

University of Alberta

A NEUROPHYSIOLOGICAL AND NEUROANATOMICAL  
INVESTIGATION OF OPTIC FLOW SENSITIVE REGIONS OF THE  
MESENCEPHALON AND OLIVOCEREBELLAR PATHWAY IN PIGEONS

by

Ian R. Winship



A thesis submitted to the Faculty of Graduate Studies and Research in partial  
fulfillment of the requirements for the degree of Doctor of Philosophy

Department of Psychology

Edmonton, Alberta

Spring, 2006



Library and  
Archives Canada

Bibliothèque et  
Archives Canada

Published Heritage  
Branch

Direction du  
Patrimoine de l'édition

395 Wellington Street  
Ottawa ON K1A 0N4  
Canada

395, rue Wellington  
Ottawa ON K1A 0N4  
Canada

*Your file* *Votre référence*  
*ISBN: 0-494-14064-X*  
*Our file* *Notre référence*  
*ISBN: 0-494-14064-X*

**NOTICE:**

The author has granted a non-exclusive license allowing Library and Archives Canada to reproduce, publish, archive, preserve, conserve, communicate to the public by telecommunication or on the Internet, loan, distribute and sell theses worldwide, for commercial or non-commercial purposes, in microform, paper, electronic and/or any other formats.

The author retains copyright ownership and moral rights in this thesis. Neither the thesis nor substantial extracts from it may be printed or otherwise reproduced without the author's permission.

**AVIS:**

L'auteur a accordé une licence non exclusive permettant à la Bibliothèque et Archives Canada de reproduire, publier, archiver, sauvegarder, conserver, transmettre au public par télécommunication ou par l'Internet, prêter, distribuer et vendre des thèses partout dans le monde, à des fins commerciales ou autres, sur support microforme, papier, électronique et/ou autres formats.

L'auteur conserve la propriété du droit d'auteur et des droits moraux qui protègent cette thèse. Ni la thèse ni des extraits substantiels de celle-ci ne doivent être imprimés ou autrement reproduits sans son autorisation.

---

In compliance with the Canadian Privacy Act some supporting forms may have been removed from this thesis.

Conformément à la loi canadienne sur la protection de la vie privée, quelques formulaires secondaires ont été enlevés de cette thèse.

While these forms may be included in the document page count, their removal does not represent any loss of content from the thesis.

Bien que ces formulaires aient inclus dans la pagination, il n'y aura aucun contenu manquant.

  
**Canada**

## **Abstract**

The Accessory Optic System (AOS), pretectum, and olivocerebellar pathway function in compensatory reflexes generated by the visual consequences of self-motion. The neurons in this pathway have large receptive fields exhibiting direction-selectivity for whole-field visual motion, termed optic flow, and connections with premotor nuclei involved in compensatory reflexes. This dissertation examined the physiology and anatomy of the AOS, pretectum, and olivocerebellar pathway as they related to the processing of optic flow. Chapter 2 demonstrated that a projection upon the hippocampal formation (HF) originating in the ventral tegmental area (VTA) arose from regions of the VTA providing input to optic flow regions of the inferior olive (IO), and that HF-projecting VTA neurons were morphological indistinguishable from IO-projecting neurons. Further, individual neurons did not project to both HF and IO, and a minority of HF-projecting, but not IO-projecting, neurons were dopaminergic. In Chapter 3, single unit recordings in response to rotational and translational optic flow identified four translation-sensitive and two rotation-sensitive classes of neurons in IO. The results reinforced that the olivocerebellar system dedicated to the analysis of optic flow is organized according to a reference frame shared with the eye muscles, semicircular canals, and postural control system. In Chapter 4, anterograde tracers injected into rotation-sensitive regions of the IO delineated four parasagittal zones spanning both folia IXcd and X of the flocculus in the vestibulocerebellum (VbC), an organization highly conserved among vertebrates. In Chapter 5, the spatio-temporal tuning of the mossy fibre (MF) and climbing

fibre (CF) inputs to the VbC was assessed using drifting sinusoidal gratings. CF input was almost exclusively tuned to high spatial frequency (SF) - low temporal frequency (TF) gratings (i.e. *slow* gratings), whereas MF input was tuned to both *slow* and *fast* (low SF - high TF) gratings. In Chapter 6, a meta-analysis of spatio-temporal tuning in the AOS and pretectum revealed that SF invariant speed tuning in the AOS and pretectum is rarer than previously estimated, and there is remarkable diversity in the impact of SF on speed tuning. Finally, in Chapter 7, complex spike activity in the VbC was assessed in response to complex stimuli designed to delineate receptive field (RF) organization. The results suggested that RFs approximated the preferred optic flowfield by pooling motion subunits of only a few different direction preferences.

## **Acknowledgements**

I owe a great debt to a great number of people for assistance during the completion of this dissertation. First, sincere thanks to my supervisor, Douglas Wong-Wylie, for being a mentor, teacher, a source of both inspiration and frustration, and a friend for the past 7 years. Hopefully I even learned something! To all the fellow Wong-Wylie lab members, especially Nathan, Janelle, and Andy, thanks for making the lab a fun place to spend time, and for offering helping hands at countless times during the completion of this dissertation. Thanks to all the academic, administrative, and psychology shop staff at the Department of Psychology who've offered assistance over the years, with special thanks to Kathryn Todd and Connie Varnhagen for being such excellent mentors and offering endless support, and to Isaac Lank, for fixing whatever broke, whenever it broke, without complaint.

Special thanks to my Mom, Dad, sister Stephanie, and brother-in-law Chris, for unconditional love and understanding, support and encouragement, and for setting the bar for academic achievement so high. Thanks also to Nancy, John, Julia, and Josh, my 'family-in-law', for thought-provoking debates and constant encouragement. Finally, infinite thanks to my beautiful wife, Jessica, for always being there for me, providing love, support, friendship, guidance, fun, and inspiration whenever needed.

**Table of Contents:**

<b><u>Chapter 1: Introduction</u></b>	1
<b>Anatomy of the AOS Pathway</b>	4
<i>The Retinal Projection to the AOS and Pretectum</i>	6
<i>Efferent Projections of the AOS and Pretectal Nuclei</i>	9
<i>The Olivo-vestibulocerebellar Pathway</i>	12
<b>Optic Flow Preferences of Neurons in the AOS-Pretectal-Olivocerebellar Pathway</b>	14
<i>Neurophysiology of Retinal Ganglion Cells</i>	15
<i>Neurophysiology of Optic Flow Neurons in the AOS and Pretectum</i>	16
<i>Spatio-Temporal Tuning in the AOS and Pretectum</i>	21
<i>Neurophysiology of the Olivocerebellar Tract</i>	24
<i>Receptive Field Structure: Bipartite Receptive Fields?</i>	26
<i>Summary and Outline of Chapters</i>	27
<i>References</i>	32
<b><u>Chapter 2: A Comparison of Ventral Tegmental Neurons Projecting to Optic Flow Regions of the Inferior Olive vs. the Hippocampal Formation</u></b>	
-	53
<b>Experimental Procedures</b>	56
<i>Surgery and Extracellular Recording</i>	56

<i>CTB/BDA Injections and Visualization</i>	58
<i>Fluorescent Tracers Injections</i>	59
<i>Tyrosine Hydroxylase Immunohistochemistry</i>	60
<i>Microscopy, Image Acquisition and Morphological Analysis</i>	61
<i>Nomenclature</i>	62
<b>Results</b>	62
<i>TH immunoreactivity – extent of the VTA/A10 in pigeons</i>	63
<i>Distribution of HF-projecting and mcIO-projecting neurons in the VTA</i>	64
<i>Morphology of HF- and mcIO-projecting VTA neurons</i>	66
<i>Retrograde Fluorescent double labeling</i>	68
<i>TH immunoreactivity of mcIO-projecting and HF-projecting neurons in the VTA</i>	69
<b>Discussion</b>	70
<i>Comparison with studies in mammals</i>	71
<i>Role of optic flow in spatial memory and path integration</i>	73
<i>The Dopaminergic Mesohippocampal Pathway</i>	74
<b>References</b>	85

**Chapter 3: Response of Neurons in the Medial Column of the Inferior Olive  
in Pigeons to Translational and Rotational Optic Flowfields**

<b>Methods</b>	101
----------------	-----

<i>Surgery</i>	101
<i>Extracellular Recordings and Optic Flow Stimulation</i>	101
<b>Results</b>	105
<i>Neurons Selective for Rotational Optic Flow</i>	106
<i>Neurons Selective for Translational Optic Flow</i>	110
<i>Ocular dominance</i>	115
<i>Functional organization of the inferior olive</i>	115
<b>Discussion</b>	116
<i>Comparison with studies of the pigeon VbC, nBOR and LM</i>	116
<i>Comparison with Mammalian Species</i>	119
<i>A common reference frame for the Optokinetic, Vestibular, and</i>	
<i>Oculomotor Systems</i>	120
<i>Topographical Organization of the mc</i>	122
<i>Role of the Rotation and Translation Optic Flow Neurons in</i>	
<i>Compensatory Eye and Head Movements</i>	124
<b>References</b>	139
<b><u>Chapter 4: Zonal Organization of the Vestibulocerebellum in Pigeons</u></b>	
<b><u>(Columba livia): I. Climbing Fibre Input to the Flocculus</u></b>	149
<b>Methods</b>	152
<i>Nomenclature</i>	155
<b>Results</b>	156

<i>Summary of rH45 injections</i>	164
<i>Summary of rVA injections</i>	167
<b>Discussion</b>	167
<i>CTB and the Potential Problem of Uptake by Fibres of Passage</i>	169
<i>Comparison with the Zonal Organization of the Mammalian Flocculus</i>	171
<b>References</b>	185
<b><u>Chapter 5: Spatio-temporal Tuning of Optic Flow Inputs to the</u></b>	
<b><u>Vestibulocerebellum in Pigeons: Differences between Mossy and</u></b>	
<b><u>Climbing Fibre Pathways</u></b>	
	193
<b>Methods</b>	197
<i>Surgery and Extracellular Recording</i>	197
<i>Stimuli and Stimulus Presentation</i>	198
<i>Quantification and Illustration of Spatio-Temporal Tuning</i>	199
<i>Quantification of Velocity Tuning</i>	201
<i>Histology</i>	203
<b>Results</b>	203
<i>Spatio-Temporal Tuning of GL units</i>	204
<i>Spatio-Temporal Tuning of the CSA of Purkinje Cells</i>	206

<i>Velocity-Like Tuning</i>	208
<b>Discussion</b>	210
<i>Comparison with Spatio-Temporal Tuning in the Pretectum and AOS</i>	210
<i>Projections of Fast and Slow Neurons in the AOS and Pretectum to the VbC</i>	212
<i>Function of Fast and Slow Neurons</i>	214
<i>Velocity-Like Tuning vs. Spatio-Temporal Independence</i>	214
<i>GL units: Granule Cells or Mossy Fibre Rosettes?</i>	215
<b>References</b>	228

## **CHAPTER 6: A Quantitative Reassessment of Speed Tuning in the Accessory**

<b><u>Optic System and Pretectum of Pigeons</u></b>	242
<b>Methods</b>	245
<i>Analysis of Speed Tuning vs. TF Tuning</i>	246
<b>Results</b>	248
<b>Discussion</b>	251
<b>References</b>	260

## **Chapter 7: Receptive Field Structure of Optic Flow Responsive Purkinje**

<b><u>Cells in the Vestibulocerebellum of Pigeons</u></b>	264
---	-----

<b>Methods</b>	268
<i>Surgery</i>	268
<i>Extracellular Recordings and Optic Flow Stimulation</i>	268
<i>Subfield Stimuli</i>	269
<i>Vector Analysis of Subfield Responses</i>	271
<i>Composite Largefield Stimuli and Rationale</i>	272
<b>Results</b>	274
<i>Responses to Composite Largefield Stimuli</i>	275
<i>Responses to Subfield Stimulation</i>	278
<b>Discussion</b>	281
<i>Responses to Composite Large Field Stimuli</i>	282
<i>Subfield Stimulation</i>	283
<i>Comparison to Optic Flow Sensitive Neurons in the MST of Primates</i>	284
<i>Comparison to Optic Flow Sensitive Neurons in Invertebrate</i>	286
<i>Constructing Bipartite Receptive fields for Rotation Expansion,     Contraction and Rotation</i>	287
<b>References</b>	300
<b><u>Chapter 8: Summary and Future Directions</u></b>	311

<b>Conclusions</b>	318
<b>References</b>	320

**List of Tables:**

Table 2.1	84
Table 5.1	227

**List of Figures:**

Figure 1.1	30
Figure 1.2	31
Figure 2.1	76
Figure 2.2	77
Figure 2.3	79
Figure 2.4	80
Figure 2.5	82
Figure 3.1	126
Figure 3.2	127
Figure 3.3	129
Figure 3.4	130
Figure 3.5	131
Figure 3.6	132
Figure 3.7	134
Figure 3.8	135
Figure 3.9	136
Figure 3.10	137
Figure 4.1	174
Figure 4.2	176
Figure 4.3	177
Figure 4.4	179
Figure 4.5	180

Figure 4.6	181
Figure 4.7	182
Figure 4.8	183
Figure 5.1	217
Figure 5.2	219
Figure 5.3	220
Figure 5.4	221
Figure 5.5	223
Figure 5.6	225
Figure 5.7	226
Figure 6.1	255
Figure 6.2	256
Figure 6.3	258
Figure 7.1	291
Figure 7.2	292
Figure 7.3	294
Figure 7.4	296
Figure 7.5	297
Figure 7.6	298
Figure 7.7	299

## **CHAPTER 1: INTRODUCTION**

Self-motion through an environment consisting of numerous stationary objects and surfaces induces distinct patterns of visual motion, termed optic flow or flowfields (Gibson 1954), across the entire retina. Optic flowfields can be described as vector fields where the length and orientation of each vector give the velocity and direction, respectively, of the corresponding image shift (Koenderink and van Doorn 1987; Nakayama and Loomis 1974; Krapp et al. 1998). The global organization of optic flowfields is dependent on the nature of the movement being performed at a particular instant in time. Figure 1.1 shows schematics of optic flowfields resulting from self-rotation (A) and self-translation (B,C), as projected onto a sphere surrounding the observer. Self-rotation produces a circular flow (in the direction opposite head rotation) about the axis of rotation and laminar (planar) flow along the “equator” of this sphere. Self-translation also results in planar motion along the equator, but radial optic flow along the vector of translation. There is a focus of expansion (FOE; see Fig. 1.1C) in the direction of motion from which the visual image radiates outward and a focus of contraction (FOC) opposite the FOE where the visual image converges (see Fig. 1.1B). It is important to note, however, that optic flow patterns generated by moving animals are rarely as straightforward as the examples in Figure 1.1. Self-motion generally produces optic flowfields with both rotational and translational components because the anatomy upon which the retina is placed is not fixed in space (e.g. eyeball, head, and torso can all move independently during self-motion; van den Berg 2000).

Optic flow can be used to determine the location, orientation, and movement of the body (Gibson 1966) in 3-dimensional space. Through the analysis of optic flow, a visual system can act as a proprioceptive sense, providing information about the animal's own self-motion relative to the surrounding environment. Indeed, the analysis of optic flow can provide information on heading of self-motion, time to collision, object motion, and object segmentation (Andersen 1997; Lappe et al. 1999). As such, optic flowfields provide information vital for the generation of visuomotor behaviours, including the compensatory eye movements and head movements necessary for retinal image stabilization. Visual acuity degrades when the visual motion moves across the retina at speeds exceeding  $4^\circ/\text{s}$  (i.e. retinal slip greater than  $4^\circ/\text{s}$ ), making retinal image stabilization essential for optimal visual acuity and velocity discrimination (Westheimer and McKee 1973, 1975; Carpenter 1977; Murphy 1978; Barnes and Smith 1981; Nakayama 1981). Reflexes involved in maintenance of retinal image stability include optokinetic nystagmus (OKN), the opto-collic reflex (OCR), the vestibulo-ocular reflex (VOR), the vestibulo-collic reflex (VCR), the cervico-ocular reflex (COR), and the cervico-collic reflex (CCR) (Wilson and Melvill Jones 1979; Gioanni 1988ab; Ilg 1997). The visually driven reflexes (OKN and OCR) involved in stabilization of retinal slip are together termed the optokinetic response (OKR). OKN refers to reflexive eye movements in response to large field visual motion, while the optocollic reflex (OCR) refers to reflexive head movements in response to large moving patterns. OKN has two phases: in the slow phase, the eyes track the large field motion and attempt to stabilize this motion on the

retina (i.e. reduce retinal slip velocity to zero); the fast phase involves rapid, saccade-like eye movements where eye position is reset to its original position. OCR involves a similar series of reflexive movements but involves movement of the head rather than the eyes (Gioanni 1988a; Ilg 1997). The parallel vestibular reflexes, VOR and VCR, are also involved in retinal image stabilization during self-motion, but are driven by vestibular stimulation rather than visual (Wilson and Melvill Jones 1979; Gioanni 1988b). The VOR and VCR respectively refer to rotations of the eye and head opposite the direction of self-motion in order to reduce retinal image velocity. Finally, CCR and COR refer to compensatory movements of the head and eye, respectively, driven by corollary proprioceptive input from the neck muscles (Maurice and Gioanni 2004).

In vertebrates, numerous studies utilizing micro-stimulation, lesion, and electrophysiological methods have implicated a sub-cortical visual pathway in the analysis of optic flow and the generation of optokinetic responses. Structures in this pathway include nuclei in the Accessory Optic System (AOS) and associated pretectal, oculomotor, and vestibular nuclei, as well as the inferior olive (IO) and the vestibulocerebellum (VbC) (for reviews see Simpson 1984; Simpson et al. 1988b; Grasse and Cynader 1990).

### **Anatomy of the AOS Pathway**

Although recognized anatomically for over 100 years and identified in all vertebrate classes (Mai 1978), relatively little was known about the AOS until the

early 1970's. Since then, the anatomy of the AOS has been delineated in numerous mammalian and non-mammalian vertebrate species and its role in the analysis of the visual consequences of self-motion has been elucidated. A simplified wiring diagram of the AOS pathway is shown in Figure 1.2: it is highly conserved, and structure names are indicated for mammals and birds (see Simpson 1984 for a review of the anatomy). Briefly, in mammals the medial, lateral, and dorsal terminal nuclei (MTN, LTN, and DTN, respectively; see Figure 1.2) of the AOS, located near the mesodiencephalic junction, receive direct retinal projections, as do optic flow sensitive neurons in the associated nucleus of the optic tract (NOT) of the pretectum (found immediately adjacent to DTN) (Kimm et al. 1979; Oyster et al. 1980; Farmer and Rodieck 1982). Efferent projections from these retinal recipient nuclei synapse on neurons in the dorsal cap (dc) of Kooy and ventrolateral outgrowth (vlo) of the inferior olive (Giolli et al. 1984, 1985; Blanks et al. 1995), which then provide climbing fibre input to Purkinje cells in the vestibulocerebellum (VbC; Gerrits and Voogd, 1982; Hess and Voogd 1986; Voogd et al. 1987ab; Ruigrok et al. 1992; Tan et al. 1995a; Sugihara et al. 2004; Sugihara and Shinoda 2004). The VbC consists of medial and lateral regions, the nodulus and ventral uvula and the flocculus, respectively. Direct projections from the AOS and pretectum to vestibular and premotor nuclei in the brainstem have also been reported (Giolli et al. 1984, 1985; Blanks et al. 1995). Efferents from the VbC synapse primarily on deep cerebellar nuclei and vestibular nuclei in the brainstem (Wylie et al. 1994; Tan et al. 1995b). This organization allows for direct (from retinal recipient nuclei) and indirect (via the

olivocerebellar pathway) transmission of optic flow information to premotor structures.

A homologous AOS-pretectal-olivocerebellar pathway has been identified in birds. As in mammals, retinal recipient nuclei within the AOS and in the associated pretectum have been identified. Within the AOS, the nucleus of the basal optic root (nBOR) complex receives direct retinal input from displaced ganglion cells in the retina and can be divided into three subdivisions: nBOR dorsalis, lateralis, and proper (nBORd, nBORl, and nBOR, respectively; Brecha et al. 1980). In the pretectum, the nucleus lentiformis mesencephali (LM) receives retinal input from ganglion cells in the ganglion cell layer proper and can be subdivided into two subnuclei, the LM pars lateralis and pars medialis (LMl and LMm, respectively; Gamlin and Cohen 1988ab). The AOS and pretectum project to the medial column of the inferior olive (mIO; equivalent to the dc), which provides climbing fibre input to Purkinje cells of the VbC (Brecha et al. 1980; Gamlin and Cohen 1988b; Wylie et al. 1997). In birds, the AOS and pretectum provide direct mossy fibre input to the granule cell layer of the VbC, thus allowing for direct and indirect (olivocerebellar) input to the VbC (Wylie et al. 1997). As in mammals, efferents from the VbC synapse primarily in the cerebellar and vestibular nuclei.

#### *The Retinal Projection to the AOS and Pretectum*

Using retrograde tracer compounds, the morphology and retinal distribution of ganglion cells projecting to the retinal recipient nuclei of the AOS have been studied

in several avian, amphibian, and mammalian species (*pigeon*, Karten et al. 1977; Fite et al. 1981; Gamlin and Cohen 1988a; *chicken*, Reiner et al. 1979; *chinchilla*, Kimm et al. 1979; *rabbit*, Oyster et al. 1980; *frog*, Montgomery et al. 1981; *turtle*, Reiner 1981; *cat*, Farmer and Roderick 1982). In birds, the retinal input to the nBOR originates almost exclusively from the displaced ganglion cells (DGCs) of Dogiel in the contralateral retina (*pigeons*, Karten et al. 1977; Fite et al. 1981; *chickens*, Reiner et al. 1979). DGCs are easily distinguishable from neurons in the ganglion cell layer proper since the large-diameter somas of DGCs are found in the inner nuclear layer, with dendrites confined to the first striatum of the inner plexiform layer (Karten et al. 1977). The retinal distribution of labeled displaced ganglion cells indicates that the higher acuity regions of the pigeon retina, the fovea and red field, are relatively devoid of DGCs but have a high concentration of ganglion cells in the ganglion cell layer proper. Lower acuity areas in the periphery of the retina have a reduced concentration of ganglion cells in the ganglion cell layer proper and an increased concentration of DGCs (Fite et al. 1981). While DGCs provide the exclusive retinal input to the nBOR in birds, the same cannot be said of mammals and amphibians. Only a small portion of the retinal projection to the AOS nuclei (MTN, DTN, LTN or amphibian homologues) arises from DGCs in the chinchilla, turtle, and frog, while no labeled DGCs are found after injection of retrograde tracers into the MTN of cats and rabbits (*chinchilla*, Kimm et al. 1979; *rabbit*, Oyster et al. 1980; *frog*, Montgomery et al. 1981; *turtle*, Reiner, 1981; *cat*, Farmer and Roderick, 1982). Instead, the major retinal input to the AOS nuclei arises from the contralateral retina (only 3% of the projection to the MTN

of cats is uncrossed, while only 0.3% is uncrossed in rabbits) from ganglion cells in the ganglion cell layer proper. Whereas DGCs projecting to the nBOR in birds are concentrated in lower acuity regions of the retina, the retinal distribution of ganglion cells projecting to the AOS nuclei in mammals mirrors that of the overall ganglion cell distribution, with fewer cells labeled in the far retinal periphery. Non-retinal afferents to the nBOR originate in the ipsilateral LM (Azevedo et al. 1983), contralateral nBOR (Brecha et al. 1980), the lateral cerebellar nucleus (Arends and Zeigler 1991), and the ipsilateral visual Wulst (Miceli et al. 1979; Rio et al. 1983; Wylie et al. 2005). Visual Wulst is thought to be the avian homologue of the mammalian primary visual cortex (Karten and Shimizu 1989; Medina and Reiner 2000).

The retinal projection to the LM of pigeons has been investigated using anterograde degeneration (Reperant 1973) and retrograde tracing techniques (Gamlin and Cohen, 1988a). Gamlin and Cohen (1988a) showed that three pretectal nuclei, the LM, tectal grey, and area pretectalis, receive input from ganglion cells in the ganglion cell layer proper of the retina. The LM can be divided into two closely apposed, cytoarchitecturally similar subnuclei, the LM, pars lateralis (LMI) and pars medialis (LMm). The retinal representation in LMm and LMI is retinotopic, such that in LMm the nasal retina is represented dorsomedially, the ventral retina dorsolaterally, the dorsal retina ventromedially, and the temporal retina is represented ventrolaterally. The LMI has a mirror image of this representation. The mammalian homologue of the LM, the NOT, also receives retinal input from ganglion cells in the ganglion cell layer

proper: the projection has been confirmed in several species (e.g. *rat*, Scalia and Arango 1979; *cat*, Scalia 1972; *primate*, Hutchins and Weber 1985). As in the pigeon, some studies have suggested that this projection is retinotopically organized (Scalia and Arango 1979; Weber 1985). Non-retinal input to the LM includes the ipsilateral nBOR (Brecha et al. 1980; Wylie et al. 1997), the lateral cerebellar nucleus (Arends and Zeigler 1991), and the ipsilateral Wulst (Miceli et al. 1979; Wylie et al. 2005).

#### *Efferent Projections of the AOS and Pretectal Nuclei*

The efferent projections of the nBOR complex have been mapped extensively in pigeons using a variety of anterograde/retrograde tracers (Brecha et al. 1980; Casini et al. 1986; Wylie et al. 1997; Wylie 2001). Brecha et al. (1980) used injections of H-leucine into the nBOR complex to demonstrate prominent bilateral projections upon the VbC, the medial column (mc) of the inferior olive, the oculomotor nuclear complex (nucleus of cranial nerve III), and the nucleus interstitialis of Cajal; a contralateral projection to the contralateral nBOR complex; and a major ipsilateral projection upon the LM. These projections were confirmed using retrograde transport of horseradish peroxidase. Wylie et al. (1997) confirmed these projections and identified previously unreported bilateral projections to the nucleus Darkschewitsch, the red nucleus, the mesencephalic reticular formation, and the ventral tegmental area (VTA), as well as ipsilateral projections to the central grey, the pontine nuclei, the cerebellar and vestibular nuclei of the brainstem, the processus cerebellovestibularis, and the dorsolateral thalamus. For most injections, the largest projections from nBOR

were to the ipsilateral LM and the mcIO. Input to contralateral mcIO arises primarily from a discrete group of cells localized in the dorsal portion of the rostral nBORp and the adjacent nBORd; input to the ipsilateral mcIO originates in a diffuse group of cells caudally in the nBORd and outside the nBOR complex in the VTA and the reticular formation (Wylie 2001). Wylie et al. (1997) reconstructed individual fibres from serial sections and demonstrated collaterals to various nuclei: collaterals of fibres projecting to the VbC terminated in the vestibular or cerebellar nuclei of the brainstem; collaterals of fibres to the inferior olive terminated in the pontine nuclei; neurons projecting to the interstitial nucleus of Cajal, the nucleus Darkshewitsch, and the central grey often had collaterals to the red nucleus and the mesencephalic reticular formation; collaterals of fibres to the contralateral nBOR terminated in the mesencephalic reticular formation or the VTA; and neurons projecting to the LM also terminated in the dorsolateral thalamus. Wylie et al. (1997) suggested that projections to the oculomotor complex, vestibular nuclei, cerebellar nuclei, VbC, LM, inferior olive, pontine nuclei, and interstitial nucleus of Cajal from the nBOR contribute to oculomotor function, projections to the interstitial nucleus of Cajal, reticular formation, and red nucleus contribute to OCR, and projections to the interstitial nucleus of Cajal, reticular formation, red nucleus, nucleus Darkshewitsch, and central grey participate in control of posture and locomotion.

Like nBOR, the pretectal nucleus LM also sends the majority of its efferent projection to pre-oculomotor structures. Gamlin and Cohen (1988b) investigated the efferent projections of the LM using anterograde autoradiographic and retrograde

tracer techniques in pigeons and found that the projection was primarily ipsilateral and caudal. They described a projection from large, multipolar neurons in LM to folia VI through IX (which constitutes part of the VbC) of the cerebellum. These mossy fibre (MF) projections terminated in the same region of the granule cell layer of the VbC innervated by the nBOR. Other targets for efferents from neurons in LM include the mcIO, nBOR, VTA, lateral pontine nucleus, nucleus pappillioformis, pedunclopontine tegmental nucleus, nucleus principalis precommissuralis, and the stratum cellulare externum. Wylie et al. (1998b) reported a projection from LM to the dorsolateral thalamus. A direct projection from the VTA to the hippocampal formation (HF) has also been reported in pigeons (Casini et al. 1986; Wylie et al. 1999b). The distribution, morphology, and neurochemical profile of neurons in VTA providing direct input to the HF or the mcIO is examined in detail in the study described in Chapter 2.

As in birds, the nuclei of the AOS and the pretectal NOT of mammals provide a major input to the olivo-vestibulocerebellar pathway. NOT has been shown to provide a direct projection to the dorsal cap of Kooy (dc) of the inferior olive in rabbits (Takeda and Maekawa 1976). However, the projection from the AOS nuclei to the dc is primarily indirect. AOS nuclei project to a group of neurons in the VTA designated as the visual tegmental relay zone (VTRZ). In turn, AOS-derived input to the dc arises from the VTRZ (Maekawa and Takeda 1979). Wylie et al. (1999a) proposed that VTRZ may be a mammalian analogue of nBORd. In addition to the connections to the olivocerebellar pathway, in mammals there is an extensive,

predominantly contralateral connection from the AOS nuclei to the superior and lateral vestibular nuclei, basilar pontine complex, reticular formation, and nucleus reticularis tegmenti pontis (Giolli et al. 1984, 1985; Blanks et al. 1995). A direct projection from the AOS to the VbC has been reported in the chinchilla (Winfield et al. 1978; though this projection has been contested, see Giolli et al. 1984), but not in other mammalian species (for review, see Simpson et al. 1988b; Grasse and Cynader 1990).

#### *The Olivo-vestibulocerebellar Pathway*

As described above, the nBOR provides bilateral input to the mcIO and the LM projects to the ipsilateral mcIO. Wylie (2001) used small iontophoretic injections of retrograde tracers in the mcIO to delineate the topographical organization of these projections. Injections into the caudal mcIO resulted in a greater proportion of retrogradely labeled cells in the LM, whereas a greater proportion of cells were found in the nBOR from injections into the rostral mcIO. As will be discussed in detail in Chapter 3, the differential projections from LM and nBOR to different regions of the mcIO are consistent with the optic flow preferences of the neurons in mcIO.

The major climbing fibre (CF) input to the VbC originates in the mcIO of pigeons and the mammalian dc and vlo. A topographical organization of mcIO neurons providing input to the VbC of pigeons was initially suggested using the injection of retrograde tracers at physiologically identified neurons in the flocculus and nodulus of pigeons and subsequent examination of retrogradely labeled cells in

the mcIO (Lau et al. 1998; Wylie et al. 1999c; Crowder et al. 2000). Briefly, in the VbC of pigeons, two types of neurons sensitive to rotational optic flow have been identified and localized to the flocculus (Wylie et al. 1993), whereas four types of neurons sensitive to translational optic flow have been identified and localized to the nodulus and ventral uvula (Wylie and Frost 1999a). Lau et al. (1998) used pressure injections of retrograde tracers in the VbC to localize the origin of climbing fibre input to Purkinje cells in the flocculus and nodulus to the dorsomedial and ventrolateral mcIO, respectively. Subsequently, Wylie and colleagues (Wylie et al. 1999c; Crowder et al. 2000) used smaller iontophoretic injections of retrograde tracers to correlate the topographical origins of the inputs to each individual type of neuron in the flocculus and nodulus. The topographical organization and the response properties of neurons in these different areas of the mcIO is the focus of the study described in Chapter 3.

A pattern of connectivity from AOS and pretectum to inferior olive similar to that of birds has been found in mammals: the caudal dc receives input from the NOT (Mizuno et al. 1973; Takeda and Maekawa 1976; Holstege and Collewyn 1982) whereas most of the visual input to the rostral dc and ventrolateral outgrowth (vlo) of the inferior olive arrive indirectly from the MTN and LTN via the VTRZ (Maekawa and Takeda 1979).

The organization of optic flow sensitive neurons in the flocculus has been investigated using anterograde tracers injected in the inferior olive and retrograde tracers injected in the VbC in a number of mammalian species (*rabbits*, De Zeeuw et

al. 1994; Wylie et al. 1994a; Tan et al. 1995b; *rats*, Ruigrok et al. 1992; Sugihara et al. 2004; Sugihara and Shinoda 2004; Tan et al. 1995b; *cats*, Gerrits and Voogd 1982; *primates*, Hess and Voogd 1986; Voogd et al. 1987ab). Collectively, the results of these experiments indicate that Purkinje cells in the mammalian VbC receiving input from dc and vlo are organized into distinct, interdigitated, parasagittal bands, though the number of bands may vary by species (Voogd and Wylie 2004). The zonal organization described using neuronal tracers correlates well with white matter compartments revealed with acetylcholinesterase histochemistry (Tan et al. 1995ab) and zonal patterns identified with aldolase C (zebrin; Sugihara and Shinoda 2004). The zonal organization of the rotation-sensitive Purkinje cells of the pigeon flocculus is examined in detail using iontophoretic injections of anterograde tracers at physiologically identified sites in the mcIO in Chapter 4, and has been the focus of more recent work in our lab (Wylie et al. 2003; Pakan et al. 2005). Briefly, the study described in Chapter 4 showed that the two classes of rotation-sensitive neurons, termed *rVA* and *rH45c* cells (described in detail below), are organized into four parasagittal bands (two of each type) in the flocculus. Based on this zonal organization, Wylie et al. (2003) identified a differential pattern of projections upon vestibular and cerebellar nuclei.

### **Optic Flow Preferences of Neurons in the AOS-Pretectal-Olivocerebellar Pathway**

The first studies of the physiology of neurons in the AOS were performed in 1959 (Marg et al. 1959), and as recently as 1973 the function of the AOS was unknown (Marg 1973). More recent studies have shown that neurons in the AOS respond preferentially to large, moving visual stimuli rich in visual texture which simulate the optic flowfields produced by self-motion (*mammals*, Simpson and Alley 1974; Westheimer and Blair 1974; Collewijn 1975ab; Simpson et al. 1979, 1988ab; Maekawa et al. 1984; Hoffmann and Schoppmann 1981; Grasse and Cynader 1982, 1984, 1990; Natal and Britto 1987, 1988; Hoffmann et al. 1988; Mustari and Fuchs 1989; Volchan et al. 1989; Ibboston et al. 1994; *birds*, Burns and Wallman 1981; McKenna and Wallman 1981, 1985; Britto et al. 1981; Morgan and Frost 1981; Winterson and Brauth 1985; Wylie and Frost 1990ab, 1999a; Wolf-Oberhollenzer and Kirschfeld 1994; Wylie 2000). In the retinal recipient nuclei of the AOS and pretectum, the majority of neurons have large, monocular receptive fields and exhibit direction-selectivity for large field moving visual stimuli. Neurons in the inferior olive and VbC also respond to large-field moving visual stimuli, but generally have panoramic, binocular receptive fields (*pigeons*, Wylie and Frost 1991, 1993, 1999b; Wylie et al. 1993, 1998a; *mammals*, Leonard et al. 1988; Graf et al. 1988; Simpson et al. 1981, 1989ab). In the remainder of this chapter, the response properties of neurons in the AOS-pretectal-olivo-vestibulocerebellar pathway illustrated in Figure 1.2 will be reviewed.

### *Neurophysiology of Retinal Ganglion Cells*

The direction and speed selectivity of ON-direction-selective ganglion cells in the rabbit retina in response to optokinetic stimuli has been assessed using single-unit recording in response to large textured visual stimuli moving through the receptive field of individual neurons. These ganglion cells are termed ON-direction-selective cells because they are excited only at the onset of steady illumination and due to their clear direction selectivity in response to moving visual stimuli (Oyster 1968; Oyster et al. 1972; see Simpson 1984). The speed selectivity of ganglion cells shows a preference for stimuli moving 0.2 to 2 degrees per second (Oyster et al. 1972). ON-direction-selective ganglion cells prefer visual motion either upward with a posterior component, downward with a posterior component, or anterior in the horizontal plane. As will be discussed below, these response properties are common to the nuclei of the AOS and pretectum in mammals and birds, providing support for a projection from ON-direction-selective ganglion cells to the AOS and pretectum (Oyster et al. 1972; Simpson et al. 1979).

#### *Neurophysiology of Optic Flow Neurons in the AOS and Pretectum*

In mammals, birds, and amphibians it is generally accepted that retinal slip signals (i.e. optic flow induced by movement of the visual world relative to the stationary or moving eye) are processed in the AOS nuclei, pretectum, and the associated olivocerebellar pathway. A significant role for the AOS and pretectal nuclei in optokinetic nystagmus (OKN), the reflexive eye movements in response to whole-

field visual motion, has been supported by lesion studies, metabolic mapping studies, and electrophysiological data in response to optokinetic stimuli.

Lesion and stimulation studies provide compelling evidence that AOS and pretectal nuclei contribute to OKN. Lesions to the AOS or pretectum consistently impair OKN, while thalamofugal or tectofugal lesions leave OKN relatively unaffected (*pigeons*, Fite et al. 1979; Gioanni et al. 1983ab; for reviews see Simpson 1984; McKenna and Wallman 1985b; Simpson et al. 1988a). In birds, Fite et al. (1979) showed that bilateral lesions of nBOR mildly impaired horizontal OKN at velocities greater than 40°/sec, but did not test vertical OKN. Subsequently, it was shown that lesions of the nBOR abolish vertical and torsional OKN, as well as monocular horizontal OKN in response to nasal to temporal (N-T) motion in the contralateral eye (Wallman et al. 1981; Gioanni et al. 1983b). LM lesions disrupt monocular horizontal OKN to optic flow moving from temporal to nasal (T-N) in the contralateral eye (Gioanni et al. 1983a). These lesion results match well with the visual response properties of neurons in the nBOR and LM (e.g. Wallman et al. 1981; Winterson and Brauth 1985). A dissociation between the AOS nuclei and pretectum and their involvement in vertical and horizontal OKN, respectively, is supported by metabolic mapping studies in chickens: presenting horizontal optic flow stimuli to one eye increases metabolic activity in the contralateral LM (as indicated by uptake of 2-deoxy-D-glucose), whereas vertical visual motion increases activity in nBOR (primarily contralateral to presentation in adult chickens; McKenna and Wallman 1981, 1985a). Lesions of NOT abolish T-N OKN in the contralateral eye, while

stimulation of NOT elicits T-N (slow phase) OKN (Collewyn 1975b). Ipsiversive horizontal OKN is impaired in monkeys by lesions of the NOT and induced by stimulation of NOT and DTN (Kato et al. 1986; Schiff et al. 1988). In cats, lesions of LTN and MTN disrupt horizontal OKN to stimuli moving from T-N and N-T (Clement and Magnin 1984).

The response properties of optic flow neurons in the AOS and pretectum of numerous species of birds and mammals have been examined using single-unit recordings in response to large field visual motion. Across vertebrate species, AOS and pretectal neurons have large receptive fields and exhibit direction-selectivity to large field visual stimulation of the contralateral eye, with the preferred speed of motion ranging from 0.5-10°/sec and varying according to species (*salamanders*, Manteuffel 1982, 1984; *frogs*, Cochran et al. 1984; Gruberg and Grasse 1984; Katte and Hoffmann 1980; *turtles*, Rosenberg and Ariel 1990; *rabbits*, Collewyn 1975ab; Maekawa et al. 1984; Simpson et al. 1979; *rats*, Natal and Britto 1987, 1988; *cats*, Hoffmann and Schoppmann 1981; Grasse and Cynader 1984, 1990; *opossum*, Volchan et al. 1989; *monkey*, Hoffmann et al. 1988; Mustari and Fuchs 1989; Westheimer and Blair 1974; *chicken*, Burns and Wallman, 1981; McKenna and Wallman 1981, 1985b; *pigeon*, Britto et al. 1981; Morgan and Frost 1981; Winterson and Brauth 1985; Wylie and Frost 1990ab, 1999ab; Wolf-Oberhollenzer and Kirschfeld 1994; Wylie 2000; *wallaby*, Ibboston et al. 1994). This contrasts with the responses of neurons in the tectofugal visual system, which responds maximally to small visual stimuli and are inhibited by whole field motion (Frost 1982, 1985). Given

that vestibular information is ambiguous at low velocities, Soodak and Simpson (1988) suggested that the low velocity selectivity of AOS neurons are well suited to complement the vestibular system in detecting self-motion. The distribution of direction preferences varies by nucleus. In the avian nBOR, neurons are direction selective for upward, downward, or nasal to temporal (N-T) visual motion in the contralateral eye (Wylie and Frost 1999b; Wylie et al. 1994b). In mammals, MTN and LTN neurons respond best to movement in near vertical directions, either upward and posterior or downward and posterior (Simpson et al. 1979). MTN neurons have a bias for the former direction of motion, LTN for the latter. Neurons in the DTN respond best to horizontal optic flow and are maximally excited by temporal to nasal (T-N) movement. Most receptive fields in MTN are *uniform*, preferring the same direction of motion throughout; however, a small subpopulation of neurons in the MTN have *monocular bipartite* receptive fields (i.e. receptive fields preferring different directions of motion in different subregions of the receptive field; Simpson et al. 1988). These receptive fields have one region excited by upward optic flow juxtaposed another region excited by downward optic flow. Bipartite neurons have also been identified in pigeons (Wylie and Frost 1999b; Wylie 2000)

The pretectal NOT of mammals and the LM of birds are direction selective primarily to horizontal visual motion (*mammals*, Collewyn, 1975ab; Hoffman and Distler 1989; Hoffman and Schoppman 1975, 1981; Ibbotson et al. 1994; Mustari and Fuchs 1990; Volchan et al. 1989; *birds*, Winterson and Brauth 1985; Wylie and Frost 1996). The majority of neurons are excited by T-N motion. DTN is virtually

indistinguishable from neighboring NOT by electrophysiological techniques and, as such, is sometimes classified as NOT-DTN (Ibbotson et al. 1994).

While the majority of neurons in the AOS and pretectum are monocular, a subpopulation of neurons have binocular receptive fields. The proportion of neurons with binocular receptive fields is small in lateral eyed species such as the pigeon, but increases to nearly half of the neurons in more frontal eyed species such as the saw-whet owl (Wylie and Frost 1999b; Wylie et al. 1994b). Wylie and Frost (1999b) recorded the activity of binocular neurons in the nBOR of anaesthetized pigeons in response to panoramic translational and rotational optic flow. Translational optic flow was produced by a ‘translator’ projector that produced patterns of moving light dots on the walls, ceiling and floor of the experiment room simulating self-translation (i.e. a binocular, 360° optic flow simulation). Rotational optic flow was produced using a ‘planetarium’ projector, which projected a pattern of moving light dots simulating self-rotation. Using these stimuli, the preferred axis of rotation or translation for a particular neuron can be determined. Wylie and Frost (1999b) identified neurons selective for translational and rotational optic flowfields. Generally, rotation cells preferred rotation about either the vertical axis (termed *rVA* neurons) or about an axis oriented at 45° ipsilateral azimuth (i.e. 45° from the midline in the horizontal plane, termed *rH45i* neurons); however, it is important to note that these neurons were not tightly tuned to these axes and considerable spread in the preferred axes occurred between neurons. Translation neurons preferred optic flow upward along the vertical axis (which would correspond to downward translation of the bird), or translational

flowfields in the horizontal plane, primarily moving N-T along an axis  $45^\circ$  from the midline. Wylie (2000) identified a subpopulation of binocular neurons in the LM of pigeons and found that these neurons, like binocular neurons in nBOR, are tuned to optic flowfields resulting from either self-rotation or self-translation.

In mammals, bipartite receptive fields are rare in the MTN, but are more common in the VTRZ. Simpson et al. (1988a) recorded from 16 neurons in the VTRZ and found that all but one had *binocular* receptive fields: both *uniform* and *bipartite* receptive fields were found when each eye was examined individually, and the boundary between the two parts of bipartite fields (when found) was approximately  $45^\circ$  from the sagittal midline (again, a region selective for upward visual motion was juxtaposed next to a selectivity for downward visual motion). The boundary location suggests that these neurons would be best suited to detecting rotation about an axis  $45^\circ$  from the midline in the horizontal plane (much like binocular *rH45i* neurons in the avian nBOR). Approximately half of the optic flow neurons in the VTRZ were activated antidromically by electrical stimulation of the ipsilateral dc. Based on these results, Simpson et al. (1988a) suggested that the spatial orientations of the direction tuning of both ON-direction-selective ganglion cells and AOS neurons are consonant with the optic flowfields associated with self-rotation about the best-response axes of the semi-circular canals (i.e. the AOS and the vestibular system share a *common reference frame*).

#### *Spatio-Temporal Tuning in the AOS and Pretectum*

Almost all of the preceding studies noted tuning to a particular range of velocities in LM and NOT in response to visual stimuli consisting of random dot patterns, square-wave gratings, or checkerboards. However, using data from the presentation of drifting sinusoidal gratings of varying spatial and temporal frequency [SF (measured in cycles per degree of visual angle, cpd) and TF (measured in cycles per second, Hz) respectively] while recording from neurons in the NOT-DTN of wallabies, Ibbotson et al. (1994) determined that the cells were tuned to TF rather than velocity (velocity = TF/SF). Two types of cells were described: *Slow* cells that responded maximally to low TF (<1 Hz) and high SF (>0.5 cpd), and *fast* cells that responded best to high TF (>10 Hz) and low SF (<0.5 cpd) but had a secondary (smaller) peak at low TFs and high SFs. Wylie and Crowder (2000) extended these findings to the avian LM, using drifting sine-wave gratings to describe the existence of *fast* cells preferring low SF (<0.25 cpd) and moderate to high TF (>1 Hz), and *slow* cells preferring high SF (>0.25 cpd) and low TF (<1 Hz), in the LM of pigeons. The existence of *fast* and *slow* neurons in the nBOR of pigeons has also been described using the same procedures (Crowder and Wylie 2001; see also Wolf-Oberhollenzer and Kirschfeld 1994). All of the studies of spatio-temporal tuning in the AOS and pretectum have emphasized that pretectal and AOS neurons are tuned to TF rather than stimulus velocity (Ibbotson et al. 1994; Wylie and Crowder 2000; Crowder and Wylie 2001; Wolf-Oberhollenzer and Kirschfeld 1994). This distinction provides support for a *correlation model* of elementary motion detectors (Reichardt, 1957, 1961; Barlow and Levick, 1965; van Santen and Sperling, 1985), which predicts

motion detectors will be tuned to TF, as opposed to the *gradient model*, which predicts velocity tuning irrespective of the texture or contrast of the stimulus (e.g. Marr and Ullmann 1981; Buchner 1984, Srinivasan 1990).

The correlation model of motion detection (often referred to as Reichardt detectors) has been used to describe visual motion processing across species from insects to primates (see Borst and Egelhaaf 1989; Buchner 1984; Clifford and Ibbotson 2003; Srinivasan et al. 1999). One feature of Reichardt correlation detectors is that they are not tuned to stimulus velocity (TF/SF) but respond to a particular TF independent of the SF, i.e. they are “spatio-temporally independent” or “TF tuned” (Buchner 1984; Egelhaaf et al. 1989; Ibbotson et al. 1994; Srinivasan et al. 1999; Clifford and Ibbotson 2003). While initial studies of spatio-temporal tuning in the AOS and pretectum suggested that the responses of these neurons to drifting sine wave gratings were TF-tuned, Crowder et al. (2003) recently suggested that whereas the *fast* units in pigeon AOS and pretectum are TF tuned, most *slow* cells show apparent velocity-tuning. As the response maxima are not completely independent of SF, Crowder et al. (2003) called this “velocity-like” tuning (see also Zanker et al. 1999). In Chapter 5, we examine the spatio-temporal tuning and incidence of velocity tuning of the MF and CF inputs of the AOS-pretectum-olivo-vestibulocerebellar pathway to the VbC. In Chapter 6 we re-examine spatio-temporal tuning in the AOS and pretectum of pigeons using improved statistical analyses to more accurately assess the incidence of tuning to velocity vs. tuning to TF in pigeons.

*Neurophysiology of the Olivocerebellar Tract*

Previous studies have shown that the complex spike activity (CSA) of Purkinje cells in the VbC is modulated in response to particular patterns of optic flow (*mammals*, Simpson et al. 1981, 1989ab; Graf et al. 1988; Leonard et al. 1988; Kano et al. 1990ab; Kusunoki et al. 1990; Shojaku et al. 1991; *pigeons*, Wylie and Frost 1991, 1993, 1999a; Wylie et al. 1993, 1998a). These Purkinje cells have binocular, panoramic receptive fields and CSA responds to optic flow simulating particular directions of rotation (e.g. see Fig. 1.1A) or translation (Fig. 1.1B,C). To determine the preferred flowfield, optic flow can be generated using either the ‘translator’ projector to create translational optic flow or the ‘planetarium’ projector to produce rotational optic flow. With these stimuli, the axis of rotation or translation can be positioned to any orientation in 3-dimensional space, and a vector representing the direction in which the animal would need to translate to produce the optic flowfield that resulted in maximal modulation of that neuron can be assigned. As originally shown in the dc, vlo, and VbC (ventral uvula, nodulus, and flocculus) of rabbits (Simpson et al. 1981, 1989b; Graf et al. 1988; Leonard et al. 1988; Kano et al. 1990ab; Kusunoki et al. 1990; Shojaku et al. 1991), rotation-sensitive neurons respond best to rotational optic flow about either the vertical axis or a horizontal axis oriented at 135° ipsilateral/45° contralateral azimuth (*rVA* and *rH45c* neurons, respectively). Simpson and colleagues emphasized that the reference frame of the floccular neurons responsive to rotational optic flow, i.e. the vertical axis and horizontal axes 45° to the midline, is common to the eye muscles, vestibular

semicircular canals, and postural control system (Graf and Simpson 1981; Simpson and Graf 1981, 1985; Ezure and Graf 1984; Graf et al. 1988; Leonard et al. 1988; Simpson et al. 1989ab; van der Steen et al. 1994; see also Wylie and Frost 1996; Wylie et al. 1998a).

Neurons equivalent to the *rVA* and *rH45c* neurons of the rabbit olivocerebellar pathway have been identified in the flocculus in pigeons (Wylie and Frost 1993). However, whereas CSA in the nodulus and ventral uvula of rabbits responds best to rotational optic flow, CSA responsive to *translational* optic flow is found in the ventral uvula and nodulus of pigeons (Wylie and Frost 1991, 1999a; Wylie et al. 1993, 1998a). In fact, neurons responsive to translational optic flow have not yet been identified in any species other than the pigeon. With respect to the preferred axes of translational optic flow, there are four response types in the vermal VbC. The best axis of translational optic flow for each type is described using the following reference frame: *x*, *y*, and *z* represent the interaural, vertical and naso-occipital axes, respectively. With respect to direction, +*x*, +*y* and +*z* represent rightward, upward and forward self-translation, respectively. In the medial VbC of pigeons, CSA responds best to optic flow patterns resulting from either upward or downward self-translation along the vertical axis [*t*(+*y*) and *t*(-*y*) neurons] or self-translation along one of two horizontal axes oriented 45° to the midline [*t*(-*x-z*) and *t*(-*x+z*) neurons (assuming recording from the left VbC, i.e. best axes would be *t*(+*x-z*) and *t*(+*x+z*) for CSA in the right VbC; Wylie et al. 1998a; Wylie and Frost 1999a). Thus, in this three-axes reference frame, the vertical axis and horizontal axes 45° to the midline, is common to

both the translational and the rotational optic flow systems. In mammals, adjacent to the dc in the beta-subnucleus of the inferior olive, and in the medial-most regions of the VbC to which the beta-subnucleus projects, neurons responsive to vestibular stimulation originating in the otolith organs have been identified (Barmack and Shojaku 1992, 1995). Insofar as the beta-subnucleus is potentially processing information from linear acceleration, it has been suggested that this structure is functionally similar to translation-sensitive regions of the pigeon mcIO (see Chapter 3).

Research in pigeons has shown that the different types of translation- and rotation-sensitive Purkinje cells receive climbing fibre (CF) input from discrete regions of the contralateral mcIO (Arends and Voogd 1989; Lau et al. 1997; Wylie et al. 1999b; Crowder et al. 2000). While rotation-sensitive, but not translation-sensitive, neurons have been identified in the inferior olive of rabbits (Leonard et al. 1988), a physiological investigation of response properties of optic flow sensitive neurons of the mcIO of pigeons has not previously been done; this was one aim of the study described in Chapter 3.

#### *Receptive Field Structure: Bipartite Receptive Fields?*

While studies in rabbits and pigeons have delineated the preferred axes of rotation and translation within the binocular, panoramic receptive fields of optic flow sensitive neurons in VbC, the organization of these receptive fields has not been directly investigated. Simpson and colleagues (Leonard et al. 1988; Graf et al. 1988;

Simpson et al. 1979, 1981, 1988ab, 1989ab) suggested that the *rH45c* neurons were not precisely tuned to the rotational optic flow field. Rather it was proposed that these neurons had a RF structure that approximated the preferred optic flow field with a *bipartite* organization (described above in reference to binocular units of the VTRZ). Such a receptive field consists of a region preferring upward motion apposed to a region preferring downward motion. The preferred optic flow field would be rotation about an axis on the boundary of the two hemifields. The *bipartite* RF structure contrasts with a RF structure that is *precisely* tuned to the preferred flowfield, where the local motion preferences within particular regions of the receptive field precisely match the directions of local motion in the corresponding region of the preferred flowfield. Optic flow sensitive neurons in invertebrates have such precisely tuned receptive fields (*blowfly*, Krapp and Hengstenberg 1996; Krapp et al. 1998; *shore crab*, Barnes et al. 2002). Since Simpson and colleagues did not offer a quantitative test demonstrating that the *rH45c* neurons have a bipartite, as opposed to a precise receptive field structure, in Chapter 7 we use two novel computer-generated stimuli to assess receptive field structure in the VbC of pigeons.

### **Summary and Outline of Chapters**

It is clear that the AOS-Preteectum-Olivo-Vestibulocerebellar pathway has a definitive role in compensatory movements in response to the visual consequences of self-motion (especially OKN). Neurons in this pathway have large receptive fields and respond maximally to large moving visual stimuli rich in visual texture. Anatomically,

the pathway provides efferent projections to and receives afferent projections from numerous premotor nuclei involved in gaze stabilization and other compensatory reflexes. This pathway works in concert with the vestibular and proprioceptive sensory systems to analyse ideothetic cues from self-motion and is facilitated by a reference frame common to the AOS, vestibular system, and eye muscles.

This dissertation includes six studies of the neuroanatomy and neurophysiology of the AOS-pretectum-olivo-vestibulocerebellar pathway in pigeons. In Chapter 2, we investigate the distribution, morphology, and neurochemical profile of neurons in the VTA of pigeons providing input to the HF and the mcIO using a variety of immunohistochemical techniques, in order to determine whether the same population of neurons is providing input to the HF and the mcIO and establish the neurochemistry of the projection. In Chapter 3, the optic flow preferences and topographical organization of neurons in the mcIO is examined. Previous studies suggest that the mcIO is organized into distinct regions, each receiving input from the LM, nBOR, and/or VTA and providing input to a particular class of optic flow sensitive neurons in the VbC. In this chapter, we seek to provide physiological confirmation of the topographical organization suggested by the anatomical studies and determine the optic flow preferences of neurons in different subregions of mcIO. In Chapter 4, the zonal organization of the CF projection to the VbC arising in the mcIO is assessed using anterograde neuronal tracers. A zonal organization has been demonstrated in numerous species of mammal, but has not been assessed in pigeons. Chapter 5 is an investigation of spatio-temporal tuning in anatomically distinct MF

and CF pathways to the VbC of pigeons. In this study we determine the spatio-temporal profile of the optic flow information reaching the VbC via the MF or CF pathways and discuss the relevance for retinal image stabilization. Chapter 6 is a meta-analysis of data from studies of spatio-temporal tuning in the LM and nBOR. The aim of this study was to determine the true incidence of velocity tuning in the AOS and pretectum of pigeons. Finally, in Chapter 7 we explicitly assess the organization of the binocular, panoramic receptive fields of optic flow sensitive neurons in the VbC, and compare this structure to previous studies in mammals and invertebrates.

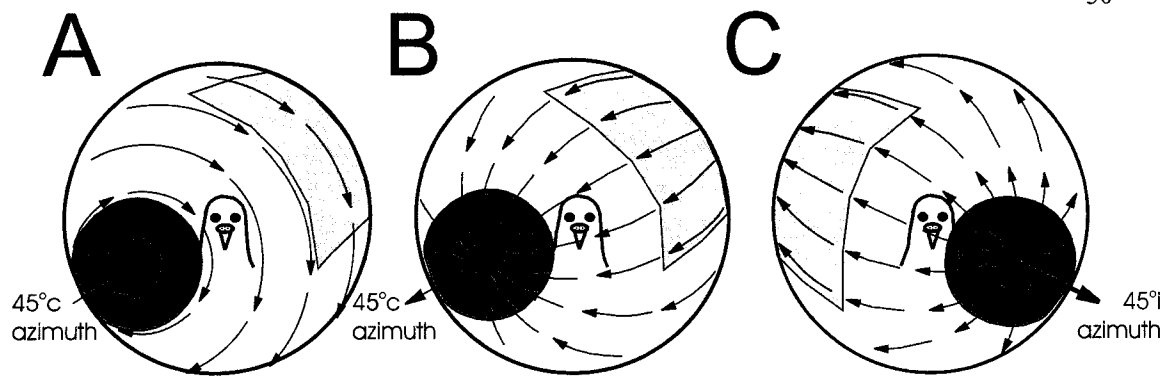


**Figure 1.1:** Optic flowfields generated by self-rotation (**A**) and self-translation (**B,C**).

Arrows indicate the motion vectors in the optic flowfield. The flowfield in **A** consists of a circular flowfield rotating about an axis oriented at  $45^\circ$  azimuth (opposite the direction of head rotation). The flowfield in **B** is produced by backward translation along an axis oriented  $45^\circ$  contralateral (c) to the midline (i.e. radial optic flow with a focus of contraction at  $45^\circ$  c azimuth), while the flowfield in **C** is produced by forward translation along an axis at  $45^\circ$  ipsilateral (i) azimuth (i.e. focus of expansion at  $45^\circ$  i).

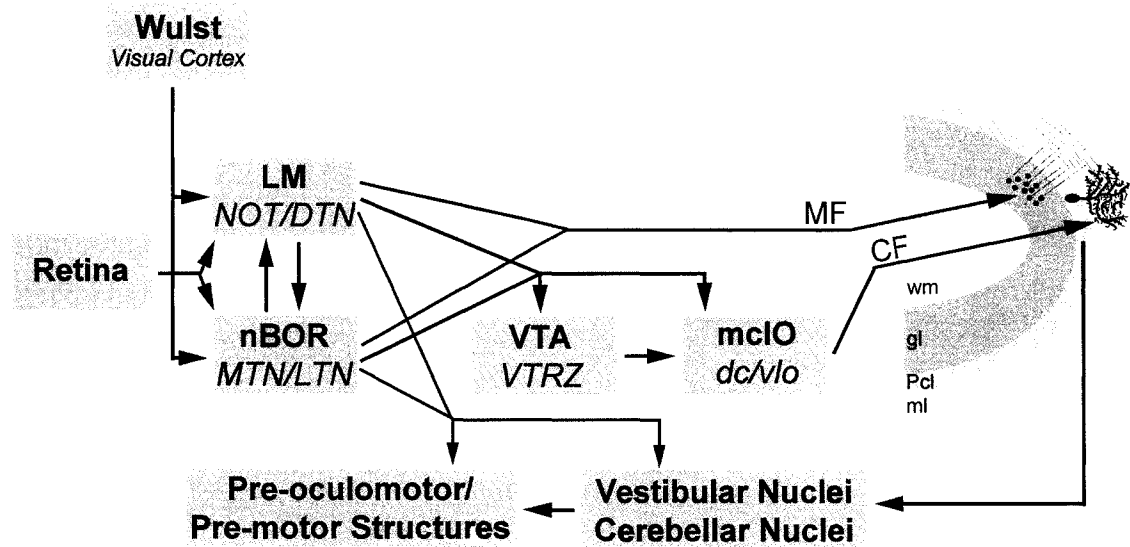


**Figure 1.2:** Simplified wiring diagram of the afferent and efferent connections of the Accessory Optic System (AOS) – Pretectum – Olivo-Vestibulocerebellar pathway.

Avian and mammalian (in italics) nomenclature is included. LM, nucleus lentiformis mesencephali; nBOR, nucleus of the basal optic root; VTA, ventral tegmental area; mcIO, medial column of the inferior olive; VbC, vestibulocerebellum; MF, mossy fibre; CF, climbing fibre; wm, cerebellar white matter; gl, granule layer; Pcl, Purkinje cell layer; ml, molecular layer; NOT, nucleus of the optic tract; DTN, dorsal terminal nucleus; MTN, medial terminal nucleus; LTN, lateral terminal nucleus; VTRZ, visual tegmental relay zone; dc, dorsal cap of Kooy of the inferior olive; vlo, ventrolateral outgrowth of the inferior olive.

## **References**

**Andersen RA.** Neural mechanisms of motion perception in primates. *Neuron* 18: 865-872, 1997.

**Arends JJA, and Voogd J.** Topographic aspects of the olivocerebellar system in the pigeon. *Exp Brain Res [Suppl]* 17: 52-57, 1989.

**Arends JJ, Zeigler HP.** Organization of the cerebellum in the pigeon (*Columba livia*): II. Projections of the cerebellar nuclei. *J Comp Neurol* 306:245-272, 1991.

**Azevedo TA, Cukiert A, Britto LRG.** A pretectal projection upon the accessory optic nucleus in the pigeon: an anatomical and electrophysiological study. *Neurosci Lett* 43: 13-18, 1983.

**Barlow HB, Levick WR.** The mechanism of directionally selective units in rabbit's retina. *J Physiol* 178: 477-504, 1965.

**Barmack NH, and Shojaku H.** Vestibularily induced slow oscillations in climbing fiber responses of Purkinje cells in the cerebellar nodulus of the rabbit (letter). *Neuroscience* 50: 1-5, 1992.

**Barmack NH, and Shojaku H.** Vestibular and visual climbing fiber signals evoked in the uvula-nodulus of the rabbit cerebellum by natural stimulation. *J Neurophysiol* 74: 2573-2589, 1995.

**Barnes WJP, Johnson AP, Horseman BG, & MacAuley MWS.** Computer-aided studies of vision in crabs. *Marine and Freshwater Behavioural Physiology* 35, 1-2, 37-56, 2002.

- Barnes GR, Smith R.** The effects of visual discrimination of image movement across the stationary retina. *Aviat Space Environ Med* 52: 466-472, 1981.
- Blanks RH, Clarke RJ, Lui F, Giolli RA, Van Pham S, and Torigoe Y.** Projections of the lateral terminal accessory optic nucleus of the common marmoset (*Callithrix jacchus*). *J Comp Neurol* 354: 511-532, 1995.
- Borst A, Egelhaaf M.** Principles of visual motion detection. *Trends Neurosci* 12: 297-306, 1989.
- Brecha N, Karten HJ, and Hunt SP.** Projections of the nucleus of the basal optic root in the pigeon: an autoradiographic and horseradish peroxidase study. *J Comp Neurol* 189: 615-670, 1980.
- Britto LGR, Natal CL, and Marcondes AM.** The accessory optic system in pigeons: receptive field properties of identified neurons. *Brain Res* 206: 149-154, 1981.
- Buchner E.** Behavioral analysis of spatial vision in insects. In: *Photoreception and Vision in Invertebrates*, edited by Ali MA. New York: Plenum Press, 1984, p. 561-621.
- Burns S, and Wallman J.** Relation of single unit properties to the oculomotor function of the nucleus of the basal optic root (AOS) in chickens. *Exp Brain Res* 42: 171-180, 1981.
- Carpenter RHS.** *Movement of the Eyes*. London: PION Ltd, 1977.
- Casini G, Bingman VP, Bagnoli P.** Connections of the pigeon dorsomedial forebrain studied with WGA-HRP and 3H-proline. *J Comp Neurol* 245: 454-70, 1986.

- Clement G, and Magnin M.** Effects of accessory optic system lesions on vestibulo-ocular and optokinetic reflexes in the cat. *Exp Brain Res* 55: 49-59, 1984.
- Clifford CW, Ibbotson MR.** Fundamental mechanisms of visual motion detection: models, cells and functions. *Prog Neurobiol* 68: 409-37, 2002.
- Cochran SL, Dieringer N, Precht W.** Basic optokinetic-ocular reflex pathways in the frog. *J Neurosci* 4: 43-57, 1984.
- Collewijn H.** Direction-selective units in the rabbit's nucleus of the optic tract. *Brain Res* 100: 489-508, 1975a.
- Collewijn H.** Oculomotor areas in the rabbit's midbrain and pretectum. *J Neurobiol*, 6: 3-22, 1975b.
- Crowder NA, Dawson MR, Wylie DR.** Temporal frequency and velocity-like tuning in the pigeon accessory optic system. *J Neurophysiol* 90: 1829-41, 2003.
- Crowder NA, Winship IR, and Wylie DRW.** Topographic organization of inferior olive cells projecting to translational zones in the vestibulocerebellum of pigeons. *J Comp Neurol* 419: 87-95, 2000.
- Crowder NA, and Wylie DRW.** Fast and slow neurons in the nucleus of the basal optic root in pigeons. *Neurosci Lett* 304; 133-136, 2001.
- DeZeeuw CI, Wylie DR, DiGiorgi PL, and Simpson JI.** Projections of individual Purkinje cells of physiologically identified zones in the flocculus to the vestibular and cerebellar nuclei in the rabbit. *J Comp Neurol* 349: 428-447, 1994.

- Egelhaaf M, Borst A, Reichardt W.** Computational structure of a biological motion-detection system as revealed by local detector analysis in the fly's nervous system. *J Opt Soc Am A* 6: 1070-87, 1989.
- Ezure K, and Graf W.** A quantitative analysis of the spatial organization of the vestibulo-ocular reflexes in lateral and frontal-eyed animals. I. Orientation of semicircular canals and extraocular muscles. *Neuroscience* 12: 85-93, 1984.
- Farmer SG, and Roderick RW.** Ganglion cells of the cat accessory optic system: Morphology and retinal topography. *J Comp Neuro* 205: 190-198, 1982.
- Fite KV, Brecha N, Karten HJ, and Hunt SP.** Displaced ganglion cells and the accessory optic system of the pigeon. *J Comp Neurol* 195: 279-288, 1981.
- Fite KV, Reiner A, Hunt SP.** Optokinetic nystagmus and the accessory optic system of pigeon and turtle. *Brain Behav Evol* 16:192-202, 1979.
- Frost BJ.** Mechanisms for discriminating object motion from self-produced motion in the pigeon. In, *Analysis of Visual Behaviour*, edited by Ingle DJ, Goodale MA, and Mansfield JW. MIT Press: Cambridge, 1982, pp. 177-196.
- Frost BJ.** Neural mechanisms for detecting object motion and figure-ground boundaries contrasted with self-motion detecting systems. In *Brain Mechanisms of Spatial Vision*, edited by Inlge D, Jeannerod M, and Lee D. Martinus Nijhoff: Dordrecht, 1985, pp. 415-449.
- Gamlin PDR, and Cohen DH.** The retinal projections to the pretectum in the pigeon (*Columba livia*). *J Comp Neurol* 269:1-17, 1988a.

- Gamlin PDR, and Cohen DH.** Projections of the retinorecipient pretectal nuclei in the pigeon (*Columba livia*), *J Comp Neurol* 269: 18-46, 1988b.
- Gibson JJ.** The visual perception of objective motion and subjective movement. *Psychol. Rev* 61: 304-314, 1954.
- Gibson JJ.** The problem of temporal order in stimulation and perception. *J Psychol* 62: 141-149, 1966.
- Gioanni H, Rey J, Villalobos J, Richard D, Dalbera A.** Optokinetic nystagmus in the pigeon (*Columba livia*). II. Role of the pretectal nucleus of the accessory optic system. *Exp Brain Res* 50: 237-247, 1983a.
- Gioanni H, Villalobos J, Rey J, Dalbera A.** Optokinetic nystagmus in the pigeon (*Columba livia*). III. Role of the nucleus ectomammilaris (nEM): interactions in the accessory optic system. *Exp Brain Res* 50: 248-258, 1983b.
- Gioanni H, Rey J, Villalobos J, Dalbera A.** Single unit activity in the nucleus of the basal optic root (nBOR) during optokinetic, vestibular and visuo-vestibular stimulations in the alert pigeon (*Columba livia*). *Exp Brain Res* 57: 49-60, 1984.
- Gioanni H.** Stabilizing gaze reflexes in the pigeon (*Columba livia*). I. Horizontal and vertical optokinetic eye (OKN) and head (OCR) reflexes. *Exp Brain Res* 69: 567-582, 1988.
- Giolli RA, Blanks RHI, and Torigoe Y.** Pretectal and brain stem projections of the medial terminal nucleus of the accessory optic system of the rabbit and rat as

studies by retrograde axonal transport of horseradish peroxidase. *J Comp Neurol* 227: 228-251, 1984.

**Giolli, RA, Blanks RHI, Torigoe Y, and Williams DD.** Projections of the medial terminal accessory optic nucleus, ventral tegmental nuclei, and substantia nigra of rabbit and rat as studied by retrograde axonal transport of horseradish peroxidase. *J Comp Neurol* 232: 99-116, 1985.

**Gerrits NM, and Voogd J.** The climbing fibre projection to the flocculus and adjacent paraflocculus of the cat. *Neuroscience*, 7: 2971-2991, 1982.

**Graf W, and Simpson JI.** The relations between the semicircular canals, the optic axis, and the extraocular muscle in lateral-eyed and frontal-eyed animals. In *Progress in Oculomotor Research. Developments in Neuroscience, vol. 12*, edited by Fuchs A, and Becker W. Amsterdam: Elsevier, 1981, pp. 409-417.

**Graf W, Simpson JI, and Leonard CS.** Spatial organization of visual messages of the rabbit's cerebellar flocculus. II. Complex and simple spike responses of Purkinje cells. *J Neurophysiol* 60: 2091-2021, 1988.

**Grasse KL, and Cynader MS.** Electrophysiology of medial terminal nucleus of accessory optic system in the cat. *J Neurophysiol* 48: 490-504, 1982.

**Grasse K.L, and Cynader MS.** Electrophysiology of lateral and dorsal terminal nucleus of the cat accessory optic system. *J Neurophysiol* 51: 276-293, 1984.

**Grasse KL, and Cyander MS.** The accessory optic system in frontal-eyed animals. In: *Vision and Visual Dysfunction. The Neuronal Basis of Visual Function*, edited by Leventhal A. New York: McMillan, 1990, p. 111-139.

- Gruberg ER, Grasse KL.** Basal optic complex in the frog (*Rana pipiens*): a physiological and HRP study. *J Neurophysiol* 51: 998-1010, 1984.
- Hess DT, and Voogd J.** Chemoarchitectonic zonation of the monkey cerebellum. *Brain Res* 369: 383-387, 1986.
- Hoffman K-P, and Distler C.** Quantitative analysis of visual receptive fields of neurons in the nucleus of the optic tract and dorsal terminal nucleus of the accessory optic tract in macaque monkeys. *J Neurophysiol* 62: 416-428, 1989.
- Hoffmann KP, Distler C, Erickson RG, Mader W.** Physiological and anatomical identification of the nucleus of the optic tract and dorsal terminal nucleus of the accessory optic tract in monkeys. *Exp Brain Res* 69: 635-644, 1988.
- Hoffman K-P, and Schoppman A.** Retinal input to direction selective cells in the nucleus tractus opticus of the cat. *Brain Res* 99: 359-366, 1975.
- Hoffman K-P, and Schoppman A.** A quantitative analysis of the direction-specific response of neurons in the cat's nucleus of the optic tract. *Exp Brain Res* 42: 146-157, 1981.
- Holstege G, and Collewyn H.** The efferent connections of the nucleus of the optic tract and the superior colliculus in rabbit. *J Comp Neurol* 209: 139-175, 1982.
- Hutchins B, and Weber JT.** The pretectal complex of the monkey: A reinvestigation of the morphology and retinal terminations. *J Comp Neurol*, 232: 425-442, 1985.
- Ibbotson MR, Mark RF, and Maddess TL.** Spatiotemporal response properties of direction-selective neurons in the nucleus of the optic tract and dorsal terminal

nucleus of the wallaby, *Macropus eugenii*. *J Neurophysiol* 72: 2927-2942, 1994.

**Ilg UJ.** Slow eye movements. *Prog Neurobiology* 53: 293-329, 1997.

**Kano M, Kano M-S, Kusunoki M, and Maekawa K.** Nature of the optokinetic response and zonal organization of climbing fibre afferents in the vestibulocerebellum of the pigmented rabbit. *Exp Brain Res* 80: 238-251, 1990a.

**Kano M, Kano M-S, and Maekawa K.** Receptive field organization of climbing fibre afferents responding to optokinetic stimulation in the cerebellar nodulus and flocculus of the pigmented rabbit. *Exp Brain Res* 82: 499-512, 1990b.

**Karten HJ, Fite KV and Brecha N.** Specific projection of displaced retinal ganglion cells upon the accessory optic system in the pigeon (*Columba livia*). *Proc Natl Acad Sci*, 74: 1752-1756, 1977.

**Karten HJ, Shimizu T.** The origins of the neocortex: connections and lamination as distinct events in evolution. *J Cognitive Neurosci* 1: 291-301, 1989.

**Kato I, Harada K, Hasegawa T, Igarashi T, Koike Y, Kawasaki T.** Role of the nucleus of the optic tract in monkeys in relation to optokinetic nystagmus. *Brain Res* 364: 12-22, 1986.

**Katte O, Hoffmann KP.** Direction specific neurons in the pretectum of the frog (*Rana esculenta*). *J Comp Physiol* 140: 53-57, 1980.

**Kimm J, Winfield JA, and Hendrickson AE.** Visual-vestibular interactions and the role of the flocculus in the vestibular-ocular reflex. In *Reflex Control of*

*Posture and Development*, eds. Granit R, and Popeiano O. *Prog Brain Res* 50: 703-713. Amsterdam/New York/Oxford: Elsevier/ North Holland, 1979.

**Koenderink JJ, van Doorn AJ.** Facts on optic flow. *Biol Cybern* 56: 247-254, 1987.

**Krapp HG, Hengstenberg B.** Estimation of self-motion by optic flow processing in single visual interneurons. *Nature* 384: 463-6, 1996.

**Krapp HG, Hengstenberg B, Hengstenberg R.** Dendritic structure and receptive-field organization of optic flow processing interneurons in the fly. *J Neurophysiol* 79: 1902-17, 1998.

**Kusunoki M, Kan M, Kano M-S, and Maekawa K.** Nature of optokinetic response and zonal organization of climbing fibre afferents in the vestibulocerebellum of the pigmented rabbit. I. The flocculus. *Exp Brain Res* 80: 225-237, 1990.

**Lau KL, Glover RG, Linkenhoker B, and Wylie DRW.** Topographical organization of inferior olive cells projecting to translation and rotation zones in the vestibulocerebellum of pigeons. *Neuroscience* 85: 605-614, 1998.

**Lappe M, Bremmer F, van Ben Berg AV.** Perception of self-motion from visual flow. *Trends Cogn Sci* 3: 329-336, 1999.

**Leonard CS, Simpson JJ, and Graf W.** Spatial organization of visual messages of the rabbit's cerebellar flocculus. I. Typology of inferior olive neurons of the dorsal cap of Kooy. *J Neurophysiol* 60: 2073-2090, 1988.

**Maekawa K, Takeda T.** Origin of descending afferents to the rostral part of dorsal cap of inferior olive which transfers contralateral optic activities to the flocculus. A horseradish peroxidase study. *Brain Res* 172: 393-405, 1979.

- Maekawa K, Takeda T, Kimura M.** Responses of the nucleus of the optic tract neurons projecting to the nucleus reticularis tegmenti pontis upon optokinetic stimulation in the rabbit. *Neurosci Res* 2: 1-25, 1984.
- Mai JK.** The accessory optic system and the retino-hypothalamic system. A review. *J Hirnforsch* 19: 213-88, 1978.
- Manteuffel G.** The accessory optic system in the newt, *Triturus cristatus*: unitary response properties from the basal optic neuropil. *Brain Behav Evol* 21: 175-184, 1982.
- Manteuffel G.** Electrophysiology and anatomy of direction-specific pretectal units in *Salamandra salamandra*. *Exp Brain Res* 54: 415-425, 1984.
- Marg E, Hamasaki D, and Giolli R.** Responses of the posterior accessory optic tract to photic stimulation of the retina and electrical stimulation of the optic nerve in rabbit. *21<sup>st</sup> Intl Congr Physiol Sci, Buenos Aires*, p. 176, 1959.
- Marg E.** Neurophysiology of the accessory optic system. *Hand Sensory Physiol*, edited by Jung R, 7/13: 103-111. Heidelberg/New York: Springer Verlag, 1973.
- Marr D, Ullman S.** Directional selectivity and its use in early visual processing. *Proceedings of the Royal Society of London - Series B: Biological Sciences*. 211: 151-180, 1981.
- Maurice M, Gianni H.** Role of the cervico-ocular reflex in the "flying" pigeon: interactions with the optokinetic reflex. *Vis Neurosci* 21: 167-80 2004.

**Mckenna OC, and Wallman J.** Identification of avian brain regions responsive to retinal slip using 2-deoxyglucose. *Brain Res* 210: 455-460, 1981.

**Mckenna OC, and Wallman J.** Functional postnatal changes in avian brain regions responsive to retinal slip: A 2-deoxy-D-glucose study. *J Neurosci* 5: 330-342, 1985a.

**McKenna OC, Wallman J.** Accessory optic system and pretectum of birds: comparisons with those of other vertebrates. *Brain Behav Evol* 26: 91-116, 1985b.

**Medina L, Reiner A.** Do birds possess homologues of mammalian primary visual, somatosensory and motor cortices? *Trends Neurosci* 23: 1-12, 2000.

**Miceli D, Gianni H, Reperant J, Peyrichoux J.** The avian visual wulst: I. An anatomical study of afferent and efferent pathways. II. An electrophysiological study of the functional properties of single neurons. In: *Neural Mechanisms of Behavior of the Pigeon*, edited by Granda, AM, Maxwell JH. New York, NY: Plenum Press, 1979, p. 223-354.

**Mizuno N, Mochizuki K, Akimoto C, and Matsushima R.** Pretectal projections to the inferior olive in the rabbit. *Exp Neurol* 39: 498-506, 1973.

**Montgomery N, Fite KV, and Bengston L.** The accessory optic system of *Rana pipiens*: neuroanatomical connections and intrinsic organization. *J Comp Neurol* 203: 595-612, 1981.

**Morgan B, Frost BJ.** Visual response characteristics of neurons in nucleus of basal optic root of pigeons. *Exp Brain Res* 42: 181-8, 1981.

- Mustari MJ, and Fuchs AF.** Discharge patterns of neurons in the pretectal nucleus of the optic tract in the behaving primate. *J Neurophysiol* 64: 77-90, 1990.
- Murphy BJ.** Pattern thresholds for moving and stationary gratings during smooth eye movement. *Vision Res* 18: 521-530, 1978.
- Nakayama K.** Differential motion hyperacuity under conditions of common image motion. *Vision Res* 21:1475-1482, 1981.
- Nakayama K, Loomis JM.** Optical velocity patterns, velocity-sensitive neurons, and space perception: a hypothesis. *Perception* 3: 63-80, 1974.
- Natal CL, Britto LR.** **The pretectal nucleus of the optic tract modulates the direction selectivity of accessory optic neurons in rats. *Brain Res* 419: 320-3, 1987.**
- Natal CL, Britto LR.** The rat accessory optic system: effects of cortical lesions on the directional selectivity of units within the medial terminal nucleus. *Neurosci Lett* 91: 154-9, 1988.
- Oyster CW.** The analysis of image motion by the rabbit retina. *J Physiol* 199: 613-35, 1968.
- Oyster CW, Simpson JI, Takahashi ES, and Soodak RE.** Retinal ganglion cells projecting to the rabbit accessory optic system. *J Comp Neurol* 190: 49-61, 1980.
- Oyster CW, Takahashi E, and Collewijn H.** Direction selective retinal ganglion cells and control of optokinetic nystagmus in the rabbit. *Vision Res* 12: 183-93, 1972.

**Pakan JM, Todd KG, Nguyen AP, Winship IR, Hurd PL, Jantzie LL, Wylie DR.**

Inferior olivary neurons innervate multiple zones of the flocculus in pigeons (*Columba livia*). *J Comp Neurol* 486: 159-68, 2005.

**Reichardt W.** Autokorrelationsauswertung als Funktionsprinzip des

Zentralnervensystems. *Z Naturforsch* 12: 448-457, 1957.

**Reichardt W.** Autocorrelation, a principle for the evaluation of sensory information

by the central nervous system. In: *Sensory Communication*, edited by

Rosenblith WA. New York: Wiley, 1961, p. 303-317. **Reiner A.** A projection

of displaced ganglion cells and giant ganglion cells to the accessory optic nuclei in turtles. *Brain Res* 204: 403-409, 1981.

**Reiner A, Brecha N, and Karten HJ.** A specific projection of retinal displaced

ganglion cells to the nucleus of the basal optic root in the chicken.

*Neuroscience* 4: 1679-1688, 1979.

**Reperant J.** Nouvelles donnees sur les projections visuelles chez le Pigeon

(*Columba livia*). *J Hirnforsch* 14: 151-187, 1973.

**Rio JP, Villalobos J, Miceli D, Reperant J.** Efferent projections of the visual wulst

upon the nucleus of the basal optic root in the pigeon. *Brain Res* 271: 145-151, 1983.

**Rosenberg AF, Ariel M.** Visual-response properties of neurons in turtle basal optic

nucleus in vitro. *J Neurophysiol* 63: 1033-1045, 1990.

- Ruigrok TJH, Osse RJ, and Voogd J.** Organization of inferior olivary projections to the flocculus and ventral paraflocculus of the rat cerebellum. *J Comp Neurol* 316: 129-150, 1992.
- Scalia F.** The termination of retinal axons in the pretectal region of mammals. *J Comp Neurol* 145: 223-57, 1972.
- Scalia F, Arango V.** Topographic organization of the projections of the retina to the pretectal region in the rat. *J Comp Neurol* 186: 271-92, 1979.
- Schiff D, Cohen B, Raphan T.** Nystagmus induced by stimulation of the nucleus of the optic tract in the monkey. *Exp Brain Res* 70: 1-14, 1988.
- Shojaku H, Barmack NH, Mizukoshi K.** Influence of vestibular and visual climbing fiber signals on Purkinje cell discharge in the cerebellar nodulus of the rabbit. *Acta Otolaryngol Suppl* 481: 242-6, 1991.
- Simpson JI.** The accessory optic system. *Ann Rev Neurosci* 7: 13-41, 1984.
- Simpson JI, Alley KE.** Visual climbing fiber input to rabbit vestibulo-cerebellum: a source of direction-specific information. *Brain Res* 82: 302-8, 1974.
- Simpson JI, and Graf W.** Eye-muscle geometry and compensatory eye movements in lateral-eyed and frontal-eyed animals. *Ann New York Acad Sci* 374: 20-30, 1981.
- Simpson JI, and Graf W.** The selection of reference frames by nature and its investigators. In *Adaptive Mechanisms in Gaze Control: Facts and Theories*, edited by Berthoz A, and Melvill-Jones G. Amsterdam: Elsevier, 1985, pp. 3-16.

- Simpson JI, Graf W, and Leonard C.** The coordinate system of visual climbing fibres to the flocculus. In *Progress in Oculomotor Research*, edited by Fuchs AF, and Becker W. Amsterdam: Elsevier, 1981, pp. 475-484.
- Simpson JI, Graf W, and Leonard C.** Three-dimensional representation of retinal image movement by climbing fiber activity. In *The Olivocerebellar System in Motor Control: Experimental Brain Research Supplement vol. 17*, edited by Strata P. Heidelberg: Springer-Verlag, 1989a, pp. 323-327.
- Simpson JI, Leonard CS, and Soodak RE.** The accessory optic system of rabbit. II. Spatial organization of direction selectivity. *J Neurophysiol* 60: 2055-2072, 1988a.
- Simpson JI, Leonard CS, and Soodak RE.** The accessory optic system: analyzer of self-motion. *Ann New York Acad Sci* 545: 170-179, 1988b.
- Simpson JI, Soodak RE, and Hess R.** The accessory optic system and its relation to the cerebellum. In *Reflex Control of Posture and Movement*, edited by Granit R, and Pompeino O, *Prog Brain Res* 50: 715-72. Amsterdam/New York/Oxford: Elsevier/North Holland, 1979.
- Simpson JI, Van der Steen J, Tan J, Graf W, and Leonard CS.** Representations of ocular rotations in the cerebellar flocculus of the rabbit. In *Progress in Brain Research vol. 80*, edited by Allum JHJ, and Hulliger M. Amsterdam: Elsevier, 1989b, pp. 213-223.
- Soodak RE and Simpson JI.** The accessory optic system of rabbit. I. Basic visual response properties. *J Neurophysiol* 60: 2037-2054, 1988.

- Srinivasan MV.** Generalized gradient schemes for the measurement of two-dimensional image motion. *Biol Cybern* 63: 421-431, 1990.
- Srinivasan MV, Poteser M, Kral K.** Motion detection in insect orientation and navigation. *Vision Res* 39: 2749-66, 1999.
- Sugihara I, Ebata S, Shinoda Y.** Functional compartmentalization in the flocculus and the ventral dentate and dorsal group y nuclei: an analysis of single olivocerebellar axonal morphology. *J Comp Neurol* 470: 113-33, 2004.
- Sugihara I, Shinoda Y.** Molecular, topographic, and functional organization of the cerebellar cortex: a study with combined aldolase C and olivocerebellar labeling. *J Neurosci* 24: 8771-85, 2004.
- Takeda T, and Maekawa K.** The origin of the pretecto-olivary tract. A study using the horseradish peroxidase method. *Brain Res* 117: 319-325, 1976.
- Tan J, Epema AH, Voogd J.** Zonal organization of the flocculovestibular nucleus projection in the rabbit: a combined axonal tracing and acetylcholinesterase histochemical study. *J Comp Neurol* 356: 51-71, 1995a.
- Tan J, Gerrits NM, Nanhoe RS, Simpson JI, and Voogd J.** Zonal organization of the climbing fibre projection to the flocculus and nodulus of the rabbit. A combined axonal tracing and acetylcholinesterase histochemical study. *J Comp Neurol* 356: 23-50, 1995b.
- van der Steen J, Simpson JI, and Tan J.** Functional and anatomic organization of three-dimensional eye movements in rabbit cerebellar flocculus. *J Neurophysiol* 72: 31-46, 1994.

- van den Berg AV.** Human ego-motion perception. *Int Rev Neurobiol* 44: 3-25, 2000.
- van Santen JP, Sperling G.** Elaborated Reichardt detectors. *Journal of the Optical Society of America A-Optics & Image Science* 2: 300-321, 1985.
- Volchan E, Rocha-Miranda CE, Picano-Diniz CW, Zinsmeisser B, Bernardes RF, and Franca JG.** Visual response properties of pretectal units in the nucleus of the optic tract of the opossum. *Exp Brain Res* 91: 273-284, 1989.
- Voogd J, Gerrits NM, and Hess DT.** Parasagittal zonation of the cerebellum in Macaques: an analysis based on acetylcholinesterase histochemistry. In *Cerebellum and Neuronal Plasticity*, edited by Glickstein M., and Stein J. New York: Plenum, 1987a, pp. 15-39.
- Voogd J, Hess DT, and Marani E.** The parasagittal zonation of the cerebellar cortex in cat and monkey. Topography, distribution of acetylcholinesterase and development. In *New Concepts in Cerebellar Neurobiology*, edited by King JS. New York: Liss, 1987b, pp. 15.
- Voogd J, Wylie DR.** Functional and anatomical organization of floccular zones: a preserved feature in vertebrates. *J Comp Neurol* 470: 107-12, 2004.
- Wallman J.** Subcortical optokinetic mechanisms. *Rev Oculomot Res* 5: 321-42, 1993.
- Wallman J, Mckenna OC, Burns S, Velez J, and Weinstein B.** Relation of accessory optic system and pretectum to optokinetic responses in chickens. In *Progress in Oculomotor Research*, edited by Fuchs A, and Becker W. Elsevier-North Holland: New York, 1981, p.435-442.

- Weber JT.** Pretectal complex and accessory optic system of primates. *Brain Behav Evol*, 26: 117-140, 1985.
- Westheimer G, Blair SM.** Unit activity in accessory optic system in alert monkeys. *Invest Ophthalmol* 13: 533-4, 1974.
- Westheimer G, McKee SP.** Failure of Donders' law during smooth pursuit eye movements. *Vision Res.* 13: 2145-253, 1973.
- Westheimer G, McKee SP.** Visual acuity in the presence of retinal-image motion. *J Opt Soc Am* 65: 847-850, 1975.
- Wilson VJ, Melvill Jones G.** *Mammalian Vestibular Physiology*. New York: Plenum Press.
- Winfield JA, Hendrickson A, and Kimm J.** Anatomical evidence that the medial terminal nucleus of the accessory optic tract in mammals provides a visual mossy fibre input to the flocculus. *Brain Res* 151: 175-182, 1978.
- Winterson BJ, and Brauth SE.** Direction-selective single units in the nucleus lentiformis mesencephali of the pigeon (*Columba livia*). *Exp Brain Res* 60:215-226, 1985.
- Wolf-Oberhollenzer F, and Kirschfeld K.** Motion sensitivity in the nucleus of the basal optic root of the pigeon. *J Neurophysiol* 71: 1559-1573, 1994.
- Wylie DRW.** Binocular neurons in the nucleus lentiformis mesencephali in pigeons: responses to translational and rotational optic flowfields. *Neurosci Lett* 291: 9-12, 2000.

- Wylie DRW.** Projections from the nucleus of the basal optic root and nucleus lentiformis mesencephali to the inferior olive in pigeons (*Columba livia*). *J Comp Neurol*, 429: 502-513, 2001.
- Wylie DRW, Bischof WF, and Frost BJ.** Common reference frame for neural coding of translational and rotational optic flow. *Nature*, 392: 278-282, 1998a.
- Wylie DR, Brown MR, Barkley RR, Winship IR, Crowder NA, Todd KG.** Zonal organization of the vestibulocerebellum in pigeons (*Columba livia*): II. Projections of the rotation zones of the flocculus. *J Comp Neurol* 456: 140-53, 2003.
- Wylie DRW, and Crowder NA.** The spatio-temporal properties of fast and slow neurons in the pretectal nucleus lentiformis mesencephali in pigeons. *J Neurophysiol* 84: 2529-2540, 2000.
- Wylie DR, DeZeeuw CI, Digioigi PL, and Simpson JI.** Projections of identified zones in the ventral nodulus to the vestibular and cerebellar nuclei in the rabbit. *J Comp Neurol* 349: 448-463, 1994a.
- Wylie DR, and Frost BJ.** Visual response properties of neurons in the nucleus of the basal optic root of the pigeon: A quantitative analysis. *Exp Brain Res* 82: 327-336, 1990a.
- Wylie DR, Frost BJ.** Binocular neurons in the nucleus of the basal optic root (nBOR) of the pigeon are selective for either translational or rotational visual flow. *Vis Neurosci* 5: 489-95, 1990b.

- Wylie DR, and Frost BJ.** Purkinje cells in the vestibulocerebellum of the pigeon respond best to either rotational or translational visual flow. *Exp Brain Res* 86: 229-232, 1991.
- Wylie DR, and Frost BJ.** Responses of pigeon vestibulocerebellar neurons to optokinetic stimulation: II. The 3-dimensional reference frame of rotation neurons in the flocculus. *J Neurophysiol* 70: 2647-2659, 1993.
- Wylie DRW, and Frost BJ.** The pigeon optokinetic system: Visual input in extraocular muscle coordinates. *Vis Neurosci* 13: 945-953, 1996.
- Wylie DRW, and Frost BJ.** Responses of neurons in the nucleus of the basal optic root to translational and rotational flowfields. *J Neurophysiol* 81: 267-276, 1999a.
- Wylie DRW, and Frost BJ.** Complex spike activity of Purkinje cells in the ventral uvula and nodulus of pigeons in response to translational optic flowfields. *J Neurophysiol* 81: 256-266, 1999b.
- Wylie, DRW, Glover RG., and Aitchison JD.** Optic flow input to the hippocampal formation from the accessory optic system. *J Neurosci.* 19: 5514-5527, 1999b.
- Wylie DRW, Glover RG, and Lau KL.** Projections from the accessory optic system and pretectum to the dorsolateral thalamus in the pigeon (*Columba livia*): a study using both anterograde and retrograde tracers. *J Comp Neurol*, 391: 456-169, 1998b.
- Wylie DRW, Linkenhoker B, and Lau K.** Projections of the nucleus of the basal optic root in pigeons (*Columba livia*). *J Comp Neurol*, 384: 517-536, 1997.

**Wylie DR, Kripalani T-K, and Frost BJ.** Responses of pigeon vestibulocerebellar

neurons to optokinetic stimulation: I. Functional organization of neurons

discriminating between translational and rotational visual flow. *J*

*Neurophysiol* 70: 2632-2646, 1993.

**Wylie DR, Ogilvie CJ, Crowder NA, Barkley RR, and Winship IR.** Telencephalic

projections to the nucleus of the basal optic root and pretectal nucleus

lentiformis mesencephali in pigeons. *Vis Neurosci* 22: 237-47, 2005.

**Wylie DR, Shaver SW, and Frost BJ.** The visual response properties of neurons in

the nucleus of the basal optic root of the northern saw-whet owl (*Aegolius*

*acadicus*). *Brain Behav and Evol* 43: 15-25, 1994b.

**Wylie DRW, Winship IR, and Glover RG.** Projections from the medial column of

the inferior olive to different classes of rotation-sensitive Purkinje cells in the

flocculus of pigeons. *Neurosci Lett.* 268: 97-100, 1999c.

**Zanker JM, Srinivasan MV, Egelhaaf M.** Speed tuning in elementary motion

detectors of the correlation type. *Biol Cybern* 80: 109-16, 1999.

**CHAPTER 2:**  
**A COMPARISON OF VENTRAL TEGMENTAL NEURONS PROJECTING**  
**TO OPTIC FLOW REGIONS OF THE INFERIOR OLIVE VS. THE**  
**HIPPOCAMPAL FORMATION**

The ventral tegmental area (VTA; catecholaminergic group A10) is a midbrain region characterized by dense dopaminergic immunoreactivity (Lindvall and Bjorklund, 1983; for review see Oades and Halliday, 1987; Gasbarri et al., 1997). In birds, the VTA, (formerly known as the area ventralis of Tsai (AVT, Reiner et al., 2004)), resides medial to the nucleus of the basal optic root (nBOR) and lateral to the third cranial nerve (Fuxe and Ljunggren, 1965; Ikeda and Gotoh, 1971; Dube and Parent, 1981; Kiss and Péczeley, 1987; Bailhache and Balthazart, 1993; Moons et al., 1994; Wynne and Güntürkün, 1995; Durstewitz et al., 1999). The VTA gives rise to a robust dopaminergic input throughout the telencephalon that has been implicated in various behaviours including cognition, reward, motivation, and motor function (for review, see Horel, 1988; Oades and Halliday, 1987; Gasbarri et al., 1997; Wise 2004).

In the present study we characterized two efferent pathways of the VTA that have been implicated in behaviours requiring the analysis of visual motion resulting from self-motion. Because the world contains an abundance of stationary objects and surfaces, self-motion produces distinct patterns of visual motion across the retina. Gibson (1954) referred to this as “optic flow” and suggested that such information would be important for numerous behaviours including the control of posture and locomotion, and spatial navigation. The VTA has been implicated in the processing of optic flow in two respects, as indicated in the schematic in Figure 2.1. Optic flow processing begins with two retinal recipient nuclei, the nucleus of the basal optic root (nBOR) of the accessory optic system (AOS) and the pretectal nucleus lentiformis mesencephali (LM; Karten et al., 1977; Reiner et al., 1979; Fite et al., 1981; Gamlin

and Cohen, 1988a). Many electrophysiological and lesion studies have implicated the LM and nBOR, as well as their mammalian equivalents, in the processing of optic flow (birds, Gioanni et al., 1983ab; Burns and Wallman, 1981; McKenna and Wallman, 1985; Winterson and Brauth, 1985; Wylie and Frost, 1990ab: for reviews see Simpson, 1984; Simpson et al., 1988b; Grasse and Cynader, 1990). Both LM and nBOR project to the medial column of the inferior olive (mcIO), which in turn projects as climbing fibres to the vestibulocerebellum (VbC; Clarke, 1977; Brecha et al., 1980; Gamlin and Cohen, 1988b; Arends and Voogd, 1989). This pathway, and the mammalian equivalent, has been implicated in the processing of optic flow for the generation of the optokinetic response (for reviews see Simpson, 1984; Simpson et al., 1988b; Waespe and Henn, 1987). In pigeons, injections of retrograde tracer into mcIO labels neurons in LM and nBOR, but also neurons dorsomedial to nBOR (Brecha et al., 1980; Wylie 2001). Wylie (2001) ascribed these neurons to the VTA. This region also receives input from collaterals of fibres originating in the LM and nBOR (Gamlin and Cohen, 1988b; Wylie et al., 1997, 1999a). Casini et al. (1986) and Atoji and Wild (2004) have shown that the hippocampal formation (HF) receives input from the VTA, and Wylie et al. (1999a) showed that some of these neurons reside in the region that receives efferents from LM and nBOR. Wylie et al. (1999a) suggested that the VTA-HF projection might be important for conveying optic flow information for “path integration”, a form of spatial navigation whereby an animal can determine spatial relationships such as the origin and destination of motion based on ideothetic cues from self-motion. Studies in rats have shown that the HF is critical for this

behaviour (Foster et al., 1989; Wilson and McNaughton, 1993; McNaughton et al., 1995, 1996; Whishaw et al., 1997; Whishaw and Maaswinkel, 1998).

Thus, although previous studies have suggested that the VTA provides input to the mcIO and HF to mediate different behaviours that require the analysis of optic flow, several questions remain unanswered. First, because the VTA is a reticular area with indistinct borders in Nissl stained tissue, it is not clear that the mcIO projecting neurons reside within VTA/A10 as defined by dopaminergic immunohistochemical studies. Second, it is not known if the regions of the VTA that project to the HF and mcIO are exclusive or overlapping. Related, it is not known if individual neurons project to both the HF and mcIO. Finally, it is not known if the mcIO-projecting or HF-projecting VTA neurons are dopaminergic. In this study we examined the extent of tyrosine hydroxylase (TH)-immunoreactive regions of the ventral tegmentum in order to define the borders of the VTA (A10) in pigeons, and we assessed the distribution and morphology of HF-projecting and mcIO-projecting VTA neurons using retrograde tracers. Further, fluorescent retrograde tracers were used to determine whether individual neurons in the VTA send efferents to both the HF and the mcIO. Lastly, we combined fluorescent retrograde tracing with immunofluorohistochemistry to determine the extent to which catecholaminergic neurons are involved in these projections.

## **Experimental Procedures**

### *Surgery and Extracellular Recording*

The methods reported herein conformed to the guidelines established by the Canadian Council on Animal Care and were approved by the Biosciences Animal Care and Policy Committee at the University of Alberta. Twenty-five Silver King and Homing Pigeons, from a local supplier, were anesthetized with a ketamine (65 mg/kg) - xylazine (8 mg/kg) cocktail (i.m.). Depth of anesthesia was monitored via toe pinch and supplemental doses were administered as necessary. The animals were placed in a stereotaxic device with pigeon ear bars and beak adapter so that the orientation of the skull conformed to the atlas of Karten and Hodos (1967). Access to the mcIO or HF was achieved by removing bone and dura over the cerebellum or the caudo-medial HF, respectively. In the case of HF injections, the injections were based on stereotaxic coordinates targeting the caudal dorsomedial (DM; Atoji and Wild, 2004) HF. For mcIO injections, single-unit extracellular recordings were used to confirm the injection site. To record the activity of optic flow units in the mcIO, glass micropipettes filled with 2 M NaCl and having tip diameters of 4-5  $\mu\text{m}$  were advanced through the cerebellum and into the brainstem using an hydraulic microdrive (Frederick Haer & Co.). Extracellular signals were amplified, filtered, and fed to a window discriminator and data analysis system (Cambridge Electronic Designs (CED) 1401plus).

Inferior olivary units are easily identified based on their characteristically low firing rate (approximately 1 spike/sec) and proximity to the base of the brain. Upon isolation of a unit in the inferior olive, the optic flow preference of the unit was qualitatively determined. In most cases, moving a large (90 X 90°) hand-held visual

stimulus, consisting of black bars, squiggles, and dots on a white background, in the receptive field of the unit was sufficient to determine the direction-selectivity. In some cases, a computer-generated stimulus (see Winship and Wylie, 2001) was used to confirm the preferred direction. After identification of an optic flow neuron in the mcIO, the recording electrode was replaced with a glass micropipette (tip diameter, 10-20  $\mu\text{m}$ ) containing a retrograde tracer.

#### *CTB/BDA Injections and Visualization*

In 12 birds (HF injections,  $n = 5$ ; mcIO injections,  $n = 7$ ), low-salt cholera toxin subunit B (CTB; Sigma, St. Louis, MO; 1% in 0.1 M phosphate-buffered saline [PBS, pH 7.4]) was iontophoretically injected unilaterally for 5-30 minutes (+4  $\mu\text{A}$ , 7 seconds ON, 7 seconds OFF). In one case, biotinylated dextran amine (BDA; Molecular Probes; molecular weight = 3000; 10% in 0.1 M phosphate buffer [PB; pH = 7.4]) was iontophoretically injected (+3  $\mu\text{A}$ , 1 second ON, 1 second OFF) into the mcIO for 5 minutes. For the cases involving iontophoresis into the mcIO, we determined the optic flow preference at the injection site prior to the injection. The electrode was left undisturbed for an additional 5 minutes post-injection. Post-surgery, birds were given an i.m. injection of buprenorphine (0.012 mg/kg) as an analgesic. After a recovery period of 3-5 days, the animals were deeply anesthetized with sodium pentobarbital (100 mg/kg) and immediately perfused with ice cold heparinized phosphate-buffered saline (PBS; 0.9% NaCl, 1 ml/100 ml heparin, 0.1 M phosphate buffer), followed by ice-cold paraformaldehyde (4% in 0.1 M phosphate buffer (PB;

pH 7.4)). These brains were extracted and post-fixed for 2-12 hours (4% paraformaldehyde, 30% sucrose in 0.1 M PB) then placed in sucrose overnight (30% in 0.1 M PB). Frozen sections, 45  $\mu\text{m}$  thick, were collected in the coronal plane. CTB or BDA was visualized using a cobalt chloride intensification of diaminobenzidine. These procedures have been described in detail elsewhere (*BDA*, Wylie et al., 1997, 1999a, 2003ab, 2005; *CTB*, Lau et al., 1998; Wylie et al., 1999ab; Crowder et al., 2000; Pakan et al., 2005; see also Wild, 1993; Veenman et al., 1992).

#### *Fluorescent Tracers Injections*

In five cases we used green and red fluorescent microspheres (Lumafluor Corp., Naples, FL) as retrograde tracers, which were pressure injected into the HF and mcIO using a Picospritzer II (General Valve Corp, Fairfield, NJ). In two cases a single injection was made into either the mcIO (case *fIO#1*) or the HF (case *fHF#1*). In the other three cases (*HFIO#2*, *HFIO#3*, *HFIO#4*) double labeling retrograde experiments were performed in which a unilateral injection of either red or green fluorescent microspheres was made in the mcIO, while the alternate color was injected either ipsilaterally or bilaterally in the HF. One other animal (case *HFIO#1*) was also used for a double labeling experiment, but in this case fluorescent conjugated CTB (Molecular Probes, Eugene, OR) was injected using iontophoresis (+4  $\mu\text{A}$ , 7 seconds ON, 7 seconds OFF). 1% CTB-AlexaFluor 594 (red) and 488 (green) were injected into the HF and ipsilateral mcIO, respectively.

After a recovery period of 2-5 days, the animals were deeply anesthetized with sodium pentobarbital and immediately perfused with ice-cold heparinized phosphate-buffered saline. The brains were immediately extracted and then flash frozen in 2-methylbutane and stored at -80°C until sectioning. Brains were embedded in optimal cutting temperature medium and 40 µm coronal sections were cut through the brainstem and cerebellum with a cryostat and mounted on electrostatic slides.

#### *Tyrosine Hydroxylase Immunohistochemistry*

Tyrosine hydroxylase (TH)-immunoreactive neurons in the VTA were visualized in six birds. Animals were perfused with ice-cold heparinized phosphate-buffered saline, followed by ice-cold paraformaldehyde. The brains were post-fixed for 2-12 hours then placed in sucrose overnight. Frozen sections, 45 µm thick, were collected in the coronal plane and placed into wells containing 0.1M PBS. The floating sections were rinsed three times with 0.1 M PBS (5 minutes per rinse), then incubated in a solution of 0.15% H<sub>2</sub>O<sub>2</sub> in a 50% methanol solution for 15 minutes and rinsed 5 additional times with PBS. Sections were placed in a blocking solution containing 10% normal horse serum (NHS) + 0.4% Triton X-100 in PBS for 1 hour at room temperature, then incubated in Sheep Anti-TH (1:500; Novus Biologicals) + 2.5% NHS + 0.4% Triton X-100 in PBS for 24 hours at 4°C. Following incubation, sections were rinsed 3 times with PBS.

In two cases (*TH#1*, *TH#2*) a chromagen was used to visualize the TH-immunoreactivity. The sections were incubated with a solution containing the

secondary antibody (biotinylated Donkey Anti-Sheep IgG; 1:1000; Jackson Immuno) with 0.4% Triton X-100 and 2.5% NHS in PBS for 60 minutes. After rinsing with PBS, avidin biotin complex (1:100; Vector Labs, Burlingame CA) was added for 30 minutes at room temperature. Sections were then stained with metal-enhanced 3,3'-diaminobenzidine tetrahydrochloride tablets (DAB; Sigma) for 1-5 minutes, dehydrated through graded ethanols, cleared with xylene, and coverslipped with Permount.

In the other four cases (*HFTH#1*, *HFTH#2*, *IOTH#1*, *IOTH#2*), tissue was incubated with a solution containing a fluorescent secondary antibody, Texas Red Donkey Anti-Sheep IgG (1:100; Jackson Immuno), with 2.5% NHS and 0.4% Triton X-100 in PBS. Following three final rinses in PBS, the tissue was mounted on electrostatic slides. In these cases green fluorescent microspheres had been injected bilaterally into HF (cases *HFTH#1* and *HFTH#2*) or unilaterally into mcIO (*IOTH#1* and *IOTH#2*) 2-5 days earlier, as described above.

#### *Microscopy, Image Acquisition and Morphological Analysis*

Sections involving visualization with DAB were viewed using standard light microscopy (Leica Laborlux) and drawings were made with the aid of a drawing tube. The sections involving fluorescent tracers or markers were examined with a compound light microscope (Leica DMRE) equipped with the appropriate fluorescence filters: Texas Red and fluorescein isothiocyanate (FITC) filters for the CTB-AlexaFluor 594 and 488, respectively; rhodamine and FITC for the red and

green latex microspheres, respectively; and Texas Red for the TH-immunofluorohistochemistry. Images were acquired using a Retiga EXi *FAST* Cooled mono 12-bit camera (Qimaging, Burnaby BC), and analyzed with OPENLAB imaging software (Improvision, Lexington MA). The images were exported to Adobe Photoshop, which was used to compensate for brightness, colour and contrast.

### *Nomenclature*

The nomenclature used in this study was agreed upon at the Avian Brain Nomenclature Forum (Reiner et al. 2004). The ventral tegmental area (VTA) was formerly known as the area ventralis of Tsai (AVT). Localization of injection sites in subdivisions of the HF was based on the nomenclature of Atoji and Wild (2004): the parahippocampus (APH) of the atlas of Karten and Hodos (1967) corresponds to the dorsolateral (DL), dorsomedial (DM), cell-poor (Po), magnocellular (Ma), and parvocellular (Pa) regions of Atoji and Wild (2004); the hippocampus of Karten and Hodos (1967) corresponds with the medial (ml) and lateral (ll) layers of the V-shaped layer and the triangular (Tr) region (see Figure 1 of Atoji and Wild (2004)). In some cases, retrogradely labeled cells were found in the nucleus of the basal optic root (nBOR) complex of the AOS. These neurons were classified according to their location in the nBOR proper (nBORp) or the nBOR pars dorsalis (nBORd), a band of cells running along the dorsal border of the nBORp (Brecha et al., 1980).

### **Results**

The results described below were acquired in one of four types of experiments:

(i) immunohistochemistry experiments used to define the extent of the VTA (ii) single-labeling retrograde experiments utilizing either CTB, BDA, or fluorescent microspheres; (iii) double-labeling retrograde studies, using injections of fluorescent microspheres in the mcIO and HF of the same animal; and (iv) experiments combining fluorescent microspheres injected in the mcIO or HF with immunofluorohistochemistry for TH-immunoreactivity.

*TH immunoreactivity – extent of the VTA/A10 in pigeons*

Areas with high concentrations of TH-immunoreactive neurons and terminal fields define the VTA/A10. In six birds processed for TH-reactivity, cell bodies, fibre fragments, and terminals were consistently labeled in the ventral tegmentum (as well as other known catecholaminergic areas of the brain, e.g. the locus coeruleus and substantia nigra). No labeling was observed in negative controls. In Figure 2.2, darkfield photomicrographs of TH-positive labeling throughout the VTA are shown. 2.2A-D is a series of coronal sections illustrating the TH-positive regions of the VTA from a representative case (*HFTH2*). The heaviest amount of labeling was found in the region adjacent to the third cranial nerve (nIII). This region was rich with labeled neurons and terminals (Fig. 2.2F,H,I). More rostrally, the labeling was not as dense (Fig. 2.2D). In all cases the TH-labeling extended laterally along the base of the brain toward the nBOR, and a band of labeling extended across the dorsal edge of the nBORd. This band contained both cell bodies and terminals, and was about 50-100µm

in width. (see insets, Fig. 2.2A-C,E,G,J,K). Some of these terminals and cell bodies were could clearly be ascribed to nBORd, especially in more caudal sections (e.g. Fig. 2.2JK). Rostrally, the labeling in the VTA extended to the stratum cellulare internum (SCI) and labeling was seen in the adjacent lateral hypothalamus (LHy) (Fig. 2.2D). Thus, based on the distribution of TH-immunoreactive elements, we were able to define the extent of the VTA in pigeons. VTA is a continuous reticular region, the bulk of which forms a column of TH-immunoreactive tissue adjacent to nIII, medial to the nBOR and ventral to the red nucleus. A fine lateral extension of the VTA runs along the dorsal border of the nBOR, through the ventral part of the mesencephalic reticular formation. VTA/A10 also includes dopaminergic regions immediately dorsal to nIII, medial to nIII and, in the more rostral sections, dorsal to the LHy and nucleus mammillaris lateralis (ML).

The TH-positive labeling in the VTA was continuous with that in the substantia nigra pars compacta (A9) and the central gray and peri-rubral areas (A11). This is consistent with previous observations in birds and mammals (Lindvall and Bjorklund, 1983; Waldmann and Gunturkun, 1993; Gasbarri et al., 1997).

#### *Distribution of HF-projecting and mcIO-projecting neurons in the VTA*

The distribution of retrogradely labeled cells in the VTA was assessed in 8 birds with a unilateral injection of retrograde tracer in the HF and 11 birds with injections in the mcIO. Twelve of these cases involved an iontophoretic injection of low-salt CTB. In one case 3000 M.W. BDA was injected in the mcIO, while 6 cases

(*fIHF#1, fIIO#1, HFTH#1, HFTH#2, IOTH#1, IOTH#2*) used fluorescent latex microspheres as a retrograde tracer. The injections in the HF were generally large, with considerable spread of the tracer across multiple subdivisions of the HF, though DL and DM received the bulk of the injections. No significant difference in the distribution of retrogradely labeled cell bodies in the VTA was found between cases. Similarly, the distribution of labeled cells in the VTA did not differ significantly between mcIO injections, and they will be considered together<sup>1</sup>.

Figure 2.3 shows camera lucida tracings illustrating the distribution of retrogradely labeled cells (black dots) in four representative cases. Injection sites are illustrated in the top row. Below, three sections through the caudo-rostral extent of the VTA are shown for each case. The projection from VTA to HF is predominantly ipsilateral (Casini et al., 1986; Wylie et al., 1999a; Atoji and Wild 2004) but the projection from the VTA and nBOR to the mcIO is bilateral (Brecha et al., 1980; Wylie et al., 1997; Wylie, 2001). For mcIO sections (3A,B), ipsilateral labeling was concentrated in the caudal and ventral VTA, continuous with heavy labeling of the nBORd. Sparse-moderate labeling was found in more dorsal and rostral regions of the VTA. Moderate labeling of the contralateral VTA and nBOR complex, and moderate-heavy labeling of the rostral nBORp, was observed after mcIO injections. This pattern of labeling is consistent with previous observations (Wylie, 2001). After HF injections (3C,D), heavy labeling in the caudal sections was concentrated in the ventral VTA, and moderate labeling was observed in or adjacent to nBORd. Heavy labeling

---

<sup>1</sup> Note: Rostral injections in mcIO generally produce more retrogradely labeled cells in the nBOR and VTA, but the distribution of these neurons does not differ from caudal injections in the mcIO (Wylie

continued through the rostral and dorsal VTA, including areas dorsal to the LHy and ML, which were also densely labeled. While the distribution of retrogradely labeled cells did not differ significantly between injection sites in the HF, those injections including the central and medial DM and other regions of the caudo-ventral HF (Tr and the V-shaped layer) generally produced more retrograde labeling in VTA than injections more lateral in DM or restricted to DL, or injections in more rostral regions. In summary, injections in the mcIO primarily labeled the nBORp, nBORd, and the caudo-ventral regions of the VTA medial to nBOR, with significant labeling of the contralateral VTA, whereas injections in the HF included heavy labeling of the caudal and ventral VTA but had a greater proportion of retrogradely labeled cells in the dorso-medial regions of the ipsilateral VTA, with sparse labeling of nBORd. The distributions are clearly overlapping, with the region of greatest overlap found in the caudal and ventral VTA.

#### *Morphology of HF- and mcIO-projecting VTA neurons*

Based on the Golgi-like staining of retrogradely labeled cells in VTA produced by CTB, we performed a coarse morphological assessment of neuron shape and size<sup>2</sup>. The results of our morphological analysis are shown in Table 1 and tracings of representative neurons are shown in Figure 2.4. A total of 225 neurons (101 from mcIO injections, 124 from HF injections), generally small to medium sized, were

---

<sup>2</sup> Note that this analysis was not intended to describe all possible cell types found in the VTA, nor do we claim that the morphological classes we describe form exclusive, distinct classes of neurons. Our purpose was to determine whether the mcIO-projecting and HF-projecting neurons had differing

classified as multipolar, fusiform, or round based on cell shape and the number of visible neuronal processes. Length and width measurements were also recorded. As shown in Table 1, the morphological characteristics of the neurons projecting to the mcIO and to the HF were not distinguishable. In both cases, approximately half (mcIO, 50.5%; HF, 51.6%) of the neurons were classified as multipolar: the vast majority of these neurons were triangular in shape and nearly all had 3 visible processes, one extending from each pole. Examples are shown in the left column of Figure 2.4A and 4B. Approximately 40% of mcIO-projecting (39.6%) and HF-projecting (39.5%) neurons were classified as fusiform: these neurons were bipolar, with a long ovoid soma and a single process extending from each pole (see the right column of Figure 2.4A and 4B). Finally, 8.9% and 9.9% of HF-projecting and mcIO-projecting neurons were classified as round neurons: these neurons had a round soma and 1 to 4 visible processes (see the right column of Figure 2.3). Post-hoc analysis of the lengths, widths, and areas of the six classes of neurons (HF – Multipolar, HF – Fusiform, HF – Round, mcIO – Multipolar, mcIO – Fusiform, mcIO – Round) using the Tukey's HSD method revealed no significant differences ( $\alpha = .05$ ) between the HF-projecting and mcIO-projecting VTA neurons.

Morphological measurements of TH-positive neurons in the VTA are included in Table 1, and representative tracings are shown in Figure 2.4C. A total of 48 TH-immunoreactive neurons were classified as multipolar, fusiform, or round based on cell shape and the number of visible neuronal processes, length, and cell body width.

---

morphology, which would suggest that different populations of cells in the VTA project to the HF vs. the mcIO.

While the general morphology of the TH-positive neurons was comparable to the mcIO- and HF-projecting neurons, TH-positive cells were larger on average, reflecting the existence of a subset of very large TH-positive fusiform and multipolar neurons. Fusiform TH-positive neurons were also less common than in the retrogradely labeled samples. Post-hoc analysis using Tukey's HSD revealed that multipolar TH-immunoreactive neurons had significantly greater length, width, and area than multipolar neurons derived from mcIO injections (length,  $P = .000$ ; width,  $P < .000$ ; area,  $P < .000$ ), and significantly greater length and area than multipolar neurons from HF injections (length,  $P < .000$ ; area,  $P < .000$ ). Similarly, the length and area of fusiform TH-positive neurons were significantly greater than those from mcIO injections (length,  $P < .041$ ; area,  $P < .003$ ) and HF injections (length,  $P < .019$ ; area,  $P < .01$ ). The length, width, and area of TH-positive round neurons were not significantly different than their counterparts from mcIO or HF injections.

#### *Retrograde Fluorescent double labeling*

Four birds received injections of fluorescent retrograde tracer (red or green) in the HF in conjunction with injection of an alternate colour of tracer in the mcIO. Retrogradely labeled cells from both injection sites were located throughout the VTA, and intermingled especially in the caudal VTA. Despite counting over 2200 retrogradely labeled neurons in the VTA, 941 of which were labeled from injections in the mcIO and 1265 of which were labeled from HF injections, no double-labeled neurons were found. That is, no individual neurons in VTA projected to both HF and

mcIO. Figure 2.5A-C shows representative photomicrographs depicting mcIO- and HF-projecting VTA neurons from these experiments. Digital images acquired under the FITC and rhodamine filters are shown in the left and middle panels, respectively, while the right panel is an overlay of the two. Fig. 2.5A shows a low magnification shot through the VTA illustrating that retrogradely labeled cells from mcIO and HF injections were intermingled within the VTA. Fig. 2.5B shows HF-projecting neurons bordering the nBORd close to mcIO-projecting neurons within nBORd, while Fig. 2.5C shows a mcIO-projecting neuron closely apposed to a HF-projecting neuron in a rostral section of the VTA.

#### *TH immunoreactivity of mcIO-projecting and HF-projecting neurons in the VTA*

Four birds were used to determine if the HF-projecting and/or the mcIO-projecting VTA neurons are dopaminergic. The animals received either a unilateral injection of the green latex microspheres bilaterally in the HF (cases *HFTH#1* and *HFTH#2*) or a unilateral injection in the mcIO (*IOTH#1* and *IOTH#2*). The tissue through the VTA was subsequently processed for TH-immunoreactivity using a Texas Red secondary antibody. Retrogradely labeled cell bodies in VTA from both injection sites were located within and adjacent to the TH-positive areas. Double-labeled cells (i.e. cells labeled with green Lumafluor from an injection in HF and Texas Red fluorescence from the TH secondary antibody) were observed in the VTA of the two birds (*HFTH#1*, *HFTH#2*) that received bilateral injections in the HF. Cumulatively, across both of these animals, 8.2% of retrogradely labeled cell bodies (n = 487) were

TH-positive. Representative double-labeled neurons from case *HFTH#1* are shown in Figure 2.5D. These cells were located in the rostral part of VTA though double-labeled neurons were distributed throughout the VTA but not in the region bordering nBORd. Contrasting this, from the two cases with an injection in the mcIO, none of the retrogradely labeled neurons (n = 501) in the VTA or nBOR complex were TH-positive, though their somas were often located among TH-positive elements (e.g. Figure 2.5E).

## **Discussion**

Our localization of TH-immunoreactive elements in the ventral tegmentum of pigeons agrees well with previous studies in birds (Fuxe and Ljunggren, 1965; Ikeda and Gotoh, 1971; Dube and Parent, 1981; Bailhache and Balthazart, 1993; Waldmann and Güntürkün, 1993; Moons et al. 1994; Wynne and Güntürkün, 1995; Durstewitz et al., 1999). VTA/A10 is a continuous reticular region, the bulk of which forms a column of TH-immunoreactive tissue adjacent to the third cranial nerve (nIII), medial to the nBOR and ventral to the red nucleus. We do, however, show that there is a lateral extension from the VTA that runs along the dorsal border of the nBOR. Data from our retrograde tracer experiments demonstrated that the distribution of VTA neurons that project to the HF overlap with that of neurons projecting to optic flow regions of the mcIO: neurons projecting to both structures are found throughout the VTA, with the greatest overlap in the caudo-ventral VTA. Injections in the HF incorporating the central and medial DM subdivision generate more retrograde

labeling in the VTA than more dorso-lateral injections, an observation that agrees well with the findings of Atoji and Wild (2004). Furthermore, VTA neurons providing input to the HF and the mcIO were morphologically indistinguishable (see Table 1): both groups were made of small and medium sized neurons, approximately half of which are classified as multipolar, 40% are classed as bipolar fusiform; the remainder are round neurons. Additionally, we have demonstrated that individual neurons do not project to both the HF and the mcIO, and that a subset (8.2%) of neurons projecting to the HF are dopaminergic (i.e. TH-immunoreactive), but neurons projecting to the mcIO are not TH-immunoreactive.

#### *Comparison with Studies on Mammals*

Our findings agree well with studies of the mesohippocampal projection in mammals. In rats, VTA provides dopaminergic and non-dopaminergic input to the limbic system, including the HF (Fallon et al., 1984; Horel, 1988; Conde et al., 1995; Gasbarri et al., 1991, 1994ab, 1997). Injections of anterograde neuronal tracers in the VTA of rats results in concentrated terminal field labeling in the ventral subiculum and adjacent CA1 field of the HF, with fewer fibres found in the dorsal HF (Gasbarri et al., 1991; 1994a). Retrograde neuronal tracing studies demonstrated that the VTA neurons projecting to the HF are topographically organized: neurons projecting to the ventral HF, primarily subiculum and adjacent CA1 field, are found primarily in the ventral two-thirds of the VTA; neurons projecting to the dorsal subiculum and CA1 field are located in the ventral and dorsal borders of the VTA (Gasbarri et al., 1994b).

Atoji and Wild (2004) postulated that DM of the avian HF incorporates components comparable to Ammon's horn (CA1-4) and the subiculum, which suggests that neurons in VTA have homologous hippocampal targets in mammals and birds.

Wylie et al. (1999a) suggested that the HF-projecting neurons in the dorsal border of the rat VTA, just ventral to the red nucleus, were located in the visual tegmental relay zone (VTRZ), a region of the ventral tegmentum containing neurons responsive to the optic flow generated by self-motion (Giolli et al., 1985; Simpson et al., 1988b). Wylie et al. (1999a) suggested that the VTRZ is equivalent to the optic flow sensitive regions of the VTA and the nBORd in pigeons based on the optic flow sensitivity of neurons in VTRZ and the topography of its projections upon optic flow regions of the inferior olive (Giolli et al., 1985; Simpson et al. 1988ab). As in pigeons, the VTA neurons projecting to the inferior olive in rats are not dopaminergic, but are intermixed in the VTA with dopaminergic and non-dopaminergic neurons projecting to the telencephalon (Fallon et al., 1984). As such, VTRZ offers a mammalian equivalent of the HF-projecting optic flow neurons in the VTA of pigeons.

The lack of double-labeled neurons in VTA from retrograde tracers injected in the mcIO and the HF of the same animal is also consistent with mammalian studies, given that a lack of collateralization is a general characteristic of the efferent projections of VTA neurons in rats (Takada and Hattori, 1987; Gasbarri et al., 1997). Finally, the relatively low percentage of TH-positive neurons projecting to the HF in our study agrees well with previous studies in rats, which showed that 10-18% of

neurons in VTA projecting to the HF were TH-immunoreactive (Gasbarri et al., 1994b, 1997).

*Role of optic flow in spatial memory and path integration*

Although it is well established that the projection from the mclO to the vestibulocerebellum is involved in the optokinetic response and the analysis of optic flow, the assertion that the VTA – HF pathway is involved in the analysis of optic flow is more tenuous. Avian HF is considered an anatomical homologue of the mammalian HF based on developmental (Källén, 1962; Redies et al., 2001), cytoarchitectural (Montagnese et al., 1996, Tömböl et al., 2000ab), neurochemical (Erichsen et al., 1991; Krebs et al., 1991; Székely and Krebs, 1996), neural connectivity (Casini et al., 1986; Székely and Krebs, 1996; Wylie et al., 1999a; Atoji et al., 2002; Kahn et al., 2003; Atoji and Wild, 2004), and physiological grounds (Siegel et al., 2000; Siegel et al., 2005). Furthermore, behavioural studies suggest that the avian HF functions in spatial cognition in a manner similar to the mammalian HF (Bingman et al., 1990; Bingman and Yates, 1992; Fremouw et al., 1997; Colombo et al., 1997; Gagliardo et al., 2002; for review see Sherry et al., 1992; Colombo and Broadbent, 2000; Macphail, 2002). The initial studies in mammals implicating the HF in ‘path integration’ suggested that ideothetic information from self-motion originates in the vestibular system (McNaughton et al., 1995, 1996; Muller et al., 1996). Wylie et al. (1999a) proposed an additional ideothetic cue: optic flow. This assertion is supported by studies indicating that both vestibular and visual motion cues influence

head-direction cells and hippocampal place cells and may thus be used for path integration (Blair and Sharp, 1996; Terrazas et al., 2005). Wylie et al. (1999a) demonstrated that the VTA of pigeons receives input from structures dedicated to the analysis of optic flow, nBOR and LM, and that a subset of neurons in the VTA of pigeons responds to precise patterns of optic flow generated by self-rotation or self-translation. Combined with the work of Wylie et al. (1999a), the morphological and topographical similarities between HF-projecting and mcIO-projecting neurons in the VTA suggests that the same population of neurons projects to both structures, and that some of this population relays information related to the analysis of optic flow; however, it is possible that in a reticular area such as VTA cohabitant subpopulations of neurons may have distinct afferents, efferents, and functions (Fallon et al., 1984).

#### *The Dopaminergic Mesohippocampal Pathway*

While the functional significance of the dopaminergic mesohippocampal projection is unclear, a role in mediating locomotor activity and spatial memory has been suggested (Gasbarri et al., 1997) based on studies of the effects of stimulation using dopamine agonists and lesions of dopaminergic neurons in the VTA and HF of rats. These studies indicate that injections of dopamine agonists in the HF increases spontaneous and exploratory behaviour (Smialowski 1976), while lesions of the dopaminergic neurons in VTA reduces spontaneous locomotor activity (Kelly and Iversen, 1976; Koob et al., 1981). Further, catecholamine agonists injected into the dorsal HF enhance performance in a win-shift radial maze task (Packard and White,

1991) and bilateral lesions of dopaminergic neurons in the dorsal and ventral subiculum and CA1 field impair performance in the hippocampal dependent spatial water maze task (Gasbarri et al., 1996). Little work, in either mammals or birds, has examined the function of the non-dopaminergic input to the HF. Given that this accounts for 80-90% of the VTA-derived projection upon the HF, the role of this projection in hippocampal dependent memory processes remains a significant question and an avenue for future study.

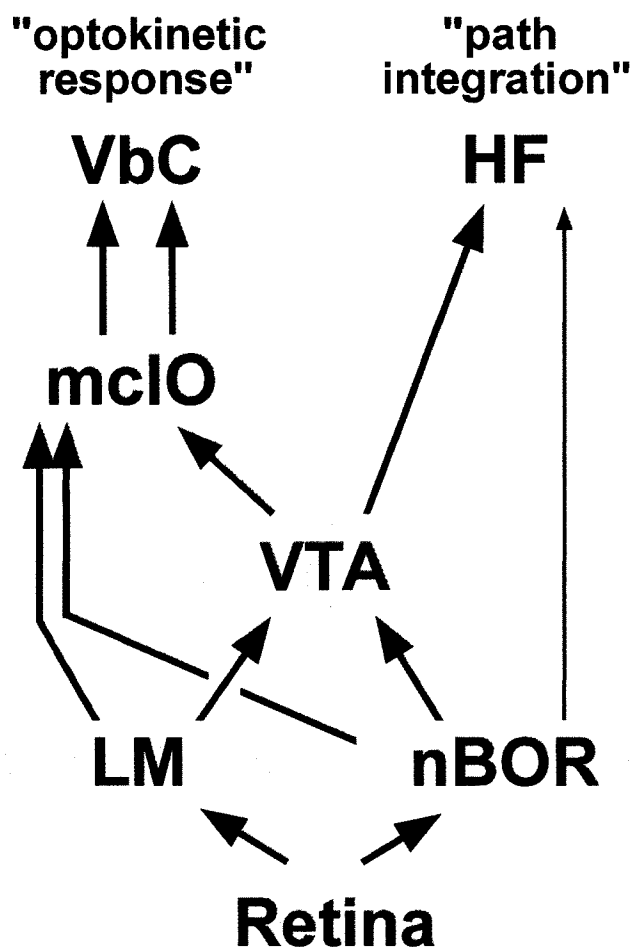


**Figure 2.1:** Schematic illustrating the interconnections of the accessory optic system (AOS), pretectum, olivocerebellar pathway, and the hippocampal formation (HF). Visual information from self-motion arrives in the nucleus of the basal optic root (nBOR) of the AOS and the nucleus lentiformis mesencephali (LM) of the pretectum directly from the retina. Optic flow information arrives at the medial column of the inferior olive (mcIO) directly from LM and nBOR and indirectly via the ventral tegmental area (VTA). mcIO provides climbing fibre input essential for the optokinetic response to the vestibulocerebellum (VbC). Optic flow information may reach the HF via a robust projection from the VTA and/or a small projection directly from the nBOR: this information may be used for path integration.

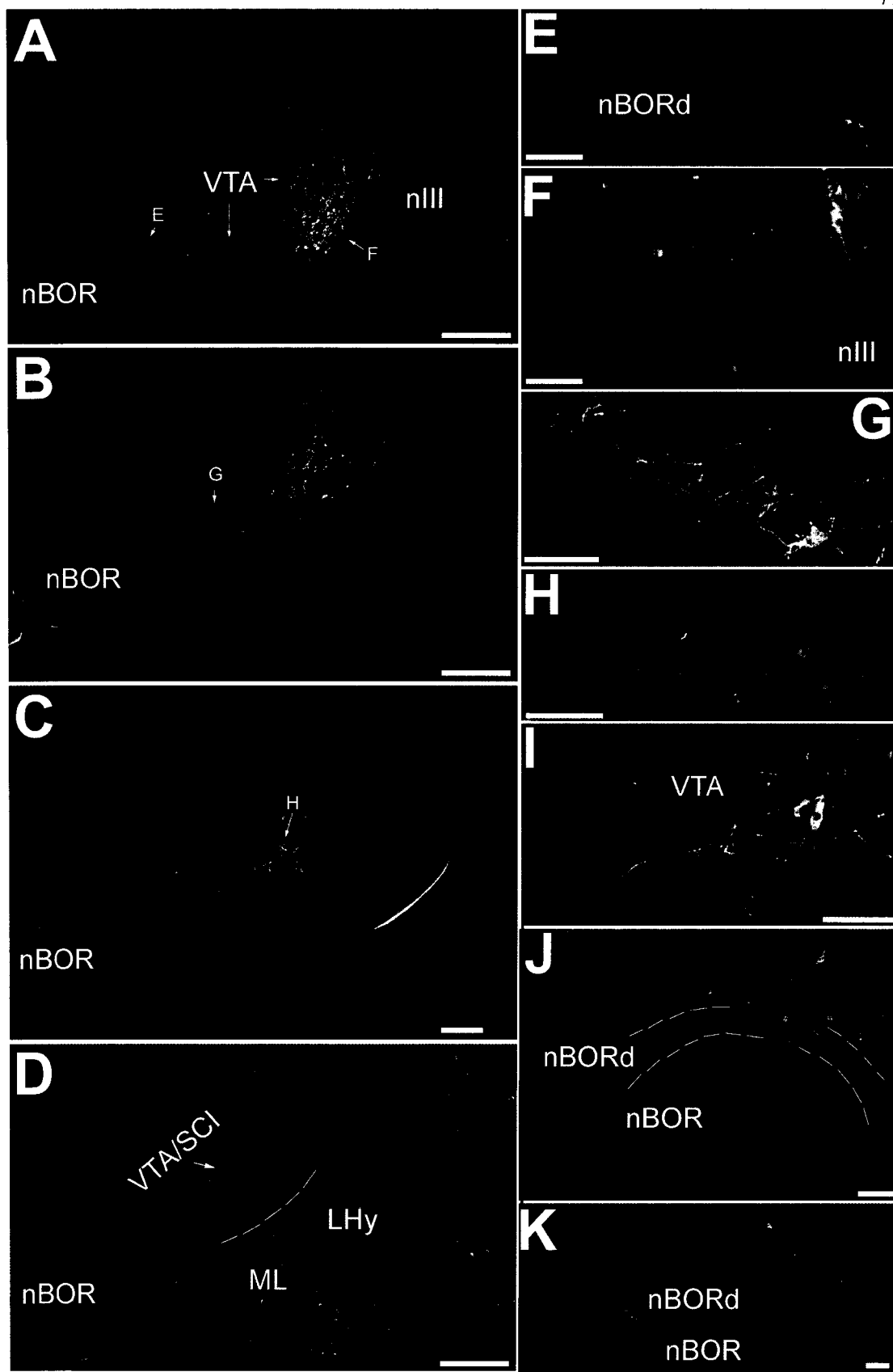
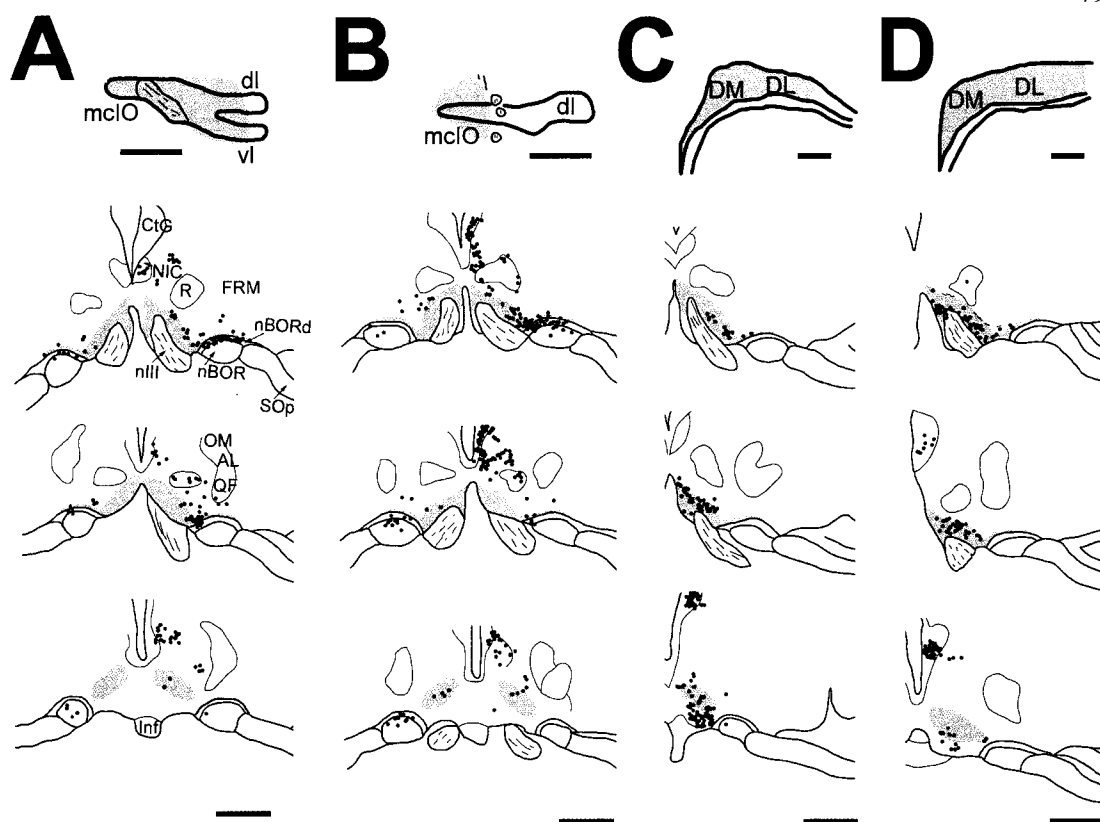


Figure 2.2: Darkfield photomicrographs of tyrosine hydroxylase (TH)-immunoreactive tissue in the ventral tegmental area (VTA). In 1A-D, low magnification images, 160  $\mu\text{m}$  apart, show the distribution of TH-positive areas in the VTA from case HFTH#2 (A, most caudal; D most rostral). E-H show enlarged digital images of regions indicated in A, B, and C. F and H show terminals and cell bodies from the heart of the VTA. G and I shows cell bodies, fibres and terminals in the caudal VTA just medial and dorsal to the nBOR. E, J and K show images from three different cases illustrating TH-positive neurons located in and immediately adjacent to the caudal part of the nucleus of the basal optic root pars dorsalis (nBORd). In all panels, lateral is to the left of the page, dorsal towards the top. nIII, third cranial nerve; nBOR, nucleus of the basal optic complex; LHy, lateral hypothalamic nucleus; SCI, stratum cellulare internum. Scale bars: A-D, 500  $\mu\text{m}$ ; E-K, 50  $\mu\text{m}$ .



**Figure 2.3:** Distribution of retrogradely labeled neurons in the ventral tegmental area (VTA) from injections in the medial column of the inferior olive (mcIO) and hippocampal formation (HF). Injections sites (grey areas) are shown in the top row; below, three midbrain sections through the VTA are illustrated, proceeding from caudal (top) to rostral. The sections are approximately 260 μm apart, and were chosen to approximately match plates from A4.00 to A4.75 of Karten and Hodós (1967). Dots show the location of retrogradely labeled cells, and grey shading on the midbrain sections approximates the distribution of the dopaminergic areas of the ventral tegmentum (catecholaminergic group A10). See Results for details. For abbreviations, see list. Scale bars for injection sites in A-B, 400 μm; all other scale bars, 1mm.

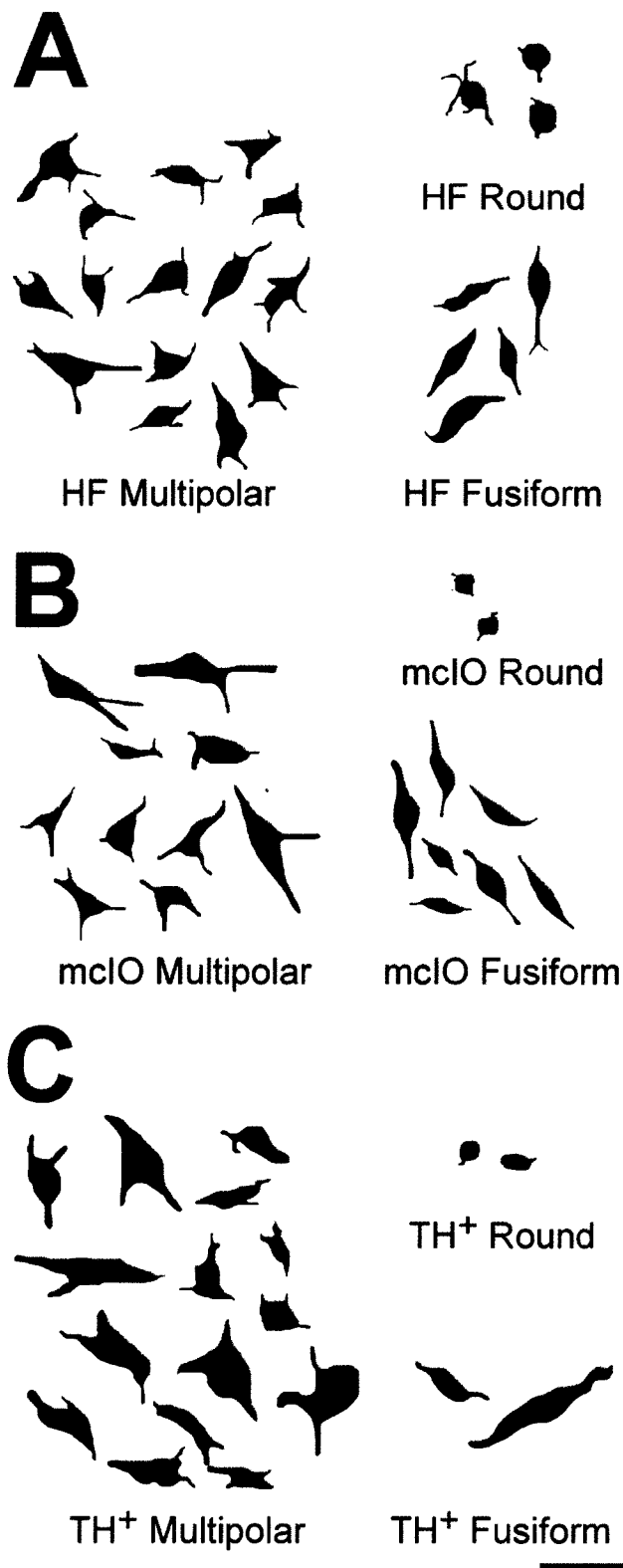


Figure 2.4: Representative silhouettes of neurons in the ventral tegmental area (VTA). In A, examples of multipolar, fusiform, and round neurons retrogradely labeled by

Figure 2.4 continued:            injections in the hippocampal formation (HF) are illustrated, while retrogradely labeled cells from injections in the medial column of the inferior olive (mcIO) are illustrated in B. C shows tracings of TH-immunoreactive neurons in the VTA. Scale bar, 50  $\mu\text{m}$ .

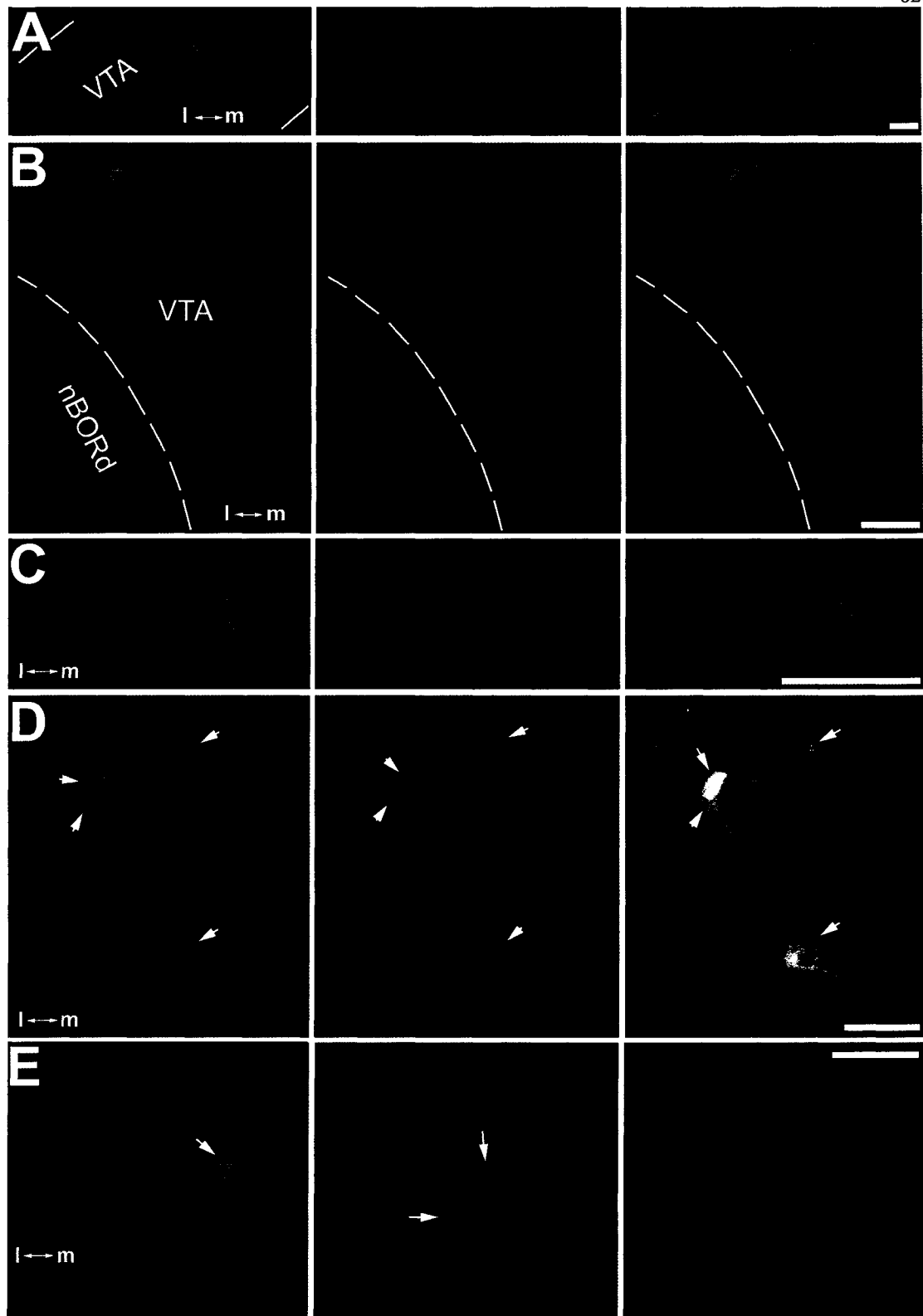


Figure 2.5: Digital images showing fluorescent-labeled neurons in the ventral tegmental area (VTA). The left column shows labeled cell bodies under the FITC

Figure 2.5 continued: filter, the middle panel shows labeled cells under the rhodamine (A-C) or Texas Red (D,E) filter, and the right panel is an overlay of the FITC and Texas Red/rhodamine images. For all panels, left is lateral and dorsal is toward the top of the page. Retrogradely labeled neurons shown in 5A-C were labeled from injections of red Lumafluor latex microspheres in the medial column of the inferior olive (mcIO) and green microspheres in the hippocampal formation (HF). A shows retrogradely labeled neurons from injections in the mcIO and HF intermingled in the VTA just medial to the nucleus of the basal optic root (nBOR). B shows retrograde the green cells from an injection in the HF bordering the nBOR pars dorsalis (nBORd), and a pair of red neurons from an injection in the ipsilateral mcIO within the borders of the nBORd. In C, a green neuron from a HF injection is juxtaposed a red neuron from an mcIO injection in a more rostral and dorsal section of the VTA. In D, the left panel shows 4 retrogradely labeled cells (white arrows) in the VTA from an injection in the HF. Two of these neurons are overlapping. The middle panel shows TH-immunoreactive cells (labeled with a Texas Red- conjugated secondary antibody) in the same section, and the right panel shows an overlay, revealing that all 4 cells are double-labeled neurons. The left panel of E shows a retrogradely labeled neuron in the VTA from an injection in the mcIO, the middle panel shows the TH-immunoreactivity in the same section, and the right panel shows the overlay. The neuron was not double-labeled, but was found immediately adjacent to TH-positive neurons (white arrows) in the heart of the VTA. l, lateral; m, medial. Scale bars, 50  $\mu$ m.

		Length $\pm$ s.e.m.	Width $\pm$ s.e.m.	%
HF	Fusiform	20.83 $\pm$ 0.45	8.71 $\pm$ 0.23	39.5
	Multipolar	17.78 $\pm$ 0.41	9.36 $\pm$ 0.20	51.6
	Round	12.59 $\pm$ 0.73	10.24 $\pm$ 0.61	8.9
IO	Fusiform	21.10 $\pm$ 0.75	8.00 $\pm$ 0.25	39.6
	Multipolar	17.94 $\pm$ 0.61	8.76 $\pm$ 0.26	50.5
	Round	11.37 $\pm$ 0.60	8.96 $\pm$ 0.58	9.9
TH +ve	Fusiform	26.08 $\pm$ 3.48	9.34 $\pm$ 0.51	27.1
	Multipolar	23.46 $\pm$ 1.16	12.34 $\pm$ 0.67	64.6
	Round	13.20 $\pm$ 1.09	10.63 $\pm$ 0.64	8.3

Table 1: Morphological Assessment of Neurons in VTA Projecting to the Hippocampal Formation (HF) and the Medial Column of the Inferior Olive (mcIO). All length and width measurements are given in  $\mu\text{m}$ . s.e.m., standard error to the mean.

## References

- Arends JJA, Voogd J (1989) Topographic aspects of the olivocerebellar system in the pigeon. *Exp Brain Res [Suppl]* 17: 52-57.
- Atoji Y, Wild JM, Yamamoto Y, Suzuki Y (2002) Intratelencephalic connections of the hippocampus in pigeons (*Columba livia*). *J Comp Neurol* 447:177-199.
- Atoji Y, Wild JM (2004) Fiber connections of the hippocampal formation and septum and subdivisions of the hippocampal formation in the pigeon as revealed by tract tracing and kainic acid lesions. *J Comp Neurol* 475:426-461.
- Bailhache T, Balthazart J (1993) The catecholaminergic system of the quail brain: immunocytochemical studies of dopamine beta-hydroxylase and tyrosine hydroxylase. *J Comp Neurol* 329:230-256.
- Bingman VP, Ioale P, Casini G, Bagnoli P (1990) The avian hippocampus: evidence for a role in the development of the homing pigeon navigational map. *Behav Neurosci* 104:906-11.
- Bingman VP, Yates G (1992) Hippocampal lesions impair navigational learning in experienced homing pigeons. *Behav Neurosci* 106:229-232.
- Brecha N, Karten HJ, Hunt SP (1980) Projections of the nucleus of the basal optic root in the pigeon: an autoradiographic and horseradish peroxidase study. *J Comp Neurol* 189:615-670.
- Britto LGR, Natal CL, Marcondes AM (1981) The accessory optic system in pigeons: receptive field properties of identified neurons. *Brain Res* 206:149-154.

- Burns S, Wallman J (1981) Relation of single unit properties to the oculomotor function of the nucleus of the basal optic root (AOS) in chickens. *Exp Brain Res* 42: 171-180.
- Casini G, Bingman VP, Bagnoli P (1986) Connections of the pigeon dorsomedial forebrain studied with WGA-HRP and 3H-proline. *J Comp Neurol* 245:454-470.
- Clarke PG (1977) Some visual and other connections to the cerebellum of the pigeon. *J Comp Neurol*. 174:535-552.
- Colombo M, Broadbent N (2000) Is the avian hippocampus a functional homologue of the mammalian hippocampus? *Neurosci Biobehav Rev* 24:465-484.
- Colombo M, Cawley S, Broadbent N (1997) The effects of hippocampal and area parahippocampalis lesions in pigeons: II. Concurrent discrimination and spatial memory. *Q J Exp Psychol B* 50:172-189.
- Conde F, Maire-Lepoivre E, Audinat E, Crepel F (1995) Afferent connections of the medial frontal cortex of the rat. II. Cortical and subcortical afferents. *J Comp Neurol* 352:567-593.
- Crowder NA, Winship IR, and Wylie DRW (2000) Topographic organization of inferior olive cells projecting to translational zones in the vestibulocerebellum of pigeons. *J Comp Neurol* 419:87-95.
- Dube L, Parent A (1981) The monoamine-containing neurons in avian brain: I. A study of the brain stem of the chicken (*Gallus domesticus*) by means of fluorescence and acetylcholinesterase histochemistry. *J Comp Neurol* 196:695-708.

- Durstewitz D, Kroner S, Gunturkun O (1999) The dopaminergic innervation of the avian telencephalon. *Prog Neurobiol* 59:161-195.
- Erichsen JT, Bingman VP, Krebs JR (1991) The distribution of neuropeptides in the dorsomedial telencephalon of the pigeon (*Columba livia*): a basis for regional subdivisions. *J Comp Neurol* 314:478-492.
- Fallon JH, Schmued LC, Wang C, Miller R, Banales G (1984) Neurons in the ventral tegmentum have separate populations projecting to telencephalon and inferior olive, are histochemically different, and may receive direct visual input. *Brain Res* 321:332-336.
- Fite KV, Brecha N, Karten HJ, Hunt SP (1981) Displaced ganglion cells and the accessory optic system of the pigeon. *J Comp Neurol* 195: 279-288.
- Foster TC, Castro CA, McNaughton BL (1989) Spatial selectivity of rat hippocampal neurons: dependence on preparedness for movement. *Science* 244:1580-1582.
- Fremouw T, Jackson-Smith P, Kesner RP (1997) Impaired place learning and unimpaired cue learning in hippocampal-lesioned pigeons. *Behav Neurosci* 111:963-975.
- Fuxe K, Ljunggren L (1965) Cellular localization of monoamines in the upper brain stem of the pigeon. *J Comp Neurol* 125:355-381.
- Gagliardo A, Odetti F, Ioale P, Bingman VP, Tuttle S, Vallortigara G (2002) Bilateral participation of the hippocampus in familiar landmark navigation by homing pigeons. *Behav Brain Res* 136:201-209.

- Gamlin PDR, Cohen DH (1988a) The retinal projections to the pretectum in the pigeon (*Columba livia*). *J Comp Neurol* 269:1-17.
- Gamlin PDR, Cohen DH (1988b) Projections of the retinorecipient pretectal nuclei in the pigeon (*Columba livia*), *J Comp Neurol* 269:18-46.
- Gasbarri A, Campana E, Pacitti C, Hajdu F, Tombol T (1991) Organization of the projections from the ventral tegmental area of Tsai to the hippocampal formation in the rat. *J Hirnforsch.* 32:429-437.
- Gasbarri A, Packard MG, Campana E, Pacitti C (1994a) Anterograde and retrograde tracing of projections from the ventral tegmental area to the hippocampal formation in the rat. *Brain Res Bull.* 33:445-452.
- Gasbarri A, Sulli A, Innocenzi R, Pacitti C, Brioni JD (1996) Spatial memory impairment induced by lesion of the mesohippocampal dopaminergic system in the rat. *Neuroscience.* 74:1037-1044.
- Gasbarri A, Sulli A, Packard MG (1997) The dopaminergic mesencephalic projections to the hippocampal formation in the rat. *Prog Neuropsychopharmacol Biol Psychiatry.* 21:1-22.
- Gasbarri A, Verney C, Innocenzi R, Campana E, Pacitti C (1994b) Mesolimbic dopaminergic neurons innervating the hippocampal formation in the rat: a combined retrograde tracing and immunohistochemical study. *Brain Res* 668:71-79.
- Gibson JJ (1954) The visual perception of objective motion and subjective movement. *Psychol. Rev* 61: 304-314.

- Gibson JJ. (1966) The problem of temporal order in stimulation and perception. *J Psychol* 62:141-149.
- Gioanni H, Rey J, Villalobos J, Richard D, Dalbera A (1983a) Optokinetic nystagmus in the pigeon (*Columba livia*). II. Role of the pretectal nucleus of the accessory optic system. *Exp Brain Res* 50: 237-247.
- Gioanni H, Villalobos J, Rey J, Dalbera A (1983b) Optokinetic nystagmus in the pigeon (*Columba livia*). III. Role of the nucleus ectomammilaris (nEM): interactions in the accessory optic system. *Exp Brain Res* 50: 248-258.
- Giolli, RA, Blanks RHI, Torigoe Y, Williams DD (1985) Projections of the medial terminal accessory optic nucleus, ventral tegmental nuclei, and substantia nigra of rabbit and rat as studied by retrograde axonal transport of horseradish peroxidase. *J Comp Neurol* 232:99-116.
- Grasse KL, Cyander MS (1990) The accessory optic system in frontal-eyed animals. In: *Vision and Visual Dysfunction. The Neuronal Basis of Visual Function* (Leventhal A, ed), p. 111-139. New York: McMillan.
- Horel JA (1988) Limbic neocortical interrelations. In: *Neurosciences (vol. 4): Comparative Primate Biology* (Steklis HD, Erwin J, eds), pp. 81-97. New York, NY: Wiley-Liss.
- Ikeda H, Gotoh J. 1971. Distribution of monoamine-containing cells in the central nervous system of the chicken. *Jpn J Pharmacol* 21:763-784.
- Kahn MC, Hough GE 2nd, Ten Eyck GR, Bingman VP (2003) Internal connectivity of the homing pigeon (*Columba livia*) hippocampal formation: an anterograde and retrograde tracer study. *J Comp Neurol* 459:127-141.

- Källén BI (1962) Embryogenesis of brain nuclei in the chick telencephalon. *Ergeb Anat Entwicklungsgesch.* 36:62-82.
- Karten HJ, Hodos W (1967) *A stereotaxic Atlas of the Brain of the Pigeon (Columba livia)*. Baltimore: Johns Hopkins Press.
- Karten HJ, Fite KV, Brecha N (1977) Specific projection of displaced retinal ganglion cells upon the accessory optic system in the pigeon (*Columba livia*). *Proc Natl Acad Sci*, 74: 1752-1756.
- Kelly PH, Iversen SD (1976) Selective 6OHDA-induced destruction of mesolimbic dopamine neurons: abolition of psychostimulant-induced locomotor activity in rats. *Eur J Pharmacol* 40:45-56.
- Kiss JZ, Peczely P (1987) Distribution of tyrosine-hydroxylase (TH)-immunoreactive neurons in the diencephalon of the pigeon (*Columba livia domestica*). *J Comp Neurol* 257:333-346.
- Koob GF, Stinus L, Le Moal M (1981) Hyperactivity and hypoactivity produced by lesions to the mesolimbic dopamine system. *Behav Brain Res* 3:341-359.
- Krebs JR, Erichsen JT, Bingman VP (1991) The distribution of neurotransmitters and neurotransmitter-related enzymes in the dorsomedial telencephalon of the pigeon (*Columba livia*). *J Comp Neurol.* 314:467-477.
- Lau KL, Glover RG, Linkenhoker B, Wylie DR (1998) Topographical organization of inferior olive cells projecting to translation and rotation zones in the vestibulocerebellum of pigeons. *Neuroscience* 85:605-614.

- Lindvall O, Björklund A (1983) Dopamine and norepinephrine containing neuron systems: Their anatomy in the rat brain. In: Chemical Neuroanatomy (Emison PC, ed), pp. 229-255. New York: Raven Press.
- Macphail EM (2002) The role of avian hippocampus in spatial memory. *Psicologica* 23:93-108.
- McKenna OC, Wallman J (1981) Identification of avian brain regions responsive to retinal slip using 2-deoxyglucose. *Brain Res.* 210:455-460.
- McKenna OC, Wallman J (1985) Accessory optic system and pretectum of birds: comparisons with those of other vertebrates. *Brain Behav Evol* 26:91-116.
- McNaughton BL, Knierim JJ, Wilson MA (1995) Vector encoding and the vestibular foundations of spatial cognition: neurophysiological and computational mechanisms. In: *The Cognitive Neurosciences* (Gazzaniga MS, ed), pp. 585-595. Cambridge, MA: MIT.
- McNaughton BL, Barnes CA, Gerrard JL, Gothard K, Jung MW, Knierim JJ, Kudrimoti H, Qin Y, Skaggs WE, Suster M, Weaver KL (1996) Deciphering the hippocampal polyglot: the hippocampus as a path integration system. *J Exp Biol* 199:173-185.
- Montagnese CM, Krebs JR, Meyer G (1996) The dorsomedial and dorsolateral forebrain of the zebra finch, *Taeniopygia guttata*: a Golgi study. *Cell Tissue Res* 283:263-282.
- Moons L, van Gils J, Ghijssels E, Vandesande F (1994) Immunocytochemical localization of L-dopa and dopamine in the brain of the chicken (*Gallus domesticus*). *J Comp Neurol.* 346:97-118.

- Morgan B, Frost BJ (1981) Visual response characteristics of neurons in nucleus of basal optic root of pigeons. *Exp Brain Res* 42:181-188.
- Oades RD, Halliday GM (1987) Ventral tegmental (A10) system: 1. Anatomy and connectivity. *Brain Res* 434: 117-165.
- Packard MG, White NM (1991) Dissociation of hippocampus and caudate nucleus memory systems by posttraining intracerebral injection of dopamine agonists. *Behav Neurosci* 105:295-306.
- Pakan JM, Todd KG, Nguyen AP, Winship IR, Hurd PL, Jantzie LL, Wylie DR. 2005. Inferior olivary neurons innervate multiple zones of the flocculus in pigeons (*Columba livia*). *J Comp Neurol* 486:159-68.
- Redies C, Medina L, Puelles L. Cadherin expression by embryonic divisions and derived gray matter structures in the telencephalon of the chicken. *J Comp Neurol*. 438:253-85.
- Reiner A, Perkel DJ, Bruce LL, Butler AB, Csillag A, Kuenzel W, Medina L, Paxinos G, Shimizu T, Striedter G, Wild M, Ball GF, Durand S, Gunturkun O, Lee DW, Mello CV, Powers A, White SA, Hough G, Kubikova L, Smulders TV, Wada K, Dugas-Ford J, Husband S, Yamamoto K, Yu J, Siang C, Jarvis ED; Avian Brain Nomenclature Forum (2004) Revised nomenclature for avian telencephalon and some related brainstem nuclei. *J Comp Neurol*. 473:377-414. Erratum in: *J Comp Neurol* 475:288.
- Reiner A, Brecha N, Karten HJ (1979) A specific projection of retinal displaced ganglion cells to the nucleus of the basal optic root in the chicken. *Neuroscience* 4:1679-1688.

- Sherry DF, Jacobs LF, Gaulin SJ (1992) Spatial memory and adaptive specialization of the hippocampus. *Trends Neurosci.* 15:298-303.
- Simpson JI (1984) The accessory optic system. *Annu Rev Neurosci* 7:13-41.
- Simpson JI, Leonard CS, Soodak RE (1988a) The accessory optic system of rabbit. II. Spatial organization of direction selectivity. *J Neurophysiol.* 60:2055-2072.
- Simpson JI, Leonard CS, Soodak RE (1988b) The accessory optic system. Analyzer of self-motion. *Ann N Y Acad Sci* 545:170-79.
- Smialowski A (1976) The effect of intrahippocampal administration of dopamine or apomorphine on EEG of limbic structures in the rabbit brain. *Pol J Pharmacol Pharm* 28:579-85.
- Szekely AD, Krebs JR (1996) Efferent connectivity of the hippocampal formation of the zebra finch (*Taenopygia guttata*): an anterograde pathway tracing study using *Phaseolus vulgaris* leucoagglutinin. *J Comp Neurol* 368:198-214.
- Siegel JJ, Nitz D, Bingman VP (2000) Hippocampal theta rhythm in awake, freely moving homing pigeons. *Hippocampus.* 10:627-631.
- Siegel JJ, Nitz D, Bingman VP (2005) Spatial-specificity of single-units in the hippocampal formation of freely moving homing pigeons. *Hippocampus.* 15:26-40.
- Takada M, Hattori T (1987) Organization of ventral tegmental area cells projecting to the occipital cortex and forebrain in the rat. *Brain Res* 418:27-33.
- Terrazas A, Krause M, Lipa P, Gothard KM, Barnes CA, McNaughton BL (2005) Self-motion and the hippocampal spatial metric. *J Neurosci.* 25: 8085-8096.

- Tömböl T, Davies DC, Nemeth A, Alpar A, Sebesteny T (2000a) A golgi and a combined Golgi/GABA immunogold study of local circuit neurons in the homing pigeon hippocampus. *Anat Embryol (Berl)*. 201:181-196.
- Tömböl T, Davies DC, Nemeth A, Sebesteny T, Alpar A (2000b) A comparative Golgi study of chicken (*Gallus domesticus*) and homing pigeon (*Columba livia*) hippocampus. *Anat Embryol (Berl)* 201:85-101.
- Veenman CL, Reiner A, Honig MG (1992) Biotinylated dextran amine as an anterograde tracer for single- and double-labeling studies. *J Neurosci Methods*. 41:239-254.
- Waespe W, Henn V (1987) Gaze stabilization in the primate. The interaction of the vestibulo-ocular reflex, optokinetic nystagmus, and smooth pursuit. *Rev Physiol Biochem Pharmacol*. 106:37-125.
- Waldmann C, Güntürkün O (1993) The dopaminergic innervation of the pigeon caudolateral forebrain: immunocytochemical evidence for a 'prefrontal cortex' in birds? *Brain Res* 600:225-234.
- Wild JM (1993) Descending projections of the songbird nucleus robustus archistrialis. *J Comp Neurol* 338:225-241.
- Winship IR, Hurd PL, Wylie DRW (2005) Spatiotemporal tuning of optic flow inputs to the vestibulocerebellum in pigeons: differences between mossy and climbing fiber pathways. *J Neurophysiol* 93:1266-1277.

- Winship IR, Wylie DR (2001) Responses of neurons in the medial column of the inferior olive in pigeons to translational and rotational optic flowfields. *Exp Brain Res* 141:63-78.
- Winship IR, Wylie DR (2003) Zonal organization of the vestibulocerebellum in pigeons (*Columba livia*): I. Climbing fiber input to the flocculus. *J Comp Neurol*. 456:127-139.
- Winterson BJ, Brauth SE (1985) Direction-selective single units in the nucleus lentiformis mesencephali of the pigeon (*Columba livia*). *Exp Brain Res* 60:215-226.
- Wise RA (2004) Dopamine, learning and motivation. *Nat Rev Neurosci* 5:1–12.
- Wolf-Oberhollenzer F, Kirschfeld K (1994) Motion sensitivity in the nucleus of the basal optic root of the pigeon. *J Neurophysiol*. 71:1559-1573.
- Wylie DR (2000) Binocular neurons in the nucleus lentiformis mesencephali in pigeons: responses to translational and rotational optic flowfields. *Neurosci Lett* 291:9-12.
- Wylie DRW (2001) Projections from the nucleus of the basal optic root and nucleus lentiformis mesencephali to the inferior olive in pigeons (*Columba livia*). *J Comp Neurol* 429:502-513.
- Wylie DR, Brown MR, Barkley RR, Winship IR, Crowder NA, Todd KG (2003a) Zonal organization of the vestibulocerebellum in pigeons (*Columba livia*): II. Projections of the rotation zones of the flocculus. *J Comp Neurol* 456:140-153.
- Wylie DR, Brown MR, Winship IR, Crowder NA, Todd KG (2003b) Zonal organization of the vestibulocerebellum in pigeons (*Columba livia*): III. Projections of the translation zones of the ventral uvula and nodulus. *J Comp Neurol* 465:179-194.

- Wylie DR, Frost BJ (1990a) Binocular neurons in the nucleus of the basal optic root (nBOR) of the pigeon are selective for either translational or rotational visual flow. *Vis Neurosci* 5:489-495.
- Wylie DR, Frost BJ (1990b) The visual response properties of neurons in the nucleus of the basal optic root of the pigeon: a quantitative analysis. *Exp Brain Res* 82:327-336.
- Wylie DR, Frost BJ (1991) Purkinje cells in the vestibulocerebellum of the pigeon respond best to either translational or rotational wholefield visual motion. *Exp Brain Res* 86:229-232.
- Wylie DR, Frost BJ (1993) Responses of pigeon vestibulocerebellar neurons to optokinetic stimulation. II. The 3-dimensional reference frame of rotation neurons in the flocculus. *J Neurophysiol* 70:2647-2659.
- Wylie DR, Frost BJ (1999) Responses of neurons in the nucleus of the basal optic root to translational and rotational flowfields. *J Neurophysiol* 81:267-276.
- Wylie DR, Glover RG, Aitchison JD (1999a) Optic flow input to the hippocampal formation from the accessory optic system. *J Neurosci* 19:5514-5527.
- Wylie DR, Linkenhoker B, Lau KL (1997) Projections of the nucleus of the basal optic root in pigeons (*Columba livia*) revealed with biotinylated dextran amine. *J Comp Neurol* 384:517-536.
- Wylie DR, Ogilvie CJ, Crowder NA, Barkley RR, Winship IR (2005) Telencephalic projections to the nucleus of the basal optic root and pretectal nucleus lentiformis mesencephali in pigeons. *Vis Neurosci* 22:237-47.

Wylie DRW, Winship IR, Glover RG (1999b) Projections from the medial column of the inferior olive to different classes of rotation-sensitive Purkinje cells in the flocculus of pigeons. *Neurosci Lett* 268: 97-100.

Wynne B, Güntürkün O (1995) Dopaminergic innervation of the telencephalon of the pigeon (*Columba livia*): a study with antibodies against tyrosine hydroxylase and dopamine. *J Comp Neurol* 357:446-64.

**CHAPTER 3:**  
**RESPONSES OF NEURONS IN THE MEDIAL COLUMN OF THE**  
**INFERIOR OLIVE IN PIGEONS TO TRANSLATIONAL AND**  
**ROTATIONAL OPTIC FLOWFIELDS**

**Full Citation:**

**Winship IR, & Wylie DRW.** Responses of neurons in the medial column of the inferior olive in pigeons to translational and rotational optic flowfields. *Experimental Brain Research*, 141: 63-78, 2001.

Self-motion of an organism through the environment containing numerous stationary objects and surfaces induces distinctive patterns of visual motion, termed optic flow or “flowfields”, across its entire retina (Gibson 1954). Thus, optic flow provides visual proprioceptive information, which, in conjunction with information from other sensory systems including the vestibular and somatosensory systems, is important for the control of posture and self-motion.

Previous research has shown that the complex spike activity (CSA) of Purkinje cells in the vestibulocerebellum (VbC) of pigeons is modulated in response to particular patterns of optic flow (Wylie and Frost 1991, 1993, 1999a; Wylie et al. 1993, 1998). Neurons in the lateral VbC (flocculus) respond best to rotational flowfields (see Fig. 3.1B), whereas neurons in the medial VbC (ventral uvula and nodulus) respond to translational flowfields (see Fig. 3.1C; Wylie et al. 1993). It was originally shown in rabbits by Simpson, Graf and colleagues (Simpson et al. 1981, 1988a,b; Graf et al. 1988; Leonard et al. 1988) that the flocculus neurons respond best to rotational optic flow about either the vertical axis or an horizontal axis oriented at 135° ipsilateral/ 45° contralateral azimuth (*rVA* and *rHI35i* neurons, respectively). This was confirmed in pigeons (Wylie and Frost 1993). Simpson and colleagues emphasized that the reference frame of the floccular neurons responsive to rotational optic flow, i.e. the vertical axis and horizontal axes 45° to the midline, is common to the vestibular canals and eye muscles (Ezure and Graf 1984; Graf et al. 1988; Leonard et al. 1988; Simpson and Graf 1981, 1985; Graf and Simpson 1981; Simpson et al. 1988a,b, 1989a,b; van der Steen et al. 1994; see also Wylie and Frost 1996).

CSA responsive to translational optic flow has only been found in the ventral uvula and nodulus of pigeons (Wylie et al. 1993, 1998; Wylie and Frost 1991, 1999a). With respect to the preferred axes of translational optic flow, there are four response types. The orientation of the best axis of translational optic flow for each of the four types is described using the reference frame depicted in Figure 3.1A.  $x$ ,  $y$  and  $z$  represent the interaural, vertical and naso-occipital axes, respectively. With respect to direction,  $+x$ ,  $+y$  and  $+z$  represent rightward, upward and forward self-translation, respectively. Neurons respond best to optic flow patterns resulting from either upward or downward self-translation along the vertical axis ( $t(+y)$  and  $t(-y)$  neurons) or self-translation along one of two horizontal axes oriented  $45^\circ$  to the midline ( $t(-x-z)$  and  $t(-x+z)$  neurons (assuming recording from the left VbC); Wylie et al. 1998; Wylie and Frost 1999a). Thus, this three axes reference frame, the vertical axis and horizontal axes  $45^\circ$  to the midline, is common to both the translational and rotational optic flow systems.

Previous anatomical research using retrograde transport from the pigeon VbC has shown that the different types of translation- and rotation-sensitive Purkinje cells receive climbing fibre (CF) input from discrete regions of the contralateral medial column (mc) of the inferior olive (IO; Wylie et al. 1999; Crowder et al. 2000). In this report we investigated the CS activity of neurons in the mc in response to translational and rotational optic flowfields.

## **Methods**

### *Surgery*

The methods reported herein conformed to the guidelines established by the Canadian Council on Animal Care and were approved by the Biosciences Animal Care and Policy Committee at the University of Alberta. Silver King or Homing pigeons were anaesthetized with a ketamine (65 mg/kg) - xylazine (8 mg/kg) mixture (i.m.) and supplemental doses were administered as necessary. The animals were placed in a stereotaxic device with pigeon ear bars and beak adapter such that the orientation of the skull conformed to the atlas of Karten and Hodos (1967). A section of bone and dura on the right side of the head starting near the midline and extending laterally was then removed to expose the cerebellum.

### *Extracellular Recordings and Optic Flow Stimulation*

After exposure of the cerebellum, birds were removed from the ear bars and beak adapter, and their heads were oriented such that their eye-beak angle was 34° (the normal orientation of the head; Erichsen et al. 1989). This involved rotating the beak upward about the inter-aural axis approximately 38° relative to the stereotaxic position of Karten and Hodos (1967). Extracellular recordings were then made with glass micropipettes filled with 2M NaCl (tip diameters of 3-5µm) or tungsten metal electrodes (Frederick Haer & Co.). To access the optic flow sensitive neurons in the mc, the electrode was oriented 10° to the sagittal plane and 38° to the frontal plane to compensate for adjustment of bird's eye-beak angle. Electrodes were advanced

through the nodulus and brainstem using an hydraulic microdrive (Frederick Haer & Co.). Extracellular signals were amplified, filtered and fed to a window discriminator, which produced TTL pulses, each representing a single spike time. TTL pulses were fed to a data analysis system (Cambridge Electronic Designs (CED) *1401plus*) and peri-stimulus time histograms (PSTHs) were constructed using *Spike2* software (CED).

IO cells were identified based on their characteristic firing rate of about 1 spike/sec. Once a cell was isolated, it was first stimulated with a large (about  $90^\circ \times 90^\circ$ ) handheld stimulus consisting of a random pattern of dots and lines to determine if the cell was sensitive to visual stimulation. Generally, by moving this stimulus in different areas of the panoramic binocular visual field, the preferred flowfield can be qualitatively determined. However, because these neurons are broadly tuned for the direction of motion, a computer-generated stimulus was used to confirm the flowfield preference. The procedure is illustrated in Figure 3.2. A screen measuring  $90^\circ \times 75^\circ$  (width  $\times$  height) was positioned in one of three locations relative to the bird's head: the frontal visual field (from  $45^\circ$  ipsilateral (i) to  $45^\circ$  contralateral (c) azimuth), the contralateral hemifield (from  $45^\circ$ c to  $135^\circ$ c azimuth), or the ipsilateral hemifield (from  $45^\circ$ i to  $135^\circ$ i azimuth; see Fig. 3.2A). Drifting sine wave gratings (in one of four orientations; illustrated in Fig. 3.2b) of an effective spatial and temporal frequency were then generated by a *VSGThree* (Cambridge Research Services) and back-projected (*InFocus* LP750) onto the screen. Direction tuning curves in each of the three areas of the visual field were obtained by moving the gratings in 8 different

directions (see Fig. 3.2b). Responses were averaged over at least 3 sweeps, where each sweep consisted of 5 seconds of motion in one direction, a 5 second pause, and 5 seconds of motion in the opposite direction, followed by a 5 second pause. Although this procedure did not elicit maximal modulation of the cell, it was quite useful for identifying the cell type for subsequent testing. (For example, translation-sensitive neurons prefer approximately the same direction of motion in both the ipsi- and contralateral hemifields, whereas rotation-neurons prefer the opposite directions of motion in the ipsi- and contralateral hemifields (e.g. Fig 3.2C-F)).

Rotation-sensitive cells were further studied using a *planetarium* projector (see Wylie and Frost 1993, 1999b). Modelled after that designed by Simpson and colleagues (Simpson et al. 1981), this device consisted of a small, hollow cylinder (3 X 7 cm (radius X height)) perforated with numerous small holes, and fixed around a small filament light source. Using a function generator and a pen motor, the cylinder was rotated such that a moving pattern of light dots was projected onto the floors, ceiling, and walls of the room. The resultant rotational flowfield covered the entire panoramic visual field except a circular area (about 60° diameter) at the base of the cylinder.

Translation-sensitive neurons were further studied with the *translator* projector (see Wylie and Frost 1999a). Similar to the planetarium projector, the translator consisted of a small, hollow metal sphere (diameter = 9 cm), the surface of which was drilled with numerous small holes. A small filament light source was moved along a path within the sphere (under computer control), such that a simulated

translational flowfield, (with a focus of expansion (FOE) at one “pole”, a focus of contraction (FOC) at the opposite pole, and laminar flow at the “equator” (see Fig. 3.1C)) was projected onto the walls, ceiling and floor of the room. As with the planetarium, this pattern essentially covered the entire binocular visual field.

For both devices, the dots subtended 1-2°. For the planetarium the dots rotated in the range of 1-2°/sec. For the translator, there is a gradient of velocity, with the dots at the poles moving slowest, and the dots along the equator moving the fastest. The “equatorial” dots moved at speeds in the range of 1-10 °/sec. By mounting the planetarium/translator in gimbals, the axis of the rotational/translational flowfield could be positioned to any orientation within three-dimensional space.

Average firing rates for each axis were determined from 5 to 15 sweeps. For the planetarium, each sweep consisted of 5 seconds of rotation in one direction, followed by 5 seconds of rotation in the opposite direction. For the translator, each sweep consisted of 5 seconds of motion in one direction along the axis of the translator, a 5 second pause, 5 seconds of translation in the opposite direction, and a 5 second pause.

Upon completion of physiological recording, in some cases electrolytic marking lesions were made (30 $\mu$ A for 10 seconds) at known locations relative to recording sites such that the topographical organization of the mc could be determined. These animals were administered an overdose of sodium pentobarbital and immediately perfused with 0.9% saline followed by 4% para-formaldehyde. The brains were extracted and cryoprotected with sucrose. Frozen sections (44  $\mu$ m thick) in the

coronal plane were collected and mounted onto gelatin coated slides. The sections were stained with Neutral Red and examined using light microscopy.

## Results

The activity of 49 neurons sensitive to optic flow stimuli was recorded from 20 pigeons. The average spontaneous firing was  $1.53 \pm 0.11$  spikes/s (mean  $\pm$  s.e.m.). These cells responded to large moving visual stimuli and preferred particular patterns of optic flow resulting from either self-translation or self-rotation. The identification of these cells was made relatively easy by examining the responses to drifting largefield sine wave gratings presented to either the frontal, contralateral and ipsilateral visual fields (see Fig. 3.2). Neurons responsive to rotational optic flow prefer approximately opposite directions of motion in the ipsi- and contralateral visual fields (e.g. Fig. 3.2B,C), whereas neurons responsive to translational optic flow prefer the same direction of motion in the ipsi- and contralateral visual fields. In response to the panoramic flowfield stimuli produced by the planetarium and translator projectors, neurons showed maximal excitation in response to rotational/translational optic flow about/along a particular axis ("best" or "preferred" axis) and maximal inhibition in response to optic flow in the opposite direction about/along the same axis. Little or no modulation occurred in response to optic flow along/about axes orthogonal to the best axis ("null" axes). A modulation index (MI) was calculated for each neuron by taking the ratio of the firing rates in response to the two directions of optic flow about/along the preferred axis (max/min). A neuron was deemed optic flow sensitive if the MI

was  $> 1.5$ . The average MI for the 49 neurons was 3.27 (range = 1.6 to 10.1). The “axis tuning” was quite broad, and the tuning curves in any particular plane approximated a cosine function. The peak of the best-fit cosine was used to assign the preferred axis for each tuning curve. It is assumed that all recordings were obtained from the mc on the right side of the brain. This facilitated comparison with previous reports of the pigeon VbC that presumed that all recordings were from the left VbC. (The projection from the IO to the VbC is exclusively contralateral).

#### Neurons Selective for Rotational Optic Flow

As expected from previous studies of the pigeon VbC (Wylie and Frost 1993), neurons selective for rotational optic flow could be classified into two types based on the orientation of the preferred axis: *rVA* neurons and *rHI35c* neurons.

##### *rVA neurons*

Recordings were made from 13 *rVA* neurons. The direction tuning curves for an *rVA* neuron to sine wave gratings drifting in the frontal, ipsi- and contralateral regions of the visual field are shown in Fig. 3.2C. In this figure, the firing rate (spikes/sec relative to the spontaneous rate (SR)) is plotted as a function of the direction of motion in polar coordinates (solid line). *rVA* neurons were excited in response to largefield stimuli moving forward (temporal-to-nasal; T-N) and backward (N-T) in the contra- and ipsilateral visual fields, respectively, and rightward motion in the frontal visual field (for neurons in the *right* IO). In the natural environment, this

type of visual stimulation would occur in response to a leftward rotation of the head about the vertical ( $y$ ) axis.

Figure 3.3 shows the responses of an  $rVA$  neuron to rotational optic flow (about several axes) produced by the planetarium projector. In Figure 3.3A an “elevation tuning curve” in the sagittal ( $yz$ ) plane is shown. The axis of the planetarium projector was placed in four orientations within the sagittal plane: the  $z$  (roll) axis, the  $y$  (yaw) axis and the two intermediate axes. The  $z$  and  $y$  axes are equivalent to  $0^\circ$  and  $90^\circ$  elevation, respectively, and the intermediate axes fall at  $+45^\circ$  and  $-45^\circ$  ( $+135^\circ$ ) elevation. The firing rate (spikes/sec) of the cell in response to rotational optic flow in both directions about each of four axes is plotted in polar coordinates. For this and subsequent figures concerned with responses to rotational optic flow (Figs. 3.4 and 3.5), a standard head-centric right-handed rule is used to represent the direction of optic flow. If the thumb of the right hand is aligned with the axis, the fingers indicate the direction of head rotation. The direction of the optic flow would be opposite to the direction of head rotation. For example, the response to the leftward/rightward head rotation about the vertical (yaw) axis is represented by the positive/negative direction along the  $y$  axis. Thus, the response to the rightward/leftward optic flow about the vertical (yaw) axis is represented by the positive/negative direction along the  $y$  axis. Likewise, in the positive direction along the  $z$  axis, the response to a clockwise (CW) roll of the head is represented. That, is the response to counter-clockwise (CCW) optic flow is plotted. Although redundant, semi-circular arrows on the figures explicitly illustrate the direction of head rotation

for each axis. In this and subsequent polar plots, the solid arrows represents the vector of maximal excitation ("best axis") determined from the phase of the best-fit cosine to the tuning curve. Figure 3.3B shows an elevation tuning curve in the frontal ( $xy$ ) plane. In both A and B, the data was obtained with both eyes open (binocular viewing conditions). In Figures 3.3C and D elevation tuning in the sagittal plane is shown for monocular stimulation of the ipsi- and contralateral eyes, respectively. For this *rVA* neurons, maximal excitation occurred in response to the optic flowfield resulting from leftward rotation of the head about the vertical axis, and optic flow about the vertical axis in the opposite direction resulted in maximal inhibition (Fig. 3.3A,B). In the sagittal plane (Fig. 3.3A), the best axis fell approximately along the vertical axis, and rotation about the z-axis resulted in no modulation. In the frontal plane (Fig. 3.3B) the best axis was about  $20^\circ$  from the vertical axis. With monocular stimulation, the best axes in the sagittal plane were approximately vertical for both ipsi- and contralateral stimulation. Clearly there was more modulation under binocular viewing conditions (Fig. 3.3A vs. 3.3C). Note that the depth of modulation was greater for stimulation of the ipsilateral eye compared to the contralateral eye. (Below, ocular dominance is discussed for all cell types.)

#### *rHI35c neurons*

Recordings were made from 13 *rHI35c* neurons in mc. The direction tuning curves for a *rHI35c* neuron to sine wave gratings drifting in the frontal, ipsi- and contralateral regions of the visual field are shown in Figure 3.2D. This neuron was

excited in response to largefield stimuli moving upward in the contralateral and frontal visual fields, and downward motion in the ipsilateral visual field. In the natural environment, this type of visual stimulation would occur in response to rotation of the head about an horizontal axis oriented at  $135^{\circ}$ c azimuth.

Figure 3.4 shows the responses of an *rHI35c* neuron to rotational optic flow produced by the planetarium projector. “Azimuth tuning curves” are shown in Fig. 3.4B,C and D for binocular, ipsilateral and contralateral viewing conditions, respectively. For azimuth tuning, the axis of the planetarium projector was placed in four orientations within the horizontal plane: the  $z$  (roll) axis, the  $x$  (pitch) axis and the two intermediate axes. The  $z$  and  $x$  axes are equivalent to  $0^{\circ}$  and  $90^{\circ}$ i azimuth respectively ( $-x = 90^{\circ}$ c azimuth). The intermediate axes fall at  $45^{\circ}$ i and  $45^{\circ}$ c azimuth. In Figure 3.4A an elevation tuning curve in a vertical plane that intersects the horizontal plane at  $45^{\circ}$ i azimuth is shown (binocular viewing). For this tuning curve, the axis of the planetarium projector was placed in four orientations within this plane: an horizontal axis at  $45^{\circ}$ i azimuth ( $0^{\circ}$  elevation), the  $y$  (yaw) axis ( $90^{\circ}$  elevation), and two intermediate axes ( $45^{\circ}$ i azimuth/ $+45^{\circ}$  elevation and  $45^{\circ}$ i azimuth/ $-45^{\circ}$  elevation). For *rHI35c* neurons, maximal modulation occurred in response to rotational optic flow about an horizontal axis oriented at  $135^{\circ}$ c azimuth (Fig. 3.4A,B). (From the bird’s point of view, maximal excitation occurred in response to CCW rotational optic flow about this axis, and maximal inhibition occurred in response to CW optic flow). Little modulation occurred in response to rotation about orthogonal axes: the vertical axis (Fig. 3.4A) and the horizontal axis through  $45^{\circ}$ c azimuth (Fig 3.4B). The best

axis for azimuth tuning was similar for stimulation of the ipsi- and contralateral eyes, but clearly there was a marked contralateral dominance.

#### *Mean Best Axes of Rotation-Sensitive Neurons in IO and VbC*

Under binocular viewing conditions, elevation tuning curves in the sagittal plane were obtained for 9 *rVA* neurons in mc and the best axes are shown in Figure 3.5A. The mean of this distribution, indicated by the larger broken arrow, was 78.3° elevation. In Figure 3.5B, the distribution of the best axes of *rVA* neurons in the pigeon VbC are shown (from Wylie and Frost 1993). The mean of this distribution was 89.0°. These two distributions were significantly different (t-test;  $p < 0.05$ ).

Azimuth tuning curves were obtained for 10 *rHI35c* neurons in mc under binocular viewing conditions and the best axes are shown in Fig. 3.5C. The mean of this distribution, indicated by the larger broken arrow, was 136.2° azimuth. In Fig. 3.5D, the distribution of the best axes of *rHI35i* neurons in the pigeon VbC are shown (mean = 135.7° azimuth; from Wylie and Frost 1993; note that this is ipsilateral for IO neurons, contralateral for VbC neurons).

#### Neurons Selective for Translational Optic Flow

As expected from previous studies of the pigeon VbC (Wylie et al. 1998; Wylie and Frost 1999a), neurons selective for translational optic flow could be classified into four types based on the orientation of the preferred axis:  $t(+y)$ ,  $t(-y)$ ,  $t(-x-z)$  and  $t(-x+z)$  neurons.

$t(+y)$  neurons.

Recordings were made from 8  $t(+y)$  neurons. In response to the drifting gratings, these neurons responded best to downward motion in the ipsi-, contralateral and frontal areas of the visual field, although for the neuron shown in Fig. 3.2E, there was little modulation in response to gratings in the contralateral hemifield. Figure 3.6 shows the responses of a  $t(+y)$  neuron to translational optic flow (produced by the translator projector) along several axes. In this figure, and subsequent figures concerning translational optic flow (Figs. 3.7,3.8,3.9), the dashed arrows along each axis represent the direction of self-motion the animal would make to cause the simulated flowfield. That is, the arrows point toward the FOE in the flowfield. For example, an arrow pointing upward along the y-axis represents the flowfield resulting from upward self-motion: a FOE above the bird's head and downward optic flow throughout most of the visual field. Elevation tuning curves in the sagittal plane (Fig. 3.6A) and frontal planes (Fig. 3.6B) under binocular viewing conditions are shown. The maximal depth of modulation occurred in response to translational optic flow along the y axis. Maximal excitation occurred in response to the optic flow that results from upward self-translation (+y); i.e. downward optic flow. Elevation tuning curves in the sagittal plane are also shown for monocular stimulation of the ipsi- and contralateral eyes (Figs. 3.6A,B). Note that there was a greater depth of modulation in response to the stimulation of the contralateral eye.

*t(-y) neurons*

Only 3 *t(-y)* neurons were encountered. In response to drifting largefield gratings, these neurons preferred upward motion in the ipsilateral, contralateral and frontal regions of the visual field (not shown). In response to panoramic flowfields produced by the translator, these neurons showed the opposite direction preference compared to the *t(+y)* neurons. Elevation tuning curves in the sagittal and frontal planes are shown for a *t(-y)* neuron in Figure 3.7A,B (binocular viewing).

*t(-x+z) neurons*

Recordings were made from 5 *t(-x+z)* neurons. In response to the drifting largefield gratings, these neurons responded best to backward (N-T) motion in the ipsilateral and contralateral hemifields, and rightward motion in the frontal area of the visual field (not shown). Figure 3.7D shows an azimuth tuning curve for a *t(-x+z)* neuron to translational optic flow under binocular viewing conditions. The best axis in this plane was at 52° azimuth. In Fig. 3.7C, an elevation tuning curve in a vertical plane that intersects the horizontal plane through 45° azimuth is shown for the same neuron. The best axis in this plane was located at +16° elevation in this plane. That is, maximal excitation occurred in response to optic flow with a FOE at about 52° azimuth / +16° elevation.

*t(-x-z) neurons*

Recordings were made from 7  $t(-x-z)$  neurons. In response to the drifting largefield gratings, these neurons responded best to forward (T-N) motion in the ipsilateral and contralateral hemifields, and rightward motion in the frontal area of the visual field. This is shown in Fig. 3.2F, although this particular neuron showed very little modulation to stimulation of the contralateral hemi-field. Figure 3.8A shows an azimuth tuning curve for a  $t(-x-z)$  neuron to translational optic flow under binocular viewing conditions. The best axis in this plane was at  $121^{\circ}$  azimuth. In Fig. 3.8B, an elevation tuning curve in a vertical plane that intersects the horizontal plane through  $45^{\circ}$  azimuth is shown for the same neuron. There was a clear elevational component to the best axis for this neuron ( $+40^{\circ}$  elevation). That is, maximal excitation occurred in response to optic flow with a FOC at about  $59^{\circ}$  azimuth /  $-40^{\circ}$  elevation. Figures 3.8C,D show azimuth tuning curves for the neuron under monocular viewing conditions. This neuron showed substantial modulation to stimulation of both the ipsilateral and contralateral eyes, but there was a disparity with respect to the best axes.

*Mean Best Axes of Translation-Sensitive Neurons in IO and VbC*

For 7  $t(+y)$  neurons the best axes determined from elevation tuning in the sagittal plane are shown in Figure 3.9A (mean =  $87.6^{\circ}$  elevation). In Fig. 3.9B the best axes of  $t(+y)$  neurons from the pigeon VbC are also shown ( $91.1^{\circ}$  elevation; from Wylie and Frost 1999a). Also in Fig. 3.9A, the best axes for the 3  $t(-y)$  neurons are

shown (mean =  $-89.5^\circ$  elevation), and in Fig. 3.9B the best axes of  $t(-y)$  neurons in the pigeon VbC are shown (mean =  $-85.5^\circ$  elevation; from Wylie and Frost 1999a).

The best axes determined from azimuth tuning curves for the 5  $t(-x+z)$  neurons in the mc, and Purkinje cells in the VbC (from Wylie and Frost 1999a) are shown in Figs. 3.9C and D, respectively. The means of the distributions for  $t(-x+z)$  neurons in the mc and VbC were  $52.6^\circ$  and  $39.7^\circ$  azimuth, respectively, but the distributions were not significantly different (Mann-Whitney  $U$  test). In Fig. 3.9E and F, the best axes from elevation tuning curves are shown for  $t(-x+z)$  neurons in the mc and VbC (from Wylie and Frost 1999a). For all neurons the best axis was located above the horizontal plane. The means for the mc and VbC distributions were  $+23.6^\circ$  and  $+29.6^\circ$  elevation, respectively.

The best axes determined from azimuth tuning curves for the 7  $t(-x-z)$  neurons in the mc, and Purkinje cells in the VbC (from Wylie and Frost 1999a) are shown in Figs. 3.9C and D, respectively. The means of the distributions for  $t(-x-z)$  neurons in the mc and VbC were  $120.8^\circ$  and  $133.1^\circ$  azimuth, respectively. These distributions were significantly different ( $p < 0.002$ ; Mann-Whitney  $U$  test). In Fig. 3.9G and H, the best axes from elevation tuning curves are shown for  $t(-x-z)$  neurons in the mc and VbC (from Wylie and Frost 1999a). The means for the mc and VbC distributions were  $+5.1^\circ$  and  $+6.2^\circ$  elevation, respectively.

### Ocular dominance

Ocular dominance (OD) for each neuron was determined using the following formula;

$$OD = \{(P_d - AP_d)/(P_{nd} - AP_{nd})\}$$

where “P” and “AP” respectively refer to the firing rate in response to translation/rotation optic flow moving in the preferred and anti-preferred directions along/about the best-response axis, “d” and “nd” refer to dominant and non-dominant eyes. The OD ratios were then used to categorize the neurons on a five-point scale that we have used previously (Wylie et al. 1993). Cells were classified as markedly dominant ( $OD > 1.5$ ), slightly dominant ( $1.5 > OD > 1.1$ ) or equi-dominant ( $OD < 1.1$ ). Overall, there was a slight bias towards a contralateral dominance. Of 38 total cells, 13 showed a marked contra- OD and 8 showed a slight contra- OD dominance. Eight cells showed a marked ipsi- OD, 5 showed a slight ipsi- OD and one cell was monocular-ipsi. Three cells were equi-dominant. There were no appreciable differences among the different cell types with the exception that 7 of the 9 *rHI35c* cells showed a marked contralateral dominance.

### Functional organization of the inferior olive

Electrolytic lesions were made at known locations relative to neurons in the mc such that the functional organization of the mc could be assessed. Figure 3.10A is a series of drawings through the IO (caudal to rostral) that shows the locations of

physiologically identified rotation- or translation-sensitive neurons. This included 8 *rVA* (!), 11 *rHI35c* (∇), 5 *t(+y)* (Γ), and 4 *t(-x-z)* (△) neurons. Unfortunately there was only one each for the *t(-y)* (O) and *t(-x+z)* (▲) groups. A clear topography is evident. The rotation cells were found medial to the translation cells, with the *rVA* neurons located caudal to the *rHI35c* neurons. With respect to the translation neurons, the *t(-x-z)* neurons were found caudal to the other three types, and lateral to the *rVA* neurons. Figure 3.10B shows a photomicrograph of a lesion in the mc. This lesion, which was almost twice as large as most, was made at the location of an *rHI35c* neuron in the most medial part of mc. This section corresponds approximately to the upper-right drawing in Figure 3.10A.

## Discussion

In this study we recorded the activity of neurons in the mc of the IO to translational and rotational panoramic optic flowfields produced by the planetarium and translator projectors. Six groups of neurons were found. Two groups, *rVA* and *rHI35c* neurons, responded best to rotational optic flow, whereas the other four groups, *t(+y)*, *t(-y)*, *t(-x+z)* and *t(-x-z)* neurons, responded best to translational optic flow.

### *Comparison with studies of the pigeon VbC, nBOR and LM*

In pigeons, the mc of the IO provides CF input to all parts of the contralateral VbC, including the ventral uvula, nodulus and flocculus (Arends and Voogd 1989;

Wylie et al. 1997). Previous electrophysiological studies of the pigeon VbC showed a clear functional distinction between the lateral VbC (flocculus) and the medial VbC (ventral uvula and nodulus) with respect to the CSA of Purkinje cells in response to translational and rotational optic flow (Wylie et al. 1993). In the flocculus, two groups of rotation-sensitive neurons were found: *rVA* and *rHI35i* neurons. In the medial VbC, four groups of translation-sensitive neurons were found: *t(+y)*, *t(-y)*, *t(-x+z)* and *t(-x-z)* neurons. As each Purkinje cell receives input from a single CF, the congruence of the findings of the present study with previous studies of the VbC is to be expected.

There were two differences from the VbC studies. First, distributions of the best axes for *rVA* neurons were significantly different ( $p < 0.05$ ) for the mc and VbC, although the magnitude of the difference was not striking (about  $10^\circ$ ). Upon re-examination of the VbC data (from Wylie and Frost 1993), the only other apparent difference between the two samples was that the VbC *rVA* neurons showed a stronger bias toward an overall ipsilateral OD and included 5 ipsi-monocular cells. However, OD was not correlated with the orientation of the best axis. Second, the distributions of the best axes of the *t(-x-z)* neurons in the mc and VbC were significantly different ( $p < 0.002$ ) and the magnitude of the difference was larger (about  $12^\circ$ ). Given the small number of neurons involved in the two samples, and consequently the lack of statistical power, we are inclined to accept that these differences represent sampling error. The only methodological difference between the present study and the previous studies of the VbC was with respect to the orientation of the head during recording. In

the present study the head was oriented to the normal posture observed for running, walking and flying (Erichsen et al. 1989). For the VbC studies, the head was in the stereotaxic position; pitched down  $38^\circ$  relative to the normal position (Wylie and Frost 1993, 1999a). It is possible that otolithic inputs signalling static head tilt could account for the differences that were observed.

The mc receives visual input from two retinal-recipient nuclei: the pretectal nucleus lentiformis mesencephali (LM; Clarke 1977; Gamlin and Cohen 1988a,b; Wylie, 2001) and the nucleus of the basal optic root (nBOR) of the accessory optic system (AOS; Karten et al. 1977; Reiner et al. 1979; Brecha et al. 1980; Fite et al. 1981; Wylie et al. 1997; Wylie, 2001). Most neurons in the LM have monocular receptive fields in the contralateral eye and respond best to moving largefield stimuli (Burns and Wallman 1981; Morgan and Frost 1981; Gioanni et al. 1984; Winterson and Brauth 1985; Wylie and Frost 1990a; Wylie and Crowder, 2000). These units are the building blocks of the panoramic receptive fields in the mc and VbC that process particular patterns of optic flow resulting from self-translation and rotation. The construction of such higher-order receptive fields appears to begin before the mc. There is a small sub-population (<10%) of neurons in both the nBOR and the LM that have binocular receptive fields and have a receptive field structure conducive to the detection of optic flow patterns resulting from either self-translation or self-rotation (Wylie and Frost 1990b, 1999b; Wylie 2000). These binocular units in the nBOR appear to reside in the dorsalis subnucleus, which is the portion of the nBOR that provides most of the input to the mc (Brecha et al. 1980; Wylie, 2001). However,

there is clearly further integration of information from the LM and nBOR in the mc for two reasons. First, most of the binocular nBOR and LM cells show a very pronounced contralateral OD (Wylie and Frost 1990b, 1999b; Wylie 2000) compared to units in the mc and VbC (Wylie et al. 1993). Second, the best axes of these LM and nBOR units selective for either translational or rotational optic flow do not cluster as tightly about the principal axes observed for mc and VbC neurons (Wylie and Frost 1999b; Wylie 2000).

#### *Comparison with Mammalian Species*

Previous studies of the IO in rabbits have found neurons responsive to rotational optic flow. Both *rVA* and *rHI35c* neurons have been found in the dorsal cap (dc) of Kooy (Leonard et al. 1988). The dc provides CF input to the flocculus and to the ventral uvula and nodulus (Takeda and Maekawa 1989a,b; Tan et al. 1995). Neurons responsive to translational optic flow have not been found in the IO or VbC in species other than the pigeon. However, adjacent to the dc in the beta-subnucleus of the IO, and in the medial most zone of the nodulus and ventral uvula to which the beta-subnucleus projects, neurons are responsive to vestibular stimulation originating in the otolith organs (Barmack and Shojaku 1992, 1995). Insofar as the beta-subnucleus is potentially processing information about linear acceleration, we suggest that this structure is functionally similar to the areas of the pigeon mc that process translational optic flow.

*A common reference frame for the Optokinetic, Vestibular, and Oculomotor Systems*

Simpson, Graf and colleagues (Ezure and Graf 1984; Graf et al. 1988; Leonard et al. 1988; Simpson and Graf 1981, 1985; Simpson et al. 1988a,b, 1989a,b; van der Steen et al. 1994) noted that the principal axes of the floccular neurons sensitive to rotational optic flow are common to the vestibular system and the extraocular muscles (for pigeons see Baldo 1990; Dickman 1996; Wylie and Frost 1993, 1996). That is, the neural systems underlying rotational optic flow analysis, the semi-circular canals and the eye muscles, are organized with respect to a reference frame consisting of three orthogonal axes: the vertical axes and two horizontal axes oriented  $45^\circ$  to the midline. The studies of the translation-sensitive neurons in the pigeon VbC (Wylie et al. 1998; Wylie and Frost 1999a) and the present study of the mc emphasize that the translational optic flow system shares this same frame of reference: the vertical axis ( $t(-y)$  and  $t(+y)$  neurons), and two horizontal axes oriented  $45^\circ$  to the midline ( $t(-x-z)$  and  $t(-x+z)$  neurons). The potential benefits and economics of such an organization has been presented in detail in previous reports (Simpson and Graf 1985; Wylie and Frost 1999a; Frost and Wylie 2000).

The principal axes of the translational optic flow system are not quite orthogonal. Although the best axes of the  $t(-x-z)$  neurons are, on average, aligned with the horizontal plane (Fig. 3.9G,H), this is not the case for the  $t(-x+z)$  neurons. This is clearly illustrated in Fig. 3.9E and F for both mc and VbC neurons. The mean of the best axes is about  $25^\circ$  above the horizontal plane. However, these results are consistent with what is known about the direction preferences of AOS neurons. Most

neurons in the nBOR prefer either upward, downward or backward (N-T) largefield motion in the contralateral eye (Wylie and Frost 1990a), whereas most neurons in the LM prefer forward (T-N) motion (Winterson and Brauth 1985; Wylie and Frost 1996; Wylie and Crowder, 2000). We have previously emphasized that the direction preference of N-T nBOR neurons and T-N LM neurons are not co-linear. For N-T neurons, the average direction preference is about  $25^\circ$  down from the horizontal plane. (This is correlated with an asymmetry in the horizontal recti (see Wylie and Frost (1996) for a detailed discussion)). The  $t(-x+z)$  neurons prefer N-T motion in the central areas of both hemifields. As much of the receptive field of a  $t(-x+z)$  neuron is constructed from N-T neurons in the nBOR, it is not surprising that there is an elevation component to the best axes of  $t(-x+z)$  neurons.

There remains doubt as to whether the signals from the otolith organs share the same three-axes reference frame. The primary afferents innervating the utricle in pigeons do not share this coordinate system. Si and colleagues (1997) have shown that most utricular afferents in pigeons respond best to linear translation along the interaural ( $x$ ) axis. However, Hess and Dieringer (1991) recorded eye movements in rats to linear acceleration. Their results suggested that the otolith signals are organized in semicircular canals coordinates. Furthermore, there is evidence suggesting that the neural systems controlling postural responses to translation may be organized according to a three-axes system. In response to translation of the floor in different directions in the horizontal plane, Macpherson (1988) found that forelimb

and hind limbs of cats were maximally responsive to displacement directions approximately  $45^\circ$  to the midline.

### *Topographical Organization of the mc*

By making electrolytic lesions at known locations relative to recordings sites we were able to illustrate a topographical organization of the mc (Fig. 3.10). Previous anatomical work, using retrograde transport of cholera toxin subunit B (CTB) from the pigeon VbC, also suggested a topographic organization of the mc. The results of the present study are in agreement with these previous studies on several accounts. Lau et al. (1998) made large injections of CTB into either the flocculus (rotation-sensitive cells) or medial VbC (translation-sensitive cells). From the injections into the flocculus, retrogradely labeled neurons were seen in the dorso-medial margin of the mc whereas, from injections in the medial VbC, retrograde labelling was found in the ventro-lateral mc. In the present study, the *rVA* and *rHI35c* neurons were found medial to the translation-sensitive neurons.

Crowder et al. (2000) were able to determine the projection of the mc to different classes of translation-sensitive cells by making small iontophoretic injections of CTB into specific zones of the medial VbC. After injections into the  $t(-x-z)$  zone in the VbC, retrogradely labelled cells were found caudally in the lateral margin of the VbC. Retrograde labelled neurons from injections into the other three zones were found rostral to the  $t(-x-z)$  neurons in the mc. There was quite a bit of overlap among the locations of retrograde labelled cells from the  $t(-y)$ ,  $t(+y)$  and  $t(-x+z)$  zones, but the

$t(-y)$  neurons were found most rostrally, the  $t(-x+z)$  neurons were caudal to these, and the  $t(+y)$  neurons were found caudal and slightly medial to  $t(-x+z)$  neurons. In the present study, the  $t(-x+z)$  neurons were found caudally in the lateral mc. The  $t(-y)$ ,  $t(+y)$  and  $t(-x+z)$  neurons were found rostral to these, however, there is insufficient data to determine any segregation of these three groups.

Wylie et al. (1999) made small iontophoretic injections of CTB in the pigeon flocculus at locations containing either  $rVA$  or  $rHI35i$  Purkinje cells. There was a clear rostro-caudal separation of the retrograde cells in the mc. After injections at locations containing  $rVA$  neurons, retrogradely labelled cells were found caudally in the medial mc. After injections at locations containing  $rHI35i$  neurons, retrogradely labelled cells were found rostrally in the medial mc. In the present study  $rVA$  cells were found in the medial mc, caudal to the  $rHI35c$  cells. The organization of the rotation-sensitive cells in the rabbit IO is strikingly similar:  $rVA$  neurons are found in the caudal dc, whereas  $rHI35c$  neurons are found in the rostral dc and ventro-lateral outgrowth (Leonard et al. 1988).

Recently, Wylie (2001) has shown that input to the caudal mc is mainly from the LM, whereas the nBOR provides the majority of the input to the rostral mc. (A similar pattern of connectivity to the dc has been shown in mammals (Mizuno et al. 1973; Takeda and Maekawa 1976; Maekawa and Takeda 1977; Holstege and Collewyn 1982)). This is consistent with the findings of the topographical organization revealed in the present study. Recall that most LM and nBOR neurons have receptive fields restricted to the contralateral eye, and that most LM neurons

prefer forward motion, whereas nBOR neurons prefer largefield stimuli moving either upward, downward or backward (Burns and Wallman 1981; Morgan and Frost 1981; Gioanni et al. 1984; Winterson and Brauth 1985; Wylie and Frost 1990a, 1996; Wylie and Crowder, 2000). The caudal mc contains *rVA* and *t(-x-z)* neurons. The preferred optic flowfield for both *rVA* and *t(x-z)* neurons consists of forward motion in the contralateral hemifield (e.g. Fig. 3.2B,E). In contrast, in the rostral mc, the preferred flowfields of *rHI35c*, *t(-y)*, *t(+y)* and *t(x+z)* neurons consist of either upward, downward or backward motion in the contralateral hemifield (e.g. Fig. 3.2C,D). Thus, one would expect that the input to the caudal mc would be from the LM primarily, whereas the rostral mc would receive a heavier input from the nBOR.

#### *Role of the Rotation and Translation Optic Flow Neurons in Compensatory Eye and Head Movements*

There are several mechanisms to generate compensatory eye and head movements in an attempt to stabilize the retinal image. These include optokinetic eye movements (optokinetic nystagmus; OKN), optokinetic head movements (opto-collic reflex; OCR), the vestibulo-ocular reflex (VOR) and the vestibulo-collic reflex (VCR) (e.g. Wilson and Melvill Jones, 1979). Pigeons exhibit robust VOR and VCR in response to head rotation (Anastasio and Correia 1988; Gioanni 1988b; Dickman et al 2000) and robust OKN and OCR in response to rotational visual stimuli (Gioanni et al. 1981; Gioanni 1988a). The resultant head and eye movements appear to be compensatory to rotation about any axis (Gioanni 1988a; Dickman et al 2000). The

*rVA* and *rHI35c* olivary cells are most certainly involved in these rotational head and eye movements. The rotational OKN and OCR are severely compromised by lesions of the nBOR and LM, the structures that are providing input to the *rVA* and *rHI35c* olivary neurons (Fite et al. 1979; Gioanni et al. 1983ab). Moreover, it is thought that the olivary projection to the flocculus is involved in the adaptive modification of the rotational VOR (e.g. Ito, 1972) although the role of the visual information carried by the CFs is debatable (Simpson et al. 1996). Few studies have measured compensatory eye and head movements to translation in pigeons. Dickman and Angelaki (1999) measured the VOR (in the dark) to translation in the horizontal plane. Compensatory eye movements were not observed, but torsional and vertical eye movements compensatory to the perceived head tilt were observed. Given these findings, we would suggest that the translational olivary neurons do not assist the linear VOR, at least not in the way that the rotational olivary neurons assist the rotational VOR. Although it has not been demonstrated, we suggest that the translational olivary neurons are important for generating optokinetic head movement during self-translation. The stereotypical head-bobbing of pigeons is an optokinetic head movement produced during forward translation (Friedman 1975; Frost 1978).

Acknowledgement: This research was supported by a grant from the Natural Sciences and Engineering Research Council of Canada (NSERC) to DRWW. We thank X. Lu for technical assistance.

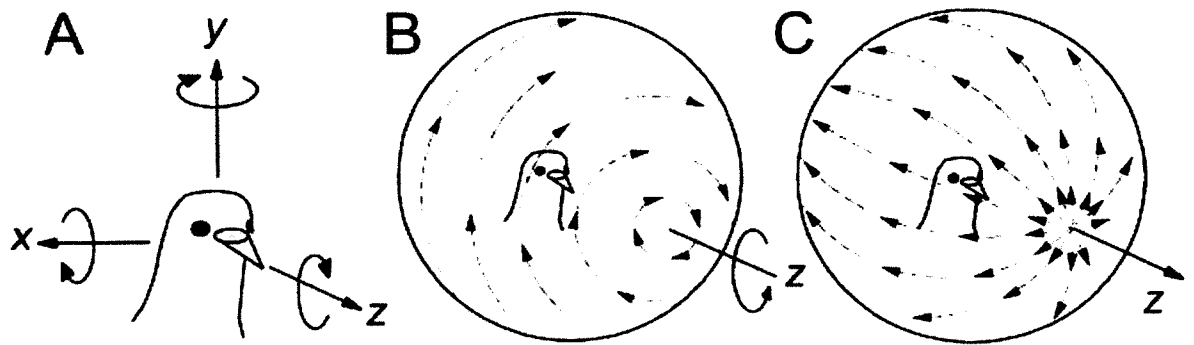


**Figure 3.1.** A shows the standard coordinate system for motion of an object in three-dimensional space. It is sufficient to describe motion using a reference frame consisting of three orthogonal axes ( $x, y, z$ ), and six degrees of freedom, three of translation and three of rotation. In vision research,  $x$ ,  $y$  and  $z$  represent the interaural, vertical and naso-occipital axes, respectively. With respect to the direction of translation,  $+x$ ,  $+y$  and  $+z$  represent rightward, upward and forward self-motion respectively. B illustrates the optic flowfield resulting from clockwise head rotation about the  $z$ -axis. The arrows, as projected onto a sphere, illustrate the counter clockwise rotation of local motion in the flowfield, which collectively constitute the wholefield rotational optic flow. C shows a schematic of the optic flowfield resulting from translation along the  $+z$ -axis. At the “pole” in the direction of translation, the arrows diverge from a point; the focus of expansion (FOE). Likewise, at the opposite pole (not shown) the vectors would converge to a point; the focus of contraction (FOC). At the “equators” of the sphere, the flowfield is laminar, with all vectors pointing in approximately the same direction.

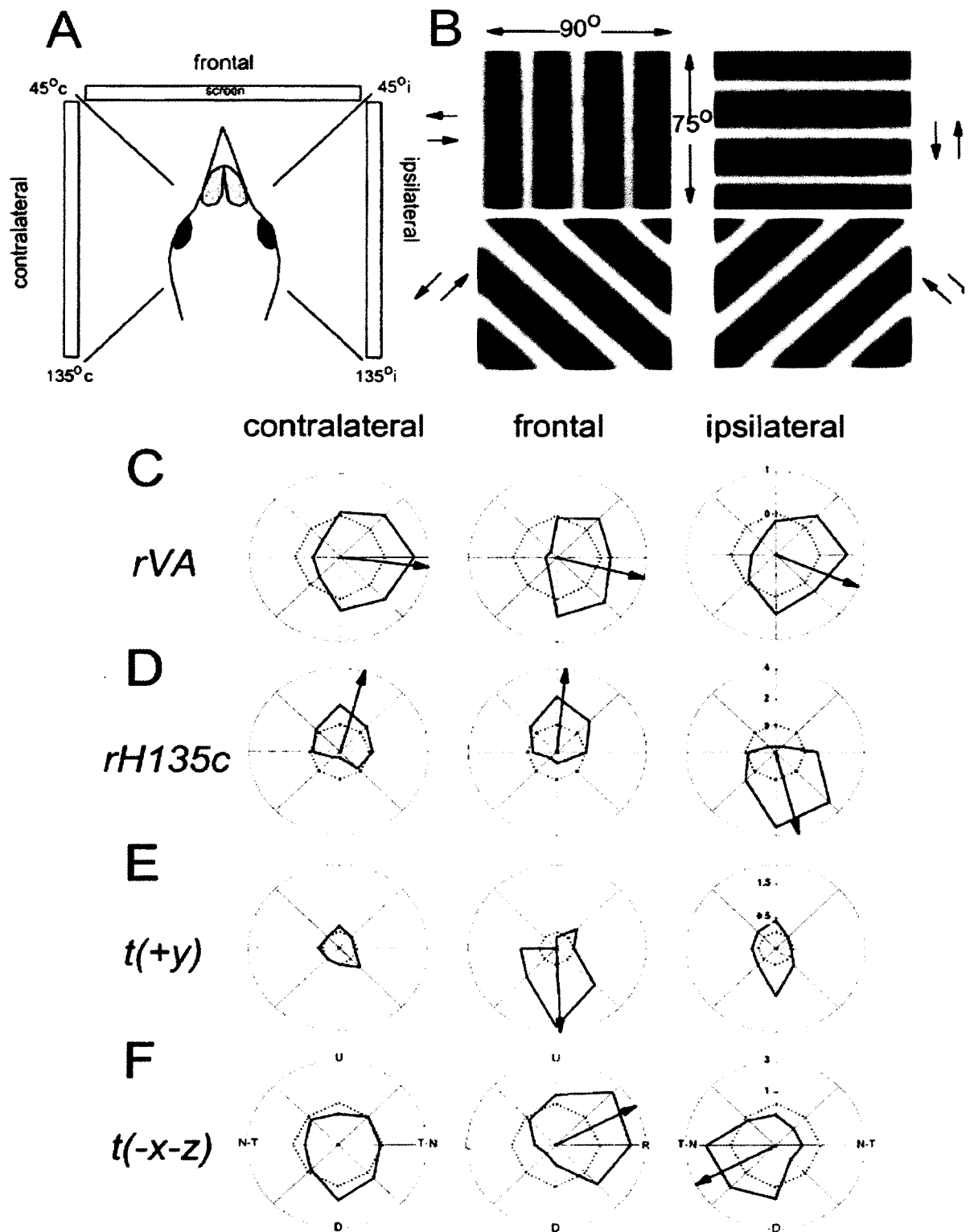
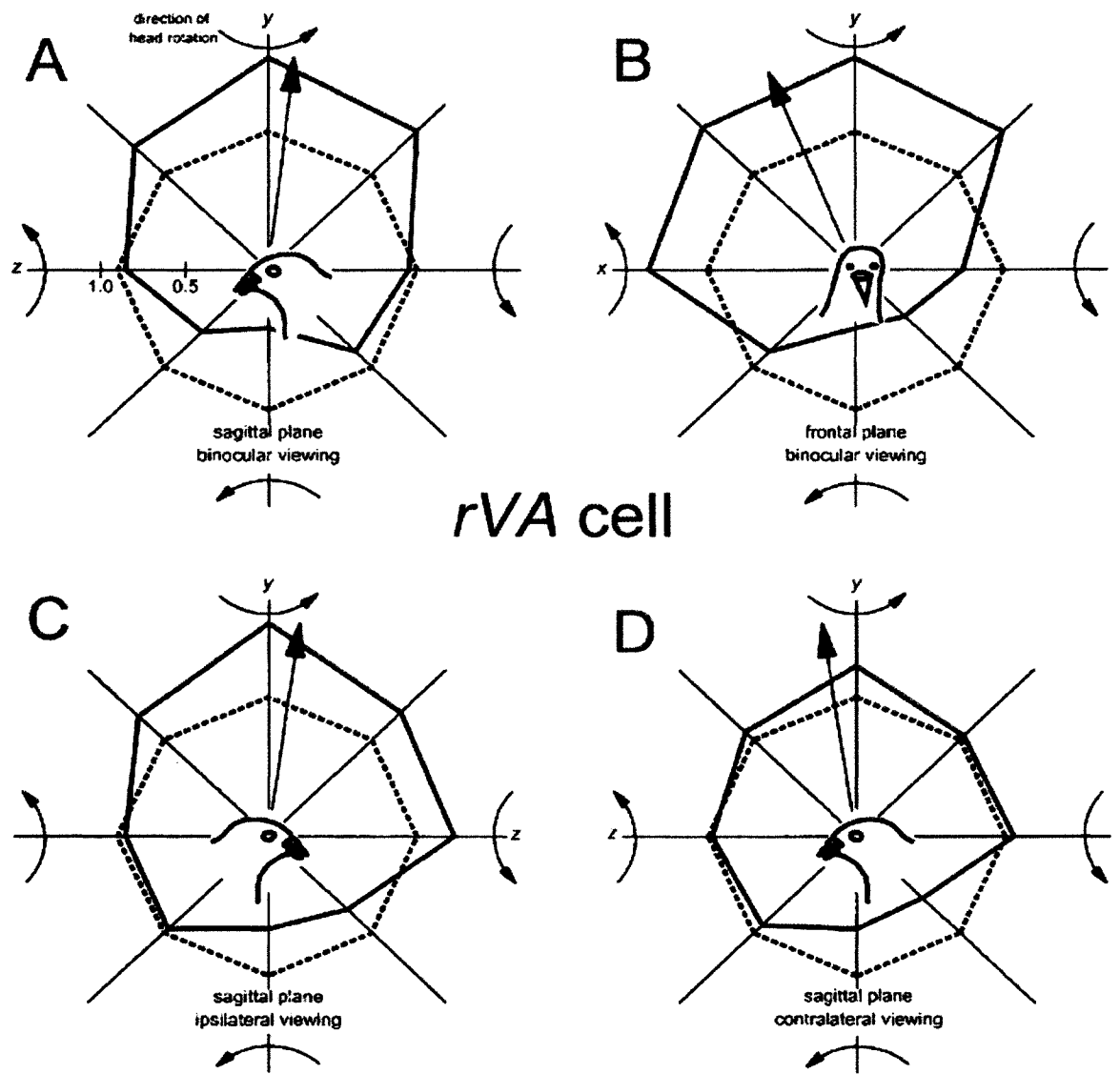
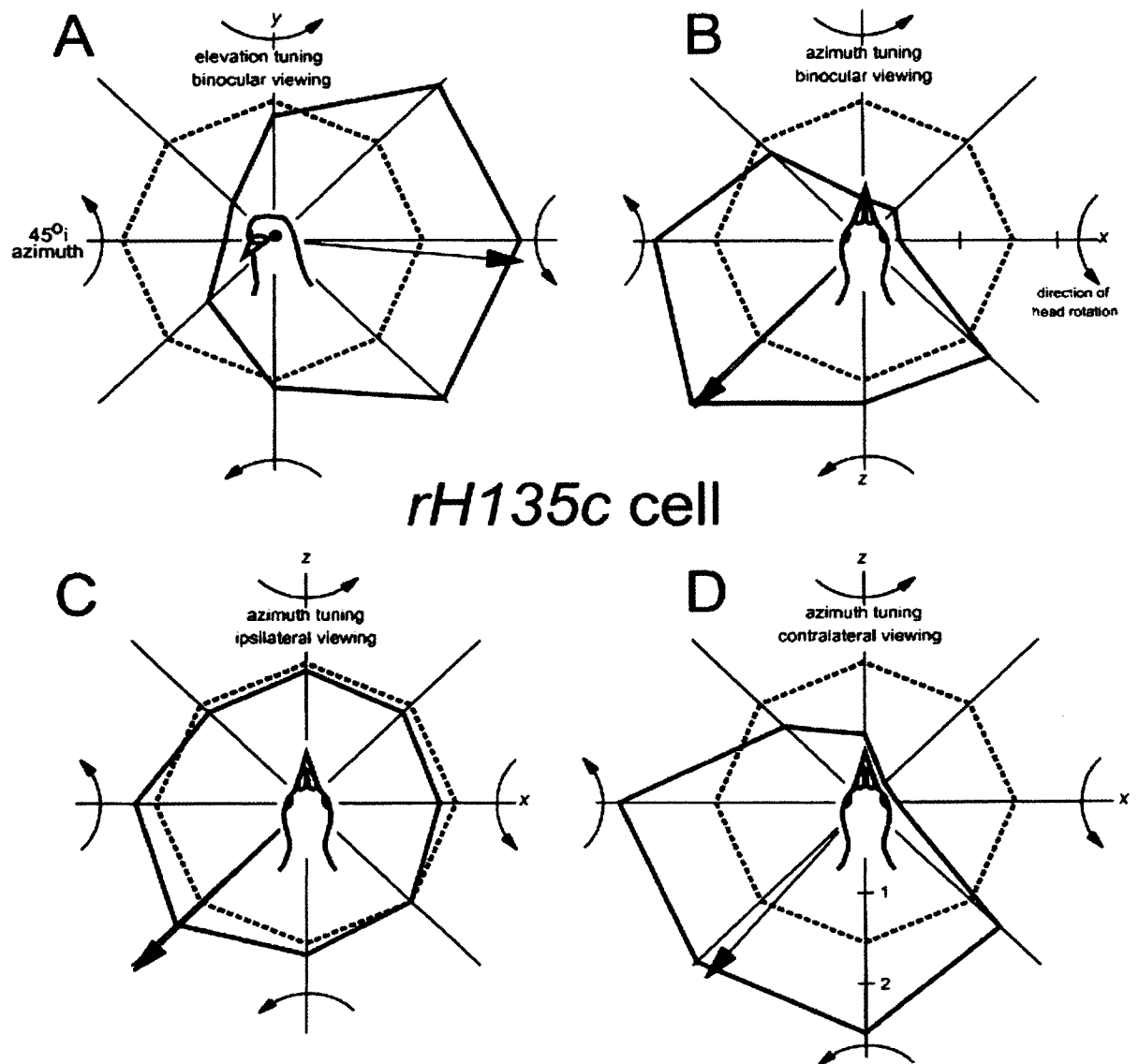


Figure 3.2. Response of medial column neurons to moving largefield sine wave gratings presented in different regions of the visual field. Drifting sine wave gratings

Figure 3.2 caption continued: were back projected onto the screen that measured  $90^\circ \times 75^\circ$  (width  $\times$  height). As illustrated in **A**, the screen was positioned at one of three locations relative to the bird: the contralateral, ipsilateral, and frontal regions (assuming recordings were made in the right inferior olive). **B** shows the four grating orientations used to determine tuning curves in each location. Each grating moved in both directions, perpendicular to the orientation of the grating, to produce a tuning curve with a total of 8 directions ( $45^\circ$  increments). **C-F** show responses of *rVA* (**C**), *rHI35c* (**D**), *t(+y)* (**E**), and *t(-x-z)* (**F**) neurons to the drifting gratings in each of the three regions. Polar plots of direction tuning are shown (firing rate (spikes/sec re. spontaneous rate (SR)) as a function of the direction of largefield motion). The broken circles represent the SR (set to 0 spikes/sec) and the arrows represent the peak of the best-fit cosine (i.e. the preferred or “best” direction). Best-fit cosines were only done for those tuning curves that had a modulation index  $\geq 1.5$  (see Results). U, D, L and R = upward, downward, leftward and rightward motion, respectively. N-T and T-N = nasal-to-temporal and temporal-to-nasal motion, respectively. i = ipsilateral; c = contralateral.



**Figure 3.3.** Responses of an *rVA* neuron. **A** and **B** show polar plots of elevation tuning curves in the sagittal and frontal planes, respectively, under binocular viewing conditions. **C** and **D** show elevation tuning curves in the sagittal plane under monocular viewing conditions. Firing rate (spikes/sec) is plotted as a function of the orientation of the axis of rotational optic flow (solid line). Broken circles represent the spontaneous firing rate, and the solid arrows indicate the preferred axes from the best-fit cosines. A standard head-centric right-handed rule is used to represent the direction of optic flow (see text). Semicircular arrows represent the direction of head rotation, which is opposite the direction of optic flow. Note that this cell responded best to the flowfield that results from leftward rotation of the head about the vertical (yaw) axis (i.e. rightward optic flow: backward motion in the ipsilateral hemifield, forward motion in the contralateral hemifield). See text for a detailed description.



**Figure 3.4.** Responses of an *rH135c* neuron. Azimuth tuning curves for binocular, ipsilateral, and contralateral viewing conditions are illustrated in **B**, **C**, and **D**, respectively. **A** shows an elevation tuning curve in a vertical plane intersecting the horizontal plane at  $45^\circ$  azimuth. Broken circles represent the spontaneous firing rate, and the solid arrows indicate the preferred axes from the best-fit cosines. A standard head-centric right-handed rule is used to represent the direction of optic flow (see text). Semicircular arrows represent the direction of head rotation, which is opposite the direction of optic flow. This neuron responded best to rotational optic flow resulting from rotation of the head about an axis oriented in the horizontal plane at about  $135^\circ$  azimuth. See text for a detailed description.

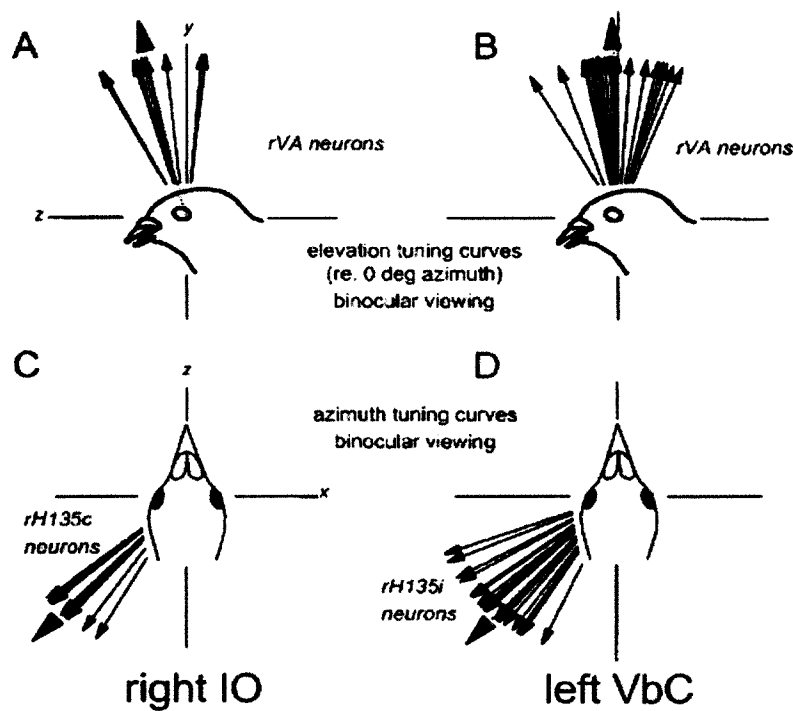


**Figure 3.5.** Best axes of *rVA* and *rH135c* neurons in the inferior olive (IO) and vestibulocerebellum (VbC). Best axes for the elevation tuning curves (sagittal plane) of *rVA* neurons in IO from this study are represented by the smaller arrows in **A**. Best axes for the complex spike activity of *rVA* Purkinje cells in the flocculus of the pigeon VbC are shown in **B**. **C** and **D** show best axes from azimuth tuning curves for *rH135c* neurons in the IO and *rH135i* neurons in the flocculus of the pigeon VbC, respectively. The larger dashed arrows represent the means of the respective distributions. The VbC data was obtained from Wylie and Frost (1993). It is assumed that recordings were made from the right IO and left VbC as the projections from the mc of the IO to the VbC are exclusively contralateral.

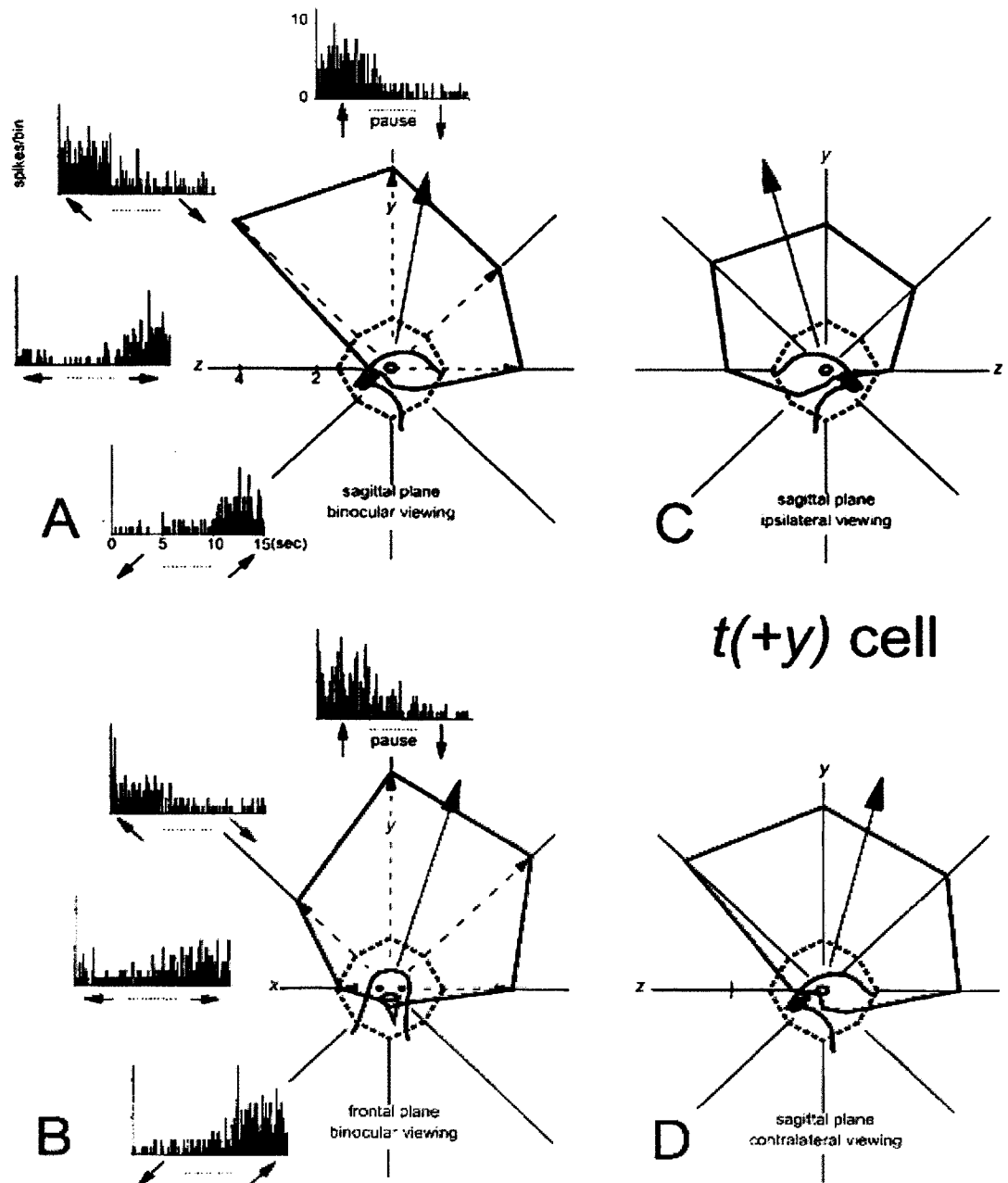


**Figure 3.6.** Elevation tuning curves for a  $t(+y)$  neuron. **A** and **B** show elevation tuning curves in the sagittal and frontal planes, respectively, under binocular viewing conditions. Firing rate (spikes/sec) in response to translational optic flowfields is plotted as a function of the orientation of the axis of translation (solid line). Dashed arrows along each axis represent the direction of self-motion the animal would make to cause the simulated flowfield (i.e. the arrows point toward the FOE in the flowfield). Broken circles represent the spontaneous firing rate, and the solid arrows indicate the axes of maximal modulation (i.e. direction of self-translation resulting in

Figure 3.6 caption continued: maximal modulation) from the best-fit cosines. The responses are also shown in peri-stimulus time histograms (PSTHs) for each axis. For each sweep there was 5 sec of translation in one direction, followed by a 5 sec pause, followed by 5 sec translation in the opposite direction. The PSTHs were summed from 10 consecutive sweeps. **C** and **D** show tuning curves in the sagittal plane under monocular viewing conditions. For this cell maximal modulation occurred in response to optic flow corresponding to upward translation (i.e. downward optic flow). See text for additional details.

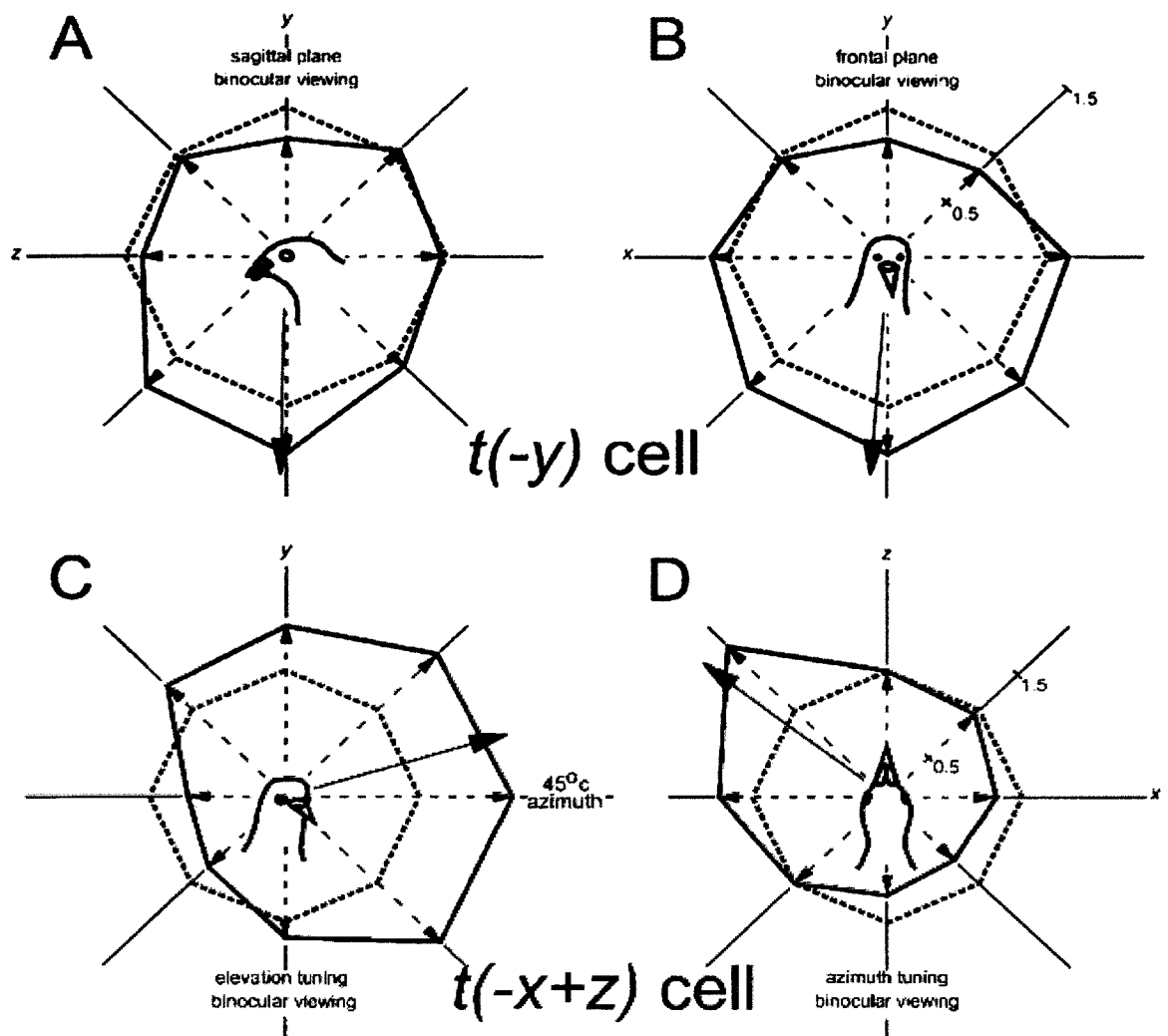


**Figure 3.7.** Binocular tuning curves for  $t(-y)$  and  $t(-x+z)$  neurons. Elevation tuning curves for binocular viewing in the sagittal and frontal planes are shown for a  $t(-y)$  neuron in **A** and **B**, respectively. **C** and **D** respectively show azimuth and elevation tuning curves for a  $t(-x+z)$  neuron. Dashed arrows along each axis represent the direction of self-motion the animal would make to cause the simulated flowfield. Broken circles represent the spontaneous firing rate, and the solid arrows indicate the best axes from the best fit cosines. For the  $t(-y)$ , note the preference for downward translation along the y-axis (**A** and **B**, i.e. upward optic flow). For the  $t(-x+z)$  neuron, the best axis in the horizontal plane was  $52^\circ$  azimuth (**D**). The elevation tuning curve was done in the vertical plane intersecting the horizontal plane through  $45^\circ$  azimuth. The best axis was  $+16^\circ$  elevation.

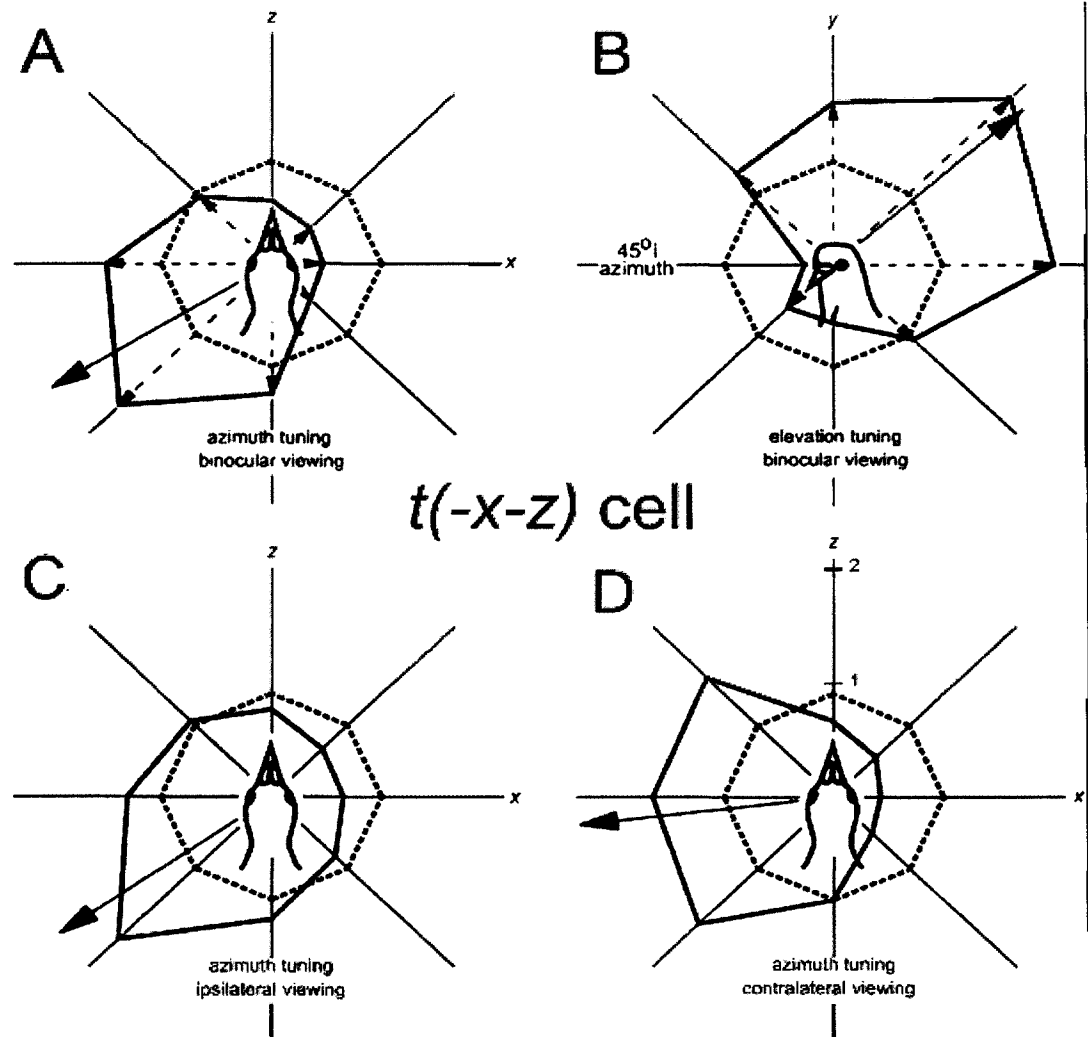


**Figure 3.8.** Axis tuning for a  $t(-x-z)$  neuron. **A** and **B** respectively show azimuth tuning and elevation tuning (in a vertical plane intersecting the horizontal plane through  $45^\circ$  azimuth) under binocular viewing conditions. Dashed arrows along each axis represent the direction of self-motion the animal would make to cause the simulated flowfield. Broken circles represent the spontaneous firing rate, and the solid arrows indicate the axes of maximal modulation from the best-fit cosines. Maximal excitation of this neuron occurs in response to an optic flowfield with FOC at  $59^\circ$  azimuth (**A**) and  $-40^\circ$  elevation (**B**). **C** and **D** show azimuth tuning curves in the horizontal plane under monocular viewing conditions. This neuron was modulated by stimulation of both ipsilateral and contralateral eyes, but there was a disparity with respect to the best axes.

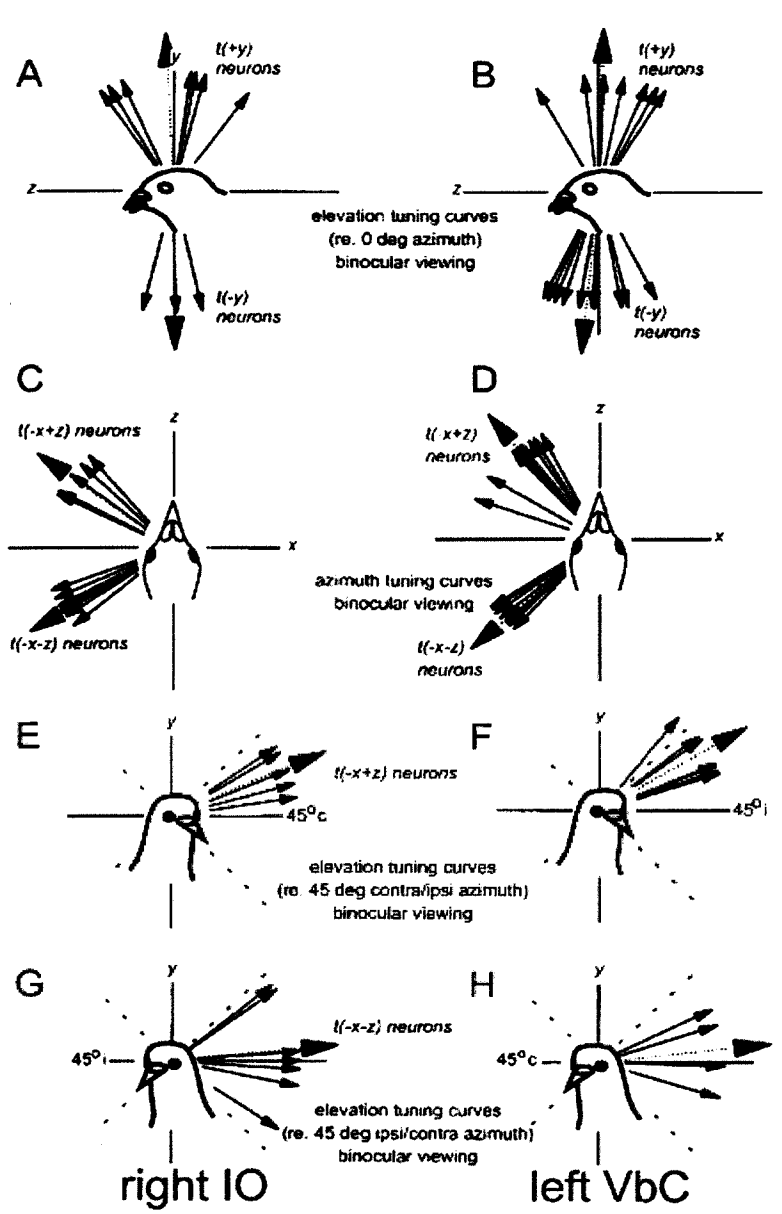
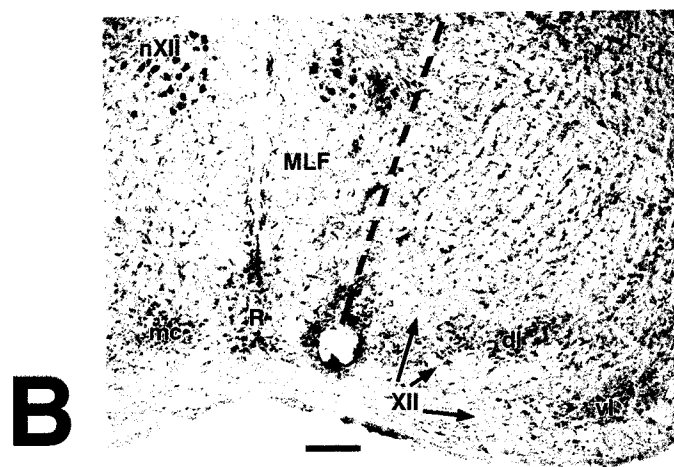
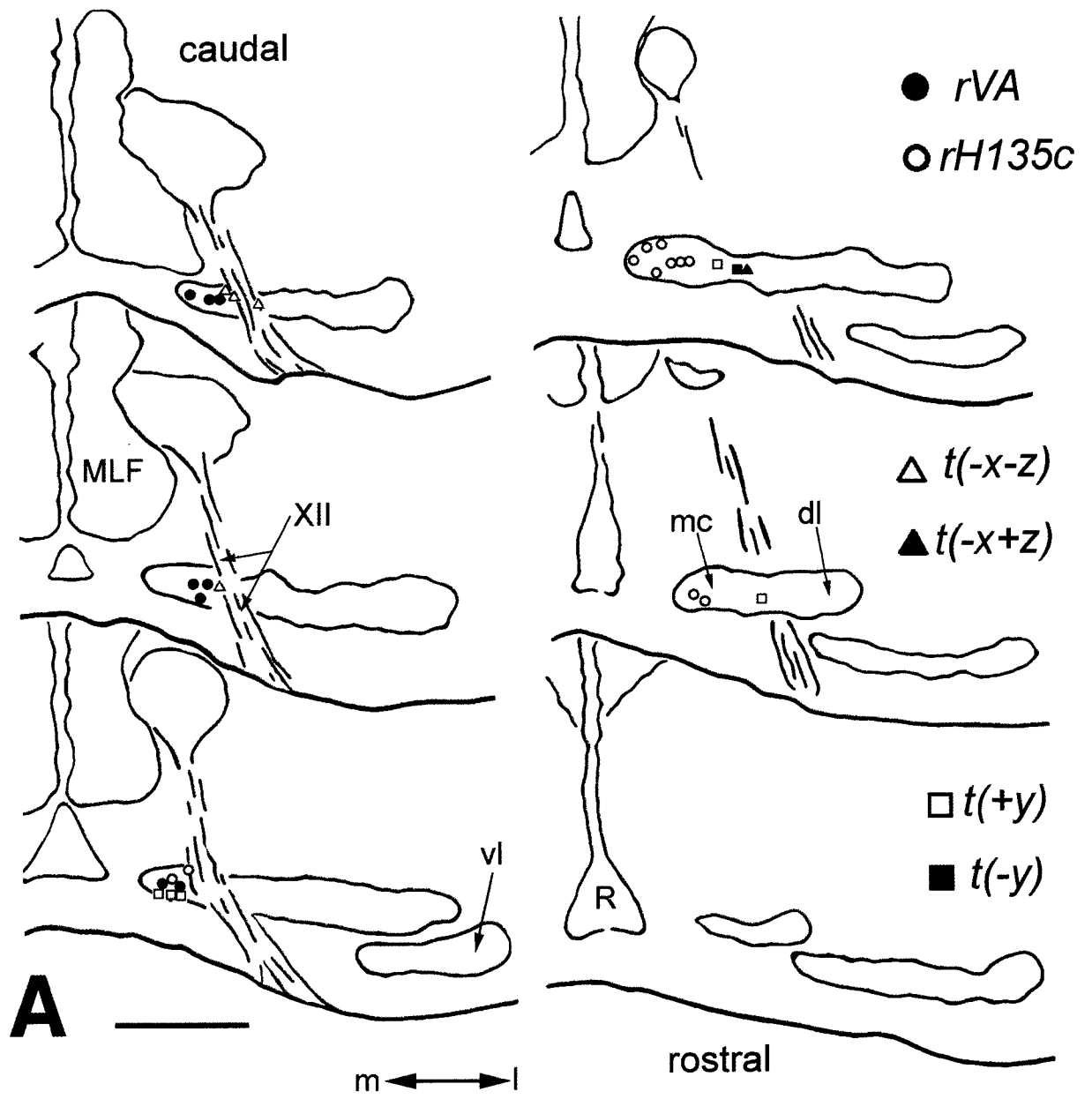


Figure 3.9. Axes of maximal modulation of translation-sensitive neurons in the inferior olive (IO) and vestibulocerebellum (VbC). Small arrows represent best axes for individual neurons and the larger dashed arrows represent the means of the distributions. **A** and **B** show the best axes for elevation tuning curves in the sagittal plane for  $t(+y)$  and  $t(-y)$  neurons in the IO and VbC, respectively. **C** and **D** show the best axes for azimuth tuning curves in the horizontal plane conditions for  $t(-x+z)$  and  $t(-x-z)$  neurons in IO and VbC, respectively. **E** and **F** show the best axes from elevation tuning curves for  $t(-x-z)$  and  $t(-x+z)$  neurons in IO and VbC, respectively. Note that best axes for  $t(-x+z)$  neurons in both IO and VbC contained a  $+y$  elevation component. The VbC data was obtained from Wylie and Frost (1999a). It is assumed that recordings were made from the right IO and left VbC.



**Figure 3.10.** Functional organization of the inferior olive (IO). **A** is a series of drawings through the IO (caudal to rostral, approximately 260 $\mu$ m apart) showing the locations of physiologically identified rotation- or translation-sensitive neurons. This included 8 *rVA* (black circles), 11 *rHI35c* (open circles), 5 *t(+y)* (open squares), 4 *t(-x-z)* (open triangles), 1 *t(-y)* (black squares) and 1 *t(-x+z)* (black triangles) neuron. **B** shows a photomicrograph of a lesion in the mc. The dashed line indicates the electrode track. This large lesion was made at the location of an *rHI35c* neuron in the most medial part of mc. MLF, medial longitudinal fasciculus; XII, twelfth cranial nerve; nXII, nucleus of the twelfth nerve; mc, medial column; dl, dorsal lamella; vl, ventral lamella; m, medial; l, lateral. Scale bars: **A**, 500 $\mu$ m, **B**, 250 $\mu$ m.

**References**

- Anastasio TJ, Correia MJ (1988) A frequency and time domain study of the horizontal and vertical vestibuloocular reflex in the pigeon. *J Neurophysiol* 59: 1143-1161
- Arends JJA, Voogd J (1989) Topographic aspects of the olivocerebellar system in the pigeon. *Exp Brain Res Suppl* 17: 52-57
- Baldo MV (1990) The spatial arrangement of the semicircular canals of the pigeon. *Braz J Med Biol Res* 23: 914-917
- Barmack NH, Shojaku H (1992) Vestibularly induced slow oscillations in climbing fiber responses of Purkinje cells in the cerebellar nodulus of the rabbit [letter]. *Neuroscience* 50(1): 1-5
- Barmack NH, Shojaku H (1995) Vestibular and visual climbing fiber signals evoked in the uvula-nodulus of the rabbit cerebellum by natural stimulation. *J Neurophysiol* 74: 2573-2589
- Brecha N, Karten HJ, Hunt SP (1980) Projections of the nucleus of basal optic root in the pigeon: An autoradiographic and horseradish peroxidase study. *J Comp Neurol* 189: 615-670
- Burns S, Wallman J (1981) Relation of single unit properties to the oculomotor function of the nucleus of the basal optic root (AOS) in chickens. *Exp Brain Res* 42: 171-180
- Clarke PGH (1977) Some visual and other connections to the cerebellum of the pigeon. *J Comp Neurol* 174: 535-552

- Crowder NA, Winship IR, Wylie DRW (2000) Topographic organization of inferior olive cells projecting to translational zones in the vestibulocerebellum of pigeons. *J Comp Neurol* 419: 87-95
- Dickman JD (1996) Spatial orientation of semicircular canals and afferent sensitivity vectors in pigeons. *Exp Brain Res* 111: 8-20
- Dickman JD, Angelaki DE (1999) Three-dimensional organization of vestibular-related eye movements to off-vertical axis rotation and linear translation in pigeons. *Exp Brain Res* 129: 391-400
- Dickman JD, Beyer M, Hess BJM (2000) Three-dimensional organization of vestibular related eye movements to rotational motion in pigeons. *Vis Res* 40: 2831-2844
- Erichsen JT, Hodos W, Evinger C, Bessette BB, Philips SJ (1989) Head orientation in pigeons: postural, locomotor, and visual determinants. *Brain Behav Evol* 33: 268-578
- Ezure K, Graf W (1984) A quantitative analysis of the spatial organization of the vestibulo-ocular reflexes in lateral and frontal-eyed animals. I. Orientation of semicircular canals and extraocular muscles. *Neuroscience* 12: 85-93
- Fite KV, Reiner T, Hunt S (1979) Optokinetic nystagmus and the accessory optic system of pigeon and turtle. *Brain Behav Evol* 16: 192-202
- Fite KV, Brecha N, Karten HJ, Hunt SP (1981) Displaced ganglion cells and the accessory optic system of the pigeon. *J Comp Neurol* 195: 279-288

Friedman MB (1975) Visual control of head movements during avian locomotion.

Nature 225: 67-69

Frost BJ (1978) The optokinetic basis of head-bobbing in the pigeon. J Exp Biol 74:

187-195

Frost BJ, Wylie DRW (2000) A common frame of reference for the analysis of optic

flow and vestibular information. Int Rev Neurobiol 44: 121-137

Gamlin PDR, Cohen DH (1988a) The retinal projections to the pretectum in the

pigeon (*Columba livia*). J Comp Neurol 269: 1-17

Gamlin PDR, Cohen DH (1988b) Projections of the retinorecipient pretectal nuclei

in the pigeon (*Columba livia*). J Comp Neurol 269:18-46

Gibson JJ (1954) The visual perception of objective motion and subjective movement.

Psychol Rev 61: 304-314

Gioanni H (1988a) Stabilizing gaze reflexes in the pigeon (*Columba livia*): I.

Horizontal and vertical optokinetic eye (OKN) and head (OCR) reflexes. Exp

Brain Res 69: 567-582

Gioanni H (1988b) Stabilizing gaze reflexes in the pigeon (*Columba livia*): II.

Vestibulo-ocular (VOR) and vestibulo-collic (closed loop VCR) reflexes. Exp

Brain Res 69: 583-593

Gioanni H, Rey J, Villalobos J, Bouyer JJ, Gioanni Y (1981) Optokinetic nystagmus

in the pigeon (*Columba livia*): I. Study in monocular and binocular vision. Exp

Brain Res 44: 362-370

- Gioanni H, Rey J, Villalobos J, Dalbera A (1983b) Optokinetic nystagmus in the pigeon (*Columba livia*): III. Role of the nucleus ectomamillaris (nEM): interactions in the accessory optic system (AOS). *Exp Brain Res* 50: 248-258
- Gioanni H, Rey J, Villalobos J, Dalbera A (1984) Single unit activity in the nucleus of the basal optic root (nBOR) during optokinetic, vestibular and visuo-vestibular stimulations in the alert pigeon (*Columba livia*). *Exp Brain Res* 57: 49-60
- Gioanni H, Rey J, Villalobos J, Richard D, Dalbera A (1983a) Optokinetic nystagmus in the pigeon (*Columba livia*): II. Role of the pretectal nucleus of the accessory optic system (AOS). *Exp Brain Res* 50: 237-247
- Graf W, Simpson JI (1981) The relations between the semicircular canals, the optic axis, and the extraocular muscle in lateral-eyed and frontal-eyed animals. In: Fuchs, A, Becker, W (Eds) *Progress in Oculomotor Research. Developments in Neuroscience*, vol 12. Elsevier, Amsterdam, pp. 409-417
- Graf W, -Simpson JI, Leonard CS (1988) Spatial organization of visual messages of the rabbit's cerebellar flocculus. II. Complex and simple spike responses of Purkinje cells. *J Neurophysiol* 60: 2091-2121
- Hess BJ, Dieringer, N (1991) Spatial organization of linear vestibuloocular reflexes of the rat: responses during horizontal and vertical linear acceleration. *J Neurophysiol* 66: 1805-1818
- Holstege G, Collewyn H (1982) The efferent connections of the nucleus of the optic tract and the superior colliculus in rabbit. *J Comp Neurol* 209: 139-175

- Ito M (1972) Cerebellar control of the vestibular neurones: Physiology and pharmacology. *Prog Brain Res* 37: 377-390
- Karten HJ, Hodos W (1967) A Stereotaxic Atlas of the Brain of the Pigeon (*Columba Livia*). Johns Hopkins Press, Baltimore.
- Karten HJ, Fite KV, Brecha N (1977) Specific projection of displaced retinal ganglion cells upon the accessory optic system in the pigeon (*Columba livia*). *Proc Natl Acad Sci* 74: 1752-1756.
- Kusunoki, M., Kan, M., Kano, M-S., and K. Maekawa (1990) Nature of optokinetic response and zonal organization of climbing fibre afferents in the vestibulocerebellum of the pigmented rabbit. I. The flocculus. *Exp. Brain Res.* 80: 225-237.
- Lau KL, Glover RG, Linkenhoker B, Wylie DRW (1998) Topographical organization of inferior olive cells projecting to translation and rotation zones in the vestibulocerebellum of pigeons. *Neuroscience* 85: 605-614
- Leonard CS, Simpson JI, Graf W (1988) Spatial organization of visual messages of the rabbit's cerebellar flocculus. I. Typology of inferior olive neurons of the dorsal cap of Kooy. *J Neurophysiol* 60: 2073-2090
- Macpherson JM (1988) Strategies that simplify the control of quadrupedal stance. I. Forces at the ground. *J Neurophysiol* 60: 204-217
- Maekawa K, Takeda T (1977) Afferent pathways from the visual system to the cerebellar flocculus of the rabbit. In: Baker, R, Berthoz, A (eds) *Control of*

Gaze by Brain Stem Neurons, *Developments in Neuroscience*, Vol 1. Elsevier, Amsterdam, pp.187-195

Mizuno N, Mochizuki K, Akimoto C, Matsushima R (1973) Pretectal projections to the inferior olive in the rabbit. *Exp Neurol* 39: 498-506

Morgan B, Frost BJ (1981) Visual response properties of neurons in the nucleus of the basal optic root of pigeons. *Exp Brain Res* 42: 184-188

Reiner A, Brecha N, Karten HJ (1979) A specific projection of retinal displaced ganglion cells to the nucleus of the basal optic root in the chicken. *Neuroscience* 4: 1679-1688

Si X, Angelaki DE, Dickman JD (1997) Response properties of pigeon otolith afferents to linear acceleration. *Exp Brain Res* 117: 242-50

Simpson JI, Graf W (1981) Eye-muscle geometry and compensatory eye movements in lateral-eyed and frontal-eyed animals. *Ann New York Acad Sci* 374: 20-30

Simpson JI, Graf W (1985) The selection of reference frames by nature and its investigators. In: Berthoz, A, Melvill-Jones, G (Eds) *Adaptive Mechanisms in Gaze Control: Facts and Theories*. Elsevier, Amsterdam, pp. 3-16

Simpson JI, Graf W, Leonard C (1981) The coordinate system of visual climbing fibres to the flocculus. In: Fuchs, AF, Becker, W (Eds) *Progress in Oculomotor Research*. Elsevier, Amsterdam, pp. 475-484

Simpson JI, Graf W, Leonard C (1989a) Three-dimensional representation of retinal image movement by climbing fiber activity. In: Strata, P (Ed) *The*

Olivocerebellar System in Motor Control: Experimental Brain Research

Supplement vol 17. Springer-Verlag, Heidelberg, pp 323-327

Simpson JI, Leonard CS, Soodak RE (1988a) The accessory optic system of rabbit. II.

Spatial organization of direction selectivity. *J Neurophysiol* 60: 2055-2072

Simpson JI, Leonard CS, Soodak RE (1988b) The accessory optic system: analyzer of

self-motion. *Ann New York Acad Sci* 545: 170-179

Simpson JI, Van der Steen J, Tan J, Graf W, Leonard CS (1989b) Representations of

ocular rotations in the cerebellar flocculus of the rabbit. In: Allum, JHJ,

Hulliger, M (Eds) *Progress in Brain Research* vol. 80. Elsevier, Amsterdam,

pp 213-223

Simpson JI, Wylie DR, De Zeeuw CI (1996) On climbing fiber signals and their

consequence(s). *Behav Brain Sci* 19: 384-398

Takeda T, Maekawa K (1976) The origin of the pretecto-olivary tract. A study using

horseradish peroxidase. *Brain Res* 117: 319-325

Takeda T, Maekawa K (1989a) Transient direct connection of vestibular mossy fibers

to the vestibulocerebellar Purkinje cells in early postnatal development of

kittens. *Neuroscience* 32(1): 99-111

Takeda T, Maekawa K (1989b) Olivary branching projections to the flocculus,

nodulus and uvula in the rabbit. II. Retrograde double labeling study with

fluorescent dyes. *Exp Brain Res* 76(2): 323-32

Tan J, Gerrits NM, Nanhoe RS, Simpson JI, Voogd J (1995) Zonal organization of the

climbing fibre projection to the flocculus and nodulus of the rabbit. A

combined axonal tracing and acetylcholinesterase histochemical study. *J Comp Neurol.* 356: 23-50

van der Steen J, Simpson JJ, Tan J (1994) Functional and anatomic organization of three-dimensional eye movements in rabbit cerebellar flocculus. *J Neurophysiol* 72: 31-46

Wilson VJ, Melvill Jones G (1979). *Mammalian vestibular physiology*. Plenum Press, New York

Winterson BJ, Brauth SE (1985) Direction-selective single units in the nucleus lentiformis mesencephali of the pigeon (*Columba livia*). *Exp Brain Res* 60: 215-226

Wylie DRW (2001) Projections from the nucleus of the Basal Optic Root and nucleus lentiformis Mesencephali to the Inferior Olive in Pigeons (*Columba livia*). *J Comp Neurol* 429:502-513

Wylie DRW (2000) Binocular neurons in the nucleus lentiformis mesencephali in pigeons: responses to translational and rotational optic flowfields. *Neurosci Lett* 291: 9-12

Wylie DRW, Bischof WF, Frost BJ (1998) Common reference frame for the coding translational and rotational optic flow. *Nature* 392: 278-282

Wylie DRW, Crowder NA (2000) Spatio-temporal properties of “fast” and “slow” direction-selective neurons in the pretectal nucleus lentiformis mesencephali in pigeons. *J Neurophysiol* 84:2529-2540

- Wylie DR, Frost BJ (1990a) Visual response properties of neurons in the nucleus of the basal optic root of the pigeon: A quantitative analysis. *Exp Brain Res* 82: 327-336
- Wylie DR, Frost BJ (1990b) Binocular neurons in the nucleus of the basal optic root (nBOR) of the pigeon are selective for either translational or rotational visual flow. *Vis Neurosci* 5: 489-495
- Wylie DR, Frost BJ (1991) Purkinje cells in the vestibulocerebellum of the pigeon respond best to either rotational or translational visual flow. *Exp Brain Res* 86: 229-232
- Wylie DR, Frost BJ (1993) Responses of pigeon vestibulocerebellar neurons to optokinetic stimulation: II. The 3-dimensional reference frame of rotation neurons in the flocculus. *J Neurophysiol* 70: 2647-2659
- Wylie DRW, Frost BJ (1996) The pigeon optokinetic system: Visual input in extraocular muscle coordinates. *Vis Neurosci* 13: 945-953
- Wylie DRW, Frost BJ (1999a) Complex spike activity of Purkinje cells in the ventral uvula and nodulus of pigeons in response to translational optic flowfields. *J Neurophysiol* 81: 256-266
- Wylie DRW, Frost BJ (1999b) Responses of neurons in the nucleus of the basal optic root to translational and rotational flowfields. *J Neurophysiol* 81: 267-276
- Wylie DR, Kripalani T-K, Frost BJ (1993) Responses of pigeon vestibulocerebellar neurons to optokinetic stimulation: I. Functional organization of neurons

discriminating between translational and rotational visual flow. *J*

*Neurophysiol* 70: 2632-2646

Wylie DRW, Linkenhoker B, Lau KL (1997) Projections of the nucleus of the basal optic root in pigeons (*Columba livia*) revealed with biotinylated dextran amine. *J Comp Neurol* 384: 517-536

Wylie DRW, Winship IR, Glover RG (1999) Projections from the medial column of the inferior olive to different classes of rotation-sensitive Purkinje cells in the flocculus of pigeons. *Neurosci Lett* 268: 97-100

**CHAPTER 4:**  
**ZONAL ORGANIZATION OF THE VESTIBULOCEREBELLUM**  
**IN PIGEONS (*COLUMBA LIVIA*):**  
**I. CLIMBING FIBRE INPUT TO THE FLOCCULUS**

**Full Citation**

Winship IR, Wylie DR. Zonal organization of the vestibulocerebellum in pigeons  
(*Columba livia*): I. Climbing fiber input to the flocculus. *J Comp Neurol* 456:  
127-39, 2003.

The complex spike activity (CSA) of Purkinje cells in the pigeon vestibulocerebellum responds best to patterns of optic flow that result from self-motion. In the medial half of the vestibulocerebellum, CSA responds best to optic flow patterns resulting from self-translation (Wylie and Frost, 1999a; Wylie et al., 1993, 1998). In the lateral half of the vestibulocerebellum, the flocculus, CSA responds best to optic flow resulting from self-rotation. The rotation cells in the flocculus respond best to rotational optic flow about one of two axes in 3-dimensional space: either the vertical axis or an horizontal axis oriented at  $45^\circ$  contralateral azimuth /  $135^\circ$  ipsilateral azimuth (Wylie and Frost, 1993). We refer to these two response types as *rVA* and *rH45* neurons, respectively (Wylie, 2001; Winship and Wylie, 2001). This was first shown in a series of studies in rabbits by Simpson, Graf and colleagues using optic flow patterns produced by a rotating planetarium projector (Simpson et al., 1981, 1988a; Graf et al., 1988). They emphasized that the rotational optokinetic system is organized with respect to a 3-axis reference frame that is common to the vestibular canals and the eye muscles (Ezure and Graf, 1984; Graf et al., 1988; Leonard et al., 1988; Simpson and Graf, 1981, 1985; Simpson et al., 1988a,b, 1989a,b; van der Steen et al., 1994; see also Wylie and Frost, 1996). In fact, the translation cells in the medial vestibulocerebellum are also organized with respect to this 3-axis reference frame (Wylie et al., 1998; Wylie and Frost, 1999a).

In the rabbit flocculus, the *rVA* and *rH45* Purkinje cells are (i) organized into parasagittal zones that receive climbing fibre (CF) input from distinct regions of the inferior olive (IO), and (ii) have differential projections to the cerebellar and

vestibular nuclei (Leonard et al., 1988; Ruigrok et al., 1992; De Zeeuw et al., 1994; Tan et al., 1995). The *rVA* neurons are found in two zones (zones FZ<sub>II</sub> and FZ<sub>IV</sub>) that are interdigitated with two zones that contain *rH45* neurons (zones FZ<sub>I</sub> and FZ<sub>III</sub>; De Zeeuw et al., 1994; Tan et al., 1995). There is a fifth zone, zone C2, where the CSA is unresponsive to optokinetic stimulation (De Zeeuw et al., 1994). The *rVA* zones receive CF input from the caudal dorsal cap (dc) whereas the *rH45* zones receive CF input from the rostral dc and ventrolateral outgrowth (vlo; Tan et al., 1995). A similar organization of floccular Purkinje cells into parasagittal zones has been confirmed in several other mammalian species (cat, Gerrits and Voogd, 1982; rat, Ruigrok et al., 1992; monkey, Hess and Voogd, 1986; Voogd et al., 1987ab; for a review, see Voogd et al., 1996).

Previous research in pigeons using retrograde transport from the vestibulocerebellum has shown that the *rVA* and *rH45* Purkinje cells receive CF input from discrete regions of the contralateral medial column of the IO (mcIO; Wylie et al. 1999). Similar to the connections in mammals, *rVA* and *rH45* neurons in the pigeon flocculus receive input from the caudal and rostral margins of the mcIO, respectively (Wylie et al., 1999). However, the zonal organization of the *rVA* and *rH45* Purkinje cells in the pigeon flocculus has yet to be determined. In the present study, we examined the zonal organization of CF projections with iontophoretic injections of anterograde tracers in the rostral and caudal mcIO in pigeons.

## Methods

The methods reported herein conformed to the guidelines established by the Canadian Council on Animal Care and were approved by the Biosciences Animal Care and Policy Committee at the University of Alberta. Silver King and Homing Pigeons (obtained from a local supplier) were anaesthetized with a ketamine (65 mg/kg) - xylazine (8 mg/kg) cocktail (i.m.). Supplemental doses were administered as necessary. The animals were placed in a stereotaxic device with pigeon ear bars and beak adapter so that the orientation of the skull conformed to the atlas of Karten and Hodos (1967). Access to the mcIO was achieved by removing bone and dura on the right side of the head over the cerebellum. Glass micropipettes, filled with 2M NaCl and having tip diameters of 4-5 $\mu$ m, were advanced through the cerebellum and into the brainstem in order to record the activity of neurons in the mcIO. Electrodes were oriented 10° to the sagittal plane and advanced using an hydraulic microdrive (Frederick Haer & Co.) in an attempt to access areas of the mcIO sensitive to rotational optic flow. Neurons in the medial margin of the mcIO respond best to rotational optic flow, whereas neurons in the lateral half of the mcIO respond to translational optic flow (Winship and Wylie, 2001; see also Lau et al., 1998; Wylie et al., 1999; Crowder et al., 2000). The *rVA* and *rH45* neurons are located in the caudal and rostral mcIO, respectively (Winship and Wylie, 2001; Wylie et al., 1999). Extracellular signals were amplified, filtered and fed to a window discriminator, which produced TTL pulses, each representing a single spike time. TTL pulses were fed to a data analysis system (Cambridge Electronic Designs (CED) *1401plus*) and

peri-stimulus time histograms (PSTHs) were constructed using *Spike2* software (CED).

IO cells were easily identified based on a low firing rate of about 1 spike/s. After a cell was isolated, the optic flow preference was determined using various procedures. These included simply listening to the response to moving a large (90° X 90°) hand-held stimulus, consisting of dots, lines and squiggles, in various areas of the visual field, or quantifying the responses to panoramic optic flow produced by a planetarium projector. This device, modeled after that of Simpson et al. (1981), and the procedure for its use has been described in detail elsewhere (Wylie and Frost 1993, 1999b). The device consisted of a small cylinder pierced with numerous small holes. A light source was positioned inside the cylinder such that dots were projected onto the walls, floor and ceiling of the room. The cylinder was rotated about its long axis by a pen motor that was controlled by a function generator, thus producing rotational optic flow. The planetarium was suspended just above the bird's head in gimbals such that the axis of rotation could be positioned to any orientation in three-dimensional space. The cylinder oscillated at 0.1 Hz and a constant speed of 1°/s. Generally, we found that the most convenient way to confirm the flowfield preference was to use a computer-generated large-field stimulus and a procedure that is illustrated in Figure 4.1A (Winship and Wylie, 2001). A screen measuring 90° X 75° (width X height) was positioned in one of three locations relative to the bird's head: the frontal visual field (from 45° ipsilateral (i) to 45° contralateral (c) azimuth), the contralateral hemifield (from 45°c to 135°c azimuth), or the ipsilateral hemifield (from

45°i to 135°i azimuth). Drifting square wave or sine wave gratings of an effective spatial and temporal frequency were generated by a *VSGThree* (Cambridge Research Services) and back-projected (*InFocus* LP750) onto the screen. Direction tuning curves in each of the three areas of the visual field were obtained by moving the gratings in 8 different directions, 45° apart. Responses were averaged over at least 3 sweeps, where each sweep consisted of 5 seconds of motion in one direction, a 5 second pause, and 5 seconds of motion in the opposite direction, followed by a 5 second pause. Although this procedure did not necessarily elicit maximal modulation of the cell, it was quite useful for identifying *rVA* and *rH45* cells. When recording from the IO on the right side of the brain, *rVA* neurons respond best to forward (temporal to nasal; T-N), rightward, and backward (N-T) motion in the contralateral, frontal, and ipsilateral visual fields, respectively, whereas *rH45* neurons respond best to upward motion in the contralateral and frontal fields, and downward motion in the ipsilateral field (Winship and Wylie, 2001).

After identification of a neuron in mcIO as either *rVA* or *rH45*, the recording electrode was replaced with a glass micropipette (tip diameter 10-20µm) containing an anterograde tracer. In 5 cases low-salt cholera toxin sub-unit B (CTB; Sigma, St. Louis, MO, USA; 1% in 0.1M phosphate-buffered saline (PBS, pH 7.4)) was iontophoretically injected for 1-3 minutes (+4 µamps, 7 seconds on, 7 seconds off). In all other cases (n = 3), biotinylated dextran amine (BDA; Molecular Probes; MW=10000; 10% in 0.1M phosphate buffer (PB; pH = 7.4)) was iontophoretically

injected (+3  $\mu$ amps, 1sec ON, 1 sec OFF) for between 2 and 5 minutes. Following the injection, the electrode was left undisturbed for an additional 5 minutes.

After a survival time of 3 to 5 days, the animals were given an overdose of sodium pentobarbital (100 mg/kg) and perfused with saline (0.9%) followed by ice-cold paraformaldehyde (4% in 0.1M phosphate buffer (PB, pH 7.4)). The brains were extracted and post-fixed for 2-12 hours (4% paraformaldehyde, 20% sucrose in 0.1M PB) and placed in sucrose overnight (20% in 0.1M PB). The brain was then embedded in gelatin (10%) and placed back in the sucrose until the block sank. Frozen sections, 45 $\mu$ m thick, were collected in the coronal plane. The BDA or CTB was visualized using a cobalt chloride intensification of diaminobenzidine. These procedures have been described in detail elsewhere (BDA, Wylie et al., 1997; CTB, Lau et al., 1998; see also Wild, 1993; Veenman et al., 1992). The tissue was mounted on gelatin chrome aluminum coated slides, lightly counter-stained with Neutral Red, and examined using light microscopy.

The photomicrographs shown in Figure 4.2 were taken using a compound light microscope (Olympus Research Microscope BX60) equipped with a digital camera (Media Cybernetics CoolSNAP-Pro color digital camera). Adobe Photoshop software was used to compensate for brightness and contrast.

### *Nomenclature*

The avian cerebellum consists of a vermis without hemispheres, as is characteristic of mammalian species (Larsell, 1948; Larsell and Whitlock, 1952;

Whitlock, 1952). The pigeon vestibulocerebellum consists of the two most ventral folia of the posterior vermis: IXcd and X using the nomenclature in Karten and Hodos (1967) which we use, or IXb and X according to Arends and Zeigler (1991). Generally, folia IXcd and X are referred to as the uvula and nodulus, respectively (Larsell, 1948; Larsell and Whitlock, 1952; Whitlock, 1952). These folia extend laterally and rostrally to form the auricle of the cerebellum, which has been referred to as the paraflocculus and/or flocculus (Larsell, 1948; Larsell and Whitlock, 1952; Whitlock, 1952). We define the flocculus as the lateral part of folia IXcd and X where the CSA responds to rotational optic flow. More medially CSA responds best to translational optic flow (Wylie et al., 1993, 1998; Wylie and Frost, 1999a). The division between the rotation and translation cells in the vestibulocerebellum is quite distinct. The border resides 1.65-1.9mm from the midline in folium X, and 1.9-2.1mm from the midline in folium IXcd (see Fig. 11 of Wylie et al., 1993). Using CTB as a retrograde tracer, it has been shown that the olivary cells projecting to the translation areas of the vestibulocerebellum reside immediately lateral to those that project to the flocculus (Lau et al. 1998; Crowder et al., 2000). What we refer to as the flocculus corresponds to zone F described by Arends and Zeigler (1991), except the lateral unfoliated cortex found rostral to the auricle. We define the auricle as the part of the flocculus that is rostral to the point where the invagination between folia IXcd and X disappears (see Fig. 4.4G, 4.7H).

## Results

Experiments were performed in 8 pigeons. Prior to injection in mcIO, optic flow preference was reliably recorded and quantitatively identified as either the *rVA* or the *rH45* response type. Generally we found 2 or 3 cells of the same optic flow preference on a given penetration. We never found *rVA* and *rH45* cells on the same track. The direction tuning of the CSA for an *rH45* neuron in response to gratings drifting in the frontal, ipsilateral and contralateral regions of the visual field is shown in Figure 4.1A. Firing rate (spikes/sec relative to the spontaneous rate) is plotted as a function of the direction of motion in polar coordinates. This neuron was excited in response to largefield stimuli moving upward in the contralateral and frontal visual fields, and downward motion in the ipsilateral visual field (the neuron was in the right mcIO). Responses of an *rH45* neuron to the planetarium projector is illustrated in Figure 4.1B. This neuron (in the right IO) showed clear modulation to rotational optic flow about an axis oriented at 45° ipsilateral azimuth. Much less modulation was seen to rotation about the vertical axis, and no modulation was seen to rotation about an horizontal axis oriented at 45° contralateral azimuth.

Figure 4.2A shows a photomicrograph of a typical BDA injection site in the mcIO (case *rH45BDA2*). Compared to the BDA injection sites, the CTB injection sites were larger and the boundaries were not as well demarcated. Anterogradely labeled CF terminals were consistently found in the vestibulocerebellum contralateral to the injection sites. B-E show anterogradely labeled CFs in the flocculus. Consistent with Freedman et al. (1977), the terminals were restricted to the basal half of the molecular layer. In B, a CF in the molecular layer of the ventral auricle is

highlighted. In addition, labeled fibres in the olivocerebellar tract (OCT) can be seen on the right-hand side, just medial to the dorsolateral vestibular nucleus. B and E were from BDA injections, whereas C and D were from CTB injections.

Figure 4.3 shows drawings of the injection sites from all eight experiments. The BDA injection sites (Fig. 4.3B,E,H) were easy to illustrate as they were a uniform dark brown or black with well demarcated borders, and surrounded by a much lighter penumbra. These are faithfully drawn in Fig. 4.3. The CTB injection sites (Fig. 4.3C,D,F,G,I) were not as easy to illustrate. Although black at the centre the borders were not as clear, and a gradation of gray radiated from the injection site. Moreover, the degree of labeling at the CTB injection sites varied from case to case. Nonetheless we have attempted to use a similar scheme to draw the CTB injections: the black indicates the centres of the injections, and the surrounding gray indicates the apparent spread. We were very liberal with our estimates of the apparent spread. The injection sites of CTB injections were generally much larger than BDA injections and resulted in a greater amount of CF labeling in the flocculus. For the four cases illustrated on the top (Fig. 4.3B-E), *rH45* responses were recorded at the injection site, whereas *rVA* responses were recorded at the injection sites illustrated on the bottom (Fig. 4.3F-I). As expected from previous studies (Winship and Wylie, 2001; Wylie et al., 1999), there was a rostral-caudal separation of the *rH45* and *rVA* injection sites.

Figure 4.3A shows the functional topography of neurons sensitive to translational and rotational optic flow in the mcIO from previous neuroanatomical and electrophysiological studies (Winship and Wylie, 2001; Crowder et al., 2000; Wylie et

al., 1999). The rostral (dark gray) and caudal (light gray) areas of the medial part of the mcIO, contain *rH45* and *rVA* neurons, respectively (Winship and Wylie, 2001; Wylie et al., 1999). The lateral parts of the mcIO (cross hatching) contain the neurons that respond to translational optic flow and project to the ventral uvula and nodulus (Lau et al., 1998; Wylie and Frost, 1999a; Crowder et al., 2000). There are actually four different types of translation neurons. They are topographically organized in the mcIO, and project to different zones within folia IXcd and X (ventral uvula and nodulus) (see Wylie and Frost, 1999; Crowder et al., 2000). The most ventro-medial portion of the mcIO, (i.e. that area not shaded in Fig. 4.3A), along with parts of the ventral lamella, project to zone E of the cerebellar cortex (Arends and Voogd, 1989; Lau et al., 1998). Zone E spans the lateral edge of all folia outside the vestibulocerebellum. The topographical organization of the mcIO illustrated in Fig. 4.3A was useful for predicting which regions of the mcIO were involved in the injection because of spread of the tracer outside the target area.

Case *rH45*CTB2 Figure 4.4 shows camera lucida drawings of 9 coronal sections from case *rH45*CTB2. The injection site, the largest of the *rH45* injections, was found rostrally in the mcIO and is shown in more detail in Fig. 4.3D. Although centred in the *rH45* region, there was considerable spread, encroaching caudally into the *rVA* region and laterally to include some of the translation regions. In Figure 4.4, CF terminals are shown as shading in the molecular layer of the cerebellar cortex, and the route of the CFs to the cerebellum (the OCT described by Arends and Voogd, 1989),

is shown. Fibres from the injection site crossed the midline at the injection site and coursed laterally through the contralateral mcIO (Fig. 4.4B). The fibres continued laterally through the ventral region of the central nucleus of the medulla oblongata, along the dorsal border of the lateral reticular nucleus (Fig. 4.4B). The fibres then turned dorsally and continued rostrally through the parvocellular reticular nucleus, the plexus of Horsley, and the nucleus of the descending trigeminal tract (Fig. 4.4C,D). Upon reaching the vestibular nuclear complex, the fibres continued dorsally and rostrally along the lateral edge of the descending vestibular nucleus, passed through the fibres innervating the tangential nucleus, then coursed along the lateral edge of nucleus angularis and the dorsolateral vestibular nucleus (Fig. 4.4E-H). Now in the cerebellum, the fibres fanned out: some traveled laterally to enter the auricle, whereas others turned caudally, most heading to the white matter of the vestibulocerebellum.

As expected from the location of the injection site, CF terminals in the molecular layer were found laterally in folia IXcd and X (i.e. the flocculus, Fig. 4.4A-F) and the auricle (Fig. 4.4G-I). Fewer terminals were found more medially in the ventral uvula and nodulus (e.g. ventral X in Fig. 4.4B and C), and some were also found laterally in folia VIII and IXab (Fig. 4.4E-I). This corresponds to zone E described by Arends and Voogd (1989), which receives input from the ventromedial mcIO (Arends and Voogd, 1989; Lau et al, 1998). There were also some very faintly labeled CF terminals in zone E of folia III, IV and V (not shown).

A zonal organization of the CF terminals in the vestibulocerebellum is apparent in Figure 4.4, but this is better illustrated in with the transformation in Figure

4.5B. This shows the locations of anterogradely labeled CFs in the molecular layers of the vestibulocerebellum plotted on an “unfolded” sheet. Both the distance from the midline, measured under the microscope, and the rostro-caudal locations, based on the section number, are indicated. This representation is quite faithful, requiring a single transformation. The auricle, which is continuous with the rostro-lateral ends of folia IXcd and X (Fig. 4.4), has been split with a horizontal slice separating it into its dorsal and ventral aspects, and is plotted as continuous with the dorsal IXcd. Plots of these measurements are shown for all *rH45* and *rVA* cases in Figures 4.5 and 4.6, respectively. The solid lines indicate the radii of the Purkinje layers and the dark dots show the location of labeled CFs.

For case *rH45CTB2* anterogradely labeled CFs in the flocculus are plotted in Fig. 4.5B. Folium X was unusually large in this case (4.5mm wide) but there were three clear zones (see also Fig. 4.4B-F). One zone was located at the lateral extreme, centred 4.0mm from the midline, a second zone was centred about 2.8mm from the midline, and a third zone was centred about 1.7mm from the midline. We believe that the most medial zone is due to spread of the injection upon the translation regions in the mcIO. (As mentioned above, the border between the translation cells and the rotation cells in folium X is about 1.65-1.9mm from the midline (Wylie et al., 1993)). In folium IXcd there were two clear zones: a rostro-lateral zone that occupied the auricle (see also Fig. 4.4G-I), and a second caudo-medial zone centred about 3.0mm lateral to the midline (see also Fig. 4.4A-E). A few labeled CFs were found medially

in ventral IXcd, possibly due to encroachment of the injection into the *rVA* region (see below).

Case *rH45CTB1* The injection site for this case, shown in Fig. 4.3C, was relatively large. While it was centred in the *rH45* region, there was considerable spread, encroaching caudally into the *rVA* region and laterally to include the translation regions. Anterogradely labeled CFs observed in the vestibulocerebellum are plotted in Fig. 4.5A. The pattern of labeling was remarkably similar to case *rH45CTB2*. In folium X, there were three clear zones. One zone was on the lateral edge of the folium, centred approximately 3.75mm lateral to the midline, and a second was centred about 2.5mm from the midline. A third zone was centred about 1.3mm from the midline. These resemble the three zones in folium X from case *rH45CTB1* but on a slightly smaller scale. The medial zone is consistent with encroachment of the injection on the translation regions of the mcIO. The labeling in folium IXcd was also similar to that observed in case *rH45CTB2*. Across both the dorsal and ventral lamellae, there was a rostro-lateral zone that occupied the auricle and a second caudo-medial zone centred about 3.0mm from the midline. There was also a little labeling more medially. In ventral IXcd there was a small group centred 1.6mm from the midline, medial to the translation/rotation border and consistent with encroachment of the injection on the translation regions. In dorsal IXcd there was a small group centred about 2.2mm from the midline. Labeling in this region was typical of *rVA* injections (see below).

Outside the vestibulocerebellum there was some faintly labeled CF terminals in folium IXab, laterally, corresponding to the E zone, and more medially, corresponding to the C zone (Arends and Voogd, 1989).

Case rH45BDA1 The injection site for this case, shown in Fig. 4.3B, was relatively compact. It was centred in the heart of the *rH45* region and the spread was minimal. The location of anterogradely labeled CFs are plotted in Fig. 4.5C. There were two distinct bands in folium X, one at the rostral extreme, centred about 3.5mm from the midline, and a second more medially, centred about 2.3mm from the midline. (Folium X was rather small in this case, ~3.7mm wide). There appeared to be two zones in folium IXcd: one rostro-lateral zone occupied the auricle, and a second caudo-medial zone, centred about 3.1mm from the midline.

There was a single CF terminal observed outside the vestibulocerebellum. It was faintly labeled and found in folium IXab.

Case rH45BDA2 The injection site for this case is shown in Fig. 4.3E. The injection site was very compact, centred in the medial margin of the *rH45* region and the spread was minimal. The location of anterogradely labeled CFs are plotted in Fig. 4.5D. Little labeling was observed in folium X. In ventral X there was only one section that contained anterogradely labeled CFs. These were located at the lateral extreme and are consistent with the lateral zone labeling from the other 3-rH45 cases. In dorsal X there was a group of CFs centred about 2.75mm from the midline, corresponding to

the medial zone labeling from the other three cases. Two zones were found in folium IXcd: a rostro-lateral zone occupying the auricle and a second medio-caudal zone centred about 3.1mm from the midline. For this case, no CF labeling was found in other folia.

Summary of *rH45* injections In Figure 4.7A the four *rH45* cases are collapsed.

Because of the variability in the size of the folia across birds, especially with respect to folium X, the rostro-caudal and medio-lateral dimensions were first normalized. The width of folium X was normalized to 80% of the lateral edge of the auricle. The medial zones from the CTB cases, which we proposed are due to spread of the injections to the translation regions, have been omitted. Two clear zones in the flocculus emerge: one at rostro-lateral extent of folia IXcd and X and extending through the auricle, and a second caudo-medial zone. The sparse labeling medially in folium IXcd is from the two CTB cases, and could be due to spread of the injections beyond the *rH45* region, caudally into the *rVA* region.

Case *rVACTB1* This injection site, shown in Fig. 4.3F was very large and heavy, with tracer spread extending to the contralateral (left) mcIO. The injection site was centred on the medial margin of the *rVA* region in the right mcIO, but spread rostrally to include much of the *rH45* area, and laterally, incorporating the translation areas and parts of the dorsal lamella. On the left side of the cerebellum, heavy anterogradely labeling was seen throughout the flocculus, ventral uvula and nodulus and the C and E

zones of folia II-IXab. Fainter labeling was observed in the A zone across folia VIII and IXab. Because of the abundance of CF labeling, and the fact that the injection site included both the *rVA* and *rH45* regions of the right IO, the CF labeling on the left side of the cerebellum was not considered.

In the left mcIO the spread of the injection appeared to be confined to the *rVA* region. CF labeling on the right side of the cerebellum was confined to the flocculus and is plotted in Fig. 4.6A. In folium X, two zones were observed: a caudo-medial zone and rostro-lateral zone centred 1.8 and 3.1mm from the midline, respectively. Note that the rostro-lateral margin was basically devoid of labeled CFs. There were also two large zones in folium IXcd: a caudo-medial group was centred 2.3mm from the midline and a rostro-lateral group that was more prominent in ventral IXcd. There was some labeling in the auricle, but it was sparse, particularly in dorsal IXcd.

Case *rVACTB2* The injection in case *rVACTB2*, shown in Fig. 4.3G, was centred on the medial-rostral margin of the *rVA* region of the mcIO. Tracer spread rostrally into the *rH45* region and may have encroached laterally on the translation regions. The locations of anterogradely labeled CFs in the vestibulocerebellum are plotted in Fig. 4.6D. Despite a significant injection and apparent spread, a poverty of labeling was observed in the flocculus relative to other CTB injections. In folium X, only one large group of labeled fibres, centred 3.3mm from the midline and a second small group of fibres near the translation/rotation border (1.6mm from the midline) were observed. Two groups of fibres were observed in folium IXcd; one zone caudo-medial to the

auricle and centred 3.3mm from the midline, and a second sparse zone found medio-caudally near the translation/rotation border, 2.0mm from the midline. Labeled CFs were also observed in a single section in the dorsal auricle.

Elsewhere in the cerebellum, labeled CF terminals were seen laterally in folia IXab and VIII (zone E). Faintly labeled CFs were also seen in the C and E zones of folium VII.

Case *rVACTB3* The injection in case *rVACTB3*, shown in Fig. 3I, was centred on the *rVA* region of the mcIO, with little spread into adjacent regions, but possibly encroaching the medial margins of the translation region. Anterogradely labeled CFs in the vestibulocerebellum are plotted in Fig. 4.6B. Folium X was quite small in this animal, but two zones are apparent: a medio-caudal zone and a rostro-lateral zone, centred 1.8mm and 3.1mm from the midline, respectively. Two bands of fibres are observed in folium IXcd; one rostro-lateral zone centred 3.1mm from the midline and a second zone medio-caudal zone centred 2.3mm from the midline.

Labeled CFs were also found 0.15-0.4mm from the midline in the nodulus and ventral uvula, consistent with spread of the injection the caudal regions of the translation region of mcIO (Crowder et al., 2000), but these were not plotted in Fig. 4.6B. Some labeled CFs were also seen in zone E of folia VIII and IXab, and a few faintly labeled CFs were seen in the C zone of these folia.

Case *rVABDA1* This injection site, illustrated in Fig. 4.3H, was centred on the *rVA* region, with spread encroaching rostrally on the *rH45* region and laterally on the translation regions. Anterogradely labeled CFs in the flocculus are plotted in Fig. 4.6C. In folium X, a single band of CFs was observed. This band was more diffuse in dorsal X. There is a suggestion of two bands in folium IXcd: a rostro-lateral zone which spills into the auricle, and a smaller second zone medial and caudal to this zone, centred 2.2mm from the midline. There is a clear space between the two zones. CF labeling outside the flocculus was not observed.

Summary of *rVA* injections In Fig. 4.7B the five *rVA* cases are normalized and collapsed. In folium X, two zones emerge: a rostro-lateral zone and a caudo-medial zone. The data for folium IXcd are not as clear, but there is a suggestion of caudo-medial and rostro-lateral zones.

In Fig. 4.7C, the data from the *rH45* cases (i.e. Fig. 4.7A) is superimposed on top of the data from the *rVA* cases (i.e. Fig. 4.7B). *rH45* and *rVA* data are represented by light gray and black circles, respectively. The two *rH45* zones are interdigitated with two *rVA* zones. This is most convincing for folium X, where there is little overlap of the zones, but also apparent in folium IXcd. Starting medio-caudally and moving rostro-laterally, an *rVA* zone is followed by an *rH45* zone, a second *rVA* zone, and an *rH45* zone, which occupies the auricle.

## **Discussion**

In the present study anterograde tracers were iontophoretically injected into physiologically identified rotation-sensitive optic flow regions in the mclO in pigeons. The locations of anterogradely labeled CFs were then measured to determine the zonal organization of rotation-sensitive Purkinje cells in the flocculus. A clear zonal organization spanning both folium IXcd and X was revealed, consisting of two *rVA* zones interdigitated with two *rH45* zones. The zonal organization is idealized in Figure 4.8. In this figure, the *rVA* and *rH45* zones were superimposed on a representative set of tracings through the cerebellum. Borders between zones were delineated based on the normalized data presented in Figure 4.7. Dark gray and light gray shading is used to indicate the approximate position of *rVA* and *rH45* zones, respectively. This summary is cleaner than the actual data presented in Figures 4.5-4.7. However, we did have to contend with spread outside of the target areas (see Fig.4.3) and a high degree of variability in the size and shape of folia IXcd and X between birds (see Figs. 4.5 and 4.6).

Electrophysiological studies provide some support for this zonal organization. In the companion paper (Wylie et al., 2003) small deposits of anterograde tracers were made at locations where *rVA* and *rH45* CSA was recorded. The locations of the injections were then plotted on the summary shown in Figure 8. Although this was a small data set, there was 100% concordance: *rVA* CSA was recorded in the *rVA* zones, and *rH45* CSA was recorded in the *rH45* zones (see Fig. 4 of Wylie et al., 2003). There is also support from the electrophysiological study by Wylie et al. (1993). This study consisted of a much larger data set of CSA recordings in the

vestibulocerebellum, although there were no recordings from the auricle (i.e. the rostro-lateral *rH45* zone). There are two apparent *rVA* zones: one just lateral to the CSA responsive to translational optic flow, and a second zone located more laterally. In between the two zones, *rH45* CSA was recorded, consistent with the caudo-medial *rH45* zone revealed in the present study.

#### *CTB and the Potential Problem of Uptake by Fibres of Passage*

Previous reports have shown that CTB can be taken up by fibres of passage (e.g. Chen and Aston-Jones, 1995), but we feel this does not pose a problem for the present study for several reasons. First, the fibres from the mcIO pass through the contralateral mcIO at the same rostro-caudal level. If fibres of passage took up the tracer, we would have seen CF terminals in the cerebellum ipsilateral to the injection site and retrogradely labeled cells in the contralateral IO. A close examination of the sections revealed that there indeed were some retrogradely labeled cells scattered throughout the contralateral and ipsilateral IO. (Most were found at the same rostro-caudal level as the injection). However, these cells were very lightly stained. Neurons in pretectum and nucleus of the basal optic root, which project to the mcIO (Wylie, 2001), were very darkly stained in the same brains. With regard to the presence of anterogradely labeled CFs ipsilateral to the injection site, we examined the route of the ipsilateral OCT in these sections. Although we saw numerous faintly labeled fibres in the brainstem, at the level of the dorsolateral vestibular nucleus few fibres were labeled and they were extremely faint. Moreover, excluding case

*rVACTB1* where the injection spread across the midline, no CF terminals were observed in the molecular layers ipsilateral to the injection site. Second, for the present study the labeling of fibres of passage only poses a problem if, for example, an injection in the *rVA* region in the caudal mcIO labeled fibres originating from cells in the *rH45* region in the rostral mcIO. However, we found that the fibres from the injection crossed the midline directly, rather than traveling rostral or caudally before crossing the midline (see Fig. 4.4B). Third, if uptake by fibres of passage had been a problem, we would not have seen the complimentary pattern of labeling that we saw from the *rVA* and *rH45c* injections. The data in this regard was quite clear-cut, particularly for folium X (Fig. 4.7). Surely the data would have been noisier if uptake by fibres of passage posed a significant problem. Indeed we believe that the minimal overlap we did see was due from spread of the injection site beyond the intended target area. Finally, the results from the BDA experiments are in concordance with the CTB experiments. The BDA injections were quite localized and uptake by fibres of passage did not seem to pose much of a problem. Although a few (< a dozen in each case) retrogradely labeled cells were seen in the mcIO contralateral to the injection site, no fibres were seen in the ipsilateral OCT, and no CF terminals were seen in the ipsilateral cerebellar cortex. Moreover, contralateral to the injection site, only a single CF terminal was found outside the flocculus in the 3 BDA cases. In summary, a close examination of our tissue strongly suggests that uptake by fibres did not pose a significant problem.

*Comparison with the Zonal Organization of the Mammalian Flocculus*

Tan et al. (1995) used anterograde transport from the IO to identify the organization of CF inputs from the IO to flocculus in rabbits. They showed that CF inputs from the rostral dc and vlo, which contain *rH45* neurons (Leonard et al., 1988) terminated in two parasagittal zones (FZ<sub>I</sub> and FZ<sub>III</sub>), while inputs from the caudal dc, which contains *rVA* neurons (Leonard et al., 1988), terminated in two parasagittal zones (FZ<sub>II</sub> and FZ<sub>IV</sub>). Acetylcholinesterase histochemistry showed that olivocerebellar fibres innervating floccular zones FZ<sub>I</sub> and FZ<sub>III</sub> or FZ<sub>II</sub> and FZ<sub>IV</sub> traversed the white matter compartments FC<sub>I</sub> and FC<sub>III</sub> or FC<sub>II</sub> and FC<sub>IV</sub>, respectively, prior to terminating in the molecular layer. CSA in the rabbit flocculus in response to optokinetic stimulation also supports this organization: *rVA* CSA is found in zones FZ<sub>II</sub> and FZ<sub>IV</sub> while *rH45* CSA is found in zones FZ<sub>I</sub> and FZ<sub>III</sub> (De Zeeuw et al., 1994; Kusunoki et al., 1990).

The zonal organization of the flocculus in cats and rats closely resembles that of rabbits. The rat flocculus can be divided into four parasagittal strips: two zones receiving CF input from the caudal dc interdigitated with one zone receiving CF input strictly from the vlo and another zone receiving a projection from the rostral dc and vlo (Ruigrok et al., 1992). In cats, Gerrits and Voogd (1982) distinguished six floccular climbing fibre zones (F1-F6), and a seventh zone, F7, in the medial extension. Zones F1 and F4 of the cat are identical to FZ<sub>II</sub> and FZ<sub>IV</sub> in the rabbit (Tan et al., 1995; Voogd et al., 1996). FZ<sub>I</sub> and FZ<sub>III</sub> of the rabbit flocculus are subdivided further in the cat. FZ<sub>I</sub> consists of zones F5 + 6 + 7 in the cat (found medially) and

zone FZ<sub>III</sub> is divided into subzones F2 + 3 (found laterally). F1 and F4 receive CF input from the caudal dc, zones F3 and F6 from the rostral dc, and zones F2 and F5 are innervated by the vlo.

Data on the zonal organization of the primate flocculus is less conclusive than that of the cat, rat, rabbit, and pigeon. Acetylcholinesterase histochemistry in the macaque cerebellum has revealed white matter compartments in the flocculus and paraflocculus (Hess and Voogd, 1986; Voogd et al., 1987ab). Three compartments restricted to the flocculus and ventral paraflocculus appear to correspond to zones FC<sub>I-III</sub> of the rabbit (Voogd et al., 1987ab). Olivocerebellar fibres in the middle compartment of the flocculus and the ventral paraflocculus have been identified using injections of tritiated leucine in the caudal dc of the macaque (Voogd et al., 1987ab). However, an equivalent to FZ<sub>IV</sub> of the rabbit flocculus has not been identified in primates.

In the present study we show that the zonal organization in the flocculus of the pigeons is quite similar to that in mammalian species, particularly rabbits, and this pattern of interdigitation of *rVA* and *rH45* zones seems highly conserved. While the order of the zones presented here in pigeons appears to be reversed in transverse sections or reconstructions of the flocculus of rabbits (insofar as the most medial section appears to be an *rH45* region in rabbits and *rVA* in pigeons), this reversal in fact represents the differing topology of the avian and mammalian flocculus. In mammals, the area of the VbC containing the flocculus, termed the terminal hook, is folded back upon itself (Bolk, 1906, cited in Glickstein and Voogd, 1995; Voogd and

Glickstein, 1998; Nieuwenhuys et al., 1998). As a result, the order of zones viewed in transverse sections becomes reversed as compared to the pigeon, where such a topological transformation does not occur.

There are some differences with respect to the olivo-cerebellar input to the flocculus. In rabbits some of the CFs innervating the flocculus send collaterals to the ventral uvula and nodulus (Takeda and Maekawa, 1989a,b). Consistent with this, CSA in the ventral uvula and nodulus of rabbits responds to rotational optic flow. There are two *rVA* zones on either side of an *rH45* zone (Kusonoki et al., 1990; Wylie et al., 1995). In pigeons, it has been shown that the CSA in the ventral uvula and nodulus responds best to patterns of translational optic flow (Wylie et al., 1993, 1998; Wylie and Frost, 1993, 1999a) and the olivary input to the translation zones is from cells that reside lateral to the floccular projecting cells in the mcIO (Lau et al., 1998; Wylie et al., 1999; Crowder et al., 2000). We have previously suggested that the translation zones in the pigeon vestibulocerebellum are analogous to the most medial zone in the rabbit ventral uvula and nodulus (Lau et al., 1998; Crowder et al., 2000). Purkinje cells in this zone receive climbing fibre input from the beta subnucleus of the IO and are responsive to head tilt originating in the otolith organs (Shojaku et al., 1991; Barmack and Shojaku, 1992; Barmack et al., 1995). What this zone has in common with the translation zones in the pigeon VbC is that both would be active during self-translation. In the companion paper (Wylie et al., 2003) we show that there are differences between rabbits and pigeons with respect to the output of floccular Purkinje cells in the *rVA* and *rH45* zones.

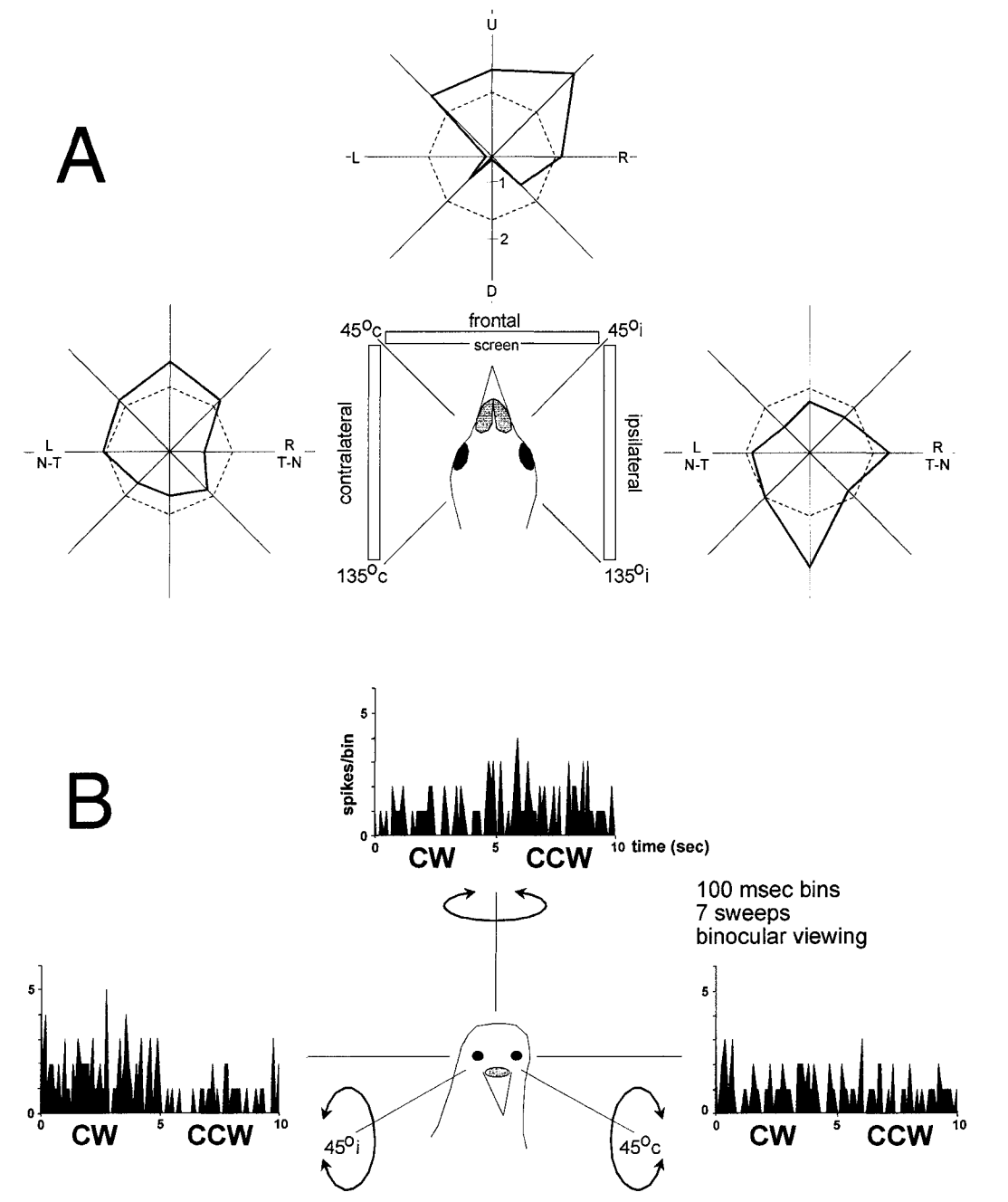


**Figure 4.1:** Largefield and optic flow stimulation of neurons in mcIO. In **A** the direction tuning of the CSA for an *rH45* neuron is shown. Cell type was confirmed by obtaining

Figure 4.1 continued: direction tuning curves in response to drifting gratings backprojected onto a screen that was positioned in one of three locations relative to the bird's head: the frontal visual field (from  $45^{\circ}$  ipsilateral (i) to  $45^{\circ}$  contralateral (c) azimuth), the contralateral hemifield (from  $45^{\circ}$ c to  $135^{\circ}$ c azimuth), or the ipsilateral hemifield (from  $45^{\circ}$ i to  $135^{\circ}$ i azimuth). Firing rate (solid line, in spikes/sec relative to the spontaneous rate) is plotted as a function of the direction of motion in polar coordinates. Spontaneous firing rate is represented by the dotted circle. This neuron was excited in response to largefield stimuli moving upward in the contralateral and frontal visual fields, and downward motion in the ipsilateral visual field (the neuron was in the right mcIO). In **B** the response of an *rH45* neuron to the panoramic optic flow produced by the planetarium projector are shown. Peri-stimulus time histograms (PSTHs) are shown for the response to rotational optic flow about three axes; the vertical axis (VA) and two horizontal axes oriented  $45^{\circ}$  to the midline. U, D, L, R = upward, downward, leftward, and rightward movement of the gratings, respectively; T-N, temporal-to-nasal; N-T, nasal-to-temporal; i, ipsilateral; c, contralateral; CW, clockwise optic flow; CCW, counter-clockwise optic flow.

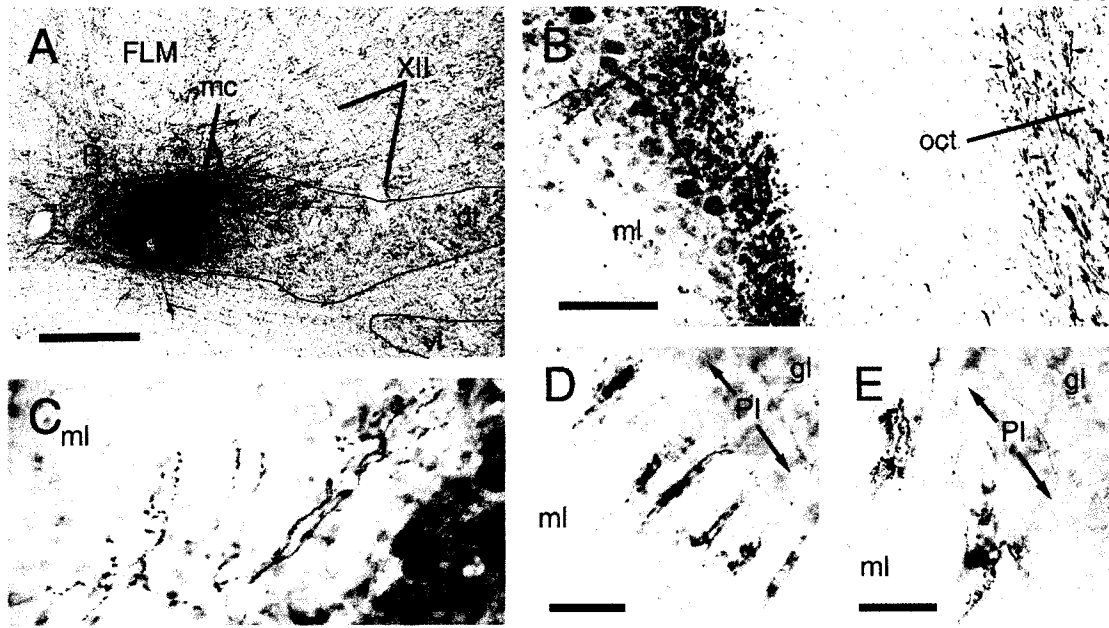


**Figure 4.2:** Photomicrographs of an injection site and labeled CFs in the flocculus. **A** shows a photomicrograph of a typical BDA injection site in the mIO (case *rH45BDA2*). **B-E** show anterogradely labeled CFs in the flocculus. In **B**, a CF in the molecular layer (ml) of the ventral auricle is highlighted. In addition, labeled fibres in the olivocerebellar tract (oct) can be seen on the right-hand side, just medial to the dorsolateral vestibular nucleus (VDL). **B** and **E** were from BDA injections, whereas **C** and **D** were from CTB injections. For other abbreviations, see list. Scale bars: **A**, 250  $\mu\text{m}$ ; **B**, 100  $\mu\text{m}$ ; **C-E**, 50  $\mu\text{m}$ .

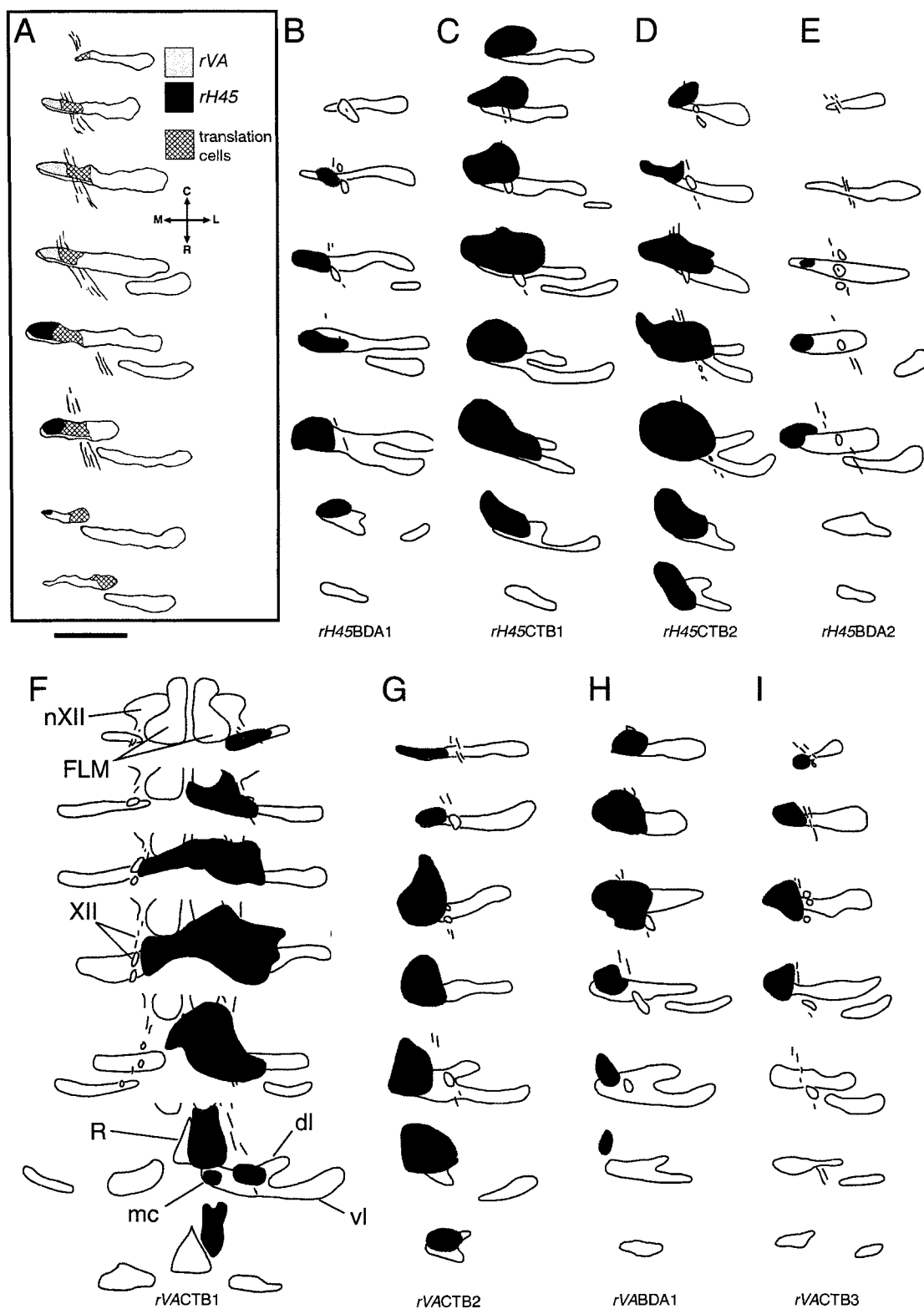


**Figure 4.3:** Injection sites at rotation-sensitive neurons in the medial column of the inferior olive (mcIO). A shows the functional topography of neurons sensitive to translational and rotational optic flow in the mcIO from previous neuroanatomical and

electrophysiological studies (Winship and Wylie, 2001; Crowder et al., 2000; Wylie et al., 1999; Lau et al., 1998). The mcIO is that part of the IO medial to the fibres of the twelfth cranial nerve (XII). The rostral and caudal areas of the medial part of the mcIO, contain *rH45* and *rVA* neurons, which are shown by the dark gray and light gray shading, respectively (Winship and Wylie, 2001; Wylie et al., 1999). The regions of the mcIO lateral to the *rVA* and *rH45c* regions contain the neurons that are sensitive to translational optic flow (cross hatching). The topographical organization of the mcIO illustrated in **A** was useful for predicting which regions of the mcIO were involved in the injection because of spread of the tracer outside the target area.

Tracings (caudal to rostral, each section approximately 260 $\mu$ m apart) of the injection sites from all eight experiments are illustrated in **B-I**. The black shading indicates the centres of the injections, and the surrounding gray indicates the apparent spread. **B-E** illustrated injections at sites where *rH45* responses were recorded, whereas *rVA* responses were recorded at the injection sites illustrated in **F-I**. C, R, M, and L = caudal, rostral, medial, and lateral, respectively. For other abbreviations, see list. Scale bar: 500 $\mu$ m.

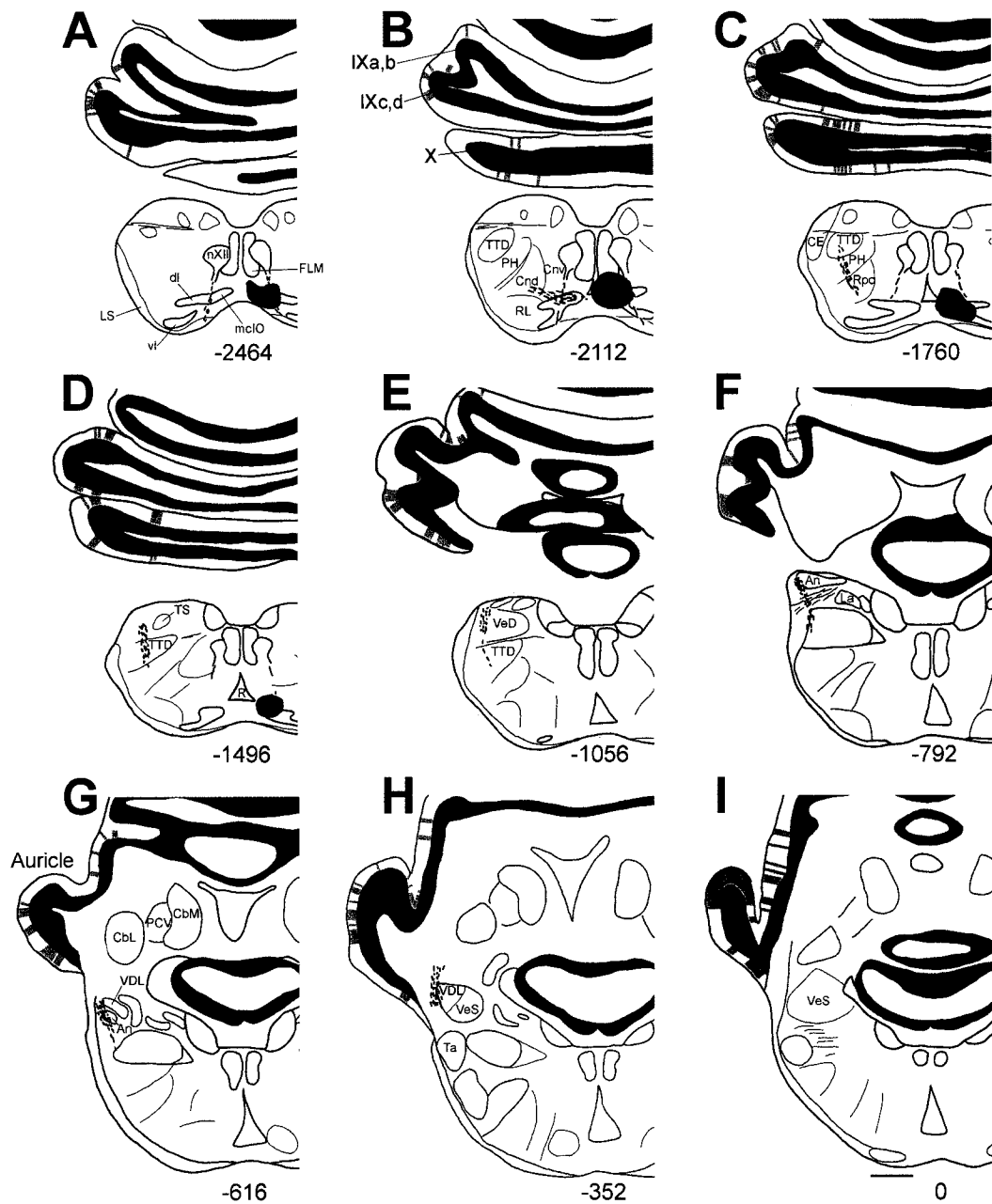


**Figure 4.4:** Reconstruction of case *rH45CTB2*. Camera lucida drawings from caudal (A) to rostral (I) are shown. The distance ( $\mu\text{m}$ ) of each section from the rostral-most section is indicated at the bottom. The injection site is shown in more detail in Fig. 4.3D. Labeled fibres crossed the midline at the injection site (Fig. 4.4B) and travelled laterally, dorsally and rostrally as the olivocerebellar tract (OCT). The labeled climbing fibre terminals are shown as shading in the molecular layer in the cerebellar cortex. For other abbreviations, see list. Scale bar: 1mm.

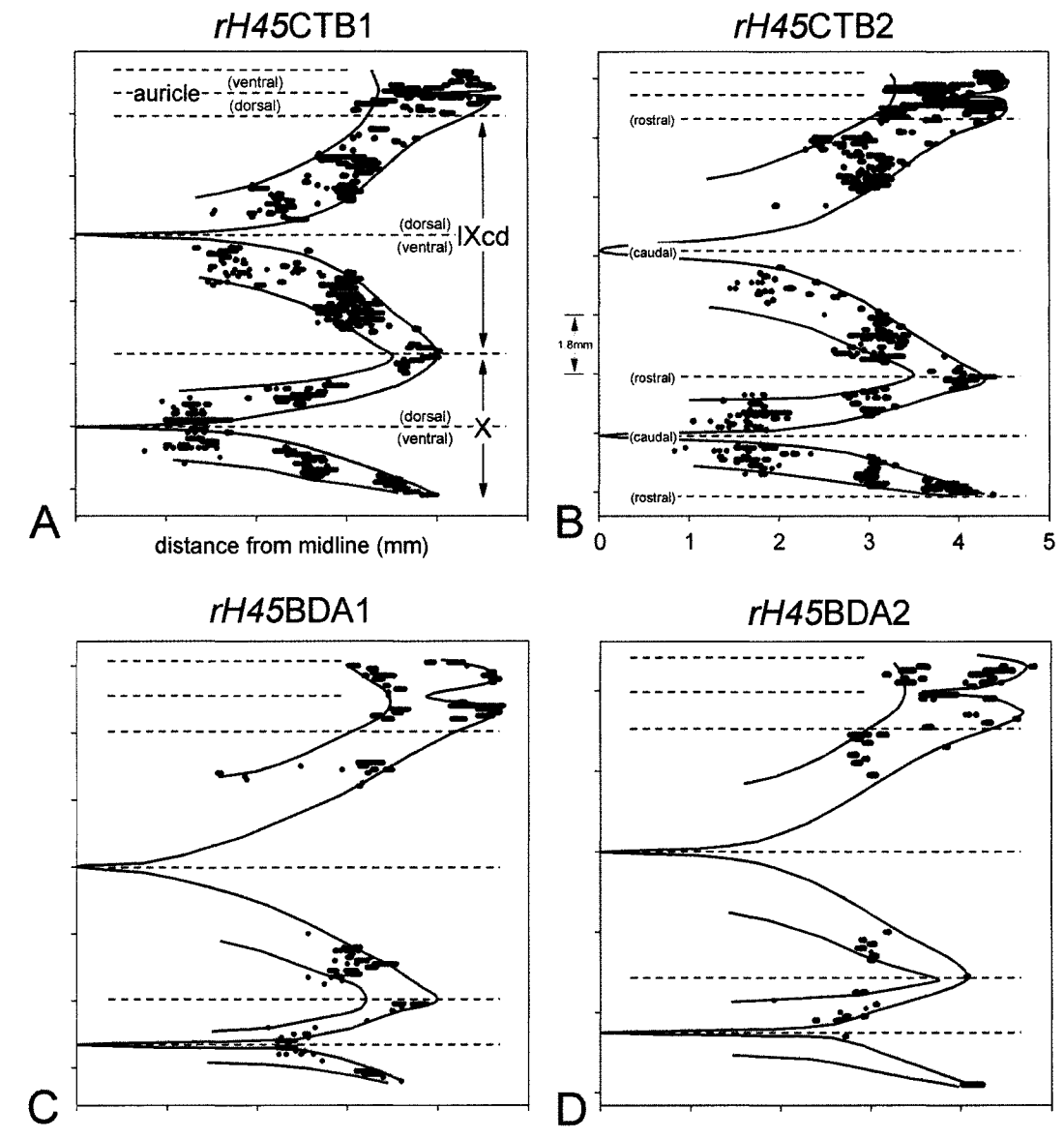


**Figure 4.5:** Labeled climbing fibres (CFs) in the flocculus contralateral to the *rH45* injection sites. The location of anterogradely labeled CFs in the molecular layer are plotted for each *rH45* case in A-D. Both the distance from the midline and the rostral-caudal location are indicated. The radii of the Purkinje layers are indicated by the solid lines and the dark dots show the location of labeled CFs.

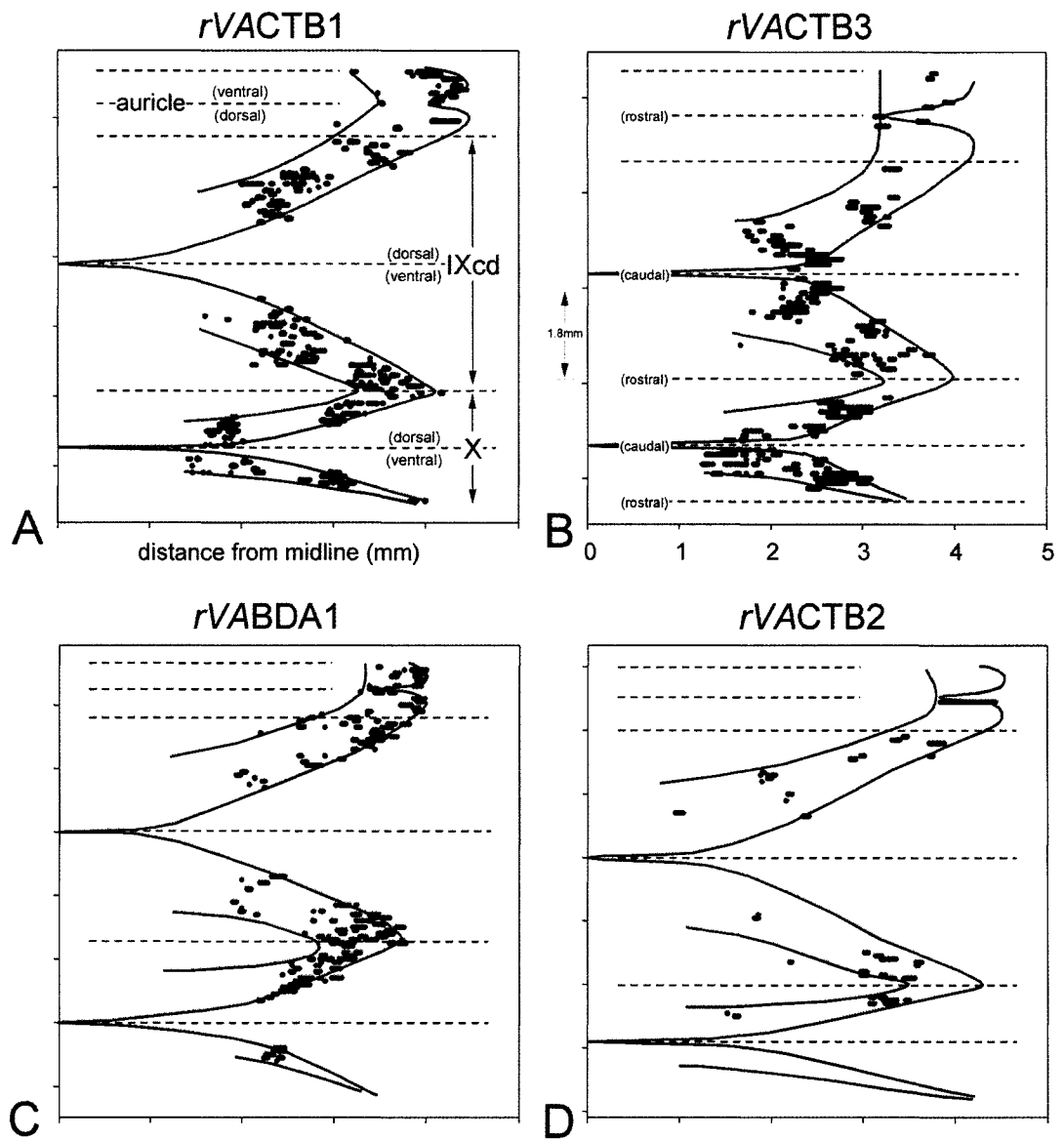
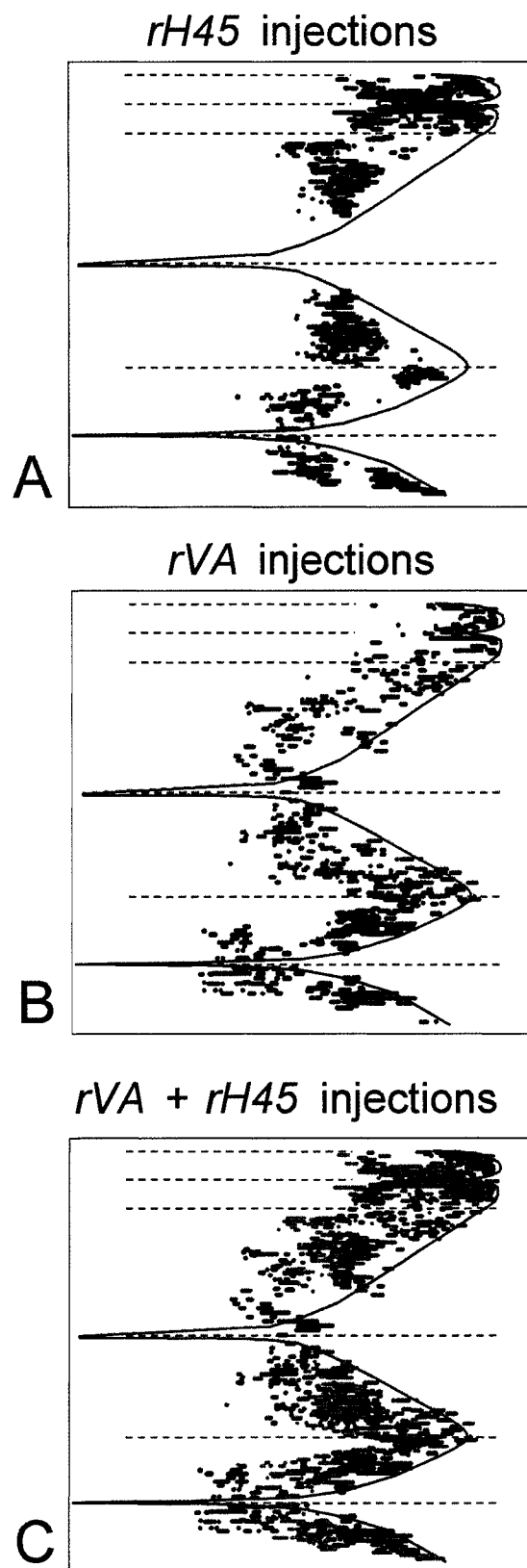


Figure 4.6: Labeled climbing fibres (CFs) in the flocculus contralateral to the *rVA* injection sites. See caption to Figure 4.5 for details.



**Figure 4.7:** Collapsed and normalized data for all cases. Because of the variability in the size of the folia across birds, especially with respect to folium X, the rostro-caudal and medio-lateral dimensions were first normalized before plotting. The four *rH45* cases are collapsed in **A**. Two clear zones in the flocculus emerge: one at rostro-lateral extent of folia IXcd and X and extending through the auricle, and a second caudo-medial zone. In **B**, the four *rVA* cases are collapsed. In folium X, two zones emerge: a rostro-lateral zone and a caudo-medial zone. The data for folium IXcd are less clear. In **C**, the data from the *rH45* cases (i.e. **A**) is superimposed on top of the data from the *rVA* cases (i.e. **B**). *rH45* and *rVA* data are represented by light gray and black circles, respectively. While considerable overlap occurred, two *rH45* zones appear to be interdigitated with two *rVA* zones.

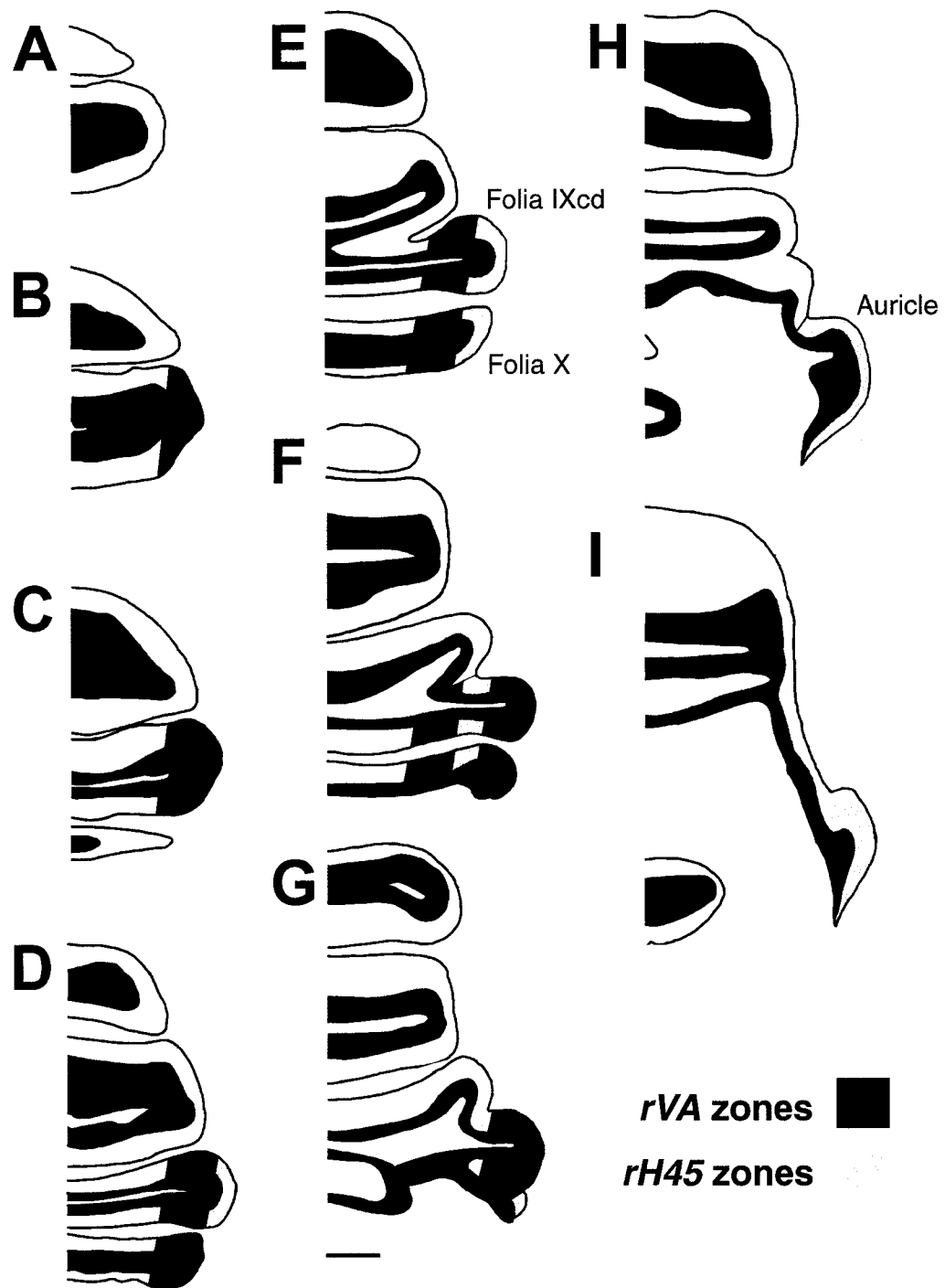


Figure 4.8: Zonal organization of the pigeon flocculus. In this figure, optic flow zones were superimposed on a representative set of tracings through the vestibulocerebellum (A-I, caudal to rostral, each approximately  $440\mu\text{m}$  apart). Borders between zones were delineated based on the normalized data presented in

Figure 4.8 continued:      Figure 7. Dark gray and light gray shading is used to indicate the approximate position of *rVA* and *rH45* zones, respectively. Scale bar: 1mm.

**References**

- Arends JJA, Voogd J. 1989. Topographic aspects of the olivocerebellar system in the pigeon. *Exp. Brain Res. Suppl.* 17:52-57.
- Arends JJA, Zeigler HP. 1991. Organization of the cerebellum in the pigeon (*Columba livia*): I. Corticonuclear and corticovestibular connections. *J Comp Neurol* 306:221-244.
- Barmack NH, Shojaku H. 1992. Representation of a postural coordinate system in the nodulus of the rabbit cerebellum by vestibular climbing fiber signals. In Shimazu H, Shimoda Y, editors: *Vestibular Control of Eye, Head and Body movements*. Basel: Japan Scientific Societies Press, Tokyo/ S. Karger, pp. 331-338.
- Barmack NH, Shojaku H. 1995. Vestibular and visual climbing fiber signals evoked in the uvula-nodulus of the rabbit cerebellum by natural stimulation. *J Neurophysiol* 74:2573-2589.
- Chen S, Aston-Jones G. 1995. Evidence that cholera toxin B subunit (CTB) can be avidly taken up and transported by fibers of passage. *Brain Res* 674:107-111.
- Crowder NA, Winship IR, Wylie DRW. 2000. Topographic organization of inferior olive cells projecting to translational zones in the vestibulocerebellum of pigeons. *J Comp Neurol* 419: 87-95.
- De Zeeuw CI, Wylie DR, DiGiorgi PL, Simpson JI. 1994. Projections of individual Purkinje cells of physiologically identified zones in the flocculus to the vestibular and cerebellar nuclei in the rabbit. *J Comp Neurol* 349:428-447.

- Ezure K, Graf W. 1984. A quantitative analysis of the spatial organization of the vestibulo-ocular reflexes in lateral and frontal-eyed animals. I. Orientation of semicircular canals and extraocular muscles. *Neuroscience* 12:85-93.
- Freedman SL, Voogd J, Vielvoye GJ. 1977. Experimental evidence for climbing fibers in the avian cerebellum. *J Comp Neurol* 175:243-52.
- Gerrits NM, Voogd J. 1982. The climbing fiber projection to the flocculus and adjacent paraflocculus in the cat. *Neuroscience* 7:2971-2991.
- Glickstein M, Voogd J. 1995. Lodewijk Bolk and the comparative anatomy of the cerebellum. *Trends Neurosci* 18:206-210.
- Graf W, Simpson JJ, Leonard CS. 1988. Spatial organization of visual messages of the rabbit's cerebellar flocculus. II. Complex and simple spike responses of Purkinje cells. *J Neurophysiol* 60:2091-2121.
- Hess DT, Voogd J. 1986. Chemoarchitectonic zonation of the monkey cerebellum. *Brain Res* 369:383-387.
- Karten HJ, Hodos W. 1967. *A Stereotaxic Atlas of the Brain of the Pigeon (Columba Livia)*. Baltimore: Johns Hopkins Press.
- Kusonoki M, Kano M, Kano M-S, Maekawa K. 1990. Nature of optokinetic response and zonal organization of climbing fibre afferents in the vestibulocerebellum of the pigmented rabbit. I. The flocculus. *Exp Brain Res* 80:225-237.
- Larsell O. 1948. The development and subdivisions of the cerebellum of birds. *J Comp Neurol* 89:123-190.

- Larsell O, Whitlock DG. 1952. Further observations on the cerebellum of birds. *J Comp Neurol* 97:545-566.
- Lau KL, Glover RG, Linkenhoker B, Wylie DRW. 1998. Topographical organization of inferior olive cells projecting to translation and rotation zones in the vestibulocerebellum of pigeons. *Neuroscience* 85:605-614.
- Leonard CS, Simpson JI, Graf W. 1988. Spatial organization of visual messages of the rabbit's cerebellar flocculus. I. Typology of inferior olive neurons of the dorsal cap of Kooy. *J Neurophysiol* 60:2073-2090.
- Kusunoki M, Kan M, Kano M-S, and Maekawa K. 1990. Nature of optokinetic response and zonal organization of climbing fibre afferents in the vestibulocerebellum of the pigmented rabbit. I. The flocculus. *Exp Brain Res* 80:225-237.
- Nieuwenhuys R, Donkelaar HJ, Nicholson C. 1998. *The Central Nervous System of Vertebrates*. Berlin: Springer-Verlag.
- Ruigrok TJH, Osse RJ, Voogd J 1992. Organization of inferior olivary projections to the flocculus and ventral paraflocculus of the rat cerebellum. *J Comp Neurol* 316:129-150.
- Shojaku H, Barmack NH, Mizukoshi K. 1991. Influence of vestibular and visual climbing fiber signals on Purkinje cell discharge in the cerebellar nodulus of the rabbit. *Acta Otolaryngol Suppl* 481:242-246.
- Simpson JI, Graf W. 1981. Eye-muscle geometry and compensatory eye movements in lateral eyed and frontal-eyed animals. *Ann New York Acad Sci* 374:20-30.

- Simpson JI, Graf W. 1985. The selection of reference frames by nature and its investigators. In: Berthoz A, Melvill-Jones G, editors: Adaptive Mechanisms in Gaze Control: Facts and Theories. Amsterdam: Elsevier. p. 3-16.
- Simpson JI, Graf W, Leonard CS. 1981. The coordinate system of visual climbing fibres to the flocculus. In Fuchs AF, Becker W, editors: Progress in Oculomotor Research. Amsterdam: Elsevier, pp. 475-484.
- Simpson JI, Graf W, Leonard CS. 1989a. Three-dimensional representation of retinal image movement by climbing fiber activity. In Strata P, editor: The Olivocerebellar System in Motor Control: Experimental Brain Research Supplement vol. 17. Heidelberg: Springer-Verlag. p. 323-327.
- Simpson JI, Leonard CS, Soodak RE. 1988a. The accessory optic system: analyzer of self-motion. *Ann New York Acad Sci* 545:170-179.
- Simpson JI, Leonard CS, Soodak RE. 1988b. The accessory optic system: II. Spatial organization of direction selectivity. *J Neurophysiol* 60: 2055-2072.
- Simpson, JI, Van der Steen J, Tan J, Graf W, Leonard CS. 1989b. Representations of ocular rotations in the cerebellar flocculus of the rabbit. In Allum JHJ, Hulliger M, editors: Progress in Brain Research vol. 80. Amsterdam: Elsevier. p. 213-223.
- Takeda T, Maekawa K. 1989b. Olivary branching to the flocculus, nodulus and ventral uvula in the rabbit. I. An electrophysiological study. *Exp Brain Res* 74:47-62.

- Takeda T, Maekawa K. 1989a. Olivary branching to the flocculus, nodulus and ventral uvula in the rabbit. II. Retorgrade double labeling study with fluorescent dyes. *Exp Brain Res* 76:323-332.
- Tan J, Gerrits NM, Nanhoe RS, Simpson JI, Voogd J. 1995. Zonal organization of the climbing fibre projection to the flocculus and nodulus of the rabbit. A combined axonal tracing and acetylcholinesterase histochemical study. *J Comp Neurol* 356:23-50.
- van der Steen J, Simpson JI, Tan J. 1994. Functional and anatomic organization of three-dimensional eye movements in rabbit cerebellar flocculus. *J Neurophysiol* 72: 31-46.
- Veenman CL, Reiner A, Honig MG. 1992. Biotinylated dextran amine as an anterograde tracer for single- and double-labeling studies. *J Neurosci Methods* 41:239-254.
- Voogd J, Gerrits NM, Hess DT. 1987a. Parasagittal zonation of the cerebellum in Macaques: an analysis based on acetylcholinesterase histochemistry. In Glickstein M, Yeo Ch, Stein J, editors: *Cerebellum and Neuronal Plasticity*. New York: Plenum. p. 15-39.
- Voogd J, Gerrits NM, Ruigrok TJH. 1996. Organization of the vestibulocerebellum. *Ann New York Acad Sci* 781: 553-79.
- Voogd J, Glickstein M. 1998. The anatomy of the cerebellum. *Trends Neurosci* 21: 370-375.

- Voogd J, Hess DT, Marani E. 1987b. The parasagittal zonation of the cerebellar cortex in cat and monkey. Topography, distribution of acetylcholinesterase and development. In King JS, editor: *New Concepts in Cerebellar Neurobiology*. New York: Liss, p.15.
- Whitlock DG. 1952. A neurohistological and neurophysiological study of afferent fibre tracts and receptive areas of the avian cerebellum. *J Comp Neurol* 97:567-635.
- Wild JM. 1993. Descending projections of the songbird nucleus robustus archistrialis. *J Comp Neurol* 338:225-241.
- Winship IR, Wylie DRW. 2001. Responses of neurons in the medial column of the inferior olive in pigeons to translational and rotational optic flowfields. *Exp Brain Res* 141:63-78.
- Wylie DRW. 2001. Projections from the nucleus of the basal optic root and nucleus lentiformis mesencephali to the inferior olive in pigeons (*Columba livia*). *J Comp Neurol* 429:502-513.
- Wylie DRW, Bischof WF, Frost BJ. 1998. Common reference frame for neural coding of translational and rotational optic flow. *Nature* 392:278-282.
- Wylie DRW, Brown MR, Barkley RR, Winship IR, Todd KG. 2003. Zonal organization of the vestibulocerebellum in pigeons (*Columba livia*): II. Projections of the rotation zones of the flocculus. *J Comp Neurol* 456: 140-53.

- Wylie DR, De Zeeuw CI, Simpson JJ. 1995. Temporal relations of the complex spike activity of Purkinje cell pairs in the vestibulocerebellum of rabbits. *J Neurosci* 15:2875-2887.
- Wylie DR, Frost BJ. 1993. Responses of pigeon vestibulocerebellar neurons to optokinetic stimulation: II. The 3-dimensional reference frame of rotation neurons in the flocculus. *J Neurophysiol* 70:2647-2659.
- Wylie DRW, Frost BJ. 1996. The pigeon optokinetic system: Visual input in extraocular muscle coordinates. *Vis Neurosci* 13:945-953.
- Wylie DRW, Frost BJ. 1999a. Complex spike activity of Purkinje cells in the ventral uvula and nodulus of pigeons in response to translational optic flowfields. *J Neurophysiol* 81:256-266.
- Wylie DRW, Frost BJ. 1999b. Responses of neurons in the nucleus of the basal optic root to translational and rotational flowfields. *J Neurophysiol* 81:267-276.
- Wylie DR, Kripalani T-K, Frost BJ. 1993. Responses of pigeon vestibulocerebellar neurons to optokinetic stimulation: I. Functional organization of neurons discriminating between translational and rotational visual flow. *J Neurophysiol* 70: 2632-2646.
- Wylie DRW, Linkenhoker B, Lau KL. 1997. Projections of the nucleus of the basal optic root in pigeons (*Columba livia*) revealed with biotinylated dextran amine. *J Comp Neurol* 384:517-536.

Wylie DRW, Winship IR, Glover RG. 1999. Projections from the medial column of the inferior olive to different classes of rotation-sensitive Purkinje cells in the flocculus of pigeons. *Neurosci Lett* 268:97-100.

**CHAPTER 5:**  
**SPATIO-TEMPORAL TUNING OF OPTIC FLOW INPUTS TO THE**  
**VESTIBULOCEREBELLUM IN PIGEONS: DIFFERENCES BETWEEN**  
**MOSSY AND CLIMBING FIBRE PATHWAYS**

**Full Citation:**

**Winship IR, Hurd PL, Wylie DR.** Spatiotemporal tuning of optic flow inputs to the vestibulocerebellum in pigeons: differences between mossy and climbing fiber pathways. *J Neurophysiol* 93:1266-77, 2005.

Self-motion through an environment consisting of stationary objects and surfaces results in distinct patterns of visual motion across the entire retina. These characteristic patterns are referred to as ‘optic flow’ or ‘flowfields’ (Gibson 1954). The analysis of optic flow is important for the generation of optokinetic responses, such as optokinetic nystagmus and the opto-collic reflex, which facilitate gaze stabilization (for review see Ilg 1997; see also Robinson 1981; Carpenter 1988; *birds*, Gioanni et al. 1981, 1983a,b; Gioanni 1988). Gaze stabilization is important to prevent the degradation of visual acuity (Westheimer and McKee 1975) and enhance velocity discrimination (Nakayama 1981).

Numerous studies, utilizing micro-stimulation, lesion, and electrophysiological methods, have implicated nuclei in the accessory optic system (AOS) and pretectum in the analysis of optic flow and the generation of optokinetic responses (for reviews see Simpson 1984; Simpson et al. 1988; Grasse and Cynader 1990). The AOS and pretectum are highly conserved, and homologous structures have been identified in mammalian and avian species (Fite 1985; McKenna and Wallman 1985a; Weber 1985). The mammalian AOS consists of the medial, lateral, and dorsal terminal nuclei (MTN, LTN, and DTN, respectively), which are equivalent to the nucleus of the basal optic root (nBOR) in birds. Likewise the pretectal nucleus of the optic tract (NOT) of mammals is equivalent to the avian pretectal nucleus lentiformis mesencephali (LM) (for reviews, see Simpson 1984; Simpson et al. 1988).

Physiological recordings from the AOS and pretectum from numerous species have shown that neurons in these nuclei have large, contralateral receptive fields and

exhibit direction-selectivity to large-field moving stimuli rich in visual texture (NOT: Collewijn 1975a,b; Hoffman and Schoppmann 1975, 1981; Hoffmann et al. 1988; Hoffmann and Distler 1989; Volchan et al. 1989; Klauer et al. 1990; Mustari and Fuchs 1990; Distler and Hoffmann 1993; Ilg and Hoffmann 1996; Yakushin et al. 2000; LM: Katte and Hoffmann 1980; McKenna and Wallman 1981, 1985b; Winterson and Brauth 1985; Fite et al. 1989; Fan et al. 1995; Wylie and Frost 1996; MTN/LTN; Simpson et al. 1979; Grasse and Cynader 1982; Grasse et al. 1984; Soodak and Simpson, 1988; *nBOR*, Burns and Wallman 1981; Morgan and Frost 1981; Gioanni et al. 1984; Wylie and Frost 1990; Rosenberg and Ariel 1990; Kogo et al. 1998, 2002; Ariel and Kogo 2001). Recent neurophysiological studies that used largefield sinusoidal gratings as stimuli showed that pretectal and AOS neurons show spatio-temporal tuning. This was first shown in the wallaby NOT (Ibbotson et al. 1994), and subsequently in the pigeon *nBOR* and LM (Wolf-Oberhollenzer and Kirschfeld 1994; Wylie and Crowder 2000; Crowder and Wylie 2001; Crowder et al. 2003a,b). These studies found that pretectal and AOS neurons fall into two groups based on a the location of the peak (maximal) response in the spatio-temporal domain: *slow* cells were maximally sensitive to motion at low temporal frequency (TF < 1 Hz) and high spatial frequency (SF > 0.25 cycles per degree, cpd), whereas *fast* cells were maximally sensitive to high TF (> 1 Hz) and low SF (< 0.25 cpd) sine wave gratings. Figure 5.1A depicts the *fast* and *slow* regions in the spatio-temporal domain. Ibbotson and Price (2001) noted that the spatio-temporal preferences of the *fast* and *slow* units in the pretectum of wallabies and pigeons were remarkably similar. We must caution

that the *fast/slow* distinction is not so simplistic. It is not uncommon for a *slow* neuron to show a secondary peak in the *fast* region, or a *fast* neuron to show a secondary peak in the *slow* region (Ibbotson et al. 1994; Wylie and Crowder 2000; Crowder and Wylie 2001; Crowder et al. 2003a). Such neurons likely receive inputs from *fast* and *slow* subunits.

The AOS and pretectum provide input to the optic flow sensitive neurons in the vestibulocerebellum (VbC) (for reviews see Simpson 1984; Simpson et al. 1988; *birds*, Clarke 1977; Brecha et al. 1980). In birds, there are two inputs from the LM and nBOR to the VbC: an indirect climbing fibre (CF) pathway through the medial column of the inferior olive (mcIO; Clarke 1977; Brecha et al. 1980; Gamlin and Cohen 1988; Arends and Voogd 1989; Lau et al. 1998; Wylie et al. 1999; Crowder et al. 2000; Wylie 2001; Winship and Wylie 2001, 2003) and a direct mossy fibre (MF) pathway that is mainly restricted to folium IXcd (Brauth and Karten 1977; Clarke 1977; Brecha and Karten 1979; Brecha et al. 1980; Gamlin and Cohen 1988; Wylie and Linkenhoker 1996; Wylie et al. 1997). The CF pathway to the VbC exists in mammals (for reviews see Simpson 1984; Simpson et al. 1988). The complex spike activity (CSA) of VbC Purkinje cells, which reflects CF input (Thach 1967), is direction-selective for particular patterns of optic flow (Simpson et al. 1981; Graf et al. 1988; Kano et al. 1990; Kusunoki et al. 1990; Wylie and Frost 1993, 1999; Wylie et al. 1998). The MF pathway has also been reported in turtles and fish (Finger and Karten 1978; Reiner and Karten 1978; Fan et al. 1993), but not in several mammalian species (Kawasaki and Sato 1980; Blanks et al. 1983; Giolli et al. 1984). Winfield et

al. (1978) reported a direct MF pathway from the MTN to the VbC in the chinchilla, although this finding has been contested (Giolli et al. 1984). In this study, in effort to determine whether the *fast* or *slow* cells in the AOS and pretectum feed the MF and CF pathways to the VbC, we recorded the responses of units in the granular layer of folium IXcd and the CSA of VbC Purkinje cells to sine wave gratings of varying TF and SF.

## **Methods**

### *Surgery and Extracellular Recording*

The methods reported herein conform to the guidelines established by the Canadian Council on Animal Care and approved by the Biosciences Animal Care and Policy Committee at the University of Alberta. Silver King pigeons (obtained from a local supplier) were anaesthetized using an intramuscular ketamine (65mg/kg) and xylazine (8mg/kg) mixture. Depth of anaesthesia was monitored via toe pinch and supplemental doses were administered as necessary. Body temperature was maintained via a thermal probe and heating pad (Fine Science Tools). The pigeons were placed in a stereotaxic apparatus with ear bars and beak adapter such that the orientation of the head conformed to the atlas of Karten and Hodos (1967). Sufficient bone and dura was removed to allow access to the VbC. Glass micropipettes with tip diameters of 4-5 $\mu$ m filled with 2M NaCl were used for the extracellular recordings. Micropipettes were advanced through the VbC via an hydraulic microdrive (Frederick Haer). The extracellular signal was amplified, filtered, and fed to a data acquisition

unit (Cambridge Electronic Designs (CED) 1401*plus*). The data was analysed off-line using Spike2 for Windows (CED). This included spike sorting and the construction of peri-stimulus time histograms (PSTHs).

### *Stimuli and Stimulus Presentation*

The procedures for stimulus construction and presentation were essentially identical to those described in previous studies from this lab that examined the spatio-temporal tuning of nBOR and LM units (Wylie and Crowder 2000; Crowder et al. 2003a,b, 2004). All stimuli were generated by a VSG*Three* (Cambridge Research Systems) graphics computer and back-projected (InFocus LP750) onto a screen measuring  $90^\circ \times 75^\circ$  (width  $\times$  height) that was positioned in the most responsive area of the receptive field. Upon identification and isolation of the CSA of P-cells or a GL unit, the direction preference and approximate receptive field boundaries were qualitatively determined by moving a large ( $90^\circ \times 90^\circ$ ) hand-held visual stimulus, consisting of black bars, squiggles, and dots on a white background, throughout the visual field. Subsequently, spatio-temporal tuning was quantified using 36-42 combinations of sine-wave gratings of varying SF (0.03-2 cycles per degree, cpd) and TF (0.03-24 cycles per second, Hz) moving in the preferred and anti-preferred direction for that unit. The contrast of the sine wave gratings was 0.95  $[(\text{Luminance}_{\text{MAX}} - \text{Luminance}_{\text{MIN}}) / (\text{Luminance}_{\text{MAX}} + \text{Luminance}_{\text{MIN}})]$  and the mean luminance was  $65 \text{cd/m}^2$ . The refresh rate was 80Hz. Each sweep for a particular SF/TF combination consisted of 4 seconds of motion in the preferred direction, a 3

second pause, 4 seconds of motion in the anti-preferred direction, followed by a 4 second pause. During the pauses the stimulus was a uniform gray of the standard mean luminance. Firing rates were averaged over 2 to 12 sweeps, and mean firing rates for motion in the preferred and anti-preferred direction were computed over the entire 4 second motion segment. For CSA, the firing rate is typically very low, thus we tried to obtain as many sweeps as possible (up to 12) for each SF/TF combination. This was generally not a problem as the units are not difficult to hold for long periods of time. For GL units, the firing rate is higher (at least 10-fold), but the units were extremely difficult to isolate and hold for long durations. We required a minimum of 2 sweeps, assuming the unit was well isolated.

#### *Quantification and Illustration of Spatio-Temporal Tuning*

To graphically illustrate tuning in the spatio-temporal domain, for each unit a contour plot of the mean firing rate as a function of SF and TF was made using *Sigma Plot*. TF and SF were plotted on the ordinate and abscissa, respectively, and firing rate (minus spontaneous rate) was plotted on the z-axis. The location of maximal excitation was referred to as the primary peak of the contour plot. A peak of lesser magnitude was termed a secondary peak. Concluding that a contour plot contained a single peak vs. two peaks was somewhat subjective (see contour plots in Figures 5.1B, 5.2 and 5.3). To be classified as a secondary peak, it had to be clearly separable from the background activity and distinct from the primary peak by visual inspection, and a consistent response of greater than 40% the magnitude of the primary peak was

necessary. (The contour plots shown in Figures 5.1B and 5.3C are representative in this regard).

To identify the precise location of the primary and secondary peaks, each peak was fit to a 2-D Gaussian function using a slightly modified version of the method of Perrone and Thiele (2001):

$$G(\mathbf{u}, \omega) = \{\exp[-(\mathbf{u}')^2 / \sigma_x^2]\} \times \{\exp[-(\omega')^2 / \sigma_y^2]\} + P$$

where

$$\mathbf{u}' = (\mathbf{u} - \mathbf{x}) \cos \theta + (\omega - \mathbf{y}) \sin \theta$$

$$\omega' = -(\mathbf{u} - \mathbf{x}) \sin \theta + (\omega - \mathbf{y}) \cos \theta$$

where  $\mathbf{u}$  is  $\ln(\text{SF})$ ,  $\omega$  is  $\ln(\text{TF})$ ,  $\theta$  is the angle of the Gaussian,  $(\mathbf{x}, \mathbf{y})$  is the location of the peak of the Gaussian,  $\sigma_x$  and  $\sigma_y$  are the spread of the Gaussian in the  $\mathbf{u}'$  and  $\omega'$  dimensions, respectively, and  $P$  is a constant reflecting the spontaneous activity of the cell.  $\sigma_x$ ,  $\sigma_y$ ,  $\mathbf{x}$ ,  $\mathbf{y}$ ,  $\theta$ , and  $P$  were optimized to minimize the sum of the mean error between the actual and  $G$  values using the solver function in *Microsoft Excel*. Not all of the data points from the contour plots were necessarily included in the Gaussian fits. In cases where there were two peaks in the contour plot, the points corresponding to each peak were fit separately (e.g. see Fig. 5.3C,D). In addition, for some contour plots with single peaks spurious values distant from the peak were omitted (e.g. Fig. 5.2A,B and C,D).

In order to determine whether the CSA and GL primary peaks were located in the *fast* or *slow* regions of the spatio-temporal domain, we first used a hierarchical cluster analysis to divide a group of 118 cells from previous studies of LM and nBOR

(Wylie and Crowder 2000; Crowder and Wylie 2001; Crowder et al. 2003a,b) into two groups based on the SF ( $x$ ) and TF ( $y$ ) of their primary peaks. (These are plotted in Figure 5.4C). Post-hoc inspection of the classification showed that the two largest clusters corresponded to *fast* and *slow* cells. We then determined a linear discriminant function to discriminate *fast* from *slow* cells using the cluster analysis results as a training set. The discriminant function was then used to calculate the posterior probabilities of *fast* or *slow* memberships for GL units and the CSA of P-cells recorded in the present study. All analyses were conducted in *R* (Ihaka & Gentleman 1996). We used the `hclust()` function from the “stats” library, with the “Ward’s” method, to perform the cluster analysis. The `lda()` function of the MASS library (Venables & Ripley 2002) was used for the linear discriminant analysis.

### *Quantification of Velocity Tuning*

In addition to providing the location of the spatio-temporal peak, the Gaussian function was also used to evaluate velocity tuning (velocity = TF/SF) following the procedure used by Priebe et al. (2003; a variant of a method devised by Levitt et al. (1994). Units showing velocity tuning would have a  $\theta$  value approaching  $45^\circ$ . When plotted on a contour plot, the peak of a unit tuned to velocity is elongated and oriented such that it has a slope of about 1 on log-log axes. This contrasts with a unit that shows “spatio-temporal independence”, i.e. it responds maximally to a given TF irrespective of the SF. Such a unit would have a non-oriented peak in the contour plot (i.e.  $\theta$  approaching  $0^\circ$  or  $90^\circ$ ). To evaluate whether a unit showed velocity tuning as

opposed to spatio-temporal independence, the primary peak for each unit was fit to a 2-D Gaussian as described above but with  $\theta$  constrained to either  $45^\circ$  to provide the velocity-tuned prediction, or to  $0^\circ/90^\circ$  to provide the independent prediction. We then computed the partial correlation of the actual response with the velocity or independent prediction using the following equations:

$$R_{\text{ind}} = \frac{(r_i - r_v * r_{iv})}{\sqrt{((1 - r_v^2)(1 - r_{iv}^2))}}$$

$$R_{\text{vel}} = \frac{(r_v - r_i * r_{iv})}{\sqrt{((1 - r_i^2)(1 - r_{iv}^2))}}$$

where  $R_{\text{ind}}$  and  $R_{\text{vel}}$  are the partial correlations of the actual response to the independent and velocity predictions, respectively;  $r_i$  is equal to the correlation of actual response with the independent prediction;  $r_v$  is the correlation of the actual data with the velocity prediction; and  $r_{iv}$  is the correlation of the two predictions.

The statistical significance of  $R_{\text{vel}}$  and  $R_{\text{ind}}$  was calculated by performing a Fisher Z-transform on the correlation coefficients  $\{Z_f = 1/2 \times \ln[(1+R)/(1-R)]\}$ , and then calculating the difference between these z-scores (Papoulis 1990):

$$z_{\text{diff}} = (Z_{f_v} - Z_{f_i}) / ((1/(N_v - 3)) + 1/(N_i - 3))^{1/2}$$

where  $Z_{f_v}$  is the Fisher Z-transform for  $R_{\text{vel}}$ ,  $Z_{f_i}$  is the Fisher Z-transform for  $R_{\text{ind}}$ , and  $N_v = N_i =$  number of SF/TF combinations used in the best-fit Gaussian. With this statistic, cells were categorized as velocity-tuned if  $z_{\text{diff}} \geq 1.65$  and  $R_{\text{vel}}$  was significantly greater than 0. Likewise cells were categorized as independent if  $z_{\text{diff}} \leq -1.65$  and  $R_{\text{ind}}$  was significantly greater than 0. Cells not meeting these criteria were

termed unclassifiable ( $1.65 > z_{diff} > -1.65$ ). The conventional criterion probability of 0.1 was used (Crow et al. 1960). This criterion has been justified by the fact that this method is not a true test for statistical significance, but a convenient way to reduce data (see Movshon et al. 1985; Gizzi et al. 1990; Scannell et al. 1996).

### *Histology*

In some cases dye spots were made at recording sites in the granular layer via iontophoretic injection of pontamine sky blue. At the end of these experiments, animals were given a lethal overdose of sodium pentobarbital (100 mg/kg) and immediately perfused with ice-cold saline followed by 4% paraformaldehyde in phosphate buffer (PB). The brains were extracted and post-fixed (4% paraformaldehyde in PB with 30% sucrose) for 2-12 hours and then placed in 30% sucrose solution in PB for 12-24 hours. Frozen coronal sections (40  $\mu$ m thick) through VbC were collected and mounted onto gelatine-coated slides. Sections were counterstained with neutral red and light microscopy was used to localize dye spots.

### **Results**

We recorded the spatio-temporal tuning of 17 GL units and the CSA of 39 P-cells in VbC from 19 birds in this study. CSA was recorded in the molecular layer of folia IXcd and X, and displayed the characteristic low spontaneous activity of about 1 spikes/s ( $0.98 \pm 0.11$  spikes/s; mean  $\pm$  s.e.m.). Visually-sensitive GL units were extremely difficult to isolate and hold, but were easily distinguished from CSA by a

much higher spontaneous rate ( $26.10 \pm 3.68$  spikes/s; mean  $\pm$  s.e.m.). The dye spots made at GL recording sites were all located in the granular layer of folia IXc,d. As expected, in response to the battery of drifting sine wave gratings, CSA and visual GL units showed clear spatio-temporal tuning.

### *Spatio-Temporal Tuning of GL units*

Consistent with previous studies, only a fraction (less than 10%) of the GL units were modulated by optic flow stimuli (Fan et al. 1993; Waespe et al. 1981). Moreover, consistent with Wylie et al. (1993), we found that the visual GL units had monocular receptive fields in either the ipsilateral ( $n = 11$ ) or contralateral ( $n = 6$ ) visual field, and showed directional tuning to largefield stimuli. Different direction preferences (similar to those in LM and nBOR) were observed, but GL units with dissimilar direction selectivity did not have any apparent differences with respect to spatio-temporal tuning.

Figure 5.1B shows a contour plot illustrating the spatio-temporal tuning of a GL unit. This unit had a primary peak in the *fast* zone, and a slightly smaller secondary peak in the slow zone. Based on the best-fit Gaussian, the primary peak was localized to SF = 0.10 cpd, TF = 13.47 Hz and the secondary peak was located at SF = 1.0 cpd, TF = 0.28 Hz. PSTHs on the right show the unit's modulation during stimulation in the preferred and antipreferred direction for gratings of three different SF – TF combinations during a single sweep. The first 4 seconds show response to movement in the preferred direction, followed by a 3 second pause, 4 seconds of

motion in the anti-preferred direction, and another 3 second pause. Clear excitation and inhibition to motion in the preferred and anti-preferred direction, respectively, are seen for PSTHs in the primary peak (SF = 0.125 cpd, TF = 16 Hz) and secondary peak (SF = 1 cpd, TF = 0.5 Hz), though this modulation is clearly greater for the primary peak. Considerably less modulation is seen outside these peaks (i.e. SF = 0.25 cpd, TF = 2 Hz). Evident in the PSTHs, the responses included both transient and steady state components. (This was the also the case for CSA). Transients and other temporal factors have been extensively analyzed in previous studies of spatio-temporal tuning in the AOS and pretectum (Ibbotson et al. 1994; Price and Ibbotson 2002; Wolf-Oberhollenzer and Kirschfeld 1994) and will not be analyzed further in this paper.

Figure 5.2 shows the contour plots of the spatio-temporal tuning of two additional GL units. The unit in Fig. 5.2A showed a single peak in the *fast* region. Figure 5.2B shows the plot of the normalized best-fit Gaussian for this unit. The peak was located at SF = 0.06 cpd, TF = 2.03 Hz. Figure 5.2C,D show the contour plot and normalized best-fit Gaussian, respectively, for a GL unit with a single peak in the *slow* zone (SF = 1.0 cpd, TF = 0.03 Hz). Eight (47.1%) GL units had a single peak in the contour plot (as in Fig. 5.2), whereas 9 of the GL units (52.9%) had secondary peaks in their contour plots (as in Fig. 5.1B). Secondary peaks were always located in the opposite spatio-temporal domain and had a magnitude, on average, 73.4% the size of the primary peak (range, 43.4 - 98.5%).

Figure 5.4A plots the locations of the primary peaks of all 17 GL units, as determined from the best-fit Gaussians. As described in the methods, the locations of

the peaks were assigned to either the *fast* or *slow* regions based on previous data of spatio-temporal tuning of LM and nBOR neurons (Wylie and Crowder 2000; Crowder and Wylie 2001; Crowder et al. 2003a,b). In Figure 5.4C the primary peaks of nBOR and LM neurons is plotted along with data from the current study. Eight (47.1%) GL units were classified as *fast* cells (low SFs/high TFs; mean = 0.13cpd/8.24Hz), whereas 9 (52.9%) GL units were *slow* cells (high SFs/low TFs; mean = 0.68cpd/0.30Hz; see also Table 1). The clustering into *fast* (white diamonds) and *slow* (grey diamonds) groups can be clearly seen in Fig. 5.4A (see also Fig. 5.4C).

Figure 5.5A and 5.5B show the normalized average contour plots of spatio-temporal tuning for *slow* and *fast* GL units, respectively. These were calculated by normalizing the contour plot of each unit, then averaging across all 9 *slow* units and 8 *fast* units. While the *slow* units clearly respond maximally to the gratings in the *slow* region, and the *fast* units clearly respond more to *fast* gratings, note the influence of the subset of units (9 GL units) that had secondary peaks in the region opposite the primary peak. Five *fast* units had secondary peaks in the *slow* zone and 4 *slow* units had secondary peaks in the *fast* regions.

#### *Spatio-Temporal Tuning of the CSA of Purkinje Cells*

Previous studies in pigeons have shown that VbC Purkinje cells have binocular, virtually panoramic receptive fields, and the CSA responds best to optic flow patterns resulting from self-translation or self-rotation along/about a particular axis in 3-dimensional space (Wylie and Frost, 1993, 1999; Wylie et al., 1998). Based

on the orientation of the preferred axis of rotation/translation, there are two classes of rotation neurons and four-classes of translation neurons. Rotation-sensitive neurons in VbC respond best to optic flow rotating about either the vertical axis (VA) or an axis orientated  $45^\circ$  contralateral to the midline in the horizontal plane ( $45^\circ$  c azimuth). Translation-sensitive neurons respond best to translational optic flow moving upward or downward along the VA, forward along an axis at  $45^\circ$  c azimuth, or backward along an axis orientated at  $45^\circ$  ipsilateral azimuth. In the present study, all six classes were represented in the sample of 39 units (24 rotation neurons, and 15 translation neurons). The different groups did not differ with respect to spatio-temporal tuning, thus they have all been grouped together.

Figure 5.3 shows representative contour plots and best-fit Gaussians for the CSA of 2 Purkinje cells. In Figure 5.3A,B, a cell with a single peak in the *slow* domain of the contour plot is illustrated. From the best-fit Gaussian, the peak was located at SF = 0.66 cpd, TF = 0.18 Hz. In Figure 5.3C,D, a cell with a primary peak in the *slow* zone and a secondary peak in the *fast* zone is shown. From the best-fit Gaussian the primary peak was located at 0.77cpd/0.10 Hz and the secondary peak was located at 0.11 cpd/18.0 Hz. Of the 39 CSA recordings, 11 (28.2%) of the contour plots showed a single peak, whereas 28 (71.8%) showed a secondary peak as well. On average, the secondary peak was 69.8% (range, 51.2 – 97.9%) the size of the primary peak. For 2 of these units the magnitude of the secondary peak was greater than 90% of the primary peak, making the assignment of primary and secondary peak more problematic.

Figure 5.4B plots the locations of the primary peaks of the CSA of 39 P-cells in this study. These are also plotted in Figure 5.4C along with the GL units and the nBOR and LM data from previous studies (Wylie and Crowder 2000; Crowder and Wylie 2001; Crowder et al. 2003a,b). Using the linear discriminate function described previously, 38 (97.4%) of the CSA units were classified as *slow* units (mean = 0.67cpd/0.35Hz; grey hexagons in 4A), while one unit was classified as a *fast* unit (white hexagon in Fig. 5.4C, primary peak at 0.10cpd/0.55Hz). This *fast* unit had a secondary peak of approximately equal magnitude (96.5%) located in the *slow* zone (0.42cpd/0.43Hz). Twenty-seven of the 38 *slow* units had secondary peaks, and 25 of these were in the *fast* region.

Figure 5.5C shows the normalized average contour plots of spatio-temporal tuning for the CSA of all 39 P-cells. The average plots clearly illustrate the dominance of *slow* spatio-temporal tuning in CSA, though the influence of secondary peaks in a subset of CSA (71.8%) is apparent with the smaller peak in the *fast* region. Note the similarity of the contour plots for the *slow* GL units and the CSA. Note also that the peaks for the *slow* GL units and CSA are sharper than that of the *fast* units, reflecting the fact that for the *fast* units the primary peaks are not as tightly clustered (Fig. 5.4A).

### *Velocity-Like Tuning*

In Figure 5.3A, note that peak for this unit is elongated, and oriented such that it has a slope of about 1 on a log-log axis. This suggests that the cell shows velocity tuning (velocity = TF/SF) to about 0.25 °/sec (see diagonal scale on the contour plot).

As the response is not independent of SF, this has been more appropriately termed velocity-like tuning (Zanker et al. 1999; Crowder et al. 2003a). In the present study, many of the peaks that were in the *slow* zone were oriented such that they approached velocity-like tuning (e.g. Fig. 5.1B, 5.2C, 5.3A). As described in the methods, following Priebe et al. (2003), neurons were classified as velocity tuned, independent, or unclassified based on the partial correlations of the actual data for each unit to velocity and independent predictions. Using the criteria described in the methods, the CSA of 10 (26.3%) *slow* P-cells showed velocity-like tuning, 5 (13.2%) showed independence, and 23 (60.5%) fell into the unclassified group. The single *fast* CSA was also unclassified. For the 8 *fast* GL units, 4 (50%) showed SF/TF independence, 1 (12.5%) was velocity-tuned and 3 (37.5%) were in the unclassified group. For the 9 *slow* GL units, all fell into the unclassified group.

Figure 5.6 shows a scatter plot of  $R_{vel}$  vs.  $R_{ind}$  for all units. For convenience, the black solid lines have been added to provide an approximation of the divisions between velocity-tuned, unclassified, and independent regions. This line represents the statistical criteria separating these groups based on 24 points in the best-fit Gaussian. (The actual number of points in the best-fit Gaussians ranged from 12-42 (mean = 24), hence this line is an approximation between the divisions). Note the CSA that showed velocity tuning in the upper left (black hexagons) and the fast GL units that showed SF/TF-independence in the bottom right (white diamonds with black borders).

## Discussion

In this study we examined the spatio-temporal tuning of the CSA of VbC Purkinje cells and GL units in folium IXcd of the VbC in response to largefield sine-wave gratings of varying SF and TF drifting in the preferred direction. We found that these units were tuned in the spatio-temporal domain. GL units could be classified into two groups: *fast* units showed a maximal response to low SF/high TF gratings, whereas *slow* units showed a maximal response to high SF/low TF. In contrast all but one of the CSA recordings was classified as a *slow* unit.

### *Comparison with Spatio-Temporal Tuning in the Pretectum and AOS*

Spatio-temporal tuning in the optokinetic system was originally demonstrated by Ibbotson et al. (1994), who recorded from the pretectum in wallabies. Subsequently, Wylie and Crowder (2000) showed strikingly similar results in the pretectal nucleus LM and the nBOR of the AOS in pigeons (Wolf-Oberhollenzer and Kirschfeld 1994; Crowder and Wylie 2001; Crowder et al. 2003a,b). The results from these previous studies closely parallel those in this study. Like CSA and GL units, LM and nBOR neurons had a primary peak located in either the *fast* or *slow* zone. In LM, *fast* units were more common than *slow* units (66% vs. 34%), but in nBOR *slow* units were more common than *fast* units (75% vs. 25%). In the present study, we found that GL units included *fast* and *slow* units, whereas CSA was clearly tuned to *slow* gratings. Table 1 summarizes the mean preferred SF/TF combinations from studies of LM, nBOR, and the VbC of pigeons (Wylie and Crowder 2000; Crowder

and Wylie 2001; Crowder et al. 2003a; present study). The average preferred SF/TF combinations for the *slow* units in LM and nBOR were 0.67cpd/0.55Hz and 0.53cpd/0.30Hz, respectively (Wylie and Crowder 2000; Crowder and Wylie 2001; Crowder et al. 2003a), which is quite close to the values for the *slow* GL units (0.68cpd/0.30Hz) and CSA (0.67cpd/0.35Hz) in the present study. Likewise, the average preferred SF/TF combinations for the *fast* units in LM and nBOR were 0.10cpd/2.49Hz and 0.08cpd/2.84Hz, respectively (Wylie and Crowder 2000; Crowder et al. 2003a), which is close to the values for the *fast* GL units (0.13cpd/8.24Hz) from the present study. In Fig. 5.4C, data from the current study of the VbC and previous studies of spatio-temporal tuning in LM and nBOR is collapsed onto a single plot: black hexagons show the primary peak locations in the spatio-temporal domain of recordings of the CSA of P-cells in VbC ( $n = 39$ ; present study); black diamonds show primary peak locations for GL units in VbC ( $n = 17$ ; present study); grey triangles show the primary peaks of LM units ( $n = 64$ ; Wylie and Crowder 2000); and the primary peaks of units from nBOR ( $n = 55$ ) are represented by grey squares (Crowder and Wylie 2001; Crowder et al. 2003a). The *fast* and *slow* populations form distinct clusters. The distribution of primary peaks within the *fast* and *slow* regions is similar for LM, nBOR, and VbC units.

In the present study we also found that the many of the contour plots of GL unit responses and CSA often included secondary peaks, almost always in the opposite region. This was also the case for many nBOR and LM neurons (Wylie and

Crowder 2000; Crowder and Wylie 2001; Crowder et al. 2003a), and some NOT neurons in wallabies (Ibbotson et al. 1994).

*Projections of Fast and Slow Neurons in the AOS and Pretectum to the VbC*

Figure 5.7 shows a cartoon of the projections of the nBOR and LM to the VbC. There is an indirect CF pathway through the medial column of the inferior olive (mcIO; Clarke 1977; Brecha et al. 1980; Gamlin and Cohen 1988; Arends and Voogd 1989; Lau et al. 1998; Wylie et al. 1999; Crowder et al. 2000; Wylie 2001; Winship and Wylie 2001, 2003) and a direct MF pathway that is restricted to folium IXcd (Brauth and Karten 1977; Clarke 1977; Brecha and Karten 1979; Brecha et al. 1980; Gamlin and Cohen 1988; Wylie and Linkenhoker 1996; Wylie et al. 1997). Our results suggest that the *slow* neurons in LM and nBOR make up the primary input to the CF pathway, while the MF pathway receives major inputs from *fast* and *slow* neurons in LM and nBOR. This is not to say that the CSA does not respond to fast gratings. Clearly many of the units have a secondary peaks in the *fast* region of the contour plot (Fig. 5.3C; see also Fig. 5.5C), as do many *slow* neurons in LM and nBOR (Wylie and Crowder 2000; Crowder and Wylie 2001; Crowder et al. 2003a), thus there is clearly an integration of *fast* and *slow* information in the CF pathway. Nonetheless we contend that the CF pathway receives input almost exclusively from cells in nBOR and LM that are maximally sensitive to *slow* gratings.

Although the CF pathway from the AOS and pretectum to the VbC exists in all mammals (for reviews see Simpson 1984; Simpson et al. 1988), a direct MF projection from the AOS and pretectum to the VbC has not been identified in mammals, with the possible exception of a controversial MTN-VbC projection in the chinchilla (Winfield et al. 1978). However, there may be several indirect MF pathways from the pretectum and AOS to the VbC. Most of the MF input to the VbC arises in the vestibular nuclei and the prepositus hypoglossi (Voogd et al. 1996; Ruijrok 2003) but there are also projections originating in the reticular formation, the raphe nuclei, and neurons located within and around the medial longitudinal fasciculus (Blanks et al. 1983; Sato et al. 1983; Gerrits et al. 1984; Langer et al. 1985; Ruijrok 2003; for review see Voogd et al. 1996). The NOT and the AOS project to many of these structures, including the vestibular nuclei, the medial and dorsolateral nuclei of the basilar pontine complex, the mesencephalic reticular formation, the prepositus hypoglossi and the nucleus reticularis tegmenti pontis (Itoh 1977; Terasawa et al. 1979; Cazin et al. 1982; Holstege and Collewyn 1982; Giolli et al. 1984, 1985, 1988; Torigoe et al. 1986a,b; for review see Simpson et al. 1988). Thus, it is possible that optic flow information reaches the VbC from the AOS and pretectum via an indirect MF pathway in mammalian species. It would be interesting to see if this information arises from *fast* and/or *slow* neurons.

### *Function of Fast and Slow Neurons*

Ibbotson et al. (1994) described the potential role of the *slow* and *fast* NOT neurons in the generation and maintenance of OKN. The *fast* units would respond maximally when retinal slip velocity (RSV) is high, whereas the slow neurons would be involved when the RSV is low, such as providing the error signal when the OKN gain is high (see Ibbotson et al. (1994) and Wylie and Crowder (2000) for detailed discussions). From the findings of the present study it follows that the MF inputs are involved when RSV is high and low, but the CF inputs are primarily involved when RSV is low. However, again we caution against such a stark simplification: the contour plots of many of the CSA recordings showed a secondary peak in the *fast* zone. Thus, the CSA of these Purkinje cells would not be silent to fast optic flow stimuli.

### *Velocity-Like Tuning vs. Spatio-Temporal Independence*

In the present study we found that many of the peaks in the *slow* zone were oriented such that they had a slope approximating one on log-log axes. That is, these units showed a peak response to a particular stimulus velocity (TF/SF), irrespective of the SF used. As the response maxima were dependent upon SF, we (Crowder et al. 2003a) have previously called this velocity-like tuning. (True velocity tuning would appear as a flattened ridge in the contour plot). Crowder et al. (2003) concluded that the majority of the *slow* units in LM and nBOR showed velocity-like tuning whereas the *fast* units were TF-tuned (i.e. SF/TF independent). However, Crowder et al.

(2003a) did not provide a quantitative test in this regard, and one can infer from Priebe et al. (2003) that there is a danger in overstating the degree of velocity-like tuning. Thus, we adopted the partial correlation outlined by Priebe et al. (2003) to compare velocity-tuned and SF/TF-independent predictions. The tendency of *slow* CSA to show velocity tuning is apparent in Figure 5.6, but only 26% showed significant velocity tuning compared to the independence prediction. 13.1% showed significant SF/TF-independence but most (60.5%) fell into the unclassified group, i.e. somewhere between velocity tuning and SF-TF independence. Consistent with Crowder et al. (2003a), SF/TF-independence was more common with the *fast* GL units (50%). Following Zanker et al. (1999), Crowder et al. (2003a) argued that velocity-like tuning reflects the properties of an ‘unbalanced’ Reichardt detector. Generally speaking, the more unbalanced the detector, the more the response approaches velocity tuning. Thus, with respect to velocity tuning vs. SF/TF-independence, the responses we observed suggest that the input units might vary with respect to the degree to which the detector is balanced.

#### *GL units: Granule Cells or Mossy Fibre Rosettes?*

There is precious little data regarding the physiological properties of MF inputs to the granule cell layer, presumably because these cells are small and difficult to isolate and hold. In fact, it is unclear whether the GL units recorded in the present study represent MF rosettes or granule cells. This is not necessarily a critical issue for the present study, as recordings from either would allow us to determine if *fast* or *slow*

units in the pretectum and AOS feed the MF pathway to the VbC. Fan et al. (1993) and Ariel and Fan (1993) recorded the visual responses of units in the GL in the turtle cerebellum using an *in vitro* preparation with eyes attached. Similar to pigeons (present study, Wylie et al. 1993), these units exhibited direction selectivity to large-field patterns but only respond to stimulation of the contralateral eye. Based on the following responses to stimulation of the nBOR, Ariel and Fan (1993) concluded that at least some (6/15) of the units they recorded were MF rosettes, as opposed to granule cells. A recent study in rats utilizing whole-cell patch clamp recordings showed that granule cells exhibited a low firing rate *in vivo*, with the mean spontaneous firing rate in the absence of holding current being  $0.5 \pm 0.2$  Hz (Chadderton et al. 2004). Based on this, it is likely that the GL units in the present study, which had high spontaneous rates (average =  $26.10 \pm 3.68$  spikes/s; mean  $\pm$  s.e.m), represent recordings from the MF rosettes in the granular layer.

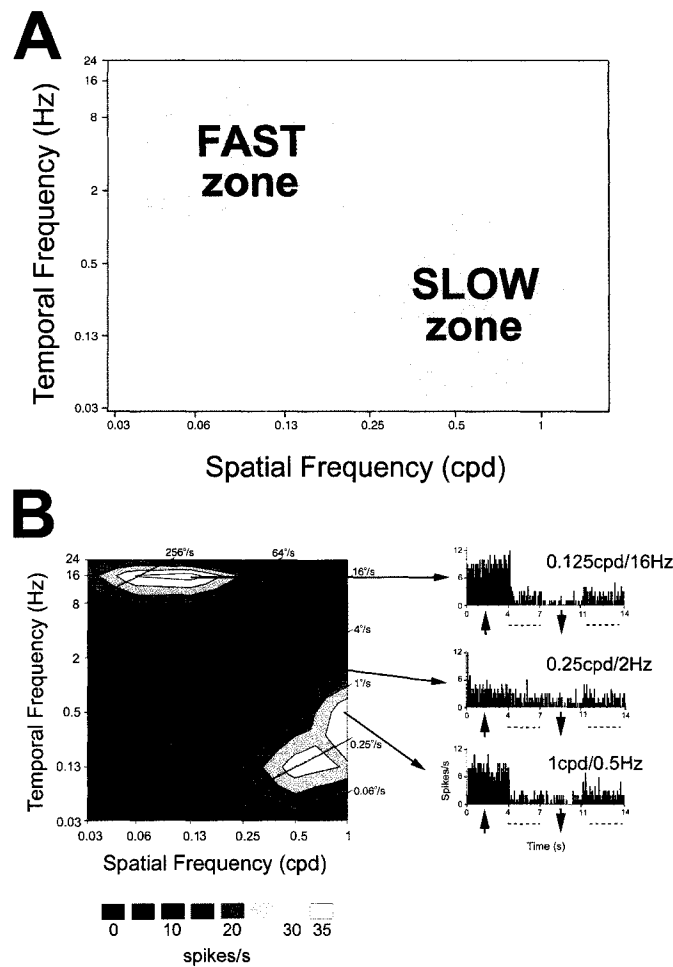


**Figure 5.1:** Spatio-temporal tuning in the accessory optic system (AOS), pretectum, and vestibulocerebellum (VbC). In Fig.5.1A, the approximate spatio-temporal preferences for *fast* and *slow* neurons in the mammalian and avian AOS and pretectum are illustrated (Ibbotson et al. 1994; Wylie and Crowder 2000; Crowder and Wylie 2001; Crowder et al. 2003a,b; Wolf-Oberhollenzer and Kirschfeld 1994). Fig. 5.1B shows the contour plot and peri-stimulus time histograms (PSTHs) of spatio-temporal tuning for a granular layer (GL) unit in the VbC. The contour plot shows the firing rate in response to sine wave gratings of varying spatial (abscissa) and temporal (ordinate) frequencies drifting in the preferred direction for the unit. The plot is shaded such that white represents the SF –TF combinations resulting in maximal excitation and black indicates minimal excitation. This unit was spatio-temporally tuned with primary peak in the *fast* zone, and a slightly lesser peak in the *slow* zone. PSTHs on the right show the unit’s modulation during stimulation in the preferred (upward) and antipreferred (downward) direction for gratings of three different SF–TF combinations during a single sweep. The top, middle, and bottom PSTHs show the unit’s response to gratings of 0.125cpd/16 Hz, 0.25cpd/2Hz, and 1cpd/0.5Hz, respectively. Firing rate is indicated by spikes per second (spikes/s) on the y-axis and

time in seconds is shown on the  $x$ -axis. Grey diagonal lines overlaying the contour plot indicate particular velocities (TF/SF) from  $0.06^\circ/\text{s}$  to  $256^\circ/\text{s}$ . See text for additional details.

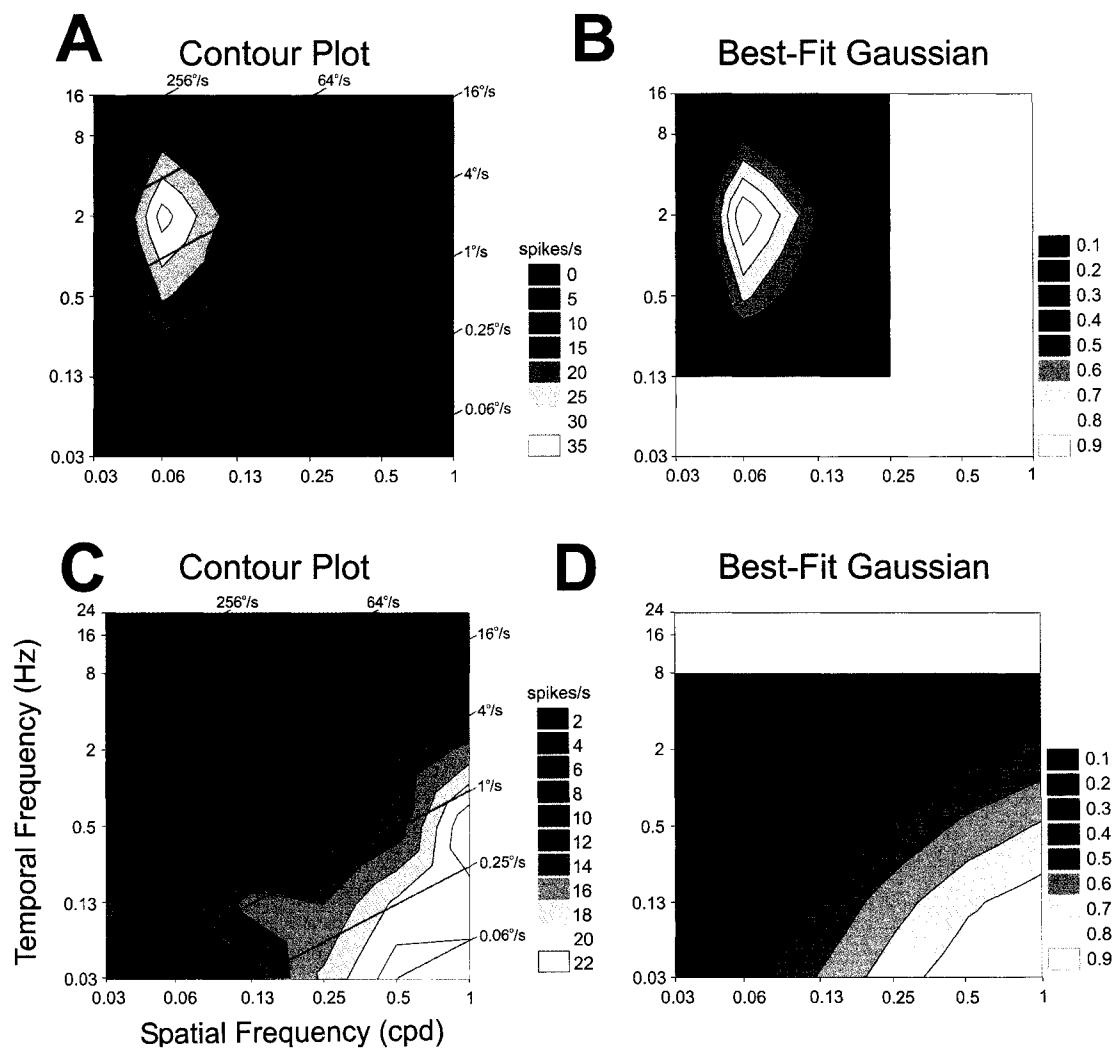


**Figure 5.2:** Contour Plots and Best-fit Gaussians for representative granular layer (GL) units. Fig. 5.2A shows the contour plot of the spatio-temporal tuning of a *fast* GL unit with a single peak. Fig. 5.2B shows the plot of the normalized Gaussian for the unit in 2A, as determined using the slightly modified equation of Perrone and Thiele (2001). Fig. 5.2C and 2D show the contour plot and best-fit Gaussian plot, respectively, of the spatio-temporal tuning of a GL unit with a single peak in the *slow* zone. See caption to Fig. 5.1 and text for additional details.

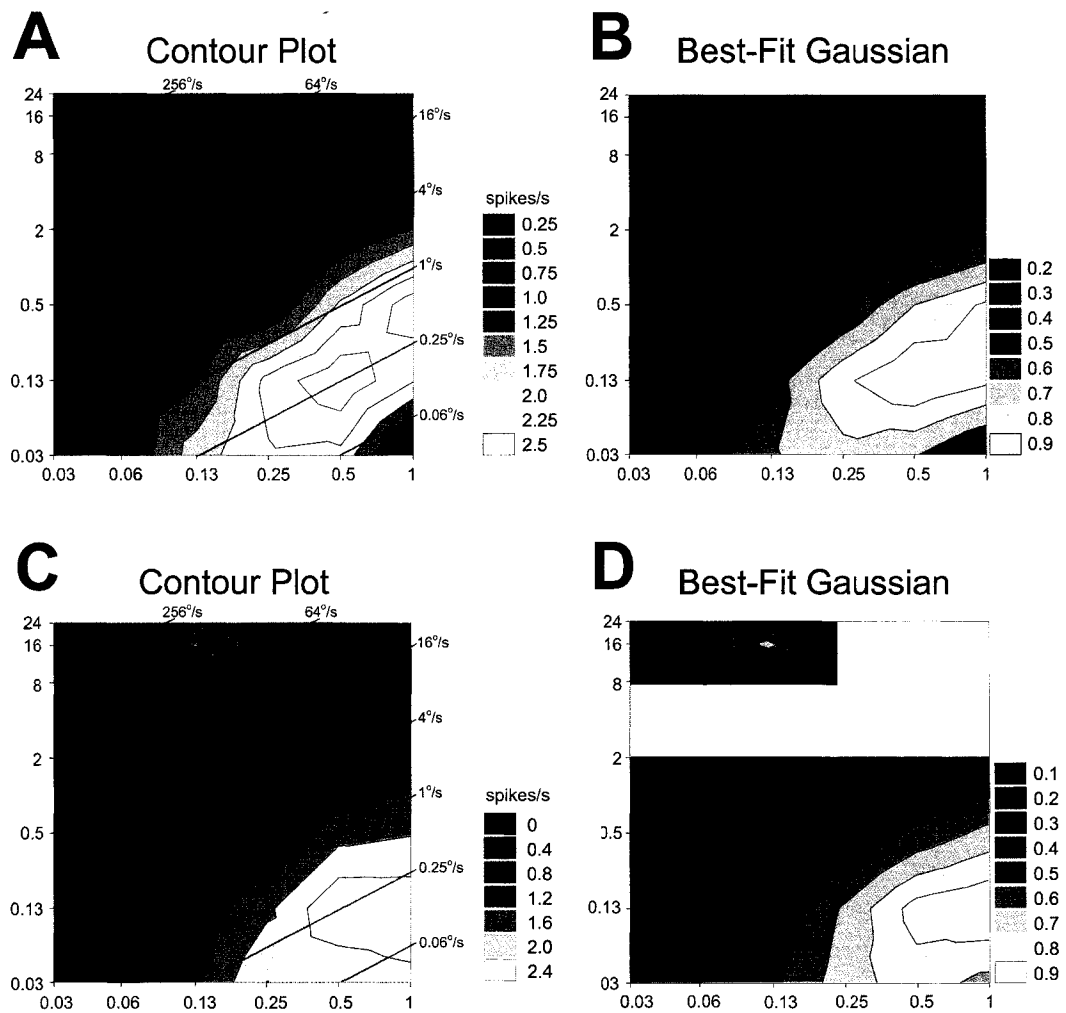


**Figure 5.3:** Contour plots and Gaussian plots for the complex spike activity of representative Purkinje cells (CSA of P-cells). Fig. 5.3A shows the contour plot of the spatio-temporal tuning of a P-cell with a single peak in the *slow* zone. Fig. 5.3B shows the plot of the normalized 2-D Gaussian for the unit in 3A. In 3C, a P-cell with a primary peak in the *slow* zone and a secondary peak in the *fast* zone is shown. The normalized 2-D Gaussian for this unit is plotted in 3D. See captions to Fig. 5.1 and 5.2 and the text for additional details.

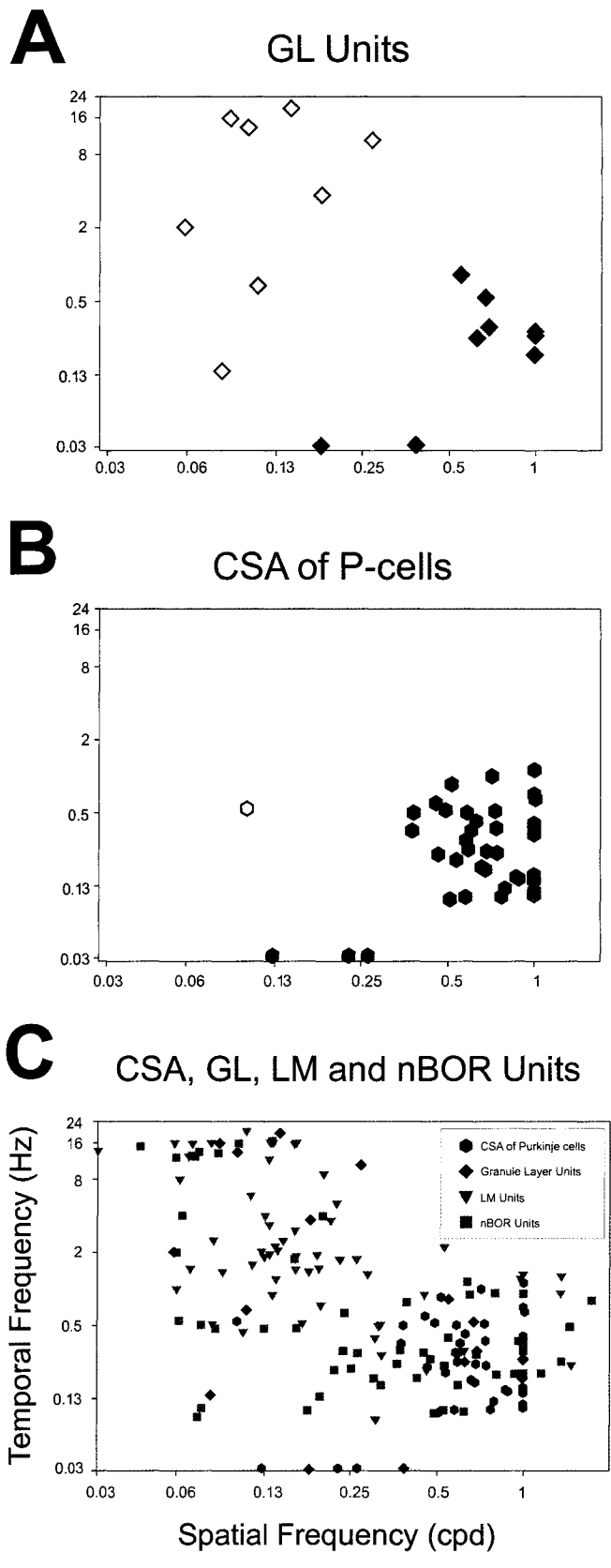


Figure 5.4: Spatio-temporal tuning of granular layer (GL) units and the complex spike activity of Purkinje cells (CSA of P-cells). In these plots, the primary peak locations in the spatio-temporal domain for all GL units (4A) and the CSA of all P-cells (4B) are indicated. In Fig. 5.4A, 8 of the units had a primary peak in the *fast* spatio-temporal domain (white diamonds), while 9 had a primary peak in the *slow* zone (grey diamonds). In Fig. 5.4B, 38 of the 39 peaks fall within the *slow* zone (grey hexagons). The remaining P-cell had a primary peak at 0.10cpd/0.55Hz (white hexagon). In Fig. 5.4C, data from the current study of the VbC and previous studies of spatio-temporal tuning in LM and nBOR is collapsed onto a single plot: black hexagons show the primary peak locations of the CSA of 39 P-cells in VbC (present study); black diamonds show primary peak locations for 17 GL units in VbC (present study); grey triangles show the primary peaks of 64 LM units (Wylie and Crowder 2000); and the primary peaks of 55 units from nBOR are represented by grey squares (Crowder and Wylie 2001; Crowder et al. 2003a). See text for details.

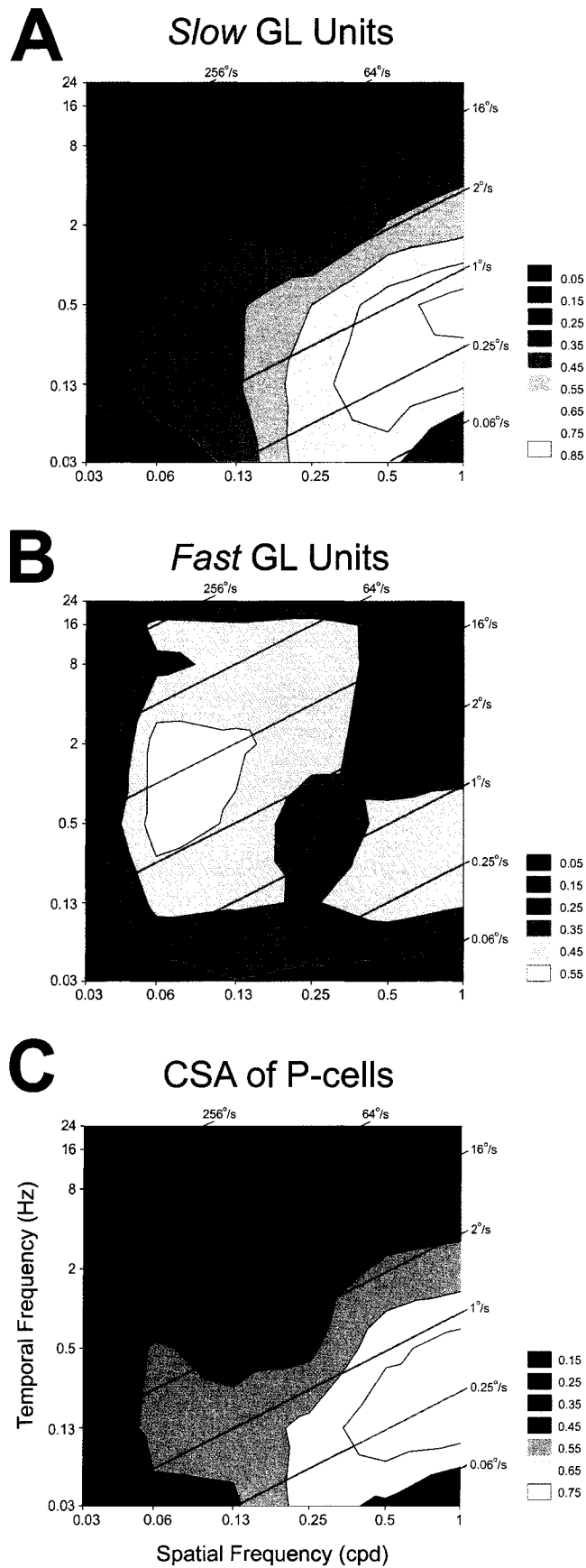
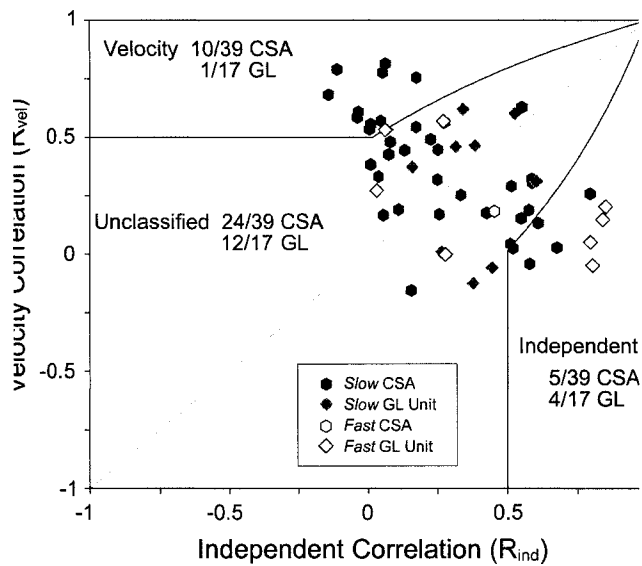
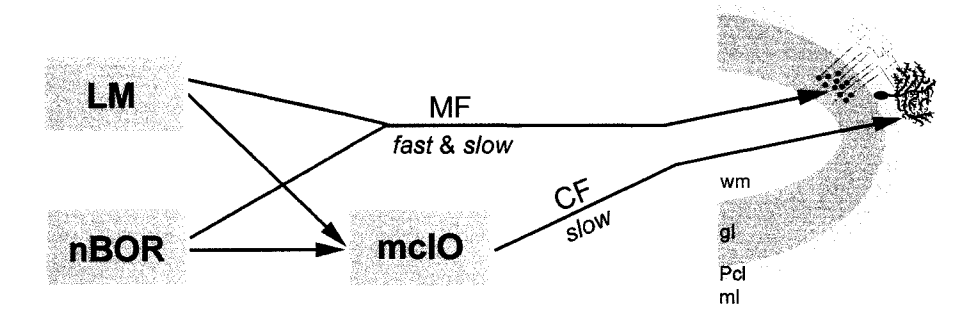


Figure 5.5: Normalized average contour plots of spatio-temporal tuning. Figures 5.5A, 5B, and 5C respectively show the normalized average plots for the 9 *slow* granular layer (GL) units, 8 *fast* GL units, and complex spike activity of 39 Purkinje cells (CSA of P-cells) recorded in this study. See captions for Figs. 5.1-5.4 and text for additional details.



**Figure 5.6:** Scatter plots of partial correlations for velocity ( $R_{vel}$ ) and spatio-temporally independent ( $R_{ind}$ ) tuning. Each data point indicates the degree to which a particular granular layer (GL) unit or the complex spike activity (CSA) of a Purkinje cell are correlated with velocity and SF/TF-independent predictions. The data space is divided into three regions based on statistical criteria approximated by the solid black lines. Velocity tuned, unclassifiable, or spatio-temporally independent cells fall in the upper left, middle, or lower right areas of the scatter plot, respectively. *Slow* CSA, *slow* GL units, *fast* CSA, and *fast* GL units are represented by black hexagons, grey diamonds, white hexagons with black borders, and white diamonds with black borders, respectively. *Slow* CSA was velocity tuned in 10 instances, while a single *fast* GL unit showed velocity tuning. See text for additional details.



**Figure 5.7:** Optic flow input from the accessory optic system (AOS) and pretectum to the vestibulocerebellum (VbC) in pigeons. This schematic illustrates the mossy fibre (MF) and climbing fibre (CF) inputs arriving at the VbC from the retinal recipient nuclei of the AOS (nucleus of the basal optic root, nBOR) and pretectum (lenticularis mesencephali, LM) and the medial column of the inferior olive (mclO), respectively. The results of this study indicate that the CF input to Purkinje cells in the VbC is primarily from *slow* cells in LM and nBOR, whereas MF input to the granular layer arises in both *fast* and *slow* cells in LM and nBOR. ml, molecular layer; Pcl, Purkinje cell layer; wm, cerebellar white matter.

	<i>Fast Cells</i>				<i>Slow Cells</i>			
	n (% total)	SF (cpd)	TF (Hz)	Velocity (°/s)	n (% total)	SF (cpd)	TF (Hz)	velocity (°/s)
Pigeon nBOR	13 (25%)	0.078	2.84	36.2 <sup>#</sup> [70.8*]	40 (75%)	0.53	0.30	0.57 <sup>#</sup> [0.75*]
Pigeon LM	23 (66%)	0.10	2.49	25.8 <sup>#</sup> [52.3*]	12 (34%)	0.67	0.55	0.82 <sup>#</sup> [1.08*]
Pigeon GL unit	8 (47%)	0.13	8.24	63.4 <sup>#</sup> [69.8*]	9 (53%)	0.68	0.30	0.4 <sup>#</sup> [0.5*]
Pigeon CSA	1 (3%)	0.10	0.55	5.5 <sup>#</sup> [5.5*]	38 (97%)	0.67	0.35	0.5 <sup>#</sup> [0.5*]

#meanTF/meanSF. \*arithmetic mean.

**Table 1**

Preferred spatial frequencies (SFs), temporal frequencies (TFs), and velocities of *fast* and *slow* neurons. Average SFs, TFs, and velocities of the primary peaks are shown for the *fast* and *slow* neurons in the pigeon nucleus of the basal optic root (nBOR; Crowder et al., 2003a) and lentiformis mesencephali (LM; from Wylie and Crowder, 2001), and granular layer (GL) units and the complex spike activity (CSA) of Purkinje cells in the vestibulocerebellum (present study).

### **References**

- Arends JJA, and Voogd J.** Topographic aspects of the olivocerebellar system in the pigeon. *Exp Brain Res Suppl.* 17: 52-57, 1989.
- Ariel M, and Fan TX.** Electrophysiological evidence for a bisynaptic retinocerebellar pathway. *J Neurophysiol* 69: 1323-30, 1993.
- Ariel M, and Kogo N.** Direction tuning of inhibitory inputs to the turtle accessory optic system. *J Neurophysiol* 86: 2919-2930, 2001.
- Blanks RH, Precht W, and Torigoe Y.** Afferent projections to the cerebellar flocculus in the pigmented rat demonstrated by retrograde transport of horseradish peroxidase. *Exp Brain Res* 52: 293-306, 1983.
- Brauth SE, and Karten HJ.** Direct accessory optic projections to the vestibulocerebellum: A possible channel for oculomotor control systems. *Exp Brain Res* 28: 73-84, 1977.
- Brecha N, and Karten HJ.** Accessory optic projections upon oculomotor nuclei and vestibulocerebellum. *Science* 203: 913-916, 1979.
- Brecha N, Karten HJ, and Hunt SP.** Projections of the nucleus of basal optic root in the pigeon: An autoradiographic and horseradish peroxidase study. *J Comp Neurol* 189: 615-670, 1980.
- Burns S, and Wallman J.** Relation of single unit properties to the oculomotor function of the nucleus of the basal optic root (AOS) in chickens. *Exp Brain Res* 42: 171-180, 1981.
- Carpenter RHS.** *Movements of the eye* (2<sup>nd</sup> edition). London: Pion, 1988.

- Cazin L, Magnin M, and Lannou J.** Non-cerebellar visual afferents to the vestibular nuclei involving the prepositus hypoglossal complex: an autoradiographic study in the rat. *Exp Brain Res* 48: 309-313, 1982.
- Chadderton P, Margrie TW, and Hausser M.** Integration of quanta in cerebellar granule cells during sensory processing. *Nature* 428: 856 – 860, 2004.
- Clarke PGH.** Some visual and other connections to the cerebellum of the pigeon. *J Physiol* 243: 267-285, 1977.
- Collewijn H.** Direction-selective units in the rabbit's nucleus of the optic tract. *Brain Res* 100: 489-508, 1975a.
- Collewijn H.** Oculomotor areas in the rabbit's midbrain and pretectum. *J Neurobiol* 6: 3-22, 1975b.
- Crow EL, Davis FA, Maxfield MW.** *Statistics Manual, With Examples Taken from Ordinance Development.* New York: Dover, 1960.
- Crowder NA, Dawson MR, and Wylie DR.** Temporal frequency and velocity-like tuning in the pigeon accessory optic system. *J Neurophysiol* 90: 1829-41, 2003a.
- Crowder NA, Dickson CT, and Wylie DR.** Telencephalic input to the pretectum of pigeons: an electrophysiological and pharmacological inactivation study. *J Neurophysiol* 91: 274-85, 2004.
- Crowder NA, Lehmann H, Parent MB, and Wylie DR.** The accessory optic system contributes to the spatio-temporal tuning of motion-sensitive pretectal neurons. *J Neurophysiol* 90: 1140-51, 2003b.

- Crowder NA, Winship IR, and Wylie DR.** Topographic organization of inferior olive cells projecting to translational zones in the vestibulocerebellum of pigeons. *J Comp Neurol* 419: 87-95, 2000.
- Crowder NA, and Wylie DRW.** Fast and slow neurons in the nucleus of the basal optic root in pigeons. *Neurosci Lett* 304: 133-136, 2001.
- Distler C, and Hoffmann KP.** Visual receptive field properties in kitten pretectal nucleus of the optic tract and dorsal terminal nucleus of the accessory optic tract. *J Neurophysiol* 70: 814-827, 1993.
- Fan TX, Rosenberg AF, and Ariel M.** Visual-response properties of units in the turtle cerebellar granular layer in vitro. *J Neurophysiol* 69: 1314-22, 1993.
- Fan TX, Weber AE, Pickard GE, Faber KM, and Ariel M.** Visual responses and connectivity in the turtle pretectum. *J Neurophysiol* 73: 2507-2521, 1995.
- Finger TE, and Karten HJ.** The accessory optic system in teleosts. *Brain Res* 153: 144-9, 1978.
- Fite KV.** Pretectal and accessory-optic visual nuclei of fish, amphibia and reptiles: themes and variations. *Brain Behav Evol* 26: 71-90, 1985.
- Fite KV, Kwei-Levy C, and Bengston L.** Neurophysiological investigation of the pretectal nucleus lentiformis mesencephali in *Rana pipiens*. *Brain Behav Evol* 34: 164-170, 1989.
- Gamlin PDR, and Cohen DH.** Projections of the retinorecipient pretectal nuclei in the pigeon (*Columba livia*). *J Comp Neurol* 269: 18-46, 1988.

- Gerrits NM, Epema AH, and Voogd J.** The mossy fiber projection of the nucleus reticularis tegmenti pontis to the flocculus and adjacent ventral paraflocculus in the cat. *Neuroscience* 11: 627-44, 1984.
- Gibson JJ.** The visual perception of object motion and subjective movement. *Psychol Rev* 61: 304-314, 1954.
- Gioanni H.** Stabilizing gaze reflexes in the pigeon (*Columba livia*). I. Horizontal and vertical optokinetic eye (OKN) and head (OCR) reflexes. *Exp Brain Res* 69: 567-582, 1988.
- Gioanni H, Rey J, Villalobos J, Bouyer JJ, and Gioanni Y.** Optokinetic nystagmus in the pigeon (*Columba livia*). I. Study in monocular and binocular vision. *Exp Brain Res* 44: 362-70, 1981.
- Gioanni H, Rey J, Villalobos J, Richard D, and Dalbera A.** Optokinetic nystagmus in the pigeon (*Columba livia*). II. Role of the pretectal nucleus of the accessory optic system. *Exp Brain Res* 50: 237-247, 1983a.
- Gioanni H, Rey J, Villalobos J, and Dalbera A.** Single unit activity in the nucleus of the basal optic root (nBOR) during optokinetic, vestibular and visuo-vestibular stimulations in the alert pigeon (*Columba livia*). *Exp Brain Res* 57: 49-60, 1984.
- Gioanni H, Villalobos J, Rey J, and Dalbera A.** Optokinetic nystagmus in the pigeon (*Columba livia*). III. Role of the nucleus ectomammilaris (nEM): interactions in the accessory optic system. *Exp Brain Res* 50: 248-258, 1983b.

- Gioli RA, Blanks RH, and Torigoe Y.** Pretectal and brain stem projections of the medial terminal nucleus of the accessory optic system of the rabbit and rat as studied by anterograde and retrograde neuronal tracing methods. *J Comp Neurol* 227: 228-251, 1984.
- Gioli RA, Blanks RH, Torigoe Y, and Williams DD.** Projections of medial terminal accessory optic nucleus, ventral tegmental nuclei, and substantia nigra of rabbit and rat as studied by retrograde axonal transport of horseradish peroxidase. *J Comp Neurol* 232: 99-116, 1985.
- Gioli RA, Torigoe Y, Blanks RH, and McDonald HM.** Projections of the dorsal and lateral terminal accessory optic nuclei and of the interstitial nucleus of the superior fasciculus (posterior fibers) in the rabbit and rat. *J Comp Neurol* 277: 608-20, 1988.
- Gizzi MS, Katz E, Schumer RA, and Movshon JA.** Selectivity for orientation and direction of motion of single neurons in cat striate and extrastriate visual cortex. *J Neurophysiol* 63: 1529-1543, 1990.
- Graf W, Simpson JI, and Leonard CS.** Spatial organization of visual messages of the rabbit's cerebellar flocculus. II. Complex and simple spike responses of Purkinje cells. *J Neurophysiol* 60: 2091-2121, 1988.
- Grasse KL, and Cynader MS.** Electrophysiology of medial terminal nucleus of accessory optic system in the cat. *J Neurophysiol* 48: 490-504, 1982.

**Grasse KL, Cyander MS, and Douglas RM.** Alterations in response properties in the lateral and dorsal terminal nuclei of the cat accessory optic system following visual cortex lesions. *Exp Brain Res* 55: 69-80, 1984.

**Grasse KL, and Cyander MS.** The accessory optic system in frontal-eyed animals. In: *Vision and Visual Dysfunction. The Neuronal Basis of Visual Function*, edited by Leventhal A. New York: McMillan, 1990, p. 111-139.

**Hoffmann KP, and Distler C.** Quantitative analysis of visual receptive fields of neurons in nucleus of the optic tract and dorsal terminal nucleus of the accessory optic tract in macaque monkey. *J Neurophysiol* 62: 416-428, 1989.

**Hoffmann KP, Distler C, Erickson RG, and Mader W.** Physiological and anatomical identification of the nucleus of the optic tract and dorsal terminal nucleus of the accessory optic tract in monkeys. *Exp Brain Res* 69: 635-644, 1988.

**Hoffmann KP, and Schoppmann A.** Retinal input to direction selective cells in the nucleus tractus opticus of the cat. *Brain Res* 99: 359-366, 1975.

**Hoffmann KP, and Schoppmann A.** A quantitative analysis of the direction-specific response of neurons in the cat's nucleus of the optic tract. *Exp Brain Res* 42: 146-157, 1981.

**Holstege G, and Collewijn H.** The efferent connections of the nucleus of the optic tract and the superior colliculus in the rabbit. *J Comp Neurol* 209: 139-75, 1982.

- Ibbotson MR, Mark RF, and Maddess TL.** Spatio-temporal response properties of direction-selective neurons in the nucleus of the optic tract and the dorsal terminal nucleus of the wallaby, *Macropus eugenii*. *J Neurophysiol* 72: 2927-2943, 1994.
- Ibbotson MR, and Price NS.** Spatio-temporal tuning of directional neurons in mammalian and avian pretectum: a comparison of physiological properties. *J Neurophysiol* 86: 2621-2624, 2001.
- Ihaka R, and Gentleman R. R.** A Language for Data Analysis and Graphics. *J Comp Graph Stats* 5: 299-314, 1996.
- Ilg UJ.** Slow eye movements. *Prog Neurobiology* 53: 293-329, 1997.
- Ilg UJ, and Hoffmann KP.** Responses of neurons of the nucleus of the optic tract and the dorsal terminal nucleus of the accessory optic tract in the awake monkey. *Eur J Neurosci* 8: 92-105, 1996.
- Itoh K.** Efferent projections of the pretectum in the cat. *Exp Brain Res* 50: 89-105, 1977.
- Kano M, Kano MS, Kusunoki M, and Maekawa K.** Nature of optokinetic response and zonal organization of climbing fiber afferents in the vestibulocerebellum of the pigmented rabbit. II. The nodulus. *Exp Brain Res* 80: 238-51, 1990.
- Karten HJ, and Hodos W.** *A stereotaxic Atlas of the Brain of the Pigeon (Columba livia)*. Baltimore: Johns Hopkins Press, 1967.
- Katte O, and Hoffmann KP.** Direction specific neurons in the pretectum of the frog (*Rana esculenta*). *J Comp Physiol* 140: 53-57, 1980.

- Kawasaki T, and Sato Y.** Afferent projection from the dorsal nucleus of the raphe to the flocculus in cats. *Brain Res* 197: 496-502, 1980.
- Klauer S, Sengpiel F, and Hoffmann KP.** Visual response properties and afferents of nucleus of the optic tract in the ferret. *Exp Brain Res* 83:178-89, 1990.
- Kogo N, Fan TX, and Ariel M.** Synaptic pharmacology in the turtle accessory optic system. *Exp Brain Res* 147: 464-472, 2002.
- Kogo N, Rubio DM, and Ariel M.** Direction tuning of individual retinal inputs to the turtle accessory optic system. *J Neurosci* 18: 2673-2684, 1998.
- Kusunoki M, Kano M, Kano MS, and Maekawa K.** Nature of optokinetic response and zonal organization of climbing fiber afferents in the vestibulocerebellum of the pigmented rabbit. I. The flocculus. *Exp Brain Res* 80: 225-37, 1990.
- Langer TA, Fuchs F, Scudder CA, and Chubb MC.** Afferents to the flocculus of the cerebellum in the rhesus macaque as revealed by retrograde transport of horseradish peroxidase. *J Comp Neurol* 235: 1-25, 1985.
- Lau KL, Glover RG, Linkenhoker B, and Wylie DR.** Topographical organization of inferior olive cells projecting to translation and rotation zones in the vestibulocerebellum of pigeons. *Neuroscience* 85: 605-14, 1998.
- Levitt JB, Kiper DC, and Movshon JA.** Receptive fields and functional architecture of macaque V2. *J Neurophysiol* 71: 2517-2542, 1994.
- McKenna OC, and Wallman J.** Identification of avian brain regions responsive to retinal slip using 2-deoxyglucose. *Brain Res* 210: 455-60, 1981.

**McKenna OC, and Wallman J.** Functional postnatal changes in avian brain regions responsive to retinal slip: a 2-deoxy-D-glucose study. *J Neurosci* 5: 330-342, 1985a.

**McKenna OC, and Wallman J.** Functional postnatal changes in avian brain regions responsive to retinal slip: a 2-deoxy-D-glucose study. *J Neurosci* 5:330-342, 1985b.

**Morgan B, and Frost BJ.** Visual response properties of neurons in the nucleus of the basal optic root of pigeons. *Exp Brain Res* 42: 184-188, 1981.

**Movshon JA, Adelson EH, Gizzi MS, and Newsome WT.** The analysis of visual moving patterns. In *Study Group on Pattern Recognition Mechanisms*, edited by Chagas C, Gattass R, Gross C. Vatican City: Pontificia Academia Scientiarum, 1985, p. 117-151.

**Mustari MJ, and Fuchs AF.** Discharge patterns of neurons in the pretectal nucleus of the optic tract (NOT) in the behaving primate. *J Neurophysiol* 64: 77-90, 1990.

**Nakayama K.** Differential motion hyperacuity under conditions of common image motion. *Vision Res* 21:1475-1482, 1981.

**Papoulis A.** *Probability and Statistics*. New York: Prentice-Hall International Editions, 1990.

**Perrone JA, and Thiele A.** Speed skills: measuring the visual speed analyzing properties of primate MT neurons. *Nature Neurosci* 4: 526-531, 2001.

- Price NS, and Ibbotson MR.** Direction-selective neurons in the optokinetic system with long-lasting after-responses. *J Neurophysiol* 88: 2224-2231, 2002.
- Priebe NJ, Cassanello CR, and Lisberger SG.** The neural representation of speed in macaque area MT/V5. *J Neurosci* 23: 5650-5661, 2003.
- Reiner A, and Karten HJ.** A bisynaptic retinocerebellar pathway in the turtle. *Brain Res* 150:163-9, 1978.
- Robinson DA.** Control of eye movements. In: *Handbook of Physiology, The Nervous System*, edited by Brooks VB. Bethesda, MD: Am. Physiol.Soc, 1981, sect. 1, vol. 2, pp. 1275-1320.
- Rosenberg AF, and Ariel M.** Visual-response properties of neurons in turtle basal optic nucleus in vitro. *J Neurophysiol* 63: 1033-1045, 1990.
- Ruigrok TJ.** Collateralization of climbing and mossy fibers projecting to the nodulus and flocculus of the rat cerebellum. *J Comp Neurol* 466: 278-98, 2003.
- Sato Y, Kawasaki T, and Ikarashi K.** Afferent projections from the brainstem to the three floccular zones in cats. II. Mossy fiber projections. *Brain Res* 272: 37-48, 1983.
- Scannell JW, Sengpiel F, Tovee MJ, Benson PJ, Blakemore C, and Young MP.** Visual motion processing in the anterior ectosylvian sulcus of the cat. *J Neurophysiol* 76: 895-907, 1996.
- Simpson JI. The accessory optic system.** *A Rev Neurosci* 7: 13-41, 1984.
- Simpson JI, Giolli RA, and Blanks RHI.** The pretectal nuclear complex and the accessory optic system. *Rev Oculomot Res* 2: 335-64, 1988.

- Simpson JI, Graf W, and Leonard C.** The coordinate system of visual climbing fibres to the flocculus. In: Progress in oculomotor research, edited by Fuchs AF, and Becker W. Amsterdam/New York/Oxford: Elsevier/North Holland, 1981.
- Simpson JI, Soodak RE, and Hess R.** The accessory optic system and its relation to the vestibulocerebellum. *Prog Brain Res* 50: 715-24, 1979.
- Soodak RE, and Simpson JI.** The accessory optic system of rabbit. I. Basic visual response properties. *J Neurophysiol* 60: 2055-2072, 1988.
- Terasawa K, Otani K, and Yamada J.** Descending pathways of the nucleus of the optic tract in the rat. *Brain Res* 173: 405-417, 1979.
- Thach WT Jr.** Somatosensory receptive fields of single units in cat cerebellar cortex. *J Neurophysiol* 30: 675-96, 1967.
- Torigoe Y, Blanks RHI, and Precht W.** Anatomical studies on the nucleus reticularis tegmenti pontis in the pigmented rat. I. Cytoarchitecture, topography, and cerebral cortical afferents. *J Comp Neurol* 243: 71-87, 1986a.
- Torigoe Y, Blanks RHI, and Precht W.** Anatomical studies on the nucleus reticularis tegmenti pontis in the pigmented rat. II. Subcortical afferents demonstrated by the retrograde transport of horseradish peroxidase. *J Comp Neurol* 243: 88-105, 1986b.
- Venables WN, and Ripley B D.** *Modern applied statistics with S-Plus* (4th edition). New York: Springer-Verlag, 2002.

- Volchan E, Rocha-Miranda CE, Picanco-Diniz CW, Zinsmeisser B, Bernardes RF, Franca JG.** Visual response properties of pretectal units in the nucleus of the optic tract of the opossum. *Exp Brain Res* 78: 380-386, 1989.
- Voogd J, Gerrits NM, and Ruigrok TJ.** Organization of the vestibulocerebellum. *Ann N Y Acad Sci* 781: 553-79, 1996.
- Waespe W, Buttner U, and Henn V.** Input-output activity of the primate flocculus during visual-vestibular interaction. *Exp Brain Res* 43: 337-348, 1981.
- Weber JT.** Pretectal complex and accessory optic system in alert monkeys. *Brain Behav Evol* 26: 117-140, 1985.
- Westheimer G, and McKee SP.** Visual acuity in the presence of retinal-image motion. *J Opt Soc Am* 65: 847-50, 1975.
- Winfield JA, Hendrickson A, and Kimm J.** Anatomical evidence that the medial terminal nucleus of the accessory optic tract in mammals provides a visual mossy fiber input to the flocculus. *Brain Res* 151: 175-82, 1978.
- Winship IR, and Wylie DRW.** Responses of neurons in the medial column of the inferior olive in pigeons to translational and rotational optic flowfields. *Exp Brain Res* 141: 63-78, 2001.
- Winship IR, and Wylie DRW.** Zonal organization of the vestibulocerebellum in pigeons (*Columba livia*): I. Climbing fibre input to the flocculus. *J Comp Neurol* 456: 127-139, 2003.

- Winterson BJ, and Brauth SE.** Direction-selective single units in the nucleus lentiformis mesencephali of the pigeon (*Columba livia*). *Exp Brain Res* 60: 215-226, 1985.
- Wolf-Oberhollenzer F, and Kirschfeld K.** Motion sensitivity in the nucleus of the basal optic root of the pigeon. *J Neurophysiol* 71: 1559-1573, 1994.
- Wylie DR.** Projections from the nucleus of the basal optic root and nucleus lentiformis mesencephali to the inferior olive in pigeons (*Columba livia*). *J Comp Neurol* 429: 502-13, 2001.
- Wylie DR, Bischof WF, and Frost BJ.** Common reference frame for neural coding of translational and rotational optic flow. *Nature* 392: 278-282, 1998.
- Wylie DR, and Crowder NA.** Spatio-temporal properties of fast and slow neurons in the pretectal nucleus lentiformis mesencephali in pigeons. *J Neurophysiol* 84: 2529-2540, 2000.
- Wylie DR, and Frost BJ.** Visual response properties of neurons in the nucleus of the basal optic root of the pigeon: A quantitative analysis. *Exp Brain Res* 82: 327-336, 1990.
- Wylie DR, and Frost BJ.** Responses of pigeon vestibulocerebellar neurons to optokinetic stimulation. II. The 3-dimensional reference frame of rotation neurons in the flocculus. *J Neurophysiol* 70: 2647-259, 1993.
- Wylie DR, and Frost BJ.** The pigeon optokinetic system: visual input in extraocular muscle coordinates. *Vis Neurosci* 13: 945-53, 1996.

- Wylie DR, and Frost BJ.** Responses of neurons in the nucleus of the basal optic root to translational and rotational flowfields. *J Neurophysiol* 81: 267-276, 1999.
- Wylie DR, Kripalani T, and Frost BJ.** Responses of pigeon vestibulocerebellar neurons to optokinetic stimulation. I. Functional organization of neurons discriminating between translational and rotational visual flow. *J Neurophysiol* 70: 2632-2646, 1993.
- Wylie DR, and Linkenhoker B.** Mossy fibres from the nucleus of the basal optic root project to the vestibular and cerebellar nuclei in pigeons. *Neurosci Lett* 219: 83-6, 1996.
- Wylie DR, Linkenhoker B, and Lau KL.** Projections of the nucleus of the basal optic root in pigeons (*Columba livia*) revealed with biotinylated dextran amine. *J Comp Neurol* 384: 517-536, 1997.
- Wylie DR, Winship IR, and Glover RG.** Projections from the medial column of the inferior olive to different classes of rotation-sensitive Purkinje cells in the flocculus of pigeons. *Neurosci Lett* 268: 97-100, 1999.
- Yakushin SB, Gizzi M, Reisine H, Raphan T, Buttner-Ennever J, and Cohen B.** Functions of the nucleus of the optic tract (NOT). II. Control of ocular pursuit. *Exp Brain Res* 131: 433-447, 2000.
- Zanker JM, Srinivasan MV, and Egelhaaf M.** Speed tuning in elementary motion detectors of the correlation type. *Biol Cybern* 80: 109-16, 1999.

**CHAPTER 6:**  
**A QUANTITATIVE REASSESSMENT OF SPEED TUNING IN THE**  
**ACCESSORY OPTIC SYSTEM AND PRETECTUM OF PIGEONS**

Manuscript *in press* with the Journal of Neurophysiology

The correlation model of motion detection has been used to describe many aspects of visual motion processing in a number of species from insects to primates (for reviews see Borst and Egelhaaf 1989; Buchner 1984; Clifford and Ibbotson 2003; Srinivasen et al. 1999). This includes motion detectors in the pretectum and Accessory Optic System (AOS; Ibbotson et al. 1994; Crowder and Wylie 2001; Crowder et al. 2003a; pretectum, Wylie and Crowder 2000; Crowder et al. 2003a,b). Motion-sensitive neurons in the pretectum and AOS exhibit direction selectivity to large field “optic flow” stimuli, and are involved in generating the optokinetic reflex. In mammals, the AOS includes the medial and lateral terminal nuclei, which are equivalent to the nucleus of the basal optic root (nBOR) in birds. Similarly, the pretectal nucleus of the optic tract (NOT) and the dorsal terminal nucleus of the AOS are the mammalian equivalent to the nucleus lentiformis mesencephali (LM) in birds (for reviews see Simpson 1984; Simpson et al. 1988).

Recent electrophysiological studies that utilized large field sinusoidal gratings as stimuli showed that pretectal and AOS neurons show spatio-temporal tuning (wallaby NOT, Ibbotson et al. 1994; pigeon nBOR and LM, Wylie and Crowder 2000; Crowder and Wylie 2001; Crowder et al. 2003a). Pretectal and AOS neurons can be classified into two groups based on spatio-temporal tuning: *slow* cells were maximally sensitive to motion at low temporal frequencies (TF < 1 Hz) and high spatial frequencies (SF > 0.25 cycles per degree, cpd), whereas *fast* cells were sensitive to high TF (> 1 Hz) and low SF (< 0.25 cpd) (see also Ibbotson and Price 2001; Winship et al. 2005).

One feature of Reichardt correlation detectors is that they are not tuned to stimulus speed (TF/SF) but respond to a particular TF independent of the SF, i.e. they are “spatio-temporally independent” (Buchner 1984; Egelhaaf et al. 1989; Ibbotson et al. 1994; Srinivasen et al. 1999; Clifford and Ibbotson 2003). Spatio-temporally independent motion detectors could be interpreted as tuned either to a particular TF (TF-tuned), a particular SF (SF-tuned), or tightly tuned to a particular SF/TF combination. Crowder et al. (2003a) quantitatively described spatio-temporal tuning in the AOS and pretectum by fitting the spatio-temporal contour plots with 2-dimensional Gaussians and suggested that *fast* units in pigeon LM and nBOR showed SF/TF-independence, whereas most of the *slow* cells showed apparent speed tuning. As the response maxima were not completely independent of SF, Crowder et al. (2003a) termed this “velocity-like” tuning (see also Zanker et al. 1999). The assertions made by Crowder et al (2003a) were based on between groups statistics that demonstrated that, for the *slow* cells, oriented Gaussians typical of velocity-like tuning provided better fits than non-oriented Gaussians typical of SF/TF-independence. Non-oriented Gaussians provided better fits for *fast* cells. Using analyses similar to these, a recent study of motion sensitive units in the middle temporal (MT) area of monkeys (Perrone and Thiele 2001; see also Simoncelli and Heeger 2001) suggested that most units were speed-tuned. However, Priebe et al. (2003) offered another quantitative test of tuning for speed vs. SF/TF-independence utilizing within groups statistics and suggested that Perrone and Thiele (2001) greatly overestimated the degree of speed tuning. We feel that the cell-by-cell classification method proposed by Priebe et al

(2003) may offer a more detailed description of the spatio-temporal tuning we've reported in the pigeon. Therefore, we have performed a meta-analysis of the spatio-temporal tuning of LM and nBOR units from previous studies (Wylie and Crowder 2000; Crowder and Wylie 2001; Crowder et al. 2003a,b, 2004) utilizing the quantitative methods outlined by Priebe et al. (2003; see also Levitt et al. 1994). Applying these criteria, speed tuning in nBOR and LM is less than previously estimated.

## **Methods**

We analysed the spatio-temporal tuning of 42 nBOR and 76 LM units collected from previous studies in pigeons (Wylie and Crowder 2000; Crowder and Wylie 2001; Crowder et al. 2003a,b, 2004). Details of the surgery, electrophysiological recording and stimulus presentation can be found in these papers. All methods conform to the guidelines established by the Canadian Council on Animal Care and approved by the Biosciences Animal Care and Policy Committee at the University of Alberta. Briefly, we recorded the responses of nBOR and LM neurons in anaesthetized pigeons to sine-wave gratings of varying SF (0.031-2 cycles per degree, cpd) and TF (0.031-24 cycles per second, Hz) moving in the preferred direction (contrast = 0.95; mean luminance = 65cd/m<sup>2</sup>; refresh rate = 80 Hz). The standard protocol consisted of 36 SF/TF combinations (0.031, 0.063, 0.125, 0.25, 0.5, and 1cpd at 0.031, 0.125, 0.5, 2, 8, and 16Hz). However, for some units we tested additional SF/TF combinations: for 15 units we also tested at TFs of 0.063, 0.25, 1

and 4 Hz; 21 units were tested with TF of 24 Hz; and 30 units were tested with SF of 2cpd. Contour plots of the mean firing rate as a function of SF (abscissa) and TF (ordinate) were generated with *Sigma Plot* (see Figure 6.2, left column). The location of maximal excitation was referred to as the primary peak of the contour plot. Many cells also display a secondary peak, but these were not considered in this analysis.

### *Analysis of Speed Tuning vs. TF Tuning*

To determine the influence of SF on speed tuning, each excitatory response contour plot was fit to a 2-D Gaussian function using the equation described by Priebe et al. (2003):

$$\mathbf{R}(\mathbf{sf}, \mathbf{tf}) = A * e^{-\frac{(\log_2(\mathbf{sf}) - \log_2(\mathbf{sf}_0))^2}{\sigma_{sf}^2}} * e^{-\frac{(\log_2(\mathbf{tf}) - \log_2(\mathbf{tf}_p(\mathbf{sf})))^2}{\sigma_{tf}^2}}$$

where  $\mathbf{tf}_p$  depends on SF and is defined as:

$$\mathbf{tf}_p(\mathbf{sf}) = 2^{(Q+1)*(\log_2(\mathbf{sf}) - \log_2(\mathbf{sf}_0)) + \log_2(\mathbf{tf}_0)}$$

Each fit was based on average of  $31.6 \pm 0.82$  (mean  $\pm$  s.e.m.) SF/TF combinations.

From this Gaussian fit, the location of maximal excitation ( $\mathbf{sf}_0$ ,  $\mathbf{tf}_0$ ) of the contour plot of spatio-temporal tuning and the relationship between preferred speed and SF (indicated by the exponent  $Q$ ) could be determined. When  $Q$  is equal to zero, there is no relationship between SF tuning and speed preference, i.e. the neuron remains tuned to a particular speed of motion across all SFs. When  $Q$  is equal to -1, preferred speed is strongly dependent on SF such that as SF increases by one log unit, the preferred

speed of the neuron decreases by one log unit. That is, a  $Q$  value of -1 indicates that the SF tuning and TF tuning of the neuron are independent, i.e. the unit is spatio-temporally independent.

The Gaussian function was used to classify units as speed-tuned or spatio-temporally independent using a partial correlation analysis (Levitt et al. 1994; Priebe et al. 2003). For the partial correlation analysis, each peak from our sample was fit to two constrained Gaussians: 1) to provide a spatio-temporally independent prediction,  $Q$  was constrained to -1 (see Fig. 6.2, right column) to provide a speed-tuned prediction,  $Q$  was constrained to 0 (see Fig. 6.2, middle column). We computed the partial correlation of the actual data with the speed-tuned or independent prediction using the following equations:

$$R_{\text{ind}} = \frac{(r_i - r_s * r_{is})}{\sqrt{((1 - r_s^2)(1 - r_{is}^2))}}$$

$$R_{\text{speed}} = \frac{(r_s - r_i * r_{is})}{\sqrt{((1 - r_i^2)(1 - r_{is}^2))}}$$

where  $R_{\text{ind}}$  and  $R_{\text{speed}}$  are the partial correlations of the real data to the spatio-temporally independent and speed-tuned predictions, respectively;  $r_i$  is equal to the correlation of real data with the independent prediction;  $r_s$  is the correlation of the real data with the speed-tuned prediction; and  $r_{is}$  is the correlation of the two predictions.

The statistical significance of  $R_{\text{speed}}$  and  $R_{\text{ind}}$  was calculated with a Fisher  $Z$ -transform on the correlation coefficients  $\{Z_f = 1/2 * \ln[(1+R)/(1-R)]\}$ , and then calculating the difference between these  $z$ -scores (Papoulis 1990):

$$z_{\text{diff}} = (Zf_{\text{ind}} - Zf_s) / ((1/(N_{\text{ind}} - 3)) + 1/(N_s - 3))^{1/2}$$

where  $Zf_s$  is the Fisher Z-transform for  $R_{\text{speed}}$ ,  $Zf_{\text{ind}}$  is the Fisher Z-transform for  $R_{\text{ind}}$ , and  $N_s = N_{\text{ind}}$  = number of SF/TF combinations used in the best-fit Gaussian. A z-score of 1.65 was selected to denote significance. With this statistic, cells were categorized as speed-tuned if  $z_{\text{diff}} \leq -1.65$  and  $R_{\text{speed}}$  was significantly greater than 0. Likewise cells were categorized as SF/TF-independent if  $z_{\text{diff}} \geq 1.65$  and  $R_{\text{ind}}$  was significantly greater than 0. Cells not meeting these criteria were termed unclassifiable ( $1.65 > z_{\text{diff}} > -1.65$ ). This partial correlation technique has been used previously to assess motion integration in visual neurons (e.g. Movshon et al. 1985; Gizzi et al. 1990; Scannell et al. 1996; Crowder and Wylie 2002). The conventional criterion of a probability of 0.1 (i.e.  $z_{\text{diff}} > 1.65$  or  $z_{\text{diff}} < -1.65$ ) (Crow et al. 1960) has been justified by the fact that this method is not a true test of statistical significance, but a convenient way to reduce data (Movshon et al. 1985; Gizzi et al. 1990; Scannell et al. 1996; Crowder and Wylie 2002).

## Results

Figure 6.1 plots primary peaks locations of all 118 units, as determined from the best-fit Gaussians. A Ward's cluster analysis on peak locations showed that the two largest clusters corresponded to *fast* and *slow* cells. Of the 76 LM units (hexagons), 45 (59.2%) were classified as *fast* cells (mean TF : mean SF = 4.28Hz : 0.15cpd; range TF = 0.45 – 16.00Hz, SF = 0.05 – 0.28cpd) and 31 (40.8%) were *slow* cells (mean TF : mean SF = 0.48Hz : 0.57cpd; range, TF = 0.09 – 2.09Hz, SF = 0.14 –

1.00cpd). Of the 42 nBOR units (triangles), 4 (9.5%) were *fast* cells (mean TF : mean SF = 5.87Hz : 0.11cpd; range 0.51 – 12.69Hz, SF = 0.07 – 0.17cpd ) and 38 (90.5%) were *slow* cells (mean TF : mean SF = 0.41Hz : 0.57cpd; range TF = 0.10 – 1.59Hz, SF = 0.18 – 1.05cpd).

Figure 6.2 shows two representative units: a *fast* LM unit (Fig. 6.2A) and a *slow* nBOR unit (Fig. 6.2B). The left column shows the contour plots of the spatio-temporal tuning for the two units; below each contour plot, the normalized response is plotted as a function of speed for all SFs. From the unconstrained Gaussian fit, the unit in Fig. 6.2A had a peak in the *fast* zone at 1.22Hz/0.14cpd, and a  $Q$  value of -1.00, strongly suggesting SF/TF-independence. The unit in Fig. 6.2B had an oriented primary peak in the *slow* region at 0.28Hz/0.68cpd, and a  $Q$  value of -0.27, suggesting that speed tuning was principally independent of SF; speed tuning curves for all SF > 0.031cpd suggested tuning for stimuli moving at approximately 0.5°/s.

Predictions used for the partial correlation analysis are also shown in Figure 6.2. The right column shows the SF/TF-independent prediction for each unit ( $Q$  constrained to -1), and the middle column shows the speed-tuned prediction ( $Q$  constrained to 0); again, contour plots are shown directly above the corresponding speed tuning curves for the tested SFs. Note that the speed tuning curves for the speed-tuned prediction show a maximal response to the same speed of motion across all SFs. Clearly, the unit in Fig. 6.2A is more closely approximated by the spatio-temporally independent prediction, while the speed-tuned prediction provides a better approximation of the unit in Fig. 6.2B. The  $Z_{\text{diff}}$  scores for these units support this

observation: the unit in 2A had a  $z_{\text{diff}}$  of 4.69, while the unit in 2B had a  $z_{\text{diff}}$  of -3.10, indicating that the *fast* and *slow* peaks were significantly SF/TF-independent and speed-tuned, respectively.

Figure 6.3A and B show scatter plots of  $R_{\text{speed}}$  vs.  $R_{\text{ind}}$  for all the nBOR and LM units, respectively. The black lines separate the data space into 3 regions (based on the criteria described in the methods): speed-tuned, SF/TF-independent, and unclassified. Of the 38 *slow* nBOR units, 15 (39.5%) showed significant speed tuning, 20 were unclassified and 3 (7.9%) were spatio-temporally independent. Of the 4 *fast* nBOR units, 3 were SF/TF independent and 1 was unclassified. Of the 31 *slow* LM units, 6 (19.4%) showed significant speed tuning, 15 were unclassified and 10 (32.2%) were spatio-temporally independent. Of the 45 *fast* LM units, 1 (2.2%) showed significant speed tuning, 13 were unclassified and 31 (68.9%) were SF/TF-independent. Thus, combining data from nBOR and LM, *fast* units tend to be SF/TF-independent (34/49, 69.4%) or unclassified (14/49, 28.6%), but not speed-tuned (1/49, 2.0%); *slow* units tend to be speed-tuned (21/69, 30.4%) or unclassified (35/69, 50.7%), but not spatio-temporally independent (13/69, 18.8%).

Overall, *fast* LM units had a mean  $Q$  value of  $-0.95 \pm 0.05$  (mean  $\pm$  s.e.m.), *slow* LM units had a mean  $Q$  value of  $-0.68 \pm 0.09$ , *fast* nBOR units had a mean  $Q$  value of  $-1.00 \pm 0.20$ , and *slow* nBOR units had a mean  $Q$  value of  $-0.42 \pm 0.06$ . Because the mean  $Q$  values suggested differences between *fast* and *slow* neurons, and LM and nBOR neurons, we performed a one-way ANOVA comparing the  $Q$  scores of the four groups of neurons. Post-hoc analysis using the Tukey's HSD method revealed

that the  $Q$  scores of *slow* nBOR units were significantly different than all other groups (*fast* LM,  $p < .001$ ; *slow* LM,  $p < .042$ ; *fast* nBOR,  $p < .034$ ). In addition, the  $Q$  values of the *fast* LM units were significantly different than *slow* LM scores ( $p < .023$ ).

Because speed tuning was more apparent for the *slow* neurons and spatio-temporal independence was more common for the *fast* units (as indicated by both mean  $Q$  values and the partial correlation analysis), in Figure 6.3C we plotted the log transform of preferred speed (TF/SF) of each nBOR (white triangles) and LM unit (black hexagons) as a function of their  $Q$  value. Regression lines for nBOR and LM units were plotted separately using *SigmaPlot*. There was a significant negative correlation between the log of preferred speed and the value of  $Q$  (all units,  $P \ll .001$ ;  $R = -0.529$ ; nBOR units,  $P < .001$ ;  $R = -0.505$ ; LM units,  $P < .001$ .  $R = -0.404$ ); i.e. as preferred speed increased,  $Q$  approached -1 (SF/TF-independence), whereas tuning for slower speeds was associated with  $Q$  values closer to 0.

## Discussion

Perrone and Thiele (2001) examined the spatio-temporal tuning of direction-sensitive neurons in area MT in rhesus monkeys. They reported that neurons had oriented peaks in contour plots of their spatio-temporal tuning and concluded that MT neurons are tuned for speed. While such an oriented response profile is necessary for speed tuning, Priebe et al. (2003) emphasized that it is not sufficient. Priebe et al. (2003) used a 2-D Gaussian function termed  $Q$  analysis, as well as a partial correlation analysis, to quantitatively test the influence of SF on the speed tuning of neurons in

MT. They concluded that only about 25% of MT neurons were tuned for speed and suggested that without such quantitative analyses there is a danger in overestimating the incidence of speed tuning<sup>3</sup>.

It seems that we (Crowder et al. 2003a) have fallen victim to the caveat noted by Priebe et al. (2003). Crowder et al. (2003a) suggested that the majority of *slow* neurons in nBOR and LM show velocity-like tuning, whereas most *fast* units were TF-tuned (i.e. SF/TF-independent). Although we (Crowder et al. 2003a) used 2-D Gaussians to quantitatively analyze the spatio-temporal peaks, and showed that oriented Gaussians provided better fits across the population, we did not statistically compare speed-tuned and SF/TF-independent fits for individual cells. This was the aim of the present re-analysis. In this study, a meta-analysis of these data suggests that speed tuning is less common than previously implied. Only 39.5% of *slow* nBOR cells, and 19.4% of *slow* LM cells, showed significant speed tuning. Consistent with what we had previously suggested, only a single *fast* unit showed speed tuning and most (69.4%) *fast* cells exhibited TF tuning (3 of 4 nBOR cells, 31 of 45 LM cells). Approximately 41.5% of all cells were unclassifiable, most of which were *slow* cells (61.2%). It is possible that we have underestimated the incidence of *fast* speed-tuned units, if these units were tightly tuned relative to our sampling resolution. We do not feel this was a problem, however, since the response peaks in the contour plots of spatio-temporal tuning spanned multiple SF/TF combinations. Following Priebe et al.

---

<sup>3</sup> Priebe et al. (2003) also noted that tests utilizing sine wave gratings of a single spatial frequency underestimate the true speed tuning of MT neurons.

(2003), we suggest that the spatio-temporal response profile for motion sensitive units in LM and nBOR is best described as a continuum between two extremes represented by the SF/TF-independent and speed-tuned predictions. *Fast* cells fall toward the spatio-temporally independent end of the distribution, whereas *slow* cells generally fall closer to the speed-tuned prediction. Additionally, Crowder et al. (2003a) noted that the speed tuning was not completely independent of SF, using the term ‘velocity-like’ tuning. The analysis in the present study supports this assertion, as speed tuning was not completely independent of SF, and was rarely observed for extremely low SFs ( $<0.125^\circ/\text{s}$ ; e.g. Fig. 6.2B, speed tuning curve for SF=0.031cpd).

*Slow* neurons in the AOS and pretectum provide input to the vestibulocerebellum (Vbc) of pigeons via climbing fibre (CF) input from the inferior olive (Winship et al. 2005). Recently, Winship et al. (2005) assessed the spatio-temporal tuning of the complex spike activity (CSA) of Purkinje cells in the VbC, which reflects CF input. A reanalysis of these data using the combined  $Q$  and partial correlation analysis from the present study suggest that, as in LM and nBOR, the degree of speed tuning of the CSA shows remarkable diversity: 25.6% of CSA showed significant velocity-like tuning (compared to 30.4% of *slow* units in this study), 61.5% was unclassified, and 12.8% was spatio-temporally independent. Combined with similar results from experiments in V2 and MT (Levitt et al. 1994; Priebe et al. 2003), our data from LM, nBOR, and VbC support the suggestion of Priebe et al. (2003) that diversity in the impact of spatial frequency on speed tuning may be a general property of motion-sensitive neurons.

Pretectal and nBOR units have been modeled with a modified version of the Reichardt detector (Crowder et al. 2003a), the hallmark of which is SF/TF-independence (Buchner 1984; Egelhaaf et al. 1989; Ibbotson et al. 1994; Srinivasen et al. 1999; Clifford and Ibbotson 2003). However, Zanker et al. (1999) demonstrated that a Reichardt detector can show velocity-like tuning if the balance between its two constituent half detectors is altered. The more ‘unbalanced’ the detector, the closer the approximation to true speed tuning. We (Crowder et al. 2003a) argued that velocity-like tuning observed in the *slow* nBOR neurons reflects the properties of an unbalanced Reichardt detector. With the continuum between speed tuning and SF/TF-independence in mind, perhaps there is a continuum with respect to the degree of balance for the *slow* cells: cells classified as speed-tuned are more unbalanced than those falling in the unclassified region. Conversely, *fast* cells would have balanced constituent half detectors.

**Acknowledgements:**

We would like to thank Peter L. Hurd for assistance with statistical analysis and the three anonymous reviewers for their insightful comments.

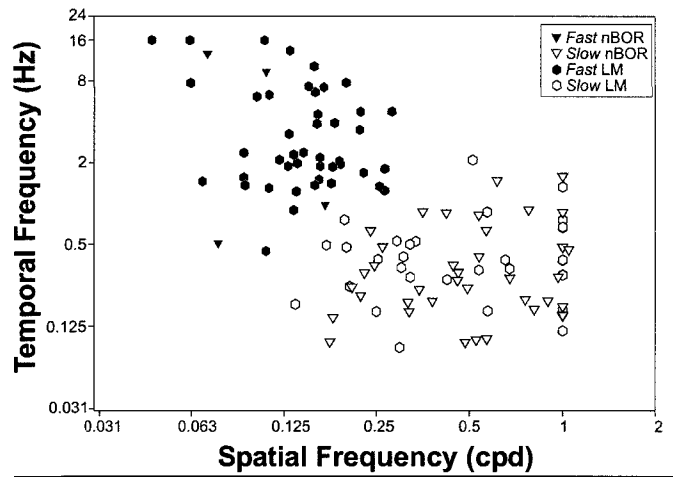


**Figure 6.1:** The locations of the primary peaks in the spatio-temporal domain for 42 units in the nucleus of the basal optic root (nBOR) and 76 units from the lentiformis mesencephali (LM) (from Wylie and Crowder 2000; Crowder and Wylie 2001; Crowder et al. 2003a,b, 2004) are indicated as a function of preferred spatial (SF, abscissa) and temporal frequency (TF, ordinate). Triangles and hexagons show peaks from nBOR and LM, respectively. As determined from the cluster analysis, black symbols indicate *fast* cells, while white symbols show *slow* cells.

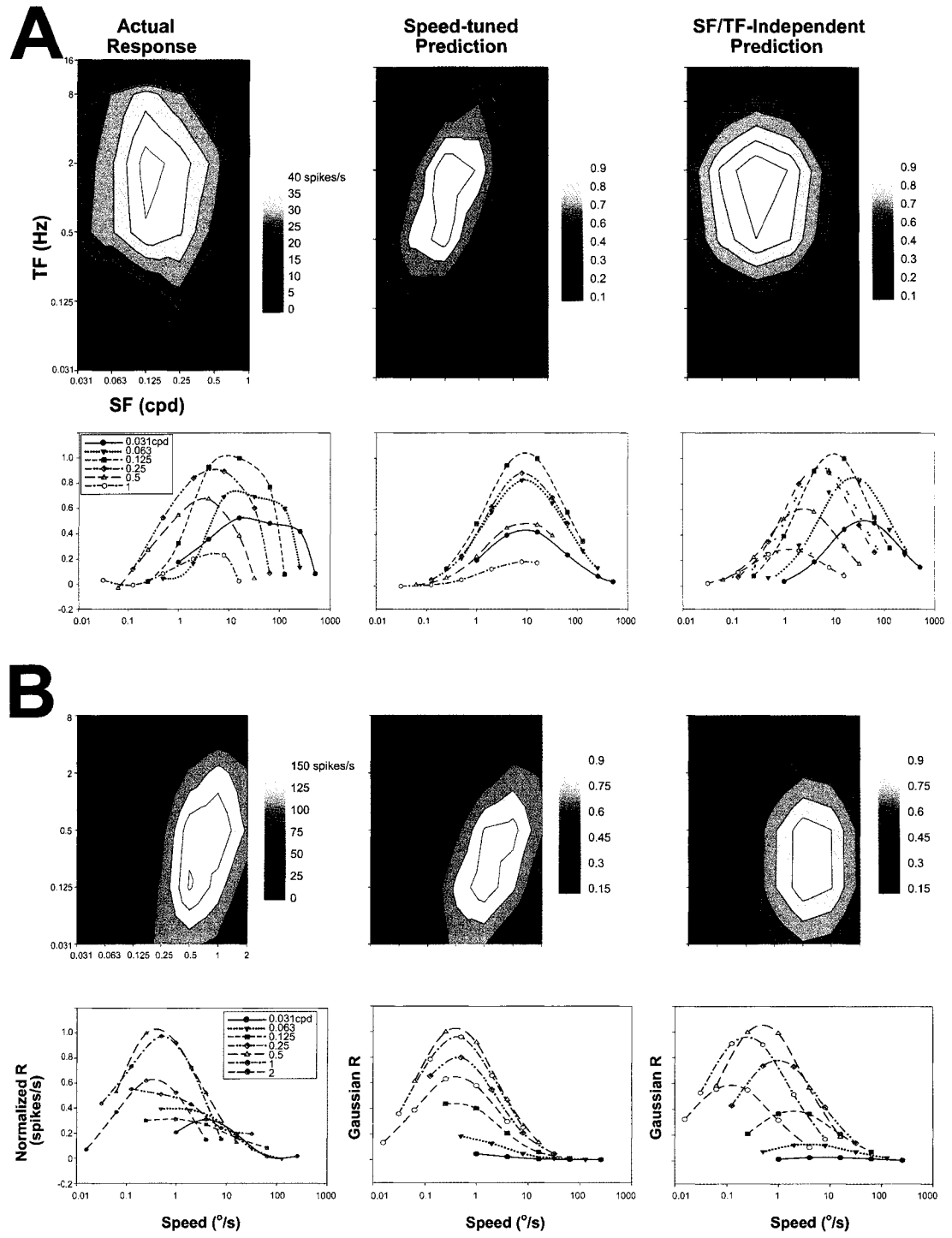
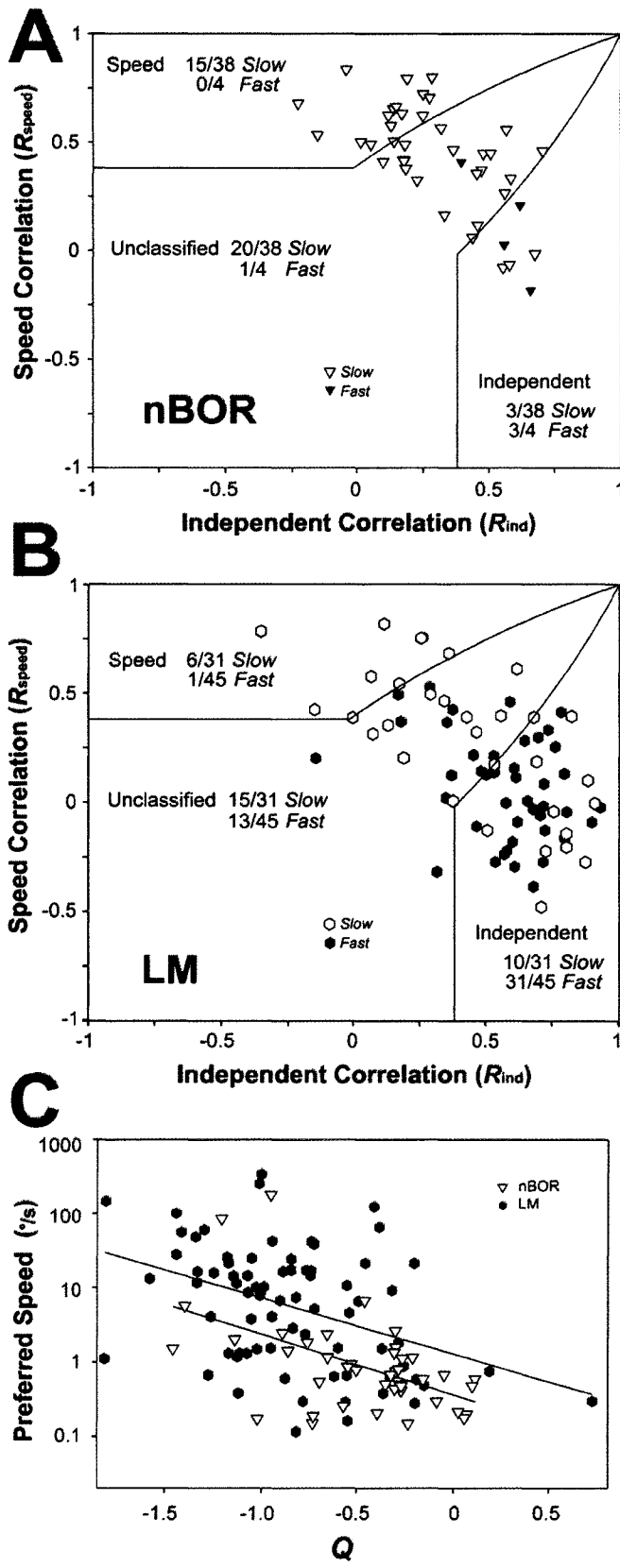


Figure 6.2: Fig. 6.2A and 6.2B respectively show the spatio-temporal tuning of units from the lentiformis mesencephali (LM) and the nucleus of the basal optic root (nBOR). The left column shows contour plots illustrating the firing rate in response to sine wave gratings of varying spatial (SF, abscissa) and temporal (TF, ordinate) frequencies. SF and TF are plotted on a logarithmic scale. The plot is shaded such that white represents the SF –TF combinations resulting in maximal excitation and black indicates minimal excitation. The unit in 2A had a primary peak in the *fast* zone, while 2B was tuned to *slow* gratings. The middle column shows the corresponding speed-tuned prediction from the Gaussian fit with  $Q$  constrained to 0. Likewise, the right column shows the spatio-temporally independent prediction from the Gaussian fit with  $Q$  constrained to -1. Below each contour plot, the unit's normalized response is plotted as a function of the speed of the gratings across all SFs. The independent prediction provides a better fit for the unit in A, whereas the unit in B is more closely approximated by the speed-tuned prediction.



**Figure 6.3:** Fig. 6.3A and 6.3B show scatter plots of partial correlations for speed ( $R_{\text{speed}}$ ) and spatio-temporally independent ( $R_{\text{ind}}$ ) tuning for units in nBOR and LM, respectively. Each data point indicates the degree to which a particular unit from the nBOR (3A) or LM (3B) is correlated with speed-tuned and independent predictions. The data space is divided into three regions by the solid black lines. These black lines are approximations, based on statistical criteria that assume 31.6 SF/TF combinations in the Gaussian fits. Speed-tuned, unclassifiable, or spatio-temporally independent cells fall in the upper left, middle, or lower right areas of the scatter plot, respectively. White and black symbols indicate *slow* and *fast* units, respectively. Figure 6.3C shows the preferred speed plotted as a function of  $Q$  values for all units (black hexagons, LM; white triangles, nBOR). Regression lines for nBOR and LM units are plotted independently. A significant negative correlation ( $P \ll .001$ ,  $R = -0.529$ ) between  $Q$  and speed preference was observed.

## References

- Borst A, Egelhaaf M.** Principles of visual motion detection. *Trends in Neurosci* 12: 297-306, 1989.
- Buchner E.** Behavioral analysis of spatial vision in insects. In: *Photoreception and Vision in Invertebrates*, edited by Ali MA. New York: Plenum Press, 1984, p. 561-621.
- Clifford CWG, Ibbotson, MR.** Fundamental mechanisms of visual motion detection: models, cells, and functions. *Progress in Neurobiology* 68: 409-437, 2003.
- Crow EL, Davis FA, Maxfield MW.** *Statistics Manual, With Examples Taken from Ordinance Development*. New York: Dover, 1960.
- Crowder NA, Dawson MR, and Wylie DR.** Temporal frequency and velocity-like tuning in the pigeon accessory optic system. *J Neurophysiol* 90: 1829-41, 2003a.
- Crowder NA, Dickson CT, and Wylie DR.** Telencephalic input to the pretectum of pigeons: an electrophysiological and pharmacological inactivation study. *J Neurophysiol* 91: 274-85, 2004.
- Crowder NA, Lehmann H, Parent MB, and Wylie DR.** The accessory optic system contributes to the spatio-temporal tuning of motion-sensitive pretectal neurons. *J Neurophysiol* 90: 1140-51, 2003b.
- Crowder NA, and Wylie DRW.** Fast and slow neurons in the nucleus of the basal optic root in pigeons. *Neurosci Lett* 304: 133-136, 2001.

- Crowder NA, Wylie DR.** Responses of optokinetic neurons in the pretectum and accessory optic system of the pigeon to large-field plaids. *J Comp Physiol A Neuroethol Sens Neural Behav Physiol* 188: 109-19, 2002.
- Egelhaaf M, Borst A, Reichardt W.** Computational structure of a biological motion-detection system as revealed by local detector analysis in the fly's nervous system. *J. Opt. Soc. Am. A.* 6: 1070-1087, 1989.
- Gizzi MS, Katz E, Schumer RA, and Movshon JA.** Selectivity for orientation and direction of motion of single neurons in cat striate and extrastriate visual cortex. *J Neurophysiol* 63: 1529-1543, 1990.
- Ibbotson MR, Mark RF, and Maddess TL.** Spatio-temporal response properties of direction-selective neurons in the nucleus of the optic tract and the dorsal terminal nucleus of the wallaby, *Macropus eugenii*. *J Neurophysiol* 72: 2927-2943, 1994.
- Ibbotson MR, and Price NS.** Spatio-temporal tuning of directional neurons in mammalian and avian pretectum: a comparison of physiological properties. *J Neurophysiol* 86: 2621-2624, 2001.
- Karten HJ, and Hodos W.** *A stereotaxic Atlas of the Brain of the Pigeon (Columba livia)*. Baltimore: Johns Hopkins Press, 1967.
- Levitt JB, Kiper DC, and Movshon JA.** Receptive fields and functional architecture of macaque V2. *J Neurophysiol* 71: 2517-2542, 1994.
- Movshon JA, Adelson EH, Gizzi MS, and Newsome WT.** The analysis of visual moving patterns. In *Study Group on Pattern Recognition Mechanisms*, edited

by Chagas C, Gattass R, Gross C. Vatican City: Pontificia Academia Scientiarum, 1985, p. 117-151.

**Papoulis A.** *Probability and Statistics*. New York: Prentice-Hall International Editions, 1990.

**Perrone JA, and Thiele A.** Speed skills: measuring the visual speed analyzing properties of primate MT neurons. *Nature Neurosci* 4: 526-531, 2001.

**Priebe NJ, Cassanello CR, and Lisberger SG.** The neural representation of speed in macaque area MT/V5. *J Neurosci* 23: 5650-5661, 2003.

**Scannell JW, Sengpiel F, Tovee MJ, Benson PJ, Blakemore C, and Young MP.** Visual motion processing in the anterior ectosylvian sulcus of the cat. *J Neurophysiol* 76: 895-907, 1996.

**Simoncelli EP, Heeger DJ.** Representing retinal image speed in visual cortex. *Nat Neurosci* 4: 461-2, 2001.

**Simpson JI.** The accessory optic system. *A Rev Neurosci* 7: 13-41, 1984.

**Simpson JI, Giolli RA, and Blanks RHI.** The pretectal nuclear complex and the accessory optic system. *Rev Oculomot Res* 2: 335-64, 1988.

**Srinivasan MV, Poteser M, Kral K.** Motion detection in insect orientation and navigation. *Vis Res* 39: 2749-2766, 1999.

**Winship IR, Hurd PL, & Wylie DRW.** Spatio-temporal tuning of optic flow inputs to the vestibulocerebellum in pigeons: Differences between mossy and climbing fibre pathways. *J Neurophysiol* 93: 1266-77, 2005.

**Wylie DR, and Crowder NA.** Spatio-temporal properties of fast and slow neurons in the pretectal nucleus lentiformis mesencephali in pigeons. *J Neurophysiol* 84: 2529-2540, 2000.

**Zanker JM, Srinivasan MV, and Egelhaaf M.** Speed tuning in elementary motion detectors of the correlation type. *Biol Cybern* 80: 109-16, 1999.

**CHAPTER 7:**  
**RECEPTIVE FIELD STRUCTURE OF OPTIC FLOW RESPONSIVE**  
**PURKINJE CELLS IN THE VESTIBULOCEREBELLUM OF PIGEONS**

Manuscript *in press* with Visual Neuroscience.

As an organism moves through an environment consisting of numerous stationary objects and surfaces, characteristic patterns of visual motion occur across the entire retina. These patterns of motion are referred to as optic flow or flowfields (Gibson, 1954). Optic flowfields can be described as vector fields where the length of each vector gives the velocity and its orientation the direction of the respective image shift (Koenderink & van Doorn, 1987; Nakayama & Loomis, 1974; Krapp et al., 1998). The global structure of these flowfields depends on the type of self-motion being performed at a particular time. Figure 1 shows examples of optic flowfields resulting from self-rotation (A) and self-translation (B,C), as projected onto a sphere surrounding the observer. Self-rotation produces a circular flow (opposite the direction of the head rotation) about the axis of rotation and laminar (planar) flow along the “equator” of this sphere. Self-translation also results in planar motion along the equator, but radial optic flow along the vector of translation. There is a focus of expansion (FOE; see Fig. 1C) in the direction of motion from which the visual image radiates outward and a focus of contraction (FOC) opposite the FOE where the visual image converges (see Fig. 1B).

In the vertebrate brain, neurons sensitive to optic flow patterns have been recorded in the the olivo-vestibulocerebellar pathway (e.g. Simpson et al. 1981; Leonard et al. 1988; Graf et al. 1988; Winship & Wylie 2001; Wylie et al. 1993, 1998), and extrastriate visual cortical areas, in particular the medial superior temporal cortex (MST) (Saito et al., 1986; Tanaka et al., 1986, 1989; Tanaka & Saito, 1989; Duffy & Wurtz, 1991a; for review, see Duffy, 2004). In the pigeon

vestibulocerebellum (VbC), the complex spike activity (CSA) of Purkinje cells in the ventral uvula and nodulus is modulated best by optic flow that results from self-translation along one of three axes in 3-dimensional space (Wylie et al., 1993, 1998; Wylie & Frost, 1999a). With respect to the preferred axes of translational optic flow, there are four relatively homogeneous response types organized into parasagittal zones (Wylie et al., 1998; Wylie & Frost, 1999a; Wylie et al., 2003b). *Ascent* and *descent* neurons prefer flowfields resulting from upward or downward translation along the vertical axis. *Expansion* neurons respond best to optic flow resulting from forward translation along an axis oriented at 45° ipsilateral (i) to the midline and approximately +20° elevation (i.e. FOE at 45°i / +20° elevation) while *contraction* neurons prefer flowfields resulting from backward translation along an axis oriented at 45° contralateral (c) azimuth (FOC at 45°c azimuth). The preferred flowfields and axes of translation are shown for *contraction* and *expansion* neurons in Figure 1B and C, respectively. In the flocculus of the VbC, CSA responds best to optic flow resulting from self-rotation. The rotation cells in the flocculus respond best to rotational optic flow about one of two axes in 3-dimensional space: either the vertical axis or an horizontal axis oriented at 45°c azimuth (Wylie & Frost, 1993). We refer to these two response types as *rVA* and *rH45c* neurons, respectively (Wylie, 2001; Winship & Wylie, 2001). The preferred flowfield and axis of rotation for an *rH45c* neuron is shown in Figure 1A. In the rabbit VbC, *rVA* and *rH45c* neurons have been recorded (Leonard et al., 1988; Graf et al., 1988; Simpson et al., 1979, 1981, 1988a,b, 1989;

Kano et al., 1990a,b; Kusunoki et al., 1990), but no translation-sensitive neurons have been found.

Simpson and colleagues (Leonard et al., 1988; Graf et al., 1988; Simpson et al., 1979, 1981, 1988a,b, 1989) suggested that the *rH45c* neurons were not precisely tuned to the rotational optic flow field. Rather it was proposed that these neurons had a RF structure that “approximated” the preferred optic flow field with a “bipartite” organization, as illustrated in Figure 2E. The RF consists of a region preferring upward motion on the left apposed to a region preferring downward motion on the right. The preferred optic flow field would be clockwise rotation about an axis centered on the boundary of the two hemifields. The bipartite RF structure contrasts with a RF structure that is “precisely” tuned to the preferred flowfield, which receives converging inputs from many direction-selective cells with small receptive fields (Tanaka et al., 1989; Orban et al., 1992; Krapp & Hengstenberg, 1996; Krapp et al., 1998). For example, a precisely tuned neuron preferring rotational optic flow would have a RF precisely matched to the flowfield shown in Figure 2D: it would prefer rightward-downward motion in the shaded region S1, downward motion in S2 and upward-leftward motion in S3. Studies of optic flow sensitive neurons in primate MST and parietal cortex suggest that they have an underlying RF with precise tuning (Steinzmetz et al., 1987; Tanaka et al., 1989; Tanaka & Saito, 1989; Orban et al., 1992; Duffy, 2004). To our knowledge, the stimuli used to show that the MST neurons do not have bipartite RFs have not been applied to the optic flow neurons in the olivo-cerebellar system.

Thus, in the present study, we investigated the RF structure of *expansion*, *contraction* and *rH45c* neurons in the VbC of pigeons with two separate tests similar to those used in previous studies of extrastriate visual neurons (Tanaka et al., 1989; Tanaka and Saito, 1989; Schaafsma and Duysens, 1996). In general our results suggest that VbC neurons have an underlying bipartite receptive field structure, as opposed to precise tuning.

## **Methods**

### *Surgery*

The methods reported herein conformed to the guidelines established by the Canadian Council on Animal Care and were approved by the Biosciences Animal Care and Policy Committee at the University of Alberta. Silver King or Homing pigeons (*Columba livia*) were anaesthetized with a ketamine (65 mg/kg) - xylazine (8 mg/kg) mixture (i.m.) and supplemental doses were administered as necessary. The animals were placed in a stereotaxic device with pigeon ear bars and beak adapter such that the orientation of the skull conformed to the atlas of Karten & Hodos (1967). A section of bone and dura was then removed to expose the cerebellum. Two different exposures were used: a medial exposure designed to access the ventral uvula and nodulus, and a lateral exposure through the anterior semicircular canal to access the flocculus.

### *Extracellular Recordings and Optic Flow Stimulation*

Pigeons were removed from the ear bars and beak adapter after exposure of the cerebellum, and attached to a head bar such that their eye-beak angle was  $34^\circ$ , which is the normal orientation of the head in a freely moving bird (Erichsen et al., 1989). This involved pitching the beak upward about the inter-aural axis by  $38^\circ$  relative to the stereotaxic position of Karten & Hodos (1967). Extracellular single unit recordings were then made using glass micropipettes filled with 2M NaCl (tip diameters of 3-5 $\mu$ m). Electrodes were advanced using an hydraulic microdrive (Frederick Haer & Co.) and raw signals were amplified, filtered and fed to a data analysis system (Cambridge Electronic Designs (CED) *1401plus*). The raw trace of the extracellular recording was spike-sorted to ensure isolation of a single unit using *Spike2* software (CED). Peri-stimulus time histograms (PSTHs) were constructed using *Spike2*.

The CSA of Purkinje cells was identified and isolated based on their characteristic spike shape and spontaneous firing rate of about 1 spike/s. Isolated units were first stimulated with a large (about  $90^\circ \times 90^\circ$ ) handheld stimulus consisting of a random pattern of dots and lines to determine if the cell was sensitive to visual stimulation. By moving this stimulus in different areas of the panoramic binocular visual field, the optic flow preference of each unit was qualitatively determined. On occasion we also recorded from the units in response to panoramic flowfields produced by planetarium projectors described in detail in previous studies (Wylie & Frost, 1993, 1999b). The test stimuli (see below) were back-projected onto a screen

measuring  $90^\circ \times 75^\circ$  (width  $\times$  height) that was positioned tangent to the preferred axis of translation or rotation for the isolated unit. The stimuli consisted of square-wave gratings (contrast =  $0.80 [(LuminanceMAX-LuminanceMIN) / (LuminanceMAX+LuminanceMIN)]$ ); mean luminance =  $65\text{cd/m}^2$ ; refresh rate = 80 Hz) of an effective spatial and temporal frequency (spatial frequency = 0.25-0.5 cycles per degree (cpd), temporal frequency = 0.125-0.5Hz; Winship et al., 2005).

### *Subfield Stimuli*

RF mapping studies in the parietal cortex of primates and in optic flow neurons in invertebrate species have typically utilized relatively small stimuli moving throughout the visual field to map visually responsive areas (e.g. *primates*, Schaafsma & Duysens, 1996; Duhamel et al. 1997; Ben Hamed et al. 2001; Bremmer et al. 2002; Avillac et al. 2005; *blowfly*, Krapp and Hengstenberg, 1996; Krapp et al. 1998; *shore crab*, Barnes et al. 2002). A larger stimulus was used in the present study, as small visual stimuli are not effective modulators of CSA in the VbC (Simpson & Alley, 1974). Thus, to determine the local motion sensitivity and local preferred direction in different areas of the RFs of *expansion*, *contraction*, and *rH45c* neurons (simply referred to as *rotation* neurons hereafter), 24 units were tested with a  $45^\circ \times 37.5^\circ$  square wave grating drifting in different subfields. These eight subfields were centred about the preferred axis of rotation or translation (i.e. *rotation* units,  $45^\circ$  c; *expansion* units,  $45^\circ$  i/+ $20^\circ$  elevation; *contraction* units,  $45^\circ$  c), and gratings of an effective SF and TF were moved in eight directions ( $45^\circ$  intervals) within each subfield to obtain a

tuning curve for direction preference in each of the eight areas. Each sweep consisted of 2 seconds (s) of motion, a 1s pause with a uniform grey screen of standard mean luminance, followed by 2s of motion in the opposite direction, and a 1s pause. Tuning curves were averaged from a minimum of 6 sweeps. The arrangement of the subfields is shown in Figure 5A. Each subfield is identified numerically. For *rotation* and *contraction* units, subfields 1, 7, and 8 would span 45-90°c azimuth, and 3, 4, and 5 would span 0-45°c; for *expansion* units, subfields 3, 4, and 5 would span 45-90°i, and 1, 7, and 8 would span 0-45°i. Note that the subfields are overlapping. e.g. subfield 2 includes the medial halves of subfields 1 and 3.

#### *Vector Analysis of Subfield Responses*

The tuning curve for each subfield was assigned a vector illustrating the preferred direction and the breadth and magnitude of the direction selectivity. The preferred direction (PD) was calculated using the following equation:

$$(1) \quad \text{PD} = \tan^{-1}[\{\sum\{R_d \sin(\theta_d)\} / \{\sum\{R_d \cos(\theta_d)\}\}]$$

where  $\theta_d$  is the direction of stimulus motion and  $R_d$  is equal to the firing rate minus spontaneous in response to that direction of stimulus motion.

Vector length was determined by calculating the sensitivity index (SI) for each tuning curve, as outlined by Vogels and Orban (1994). In circular statistics, the response  $R_d$  to each direction of motion is represented by a vector with a direction  $\theta_d$  and length  $R_d$ . The SI represents the normalized length of the sum of these vectors:

$$(2) \quad \text{SI} = \{[\sum(R_d * \sin(\theta_d))]^2 + [\sum(R_d * \cos(\theta_d))]^2\}^{1/2} / (\sum R_d)$$

where  $R_d$  is equal to the firing rate minus spontaneous and  $\theta_d$  is equal to the direction of stimulus motion. A higher SI reflects a narrower tuning curve. We then scaled the SI to the depth of modulation for that tuning curve, and these scaled SI values were then normalized among the eight subfields for each unit. In Figure 5B, vectors representing the PD and scaled SI (vector length) are superimposed on their respective subfield tuning curves. In Figure 6, the vectors from all subfields in 24 units tested with the subfield stimulus are illustrated according to cell type.

#### *Composite Largefield Stimuli and Rationale*

Because CSA showed less than maximal modulation in response to the subfield stimuli, we also constructed composite largefield stimuli similar to those used in previous studies of MST (Tanaka et al. 1989; Tanaka & Saito, 1989) to directly test the bipartite vs. precise RF structure predictions. These stimuli, illustrated in Figure 2C and F, were composed of square wave gratings drifting in different directions in different sub-regions of the RF, organized in such a way as to approximate the preferred flowfield along the axis of translation or rotation. *Expansion* neurons were tested using the stimulus illustrated in Figure 2C centred to the axis at  $45^\circ$  azimuth /  $+20^\circ$  elevation (Wylie & Frost, 1999a; Winship & Wylie, 2001). The stimulus consisted of four configurations, each presented for five seconds with gratings moving centripetally (i.e. approximated contraction), followed by a five second pause with a uniform grey screen of standard mean luminance, five seconds of centrifugal motion (i.e. approximated expansion), and another five second pause. In the first two

configurations (*horizontal bars* and *vertical bars*), the FOC/FOE was approximated using a bipartite stimulus with horizontal or vertical gratings moving in opposite directions. In the other two configurations (*X* and *cross*), the stimulus was divided into four subregions to more closely approximate the FOC/FOE. CSA modulation in response to each configuration was recorded over 3-10 sweeps. *Contraction* neurons were tested using the stimulus illustrated in Figure 2C centred along the axis at 45° azimuth.

*Rotation* neurons were tested using the stimulus illustrated in Figure 2F centred along the axis at 45° azimuth. The stimulus consisted of five configurations, each of which was presented for five seconds with CW movement of the gratings, followed by a 5.5 second pause with a uniform grey screen, five seconds of CCW motion, and another 5.5 second pause. Two configurations simulated rotational optic flow via a bipartite stimulus (*horizontal shear* and *vertical shear*), two conditions simulated rotation with a stimulus consisting of four subregions (*X* and *cross*), and a final condition projected a true rotational stimulus (*windmill*). CSA modulation in response to the stimulus was recorded over 3-10 sweeps. For units in the left flocculus, CW rotation would elicit maximal excitation, while CCW stimulus movement would inhibit the unit (neurons in the right flocculus showed the opposite direction preference).

Using these stimuli, the prediction was that if the RF were precisely tuned to their preferred optic flowfield, the CSA of translation-sensitive neurons would modulate equally to the *vertical bar* and *horizontal bar* conditions in Figure 2C, and

*rotation* neurons would modulate equally to the *horizontal shear* and *vertical shear* conditions shown in Figure 2F. For example, if the response map along the preferred axis of an *expansion* neuron was precisely tuned to the preferred flowfield (i.e. the response map around the preferred axis precisely matched the flowfield as in Figure 2A), an equal number of motion detectors would be excited by the *horizontal bar* and *vertical bar* conditions, and the neuron would show equal modulation to each condition (e.g. see Fig. 13 of Tanaka and Saito, 1989). Furthermore, modulation to the *X* and *cross* conditions should surpass that of the shear configurations since the *X* and *cross* more closely approximate the preferred flowfield (e.g. see Figs. 8,9 of Tanaka et al. 1989). However, if the tuning was approximated using a limited number of direction preferences, such as illustrated in Figure 2B, differential modulation to the two conditions would be expected. For a RF organized as in Fig. 2B, significant modulation to the *vertical bar* but not the *horizontal bar* configuration would be expected. For *rotation* neurons tested with the stimulus shown in Figure 2F, the predictions would be nearly identical: if *rotation* neurons are precisely tuned, modulation to *horizontal shear* and *vertical shear* conditions should not differ, and more modulation might be expected to the *X*, *cross*, and *windmill* conditions which more closely approximate the flowfield around the axis of rotation (see Tanka & Saito, 1989; Tanaka et al., 1989).

## Results

Experiments were performed in 19 pigeons. CSA in the VbC was isolated, and optic flow preference were reliably recorded and quantitatively identified as the *expansion*, *contraction*, or *rotation* response type. As in previous studies, we generally found several units of the same optic flow preference grouped into parasagittal bands in the VbC: *rotation* units were found laterally in the flocculus, while *contraction* neurons were found adjacent to the midline medial to *expansion* neurons in the nodulus and ventral uvula (Wylie et al., 1993; Crowder et al., 2000; Winship & Wylie, 2003; Wylie et al., 2003a,b). A total of 22 *rotation* units, 11 *expansion* units, and 22 *contraction* units were recorded and quantitatively analyzed in this study.

#### *Responses to Composite Largefield Stimuli*

In Figure 3A and 3B we compare the responses of a *rotation* unit to the *vertical shear* stimulus (B) and panoramic optic flow about the preferred axis produced by a planetarium projector (A; see Wylie & Frost, 1993, 1999a). The depth of modulation in response to these two stimuli was virtually identical. In Figure 3C, the modulation of a typical *rotation* unit in the right flocculus in response to all configurations of the simulated rotation stimulus is shown. White and black bars show the average firing rate of the unit minus spontaneous rate across 5 sweeps in response to simulated CW (white arrows) and CCW (black arrows) rotation, respectively. (Note, CW and CCW directions refer to the bird's perspective). The *horizontal shear* configuration resulted in very little modulation of this cell's CSA. All other conditions showed excitation in response to simulated CCW rotation, and inhibition

to CW rotation. The *vertical shear* and *X* conditions produced the greatest modulation of CSA. Note the difference in modulation in the *horizontal shear* versus *vertical shear* conditions. Such a difference was present in all *rotation* units recorded in this study: *vertical shear* always resulted in much greater modulation than *horizontal shear*.

In Figure 3D, the modulation of a typical *contraction* unit in response to all expansion/contraction configurations is illustrated. White and black bars respectively show the average firing rate of the unit minus spontaneous rate across 6 sweeps in response to simulated contraction (white arrows) and expansion (black arrows). Effectively no modulation occurred in response to the *horizontal bar* configuration, while in all other configurations, simulated contraction is preferred over expansion. The *vertical bar* condition showed the greatest modulation. In particular, note the difference in modulation in the *horizontal* versus *vertical bar* conditions. Such a difference was present in all *contraction* and *expansion* units recorded in this study: *vertical bars* always resulted in much greater modulation than *horizontal bars*.

Figure 4A summarizes the responses of all *rotation* (n=22) units. Depth of modulation was calculated for each of the five configurations using the following equation:

$$(3) \quad \text{Depth of Modulation} = (R_a - R_b)/(R_a + R_b)$$

where  $R_a$  and  $R_b$  respectively equal the firing rate to visual motion in the preferred and anti-preferred directions. These values were then normalized among the five stimulus configurations (i.e. the stimulus configuration eliciting the greatest modulation was

assigned a value of 1.0). The five resultant values were then averaged across all cells. *Horizontal shear* showed the least modulation of all configurations ( $0.303 \pm 0.049$ , mean  $\pm$  s.e.m.). Pair-wise comparisons (Tukey's HSD) showed that this value was significantly lower ( $\alpha = .05$ ) than those for each of the other configurations (all  $p \ll .001$ ). The depth of modulation for the *vertical shear* configuration was significantly greater than the *windmill* ( $p < .002$ ), but not different from the *X* and *cross* configurations. The depth of modulation for the *X* configuration was significantly greater than all but the *vertical shear* configuration (*cross*,  $p < .02$ ; *windmill*,  $p \ll .001$ ). It is important to note that the depth of modulation in response to the *horizontal shear* configuration was significantly greater than 0 ( $p < .001$ )

Figure 4B summarizes the response of all *contraction* ( $n=22$ ) and *expansion* ( $n=11$ ) units to the simulated contraction/expansion stimulus. As in 4A, the depth of modulation was calculated by averaging the normalized depth of modulation values for each of the four stimulus configurations (See equation (3)). White and black bars show the mean depth of modulation for *contraction* and *expansion* units to each configuration, respectively. For the *contraction* units, post-hoc analysis using Tukey's HSD revealed that mean depth of modulation was significantly greater for the *vertical bar* configuration than all other configurations ( $\alpha = .05$ ; *horizontal bar*,  $p \ll .001$ ; *cross*,  $p < .01$ ; *X*,  $p < .002$ ). In addition, the depth of modulation values in response to the *horizontal bar* configuration was significantly less than all other configurations (*vertical bar*,  $P < .000$ ; *cross*,  $P < .001$ ; *X*,  $p < .006$ ). For the *expansion* units, the depth of modulation was significantly different only for the *horizontal bar* vs. *vertical*

*bar* configurations ( $p \ll .001$ ), although differences between the depth of modulation to the *vertical bar* vs. the *X* and *cross* configurations approached significance ( $p < .051$  and  $p < .052$ , respectively). Note that the *horizontal bar* configuration was significantly greater than 0 for both the *contraction* ( $p \ll .001$ ) and *expansion* neurons ( $p < .01$ ).

### *Responses to Subfield Stimulation*

Twenty-four units (7 *rotation*, 11 *contraction*, 6 *expansion*) were tested with the subfield stimuli to determine the local motion sensitivity and direction-preference in eight different sub-regions shown in Figure 5A. Figure 5B shows a representative series of tuning curves for a *rotation* cell. The tuning curves plot the firing rate minus spontaneous rate (areas in grey represent negative values) as a function of the direction of motion in polar coordinates, and the corresponding subfields are indicated numerically. For each tuning curve, vectors illustrating the preferred direction (PD) and scaled SI (as described in the Methods) are included. Based on these vectors, this neuron preferred downward motion in subfields 1 and 8, upward motion in subfields 3, 4 and 5, downward-rightward motion in subfield 7, and rightward motion in subfield 6. Clearly there were differences between the subfields with respect to the depth of modulation: greatest for subfields 1, 8 and 6 and least for subfields 2 and 3. In addition there were differences with respect to the breadth of tuning: clearly the cell was most tightly tuned to motion in subfield 1, and the tuning curve in subfields 2 and 7 were very broad.

The subfield tuning curves can be qualitatively examined to determine if they match a bipartite RF or a precisely tuned organization. For example, for the *rotation* unit shown in Fig. 5, the tuning curves in subfields 1 and 3 lend support to a bipartite RF organization; however, the tuning curves from subfields 5, 6, and 7 seem better aligned with a precisely tuned RF. Subfield 2 clearly does not support a precise RF structure. (Note, however, that the response observed in subfields 2 and 6 are difficult to determine. If the underlying receptive field is bipartite, the direction tuning for subfields 6 could be approximated by averaging the responses to fields 5 and 7).

In Figure 6, vectors illustrating the PD and scaled SI of all subfield tuning curves are collapsed according to cell type. Dotted lines represent the mean preferred direction in each subfield as determined by vector summation i.e. the population response. Solid and open circles respectively show the predicted preferred direction for each subfield in a bipartite or precisely tuned receptive field. Figs. 6A, 6B, and 6C show the vector fields for 7 *rotation* units, 11 *contraction* units, and 6 *expansion* units, respectively. For 6A, qualitatively it appears the population direction tuning is better approximated by the bipartite prediction. The data from fields 3, 5, and 7 show bias towards the precise predictions although the vector lengths are quite small. For field 6, the weighted average vector is close to the precise prediction, but the vectors are very small. For the *contraction* units (Fig. 6B), the vectors in subfields 1 and 3 appear closely aligned with the precise prediction, whereas 5 and 7 are closer to the bipartite prediction. Conversely, for the *expansion* units (Fig. 6C), the vectors in

subfields 1 and 3 are closer to the bipartite prediction, whereas those in fields 5 to 7 are closer to the precisely tuned predictions.

To assess whether the bipartite or precisely tuned predictions offered a better estimate of true RF organization, a pair of quantitative analyses were performed. First, we calculated confidence intervals for the mean preferred angle *rotation*, *contraction*, and *expansion* units using a non-parametric bootstrap (Efron & Tibshirani, 1994). For each type of neuron, mean vectors from subfields 1, 3, 5, and 7 were reflected such that  $0^\circ$  would represent the bipartite prediction and  $45^\circ$  would be the precisely tuned prediction. Ninety-five percent confidence intervals (95% CI) for each class of neuron were then developed based on 1000 resamplings performed in *R* (*R* Development Core Team, 2005). For the *contraction* units, the 95% CI for the mean is from  $-5.22^\circ$  to  $33.71^\circ$ , while the 95% CI for means for *expansion* units was from  $-15.57^\circ$  to  $26.86^\circ$ . Thus for *contraction* and *expansion* units, the 95% CI spanned the bipartite but not the precisely tuned prediction. For the *rotation* units, the 95% CI on means was from  $6.58^\circ$  to  $26.55^\circ$  i.e. did not include either the bipartite or precise predictions, but was closer to the former.

A second quantitative analysis assessed the difference between the preferred direction for each cell in each subfield and the predicted preferred direction for a bipartite RF vs. a precisely tuned RF (illustrated by the solid and open circles in Fig. 6, respectively). Bipartite predictions for fields 2 and 6 were obtained by averaging the tuning curves of the neighbouring fields (1 and 3 for subfield 2, 5 and 7 for field 6). The differences between the actual preferred directions and the predicted values were

determined in each subfield, and a weighted average of each difference score was calculated for each unit across all subfields (using equation (2), where  $\theta_d$  is the difference score from the bipartite or precise prediction for a given subfield and  $R_d$  is the scaled SI for that subfield). Subfields 4 and 8 were not included in this analysis, as the predictions for a bipartite and precisely tuned RF are identical. Across all cell types, the mean difference score for the bipartite and precise predictions were  $30.9^\circ$  and  $40.4^\circ$ , respectively. These scores were significantly different (paired  $t$ -test,  $\alpha = .05$ ;  $P < .023$ ), suggesting the bipartite prediction is a better predictor of the RF organization. When analysed by cell type, paired  $t$ -tests showed that the bipartite prediction was significantly closer to the actual preferred directions in *rotation* ( $18.3^\circ$  vs.  $35.1^\circ$ ;  $P < .003$ ) and *expansion* ( $41.6^\circ$  vs.  $54.6^\circ$ ;  $P < .048$ ) neurons. Difference scores for the bipartite vs. precise predictions were not significantly different in *contraction* units ( $33.1^\circ$  vs.  $36.0^\circ$ ).

## Discussion

In this study, we examined the RFs of optic flow sensitive Purkinje cells in the VbC of pigeons to determine whether the RFs are precisely tuned to their preferred flowfield, as in invertebrate optic flow neurons, or represent coarse approximations of the flowfield, as had been suggested in the olivo-cerebellar system in mammals. Our results support the idea that the RF has a bipartite organization. However, we will argue that there might be a slight bias toward the precisely tuned model.

*Responses to Composite Large Field Stimuli*

Simpson and colleagues inferred the bipartite RF structure for the *rotation* neurons by noting that the rotation cells in the rabbit accessory optic system (AOS), inferior olive (IO), and VbC responded to upward motion on one side of the axis of preferred rotation, and downward motion on the other side of the axis (e.g. see Simpson et al., 1988a, Figures 2 and 3; see also Kano et al., 1990a,b; Kusunoki et al., 1990). This has also been shown for the *rotation* neurons in the pigeon VbC, and AOS (Wylie & Frost, 1993, 1999b; Wylie et al., 1993). However, it has been shown that a cortical optic flow neurons with precise tuning still respond vigorously to such a stimulus (e.g. Fig. 13 of Tanaka & Saito, 1989). These neurons respond to shear about any axis, but the bipartite RF proposed by Simpson and colleagues (Fig. 2B) should not respond strongly to horizontal shear. As shown in Figure 4A, for the *rotation* units the *vertical shear* configuration showed significantly greater modulation of CSA than the *horizontal shear* configuration. In fact, *horizontal shear* showed significantly less modulation than all of the other stimulus configurations. For both *expansion* and *contraction* units, the *vertical bar* configuration produced significantly greater modulation of CSA than the *horizontal bar* configuration. These results argue strongly against precisely tuned RFs for optic flow sensitive neurons in the VbC of pigeons, and suggest that these neurons approximate the optic flowfield via a vertically-divided bipartite RF, such as illustrated in Figure 2B for an *expansion* neuron. However, there is one observation we would like to highlight that argues against a strict bipartite RF organization. For the *rotation* units, the depth of modulation to the *horizontal shear*

configuration was significantly greater than zero, such that the response to simulated rotation in the preferred direction was greater than rotation in the opposite direction (see Figure 4A). If the RF was organized as in Figure 2E, one would not expect any modulation to this configuration. Likewise, for the *expansion* and *contraction* units, the depth of modulation to the *horizontal bar* configuration was significantly greater than zero (see Figure 4B).

### *Subfield Stimulation*

To assess direction preference in different regions of the RF, we tested the response to subfield stimulation using drifting  $45^\circ \times 37.5^\circ$  square wave gratings. A similar technique, albeit using smaller stimuli, has been used to assess the receptive field structure of visual neurons in parietal cortex (Schaafsma & Duysens, 1996; see also Duhamel et al. 1997; Ben Hamed et al. 2001; Bremmer et al. 2002; Avillac et al. 2005). While the depth of modulation in response to this stimulation was not optimal, this allowed us to assign direction-tuning curves in eight regions of the RF around the FOE, FOC, or axis of rotation for *expansion*, *contraction*, and *rotation* units, respectively. Two statistical analyses of the local vector fields support a bipartite RF more so than a precisely tuned RF. The 95% CIs on the preferred directions for *expansion* and *contraction* units included the bipartite but not the precisely tuned prediction, while the 95% CI for *rotation* units included neither but was closer to the bipartite prediction. In addition, the disparity between the actual local tuning and the bipartite prediction was significantly less than the difference between actual data and

the precisely tuned prediction. However, the spread of the vector fields is in the direction of the precisely tuned prediction, which suggests that the RF is biased towards a more precise tuning (e.g. Fig. 6A, subfields 3, 5, and 7; Fig. 6B, subfields 1 and 3; Fig. 6C, subfields 5 and 7). Furthermore, 95% CIs were not centred around the bipartite prediction but tended to bias towards the precise prediction.

Taken together, quantitative analyses of both the responses to the composite and subfield stimuli lend support to a bipartite organization. However, it would appear that the bipartite fields are biased towards a more precise organization than those illustrated in Figure 2B and 2E.

#### *Comparison to Optic Flow Sensitive Neurons in the MST of Primates*

Several groups have identified neurons in area MST and parietal cortex that respond to optic flow stimuli (e.g. Saito et al. 1986; Tanaka et al., 1986, 1989; Motter et al., 1987; Steinmetz et al., 1987; Tanaka & Saito, 1989; Duffy & Wurtz, 1991a,b, 1995; Orban et al. 1992; Lagae et al. 1994; Graziano et al. 1994; Schaafsma & Duysens, 1996; Page & Duffy 2003; for review see Duffy, 2004). There are a wide variety of cortical optic flow neurons including neurons that show “position invariance” and those that prefer combinations of planar, radial and circular optic flow (Duffy & Wurtz, 1991a,b, 1995; Graziano et al., 1994; Schaafsma & Duysens, 1996). Nonetheless, the underlying RF structure of cortical neurons responsive to expansion, contraction and rotation has been investigated using stimuli similar to those employed in the present study, thus permitting a direct comparison of cortical and VbC optic

flow neurons. Motter et al. (1987) and Steinmetz et al. (1987) stimulated contraction and expansion neurons area 7a of the primate parietal cortex with small visual stimuli moving throughout a neuron's RF. The population response of these neurons was precisely tuned to the local motion in their preferred flowfield (see Figure 12 of Steinmetz et al. 1987). Tanaka and colleagues (Tanaka & Saito, 1989; Tanaka et al. 1989; see also Orban et al., 1992) stimulated expansion, contraction and rotation neurons in MST with composite stimuli similar to those used in the present study. They approximated rotation, expansion or contraction with composite stimuli consisting of 2, 4 or 8 directions of motion, whereas we used stimuli consisting of 2 or 4 directions. Their results are in stark contrast to those of the present study. First, they found that rotation neurons responded much more strongly to true circular rotation than to shear along horizontal, vertical or oblique axes. In contrast we found that the response to vertical shear was significantly greater than that to true rotation (*windmill*, see Fig. 4A). Likewise they found that expansion/contraction neurons responded much more strongly to true expansion/contraction as opposed to axial expansion/contraction, in which the radial motion was approximated with two subregions. Second, they found that the response increased as the number of directions in the composite stimuli increased from 2 to 4 to 8 (see Figs. 8-11 from Tanaka et al. (1989)). In fact only 5% of the neurons would respond significantly to the stimuli consisting of 2 directions. In contrast, for *rotation* neurons we found that the responses to the "X" and "cross" configurations were comparable or less than the response to *vertical shear*, and for *expansion* and *contraction* neurons the responses to

the “X” and “cross” configurations were less than the responses to the *vertical bar* configuration (see Figs. 3 and 4). Finally for rotation neurons, Tanaka et al. (1989) showed that the responses to *vertical* and *horizontal shear* were essentially identical (see Fig. 13 of Tanaka and Saito (1989) and Fig. 8 of Tanaka et al. (1989)). The reduced response to bipartite stimuli and the homogenous response to vertical and horizontal bipartite stimuli contrast with the response of optic flow neurons in the VbC from the present study. Based on the response properties of MST neurons described above, Tanaka et al. (1989) suggested that expansion, contraction, and rotation sensitive neurons might receive converging inputs from many directional cells in area MT with relatively small receptive fields in different parts of the visual field (termed the ‘mosaic’ hypothesis). These receptive fields and direction preferences would have precise tuning to their preferred flowfield (see Figure 12 of Tanaka et al., 1989). Orban et al. (1992) suggested that such an RF arrangement could account for position invariance and responses to multiple optic flow components.

#### *Comparison to Optic Flow Sensitive Neurons in Invertebrates*

In the visual system of invertebrates, there are neurons responding to optic flow resulting from either self-rotation or self-translation (*e.g.* Krapp & Hengstenberg, 1996; Krapp et al., 1998; Barnes et al., 2002). Like neurons in the AOS, pretectum, and VbC, these optic flow cells are responsible for generating the optokinetic response (Hengstenberg, 1993; Simpson, 1984). In blowflies and shore crabs, RF organization was assessed using intracellular recording in response to small moving

visual stimuli (*blowfly*, Krapp & Hengstenberg, 1996; Krapp et al., 1998; *crab*, Barnes et al., 2002; Johnson et al., 2002), and it was determined that the RFs are precisely tuned to the preferred optic flowfield. Comparison to the present study is rather tenuous due to very different recording conditions and stimuli. Nonetheless, our results contrast the invertebrate studies. Thus it appears that the RFs of optic flow neurons in the VbC of vertebrates are somewhat simplistic in their design compared to those in the visual neuropile of invertebrates. Also, it should be noted that despite the precisely tuned RF organization of the optic flow units in blowflies, these neurons are surprisingly broadly tuned to global rotational and translational optic flow patterns (Karmeier et al., 2003). In light of such broad tuning, a number of recent studies have emphasized the importance of the population code among optic flow sensitive neurons for the accurate assignment of direction of motion (Lappe et al., 1996; Ben Hamed et al., 2003; Page & Duffy, 2003).

*Constructing Bipartite Receptive fields for Rotation Expansion, Contraction and Rotation*

Simpson and colleagues originally conceived the notion of the bipartite receptive field as depicted in Figure 2E for rotation neurons in the rabbit flocculus. For the rabbit VbC, the concept of the bipartite RF is consistent with (at least) two features of the physiology of the rabbit visual system. First, the visual input to the olivocerebellar pathway arises from the AOS (for reviews see Simpson 1984; Simpson et al. 1988c). These neurons have very large receptive fields, measuring at

least  $60^\circ$  in diameter (Soodak & Simpson, 1988). Thus, the bipartite RF depicted in Fig. 2E could be constructed by pooling as few as two AOS neurons; one responsive to upward motion with one responsive to downward motion (Simpson, 1984; Simpson et al., 1988b). In contrast, a neuron with precise tuning would receive input from many units with smaller RFs (Tanaka et al., 1989; Krapp & Hengstenberg, 1996; Krapp et al., 1998; Barnes et al., 2002). Second, the rabbit retina has a streak organization and, according to Oyster et al. (1980), the density of ganglion cells that project to the AOS is highest in the visual streak. Thus, the bipartite RF depicted in Fig. 2E could arise from input from AOS cells preferring vertical motion along the visual streak, with little or no input from other areas of the retina.

A final feature of the AOS that is incompatible for constructing RFs that are precisely tuned is the fact that few directions are represented. Precise tuning requires input from neurons of many different direction preferences. In pigeons the visual input to the VbC originates in the nucleus of the basal optic root (nBOR) of the AOS and pretectal nucleus leniformis mesencephali. Homologous retinal recipient nuclei have been identified in mammals: the medial, lateral, and dorsal terminal nuclei of the AOS (MTN, LTN, and DTN, respectively) and the pretectal nucleus of the optic tract (NOT) (Fite, 1985; McKenna & Wallman, 1985; Simpson, 1984; Simpson et al., 1988a,b; Weber, 1985). Most AOS neurons prefer either upward, downward or backward (nasal-temporal) visual motion, whereas most pretectal neurons prefer forward (temporal-nasal) motion (e.g. NOT, Collewijn, 1975a,b; Mustari & Fuchs, 1990; Ibbotson et al., 1994; LM, McKenna & Wallman, 1985; Winterson & Brauth,

1985; Wylie & Crowder, 2000; Wylie & Frost, 1996; MTN/LTN, Grasse & Cynader, 1982, 1984; Soodak & Simpson, 1988; nBOR, Burns & Wallman, 1981; Rosenberg & Ariel, 1990; Wylie & Frost, 1990). Whole-cell patch recordings from the nBOR in turtles indicate that these neurons receive input from a few to several retinal subunits, each having approximately the same direction preference (Kogo et al., 1998).

Whereas the precursor direction cells for *expansion*, *contraction*, and *rotation* neurons in MST have small receptive fields, the AOS and pretectal precursors for olivo-cerebellar neurons have large receptive fields. The fact that pretectal and AOS neurons are tuned to the cardinal directions, rather than acting as motion detectors across the full spectrum of motion directions, provides a physiological base for the bipartite RFs in VbC. That is, our results suggest that bipartite receptive field organization in the VbC may result from the pooling of relatively few precursor cells compared to optic flow neurons in MST. This is depicted in Figure 7. In Figure 7A, the bipartite RF of a *contraction* neuron is constructed via the juxtaposition of the RF of an LM cell selective for forward visual motion and the RF from an nBOR cell selective for backward visual motion on either side of the preferred axis at 45° azimuth (i.e. a strict bipartite organization). In 7B, the RF of a *contraction* neuron is constructed using input from four neurons in LM and nBOR, each with slightly different direction preferences and regions of peak excitability. Such a neuron would show a slight bias towards a precisely tuned RF organization.

**Supporting Grants:**

This research was supported by funding from the Natural Sciences and Engineering Research Council of Canada (NSERC; to D.R.W.W.) D.R.W.W. was supported by the Canada Research Chairs Program. I.R.W. was supported by scholarships from NSERC and the Alberta Heritage Foundation for Medical Research.

**Acknowledgements:**

We thank Peter L. Hurd for assistance with statistical analysis.

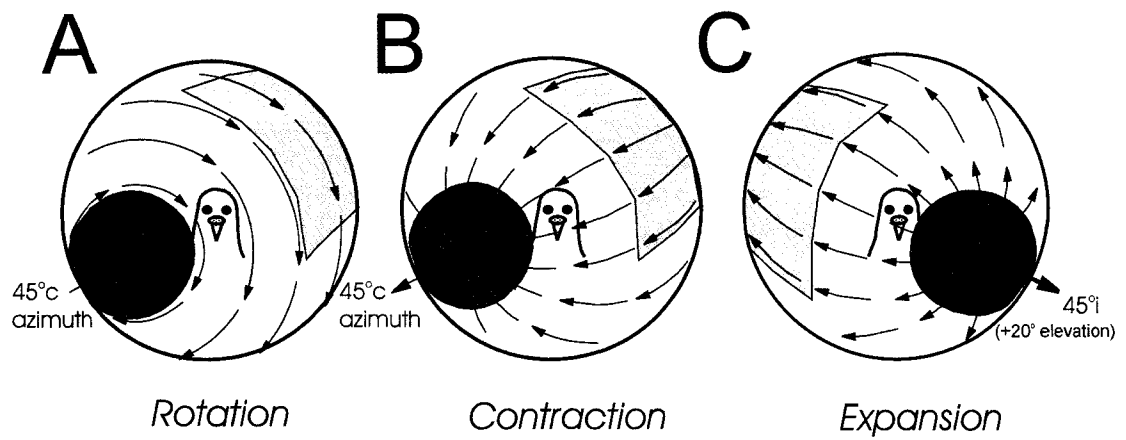


**Figure 7.1:** Preferred optic flowfields for rotation (A), contraction (B), and expansion (C) neurons in the vestibulocerebellum (VbC). Rotation neurons prefer a circular flowfield rotating about an axis oriented at 45° azimuth. Contraction neurons prefer radial optic flow with a focus of contraction (FOC) at 45° azimuth. Expansion neurons prefer a radial optic flowfield with a focus of expansion (FOE) at 45° azimuth + 20° elevation.

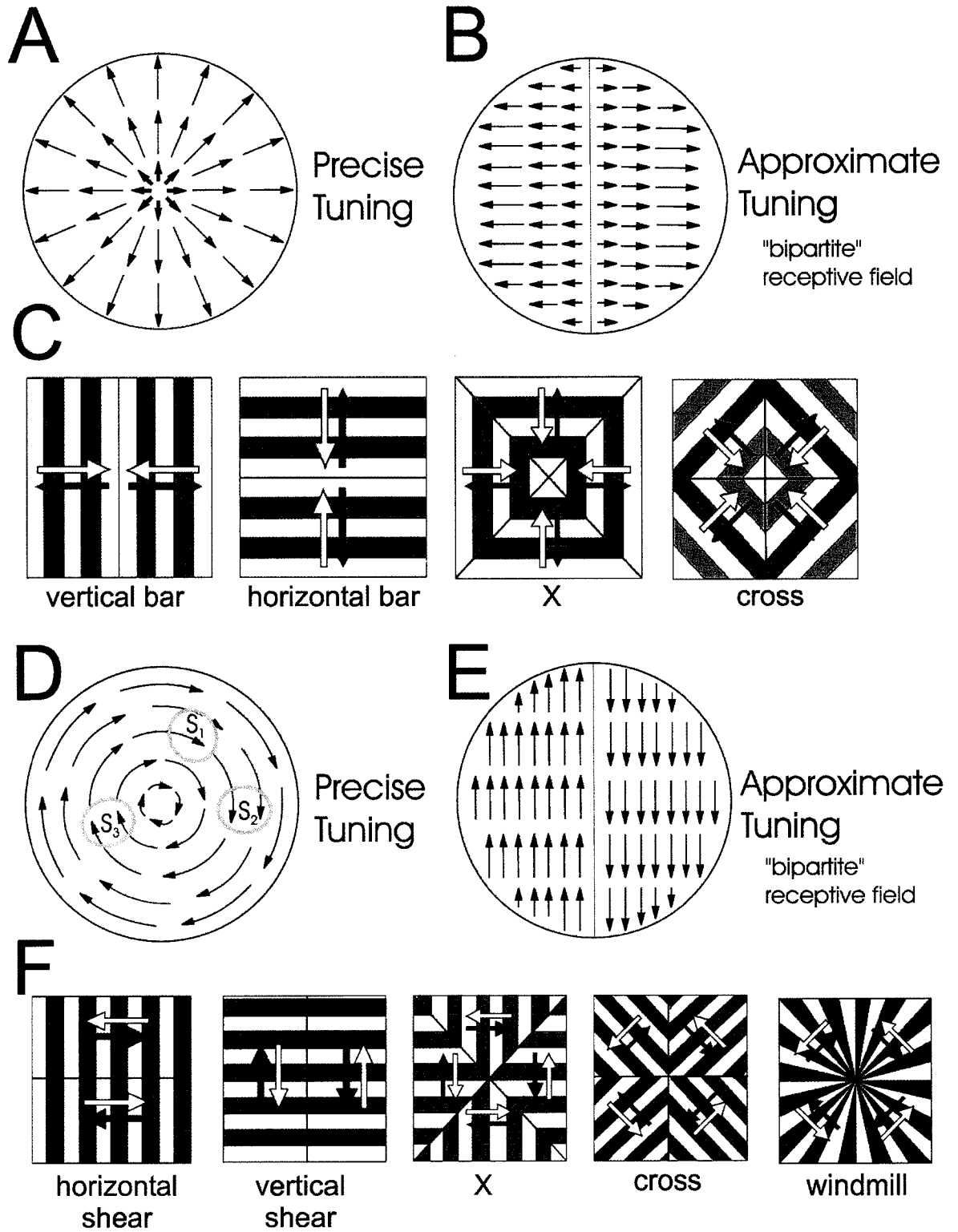
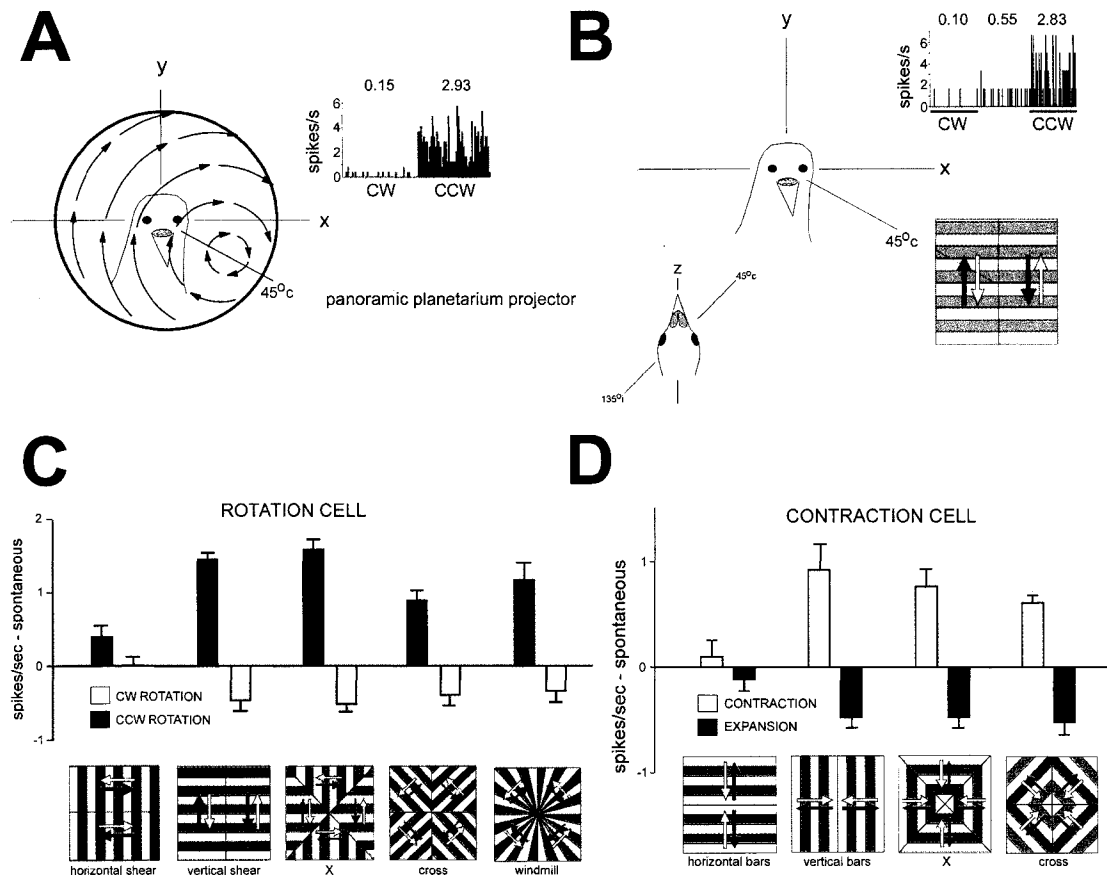
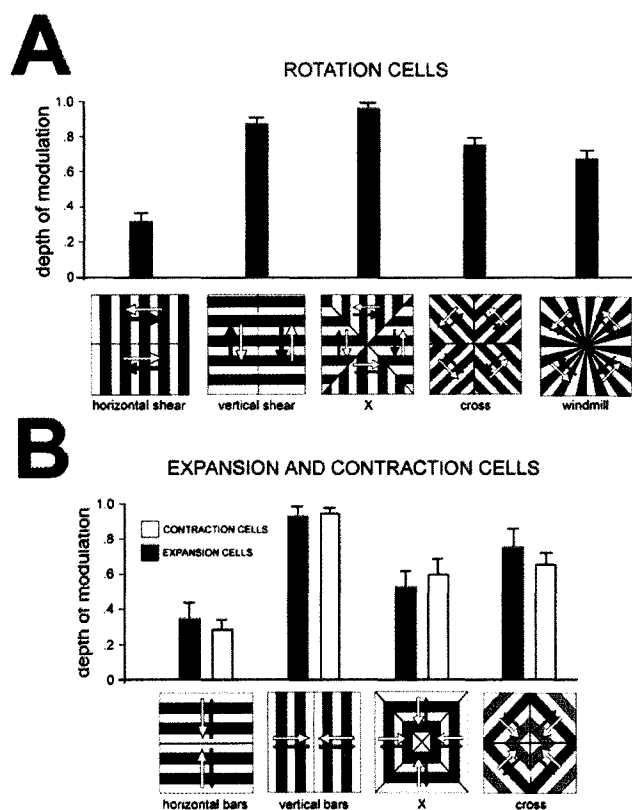


Figure 7.2: Precise and Approximate Tuning of Optic Flow Sensitive Neurons in the Vestibulocerebellum (VbC). A and B show how the response preferences of expansion neurons could be accounted for by precisely and approximately tuned receptive fields, respectively. D and E show precise and approximately tuned receptive fields for rotation neurons. C and F respectively show the composite stimuli used to test the receptive field organization of translation-sensitive and rotation neurons in the VbC. The stimuli consisted of drifting square wave gratings organized in such a way as to approximate the preferred flowfield around the preferred axis for an expansion, contraction, or rotation neuron.



**Figure 7.3:** A shows the modulation of a rotation unit in the right flocculus in response to the rotational optic flow about the preferred axis produced by a planetarium projector, recorded over 22 sweeps, where each sweep consisted of 5 s clockwise (CW) motion at a constant velocity of  $20^\circ/\text{s}$ , followed by 5 sec of counter-clockwise (CCW) motion. (Note, designation of CW or CCW rotation is from the bird's perspective). B shows the modulation of the same unit in response to the vertical shear configuration of the composite stimulus, recorded over 6 sweeps. Each sweep consisted of 5 s simulated CCW motion (generated by gratings moving upward from  $0-45^\circ$  and downward from  $45-90^\circ$ ), a 5.5 sec pause, followed by 5 sec of simulated CW motion. The average firing rate (spikes/s) for each epoch is indicated above the histograms in A and B. Note that the modulation was about the same in response to both stimuli. C shows the firing rate of another rotation unit in the right flocculus in response to all configurations of the composite stimulus (depicted below the corresponding response). White and black bars show the average firing rate of the unit (minus spontaneous rate) in response to simulated CW (white arrows) and CCW (black arrows) rotation, respectively. D shows the firing rate of a contraction unit in response to all stimulus configurations. White and black bars show the average firing rate of the unit (re. spontaneous) in response to simulated contraction (white arrows)

Figure 7.3 continued:                    and expansion (black arrows), respectively, of the stimulus configuration shown directly below.



**Figure 7.4:** A shows the normalized depth of modulation values for all rotation units ( $n=22$ ) in response to the composite stimulus configurations illustrated directly below. B shows the normalized depth of modulation values for all expansion ( $n=11$ , black bars) and contraction ( $n=22$ , white bars) units in response to the stimulus configurations illustrated directly below. A significant difference exists between modulation to horizontal shear vs. vertical shear (A) and horizontal bars vs. vertical bars (B).

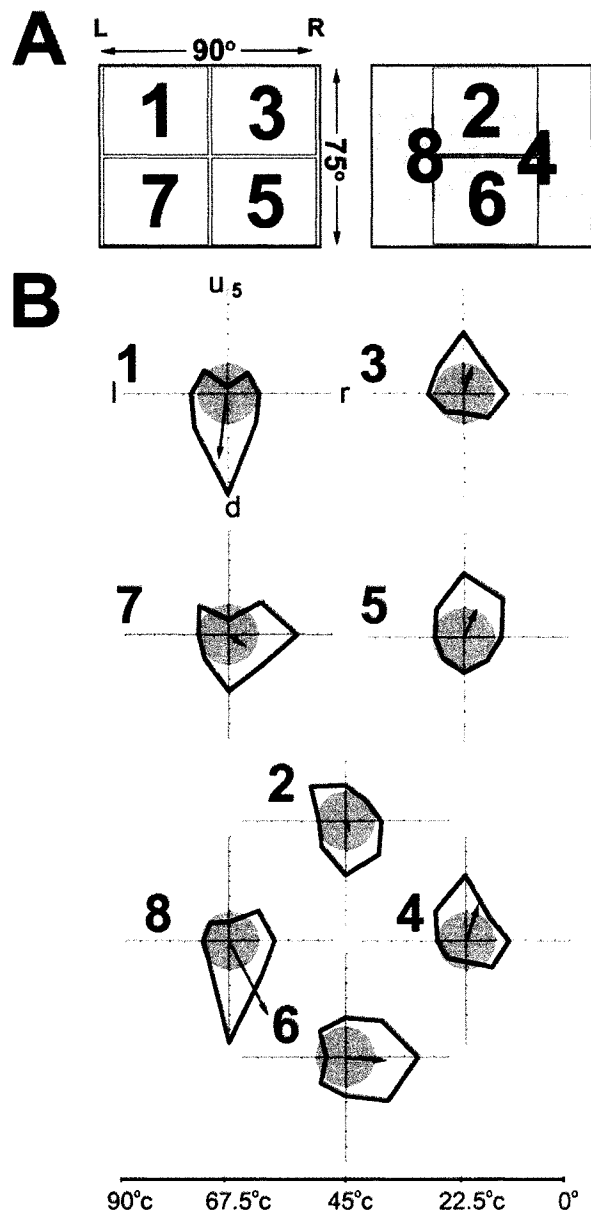


**Figure 7.5:** A shows the eight subfields for which local tuning curves of expansion, contraction, and rotation were determined using drifting square wave gratings. The screen was centred at  $45^\circ$  elevation for expansion units and  $45^\circ$  c for contraction and rotation units. Local motion tuning curves for a representative rotation unit are shown in B. The polar plots show firing rate minus spontaneous rate, with grey shading representing negative values (i.e. inhibition). Arrows are vectors indicating the direction (PD, see equation (1)) and magnitude (scaled SI, see equation (2)) of the direction selectivity for a given subfield.

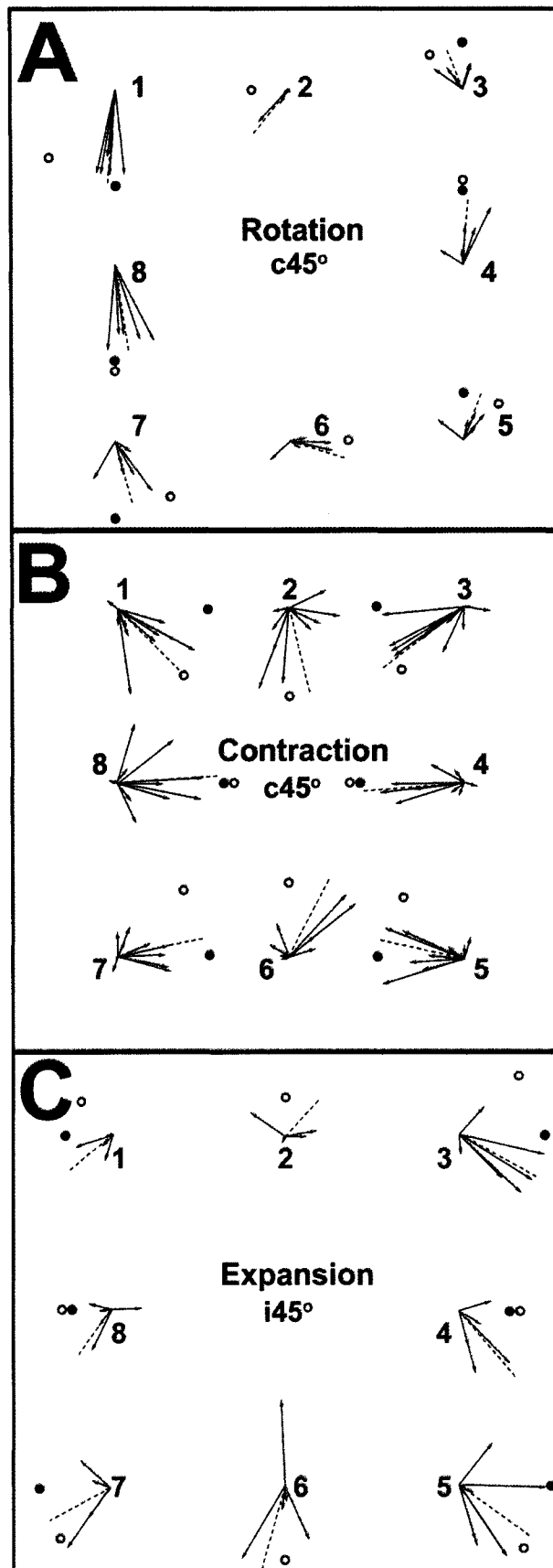
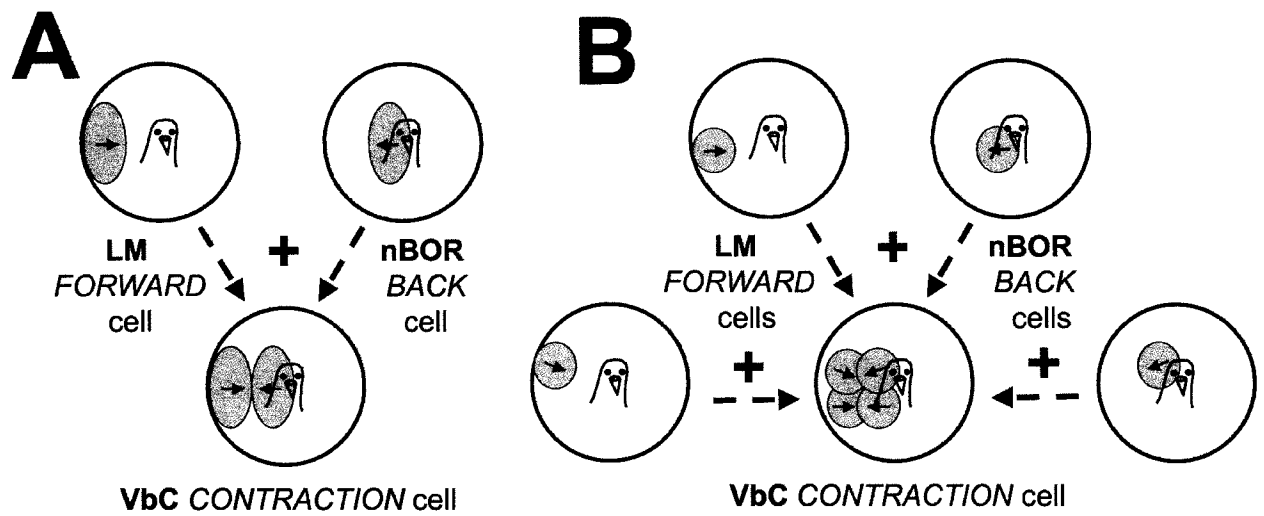


Figure 7.6: Vector fields for rotation, contraction, and expansion units are shown in A, B, and C, respectively. The direction of the arrow is the PD (equation (1)) and vector length is equal to the scaled SI (equation (2)). Each numeral 1-8 indicates the corresponding subfield, as defined in Fig. 5A. The dotted lines show the weighted mean preferred direction for each subfield calculated using equation (1), where  $R_d$  and  $\theta_d$  are the length and direction of each vector. Solid circles show the predicted preferred direction for each subfield in a bipartite RF (e.g Fig. 2B,E), while open circles show the predicted preferred direction for a precisely tuned RF (e.g. Fig. 2A,D). Note that for subfields 4 and 8 the two predictions are coincident. For fields 2 and 6, a bipartite prediction was not indicated, since in a bipartite RF the tuning curve in this subfield would simply reflect an average of the neighbouring subfields. Statistical analyses supports a bipartite RF organization more so than a precise tuning, though there is clearly bias towards the latter.



**Figure 7.7:** In A, the receptive fields of a single direction selective unit in the pretectal nucleus lentiformis mesencephali (LM) and a single unit in the nucleus of the basal optic root (nBOR) of the accessory optic system (AOS) are combined to construct a strict bipartite receptive field of a contraction unit in the vestibulocerebellum (VbC). In B, four inputs are used to construct the receptive field of a contraction unit in the VbC.

## **References**

- Avillac, M., Deneve, S., Olivier, E., Pouget, A., & Duhamel, J.R. (2005). Reference frames for representing visual and tactile locations in parietal cortex. *Nature Neuroscience* **8**, 941-9.
- Barnes, W.J.P., Johnson, A.P., Horseman, B.G., & MacAuley, M.W.S. (2002). Computer-aided studies of vision in crabs. *Marine and Freshwater Behavioural Physiology* **35**, 1-2, 37-56.
- Ben Hamed, S., Duhamel, J.R., Bremmer, F., & Graf, W. (2001). Representation of the visual field in the lateral intraparietal area of macaque monkeys: a quantitative receptive field analysis. *Experimental Brain Research* **140**, 127-44.
- Ben Hamed, S., Page, W., Duffy, C., & Newsome, W.T. (2003). MSTd neuronal basis functions for the population encoding of heading direction. *Journal of Neurophysiology* **90**, 549-58.
- Bremmer, F., Duhamel, J.R., Ben Hamed S., & Graf, W. (2002). Heading encoding in the macaque ventral intraparietal area (VIP). *European Journal of Neuroscience* **16**, 1554-68.
- Burns, S., Wallman, J. (1981). Relation of single unit properties to the oculomotor function of the nucleus of the basal optic root (AOS) in chickens. *Experimental Brain Research* **42**, 171-180.
- Collewijn, H. (1975a). Direction-selective units in the rabbit's nucleus of the optic tract. *Brain Research* **100**, 489-508.

- Collewijn, H. (1975b). Oculomotor areas in the rabbit's midbrain and pretectum. *Journal of Neurobiology* **6**, 3-22.
- Crowder, N.A., Winship, I.R., & Wylie, D.R. (2000). Topographic organization of inferior olive cells projecting to translational zones in the vestibulocerebellum of pigeons. *Journal of Comparative Neurology* **419**, 87-95.
- Duffy, C.J. (2004). The cortical analysis of optic flow. In *The Visual Neurosciences*, volume 2, ed. Chalupa, L.M., & Werner, J.S., pp 1260-1283. Cambridge: MIT Press.
- Duffy, C.J., Wurtz, R.H. (1991a). Sensitivity of MST neurons to optic flow stimuli. I. A continuum of response selectivity to large-field stimuli. *Journal of Neurophysiology* **65**, 1329-45.
- Duffy, C.J., Wurtz, R.H. (1991b). Sensitivity of MST neurons to optic flow stimuli. II. Mechanisms of response selectivity revealed by small-field stimuli. *Journal of Neurophysiology* **65**, 1346-59.
- Duffy, C.J., Wurtz, R.H. (1995). Response of monkey MST neurons to optic flow stimuli with shifted centers of motion. *Journal of Neuroscience* **15**, 5192-208.
- Duhamel, J.R., Bremmer, F., Ben Hamed, S., & Graf, W. (1997). Spatial invariance of visual receptive fields in parietal cortex neurons. *Nature* **389**, 845-8.
- Efron B & Tibshirani R.J. (1994). *Introduction to the bootstrap*. New York: Chapman & Hall.

- Erichsen, J.T., Hodos, W., Evinger, C., Bessette, B.B., & Philips, S.J. (1989). Head orientation in pigeons: postural, locomotor, and visual determinants. *Brain, Behaviour, and Evolution* **33**, 268–578.
- Fite, K.V. (1985). Pretectal and accessory-optic visual nuclei of fish, amphibia and reptiles: themes and variations. *Brain, Behaviour, and Evolution* **26**, 71-90.
- Gibson, J.J. (1954). The visual perception of objective motion and subjective movement. *Psychological Review* **61**, 304-314.
- Graf, W., Simpson, J.I., & Leonard, C.S. (1988). Spatial organization of visual messages of the rabbit's cerebellar flocculus. II. Complex and simple spike responses of Purkinje cells. *Journal of Neurophysiology* **60**, 2091-2021.
- Grasse, K.L., & Cynader, M.S. (1982). Electrophysiology of medial terminal nucleus of accessory optic system in the cat. *Journal of Neurophysiology* **48**, 490-504.
- Grasse, K.L., Cyander, M.S., & Douglas, R.M. (1984). Alterations in response properties in the lateral and dorsal terminal nuclei of the cat accessory optic system following visual cortex lesions. *Experimental Brain Research* **55**, 69-80.
- Graziano, M.S., Andersen, R.A., Snowden, R.J. (1994). Tuning of MST neurons to spiral motions. *Journal of Neuroscience* **14**, 54-67.
- Hengstenberg, R. (1993). Multisensory control in insect oculomotor systems. In *Visual Motion and Its Role in the Stabilization of Gaze*, ed. Miles, F.A., pp 285-298. Wallman, J. New York: Elsevier.

- Ibbotson, M.R., Mark, R.F., & Maddess, T.L. (1994). Spatiotemporal response properties of direction-selective neurons in the nucleus of the optic tract and the dorsal terminal nucleus of the wallaby, *Macropus eugenii*. *Journal of Neurophysiology* **72**, 2927-2943.
- Johnson, A.P., Horseman, B.G., MacAuley, M.W.S., & Barnes, W.J.P. (2002). PC-based visual stimuli for behavioural and electrophysiological studies of optic flow field detection. *Journal of Neuroscience Methods* **114**, 1,51-61.
- Kano, M., Kano, M.-S., Kusunoki, M., Maekawa, K. (1990a). Nature of the optokinetic response and zonal organization of climbing fibre afferents in the vestibulocerebellum of the pigmented rabbit. *Experimental Brain Research* **80**, 238-251.
- Kano, M., Kano, M.-S., & Maekawa, K. (1990b). Receptive field organization of climbing fibre afferents responding to optokinetic stimulation in the cerebellar nodulus and flocculus of the pigmented rabbit. *Experimental Brain Research* **82**, 499-512.
- Karmeier, K., Krapp, H.G., & Egelhaaf, M. (2003). Robustness of the tuning of fly visual interneurons to rotatory optic flow. *Journal of Neurophysiology* **90**, 1626-34.
- Karten, H.J., & Hodos, W. (1967). *A Stereotaxic Atlas of the Brain of the Pigeon (Columba Livia)*. Baltimore: Johns Hopkins Press.
- Koenderink, J.J., & van Doorn, A.J. (1987). Facts on optic flow. *Biological Cybernetics* **56**, 247-254.

- Kogo, N., McGartland Rubio, D., & Ariel, M. (1998). Direction tuning of individual retinal inputs to the turtle accessory optic system. *Journal of Neuroscience* **18**, 2673-2684.
- Krapp, H.G., & Hengstenberg, B. (1996). Estimation of self-motion by optic flow processing in single visual interneurons. *Nature* **384**, 463-6.
- Krapp, H.G., Hengstenberg, B., & Hengstenberg, R. (1998). Dendritic structure and receptive-field organization of optic flow processing interneurons in the fly. *Journal of Neurophysiology* **79**, 1902-17.
- Kusunoki, M., Kan, M., Kano, M.-S., & Maekawa, K. (1990). Nature of optokinetic response and zonal organization of climbing fibre afferents in the vestibulocerebellum of the pigmented rabbit. I. The flocculus. *Experimental Brain Research* **80**, 225-237.
- Lagae, L., Maes, H., Raiguel, S., Xiao, D.K., & Orban, G.A. (1994). Responses of macaque STS neurons to optic flow components: a comparison of areas MT and MST. *Journal of Neurophysiology* **71**, 1597-626.
- Lappe, M., Bremmer, F., Pikel, M., Thiele, A., & Hoffman, K.P. (1996). Optic flow processing in monkey STS: a theoretical and experimental approach. *Journal of Neuroscience* **16**, 6265-6285.
- Leonard, C.S., Simpson, J.I., & Graf, W. (1988). Spatial organization of visual messages of the rabbit's cerebellar flocculus. I. Typology of inferior olive neurons of the dorsal cap of Kooy. *Journal of Neurophysiology* **60**, 2073-2090.

- McKenna, O.C., Wallman, J. (1985). Accessory optic system and pretectum of birds: comparisons with those of other vertebrates. *Brain, Behaviour, and Evolution* **26**, 91-116.
- Motter, B.C., Steinmetz, M.A., Duffy, C.J., & Mountcastle, V.B. (1987). Functional properties of parietal visual neurons: mechanisms of directionality along a single axis. *Journal of Neuroscience* **7**, 154-76.
- Mustari, M.J., & Fuchs, A.F. (1990). Discharge patterns of neurons in the pretectal nucleus of the optic tract (NOT) in the behaving primate. *Journal of Neurophysiology* **64**, 77-90.
- Nakayama, K., & Loomis, J.M. (1974). Optical velocity patterns, velocity-sensitive neurons, and space perception: a hypothesis. *Perception* **3**: 63-80.
- Orban, G.A., Lagae, L., Verri, A., Raiguel, S., Xiao, D., Maes, H., & Torre, V. (1992). First-order analysis of optical flow in monkey brain. *Proceedings of the National Academy of Sciences USA* **89**, 2595-9
- Oyster, C.W., Simpson, J.I., Takahashi, E.S., & Soodak, R.E. (1980). Retinal ganglion cells projecting to the rabbit accessory optic system. *Journal of Comparative Neurology* **190**, 49-61.
- Page, W., & Duffy, C. (2003). Heading representation in MST: sensory interactions and population encoding. *Journal of Neurophysiology* **89**, 1994-2013.
- R Development Core Team. (2005). *R: A language and environment for statistical computing*. R Foundation for Statistical Computing.

- Rosenberg, A.F., & Ariel, M. (1990). Visual-response properties of neurons in turtle basal optic nucleus in vitro. *Journal of Neurophysiology* **63**, 1033-1045.
- Saito, H., Yukie, M., Tanaka, K., Hikosaka, K., Fukada, Y., & Iwai, E. (1986). Integration of direction signals of image motion in the superior temporal sulcus of the macaque monkey. *Journal of Neuroscience* **6**, 145-57.
- Schaafsma, S.J., & Duysens, J. (1996). Neurons in the ventral intraparietal area of awake macaque monkey closely resemble neurons in the dorsal part of the medial superior temporal area in their responses to optic flow patterns. *Journal of Neurophysiology*, **76**, 4056-68.
- Simpson, J.I. (1984). The accessory optic system. *Annual review of neuroscience* **7**, 13-41.
- Simpson JI, & Alley KE. (1974). Visual climbing fiber input to rabbit vestibulo-cerebellum: a source of direction-specific information. *Brain Research* **82**, 302-8.
- Simpson, J.I., Giolli, R.A., & Blanks, R.H. (1988c). The pretectal nuclear complex and the accessory optic system. *Reviews of Oculomotor Research* **2**, 335-64.
- Simpson, J.I., Graf, W., & Leonard, C. (1981). The coordinate system of visual climbing fibres to the flocculus. In *Progress in Oculomotor Research*, ed. Fuchs, A.F., & Becker, W., pp 475-484. Amsterdam: Elsevier.
- Simpson, J.I., Graf, W., & Leonard, C. (1989). Three-dimensional representation of retinal image movement by climbing fiber activity. In *The Olivocerebellar*

*System in Motor Control: Experimental Brain Research Supplement vol. 17*, ed. Strata, P., pp 323-327. Heidelberg: Springer-Verlag.

Simpson, J.I., Leonard, C.S., & Soodak, R.E. (1988a). The accessory optic system of rabbit. II. Spatial organization of direction selectivity. *Journal of Neurophysiology* **60**, 2055-2072.

Simpson, J.I., Leonard, C.S., & Soodak, R.E. (1988b). The accessory optic system: analyzer of self-motion. *Annals of the New York Academy of Sciences* **545**, 170-179.

Simpson, J.I., Soodak, R.E., & Hess, R. (1979). The accessory optic system and its relation to the vestibulocerebellum. *Progress in Brain Research* **50**, 715-24.

Soodak, R.E., & Simpson, J.I. (1988). The accessory optic system of rabbit. I. Basic visual response properties. *Journal of Neurophysiology* **60**, 2055-2072.

Steinmetz, M.A., Motter, B.C., Duffy, C.J., & Mountcastle, V.B. (1987). Functional properties of parietal visual neurons: radial organization of directionalities within the visual field. *Journal of Neuroscience*, **7**, 177-91.

Tanaka, K., Fukada, Y., & Saito, H.A. (1989). Underlying mechanisms of the response specificity of expansion/contraction and rotation cells in the dorsal part of the medial superior temporal area of the macaque monkey. *Journal of Neurophysiology* **62**, 642-56.

Tanaka, K., Hikosaka, K., Saito, H., Yukie, M., Fukada, Y., & Iwai, E. (1986). Analysis of local and wide-field movements in the superior temporal visual areas of the macaque monkey. *Journal of Neuroscience* **6**, 134-44.

- Tanaka, K., & Saito, H. (1989). Analysis of motion of the visual field by direction, expansion/contraction, and rotation cells clustered in the dorsal part of the medial superior temporal area of the macaque monkey. *Journal of Neurophysiology* **62**, 626-41.
- Vogels, R., & Orban, G.A. (1994). Activity of inferior temporal neurons during orientation discrimination with successively presented gratings. *Journal of Neurophysiology* **71**, 1428-1451.
- Weber, J.T. (1985). Pretectal complex and accessory optic system in alert monkeys. *Brain, Behaviour, and Evolution* **26**, 117-140.
- Winship, I.R., Hurd, P.L., & Wylie, D.R.W. (2005). Spatio-temporal tuning of optic flow inputs to the vestibulocerebellum in pigeons: Differences between mossy and climbing fibre pathways. *Journal of Neurophysiology* **93**, 1266-77.
- Winship, I.R., & Wylie, D.R.W. (2001). Responses of neurons in the medial column of the inferior olive in pigeons to translational and rotational optic flowfields. *Experimental Brain Research* **141**, 63-78.
- Winship, I.R., & Wylie, D.R.W. (2003). Zonal organization of the vestibulocerebellum in pigeons (*Columba livia*): I. Climbing fibre input to the flocculus. *Journal of Comparative Neurology* **456**, 127-139.
- Winterson, B.J., & Brauth, S.E. (1985). Direction-selective single units in the nucleus lentiformis mesencephali of the pigeon (*Columba livia*). *Experimental Brain Research* **60**, 215-226.

- Wylie, D.R.W. (2001). Projections from the nucleus of the basal optic root and nucleus lentiformis mesencephali to the inferior olive in pigeons (*Columba livia*). *Journal of Comparative Neurology* **429**, 502-513.
- Wylie, D.R.W., Bischof, W.F., & Frost, B.J. (1998). Common reference frame for neural coding of translational and rotational optic flow. *Nature* **392**, 278-282.
- Wylie, D.R.W., Brown, M.R., Barkley, R.R., Winship, I.R., Crowder, N.A., & Todd, K.G. (2003a). Zonal organization the vestibulocerebellum in pigeons (*Columba livia*): II. Projections of the rotation zones of the flocculus. *Journal of Comparative Neurology* **456**, 140-153.
- Wylie, DRW, Brown, M.R., Winship, I.R., Crowder, N.A., & Todd, K.G. (2003b). Zonal organization of the vestibulocerebellum in pigeons (*Columba livia*): III. Projections of the translation zones of the ventral uvula and nodulus. *Journal of Comparative Neurology* **465**, 179-194.
- Wylie, D.R., & Crowder, N.A. (2000). Spatiotemporal properties of fast and slow neurons in the pretectal nucleus lentiformis mesencephali in pigeons. *Journal of Neurophysiology* **84**, 2529-2540.
- Wylie, D.R., & Frost, B.J. (1990). Binocular neurons in the nucleus of the basal optic root (nBOR) of the pigeon are selective for either translational or rotational visual flow. *Visual Neuroscience* **5**, 489-495.
- Wylie, D.R., & Frost, B.J. (1993). Responses of pigeon vestibulocerebellar neurons to optokinetic stimulation: II. The 3-dimensional reference frame of rotation neurons in the flocculus. *Journal of Neurophysiology* **70**, 2647-2659.

- Wylie, D.R.W., & Frost, B.J. (1996). The pigeon optokinetic system: Visual input in extraocular muscle coordinates. *Visual Neuroscience* **13**, 945-953.
- Wylie, D.R.W., & Frost, B.J. (1999a). Complex spike activity of Purkinje cells in the ventral uvula and nodulus of pigeons in response to translational optic flowfields. *Journal of Neurophysiology* **81**, 256-266.
- Wylie, D.R., & Frost, B.J. (1999b). Responses of neurons in the nucleus of the basal optic root to translational and rotational flowfields. *Journal of Neurophysiology* **81**, 267-276.
- Wylie, D.R., Kripalani, T.-K., & Frost, B.J. (1993). Responses of pigeon vestibulocerebellar neurons to optokinetic stimulation: I. Functional organization of neurons discriminating between translational and rotational visual flow. *Journal of Neurophysiology* **70**, 2632-2646.

**CHAPTER 8: SUMMARY AND FUTURE DIRECTIONS**

The Accessory Optic System (AOS)-Pretectum-Olivo-Vestibulocerebellar pathway functions in compensatory movements in response to the visual consequences of self-motion, particularly those related to gaze stabilization (optokinetic nystagmus). Neurons in this pathway are well suited for this function, with large receptive fields and direction-selective responses to large moving visual stimuli rich in visual texture. The afferent and efferent connections of the pathway include premotor nuclei involved in eye movement and other compensatory reflexes (for review see Simpson 1984; Simpson et al. 1988; Grasse and Cynader 1990).

The results of six studies of the neuroanatomy and neurophysiology of the AOS-pretectum-olivo-vestibulocerebellar pathway in pigeons were discussed in this dissertation. Chapter 2 revealed a number of important findings regarding the projections from the ventral tegmental area (VTA) to the hippocampal formation (HF) and the optic flow sensitive regions of the medial column of the inferior olive (mcIO). First, this study provided a detailed definition of the topography of the VTA (catecholaminergic group A10) in pigeons beyond existing literature. Second, the study demonstrated that input to the HF and the inferior olive arises from overlapping regions of the caudo-ventral VTA, and that the morphological characteristics of the neurons providing input to the HF are indistinguishable from those sending olivary input. Using fluorescent retrograde double-labelling protocols, the study demonstrated that neurons projecting to HF or mcIO are intermingled throughout the VTA, but individual neurons do not project to both structures. Finally, this study showed that a minority of neurons providing input to the HF, but not the mcIO, are dopaminergic. A

comparison with studies in mammals suggests that an equivalent projection from optic flow regions of the VTA to the HF exists, and that the dopaminergic projection may be involved in spatial memory (see Gasbarri et al. 1997 for review). While previous research on the function of this mesohippocampal projection has focused on the dopaminergic projection, this study suggests that more research on the role of the non-dopaminergic mesohippocampal projection, which constitutes 80-90% of the projection in mammals and birds, is needed. Future studies could examine the neurochemical profile of non-dopaminergic neurons projecting to the HF and the mcIO in order to better understand the function of the projection. Further, the nature of the visual input to the HF could be confirmed via antidromic stimulation from the HF of physiologically identified optic flow sensitive neurons in the VTA. Given that most studies of spatial behaviour and path integration have been performed in rats, the extent, neurochemical profile, and neuroanatomy of the equivalent projection from optic flow regions of the VTA to the HF of rats could be further examined.

In Chapter 3, the responses of neurons in the mcIO to translational and rotational optic flow were recorded from anaesthetized pigeons. Panoramic translational or rotational flowfields were produced by mechanical devices that projected optic flow patterns onto the walls, ceiling and floor of the room, such that the axis of rotation/translation could be positioned to any orientation in 3-dimensional space and axis tuning could be determined. Each neuron was assigned a vector representing the axis about/along which the animal would rotate/translate to produce the flowfield that elicited maximal modulation. Both translation-sensitive and

rotation-sensitive neurons were found. For neurons responsive to translational optic flow, the preferred axis was described with reference to a standard right-handed coordinate system, where  $+x$ ,  $+y$  and  $+z$  represent rightward, upward and forward translation of the animal, respectively (assuming that all recordings were from the right side of the brain).  $t(+y)$  neurons were maximally excited in response to a translational optic flowfield that results from self-translation upward along the vertical ( $y$ ) axis.  $t(-y)$  neurons also responded best to translational optic flow along the vertical axis but showed the opposite direction preference. The two remaining groups,  $t(-x+z)$  and  $t(-x-z)$  neurons, responded best to translational optic flow along horizontal axes that were oriented  $45^\circ$  to the midline. There were two types of neurons responsive to rotational optic flow:  $rVA$  neurons preferred rotation about the vertical axis, and  $rHI35c$  neurons preferred rotation about an horizontal axis at  $135^\circ$  contralateral azimuth. The locations of marking lesions indicated a clear topographical organization of the six response types. In summary, the results reinforced that the olivo-cerebellar system dedicated to the analysis of optic flow is organized according to a reference frame consisting of three approximately orthogonal axes: the vertical axis, and two horizontal axes oriented  $45^\circ$  to either side the midline. Previous research has shown that the eye muscles, vestibular semicircular canals, and postural control system all share a similar spatial frame of reference. While a comparison to studies of mammals identifies near identical response properties of neurons tuned to self-rotation, no neurons responsive to translational optic flowfields have been identified in mammals

(Simpson et al. 1981, 1989ab; Graf et al. 1988; Leonard et al. 1988; Kano et al. 1990ab; Kusunoki et al. 1990).

In Chapter 4, injections of anterograde tracers into the medial column were used to investigate the zonal organization of the climbing fibre input to the flocculus of pigeons. Iontophoretic injections of either cholera toxin subunit-B or biotinylated dextrin amine were made into the mclO at locations responsive to *rVA* or *rH45* rotational optic flow. Anterogradely labeled climbing fibres in the flocculus showed a clear zonal organization. There were four parasagittal bands spanning both folia IXcd and X consisting of two *rVA* zones interdigitated with two *rH45* zones. This zonal organization is highly conserved, and comparable organizations have been identified in the mammalian flocculus (De Zeeuw et al. 1994; Tan et al. 1995). Based on the findings of Chapters 3 and 4, more recent studies in our laboratory have provided physiological confirmation of this zonal organization and further probed its afferent and efferent connections (Wylie et al. 2003; Pakan et al. 2005). Combined, the chapters demonstrated that the anatomy of the olivocerebellar extension of the AOS is highly conserved, but that interesting differences exist between mammals and birds with respect to the neurophysiology of the pathway. Future experiments could examine the synchronicity of responses in like and different zones of the flocculus using multi-electrode arrays in order to clarify the function of the zonal organization, or use fluorescent probes to assess zonal CF organization in other lobules of the cerebellum.

Recently, using drifting sine-wave gratings as stimuli, it has been shown that pretectal and AOS neurons exhibit spatio-temporal tuning (e.g. Ibbotson et al. 1994; Wylie and Crowder 2000; Crowder and Wylie 2001). In this respect there are two groups: *fast* neurons, which prefer low spatial frequency (SF) and high temporal frequency (TF) gratings, and *slow* neurons, which prefer high SF - low TF gratings. In pigeons, there are two pathways from the pretectum and AOS to the VbC: a climbing fibre (CF) pathway to Purkinje cells (P-cells) via the inferior olive and a direct mossy fibre (MF) pathway to the granular layer (GL). In Chapter 5 we assessed spatio-temporal tuning in the VbC of ketamine-anaesthetized pigeons using standard extracellular techniques. Recordings were made from optic flow sensitive units in the GL, presumably granule cells or MF rosettes, and the complex spike activity (CSA) of Purkinje cells, which reflects CF input. Based on spatio-temporal tuning to gratings moving in the preferred direction, approximately half of the GL units were classified as *fast* units, with a primary response to low SF - high TF gratings (mean = 0.13cpd/8.24Hz), and half were *slow* units preferring high SF - low TF gratings (mean = 0.68cpd/0.30Hz). CSA was almost exclusively tuned to *slow* gratings (mean = 0.67cpd/0.35Hz). We conclude that MF input to the VbC is from both *fast* and *slow* cells in the AOS and pretectum, whereas the CF input is primarily tuned to *slow* gratings.

Spatio-temporal tuning in the retinal recipient nuclei of the AOS and pretectum was the focus of Chapter 6. The correlation model of motion detection has been used to describe visual motion processing in the pretectum and Accessory Optic

System (AOS). One feature of correlation detectors is that they are tuned to a particular temporal frequency (TF) independent of the spatial frequency (SF), but not to a particular stimulus velocity (velocity = TF/SF). Previous work has suggested that a subset of neurons in the AOS and pretectum of pigeons show apparent velocity tuning (Crowder et al. 2003). However, Crowder et al. (2003) used relatively liberal between groups statistics to assess velocity tuning. From studies of the motion sensitive neurons in primate cortex, a rigorous within groups test of velocity tuning has been offered (Levitt et al. 1994; Priebe et al. 2003). In Chapter 6, a meta-analysis of the spatio-temporal tuning of units in the AOS and pretectum of pigeons using this within groups analysis of velocity tuning was performed. We concluded that velocity tuning in the AOS and pretectum is rarer than previously estimated, and there is remarkable diversity in the impact of SF on velocity tuning. TF tuning was common, but most cells fell along a continuum between velocity tuning and TF tuning. This diversity has also been noted in primate cortex, and may reflect a general property of motion-sensitive systems. Given that real world visual stimuli rarely resemble the sinusoidal gratings used in laboratory recordings, future studies of spatio-temporal tuning could examine speed tuning as a function of stimulus texture or contrast using more naturalistic stimuli, or examine spatio-temporal tuning in the AOS and pretectum of behaving animals.

Previous studies have suggested that rotation and translation sensitive neurons in the VbC have a receptive field (RF) structure that “approximates” the preferred optic flow field with a “bipartite” organization. Contrasting this, studies in some

invertebrate species indicate that optic flow sensitive neurons in these species are precisely tuned to their preferred flowfield, such that the local motion sensitivities and local preferred directions within their RFs precisely match the local motion in that region of the preferred flowfield. In Chapter 7, CSA in the VbC of pigeons was recorded in response to a set of novel computer generated stimuli, designed to allow discrimination between precise and approximate tuning of RFs. Results show that these RFs were not precisely tuned to optic flow patterns. Rather, these neurons have a bipartite RF structure that approximates the preferred optic flowfield by pooling motion subunits of only a few different direction preferences. A similar receptive field structure has been suggested in mammals (Graf et al. 1988; Leonard et al. 1988; Simpson et al. 1988b, 1989ab), but the approximate RFs starkly contrast findings in the invertebrate optic flow system (Krapp and Hengstenberg 1996; Krapp et al. 1998; Barnes et al. 2002). Again, studies using a more naturalistic stimulus, in awake behaving animals, or using multi-electrode arrays in the VbC to assess the population code to complex stimuli could be performed in order to better understand how this receptive field structure translates to the optokinetic response.

## **Conclusions**

Typically, the AOS and associated structures in the pretectum and olivo-vestibulocerebellum have been regarded as vestigial and considered merely as slaves to the oculomotor system. Clearly, the AOS - pretectum - olivo-vestibulocerebellar pathway is highly conserved, as evidenced by the tremendous similarity in the

response properties and zonal organization of the rotation-sensitive neurons in the inferior olive and flocculus between mammals and birds. Nonetheless, interesting differences remain, not the least of which is the complete absence of neurons sensitive to translational optic flow in the brainstem and cerebellum of mammals. Further, despite being only one synapse from the retina, neurons in the AOS and pretectum have complex responses to large moving visual stimuli and show tremendous variance in the degree to which the physical attributes of the stimulus affect the speed tuning of a neuron. Only two synapses from the retina, binocular panoramic receptive fields are constructed in the inferior olive, where neurons are tuned to precise patterns of optic flow from self-motion, and share a common reference frame with the eye muscles and semi-circular canals of the vestibular system. Interestingly, these binocular receptive fields respond to optic flowfields nearly identical to those preferred by neurons in some invertebrate optic flow systems, but do so with a completely different receptive field structure. While the AOS and associated structures do play an essential role in compensatory responses to the visual consequences of self-motion, they are not restricted to this role. Neurons within this pathway provide input to the HF, and given that optic flow can be used as an ideothetic cue to estimate direction and speed of self-motion, it is possible that this projection aids in complex tasks such as spatial cognition. By examining the interconnections and response properties of neurons in this subcortical pathway, a better understanding of how all visual systems cope with the challenges associated with self-movement through the environment can be attained.

### ***References***

- Barnes WJP, Johnson AP, Horseman BG, & MacAuley MWS.** Computer-aided studies of vision in crabs. *Marine and Freshwater Behavioural Physiology* 35, 1-2, 37-56, 2002.
- Crowder NA, Winship IR, and Wylie DRW.** Topographic organization of inferior olive cells projecting to translational zones in the vestibulocerebellum of pigeons. *J Comp Neurol* 419: 87-95, 2000.
- Crowder NA, W Wylie DR.** Fast and slow neurons in the nucleus of the basal optic root in pigeons. *Neurosci Lett* 304:133-6, 2001.
- DeZeeuw CI, Wylie DR, DiGiorgi PL, and Simpson JI.** Projections of individual Purkinje cells of physiologically identified zones in the flocculus to the vestibular and cerebellar nuclei in the rabbit. *J Comp Neurol* 349: 428-447, 1994.
- Gasbarri A, Sulli A, Packard MG.** The dopaminergic mesencephalic projections to the hippocampal formation in the rat. *Prog Neuropsychopharmacol Biol Psychiatry*. 21:1-22, 1997.
- Graf W, Simpson JI, and Leonard CS.** Spatial organization of visual messages of the rabbit's cerebellar flocculus. II. Complex and simple spike responses of Purkinje cells. *J Neurophysiol* 60: 2091-2021, 1988.

**Grasse KL, and Cyander MS.** The accessory optic system in frontal-eyed animals.

In: *Vision and Visual Dysfunction. The Neuronal Basis of Visual Function*, edited by Leventhal A. New York: McMillan, 1990, p. 111-139.

**Ibbotson MR, Mark RF, Maddess TL.** Spatiotemporal response properties of direction-selective neurons in the nucleus of the optic tract and dorsal terminal nucleus of the wallaby, *Macropus eugenii*. *J Neurophysiol* 72:2927-43, 1994.

**Kano M, Kano M-S, Kusunoki M, and Maekawa K.** Nature of the optokinetic response and zonal organization of climbing fibre afferents in the vestibulocerebellum of the pigmented rabbit. *Exp Brain Res* 80: 238-251, 1990a.

**Kano M, Kano M-S, and Maekawa K.** Receptive field organization of climbing fibre afferents responding to optokinetic stimulation in the cerebellar nodulus and flocculus of the pigmented rabbit. *Exp Brain Res* 82: 499-512, 1990b.

**Krapp HG, Hengstenberg B.** Estimation of self-motion by optic flow processing in single visual interneurons. *Nature* 384: 463-6, 1996.

**Krapp HG, Hengstenberg B, Hengstenberg R.** Dendritic structure and receptive-field organization of optic flow processing interneurons in the fly. *J Neurophysiol* 79: 1902-17, 1998.

**Kusunoki M, Kan M, Kano M-S, and Maekawa K.** Nature of optokinetic response and zonal organization of climbing fibre afferents in the vestibulocerebellum of the pigmented rabbit. I. The flocculus. *Exp Brain Res* 80: 225-237, 1990.

- Lau KL, Glover RG, Linkenhoker B, and Wylie DRW.** Topographical organization of inferior olive cells projecting to translation and rotation zones in the vestibulocerebellum of pigeons. *Neuroscience* 85: 605-614, 1998
- Leonard CS, Simpson JI, and Graf W.** Spatial organization of visual messages of the rabbit's cerebellar flocculus. I. Typology of inferior olive neurons of the dorsal cap of Kooy. *J Neurophysiol* 60: 2073-2090, 1988.
- Pakan JM, Todd KG, Nguyen AP, Winship IR, Hurd PL, Jantzie LL, Wylie DR.** Inferior olivary neurons innervate multiple zones of the flocculus in pigeons (*Columba livia*). *J Comp Neurol* 486: 159-68, 2005.
- Priebe NJ, Cassanello CR, and Lisberger SG.** The neural representation of speed in macaque area MT/V5. *J Neurosci* 23: 5650-5661, 2003.
- Simpson JI.** The accessory optic system. *Ann Rev Neurosci* 7: 13-41, 1984.
- Simpson JI, Graf W, and Leonard C.** The coordinate system of visual climbing fibres to the flocculus. In *Progress in Oculomotor Research*, edited by Fuchs AF, and Becker W. Amsterdam: Elsevier, 1981, pp. 475-484.
- Simpson JI, Graf W, and Leonard C.** Three-dimensional representation of retinal image movement by climbing fiber activity. In *The Olivocerebellar System in Motor Control: Experimental Brain Research Supplement vol. 17*, edited by Strata P. Heidelberg: Springer-Verlag, 1989a, pp. 323-327.
- Simpson JI, Leonard CS, and Soodak RE.** The accessory optic system of rabbit. II. Spatial organization of direction selectivity. *J Neurophysiol* 60: 2055-2072, 1988a.

- Simpson JI, Leonard CS, and Soodak RE.** The accessory optic system: analyzer of self-motion. *Ann New York Acad Sci* 545: 170-179, 1988b.
- Simpson JI, Van der Steen J, Tan J, Graf W, and Leonard CS.** Representations of ocular rotations in the cerebellar flocculus of the rabbit. In *Progress in Brain Research vol. 80*, edited by Allum JHJ, and Hulliger M. Amsterdam: Elsevier, 1989b, pp. 213-223.
- Tan J, Gerrits NM, Nanhoe RS, Simpson JI, and Voogd J.** Zonal organization of the climbing fibre projection to the flocculus and nodulus of the rabbit. A combined axonal tracing and acetylcholinesterase histochemical study. *J Comp Neurol* 356: 23-50, 1995.
- Wylie DR, Crowder NA.** Spatiotemporal properties of fast and slow neurons in the pretectal nucleus lentiformis mesencephali in pigeons. *J Neurophysiol* 84(5):2529-40, 2000.
- Wylie DRW, Winship IR, and Glover RG.** Projections from the medial column of the inferior olive to different classes of rotation-sensitive Purkinje cells in the flocculus of pigeons. *Neurosci Lett.* 268: 97-100, 1999.
- Wylie DR, Brown MR, Barkley RR, Winship IR, Crowder NA, Todd KG.** Zonal organization of the vestibulocerebellum in pigeons (*Columba livia*): II. Projections of the rotation zones of the flocculus. *J Comp Neurol* 456: 140-53, 2003.

